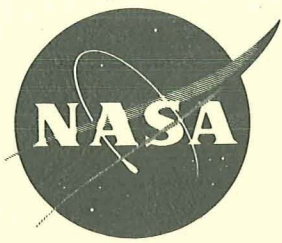


N 70 11548
19

Paul Herr
R. J. Fiorito

NASA CR-72526
MARQUARDT 6147



SPACE STORABLE THRUSTOR INVESTIGATION

748619

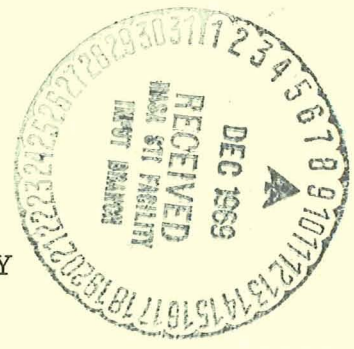
by

**CASE FILE
COPY**

C. D. Coulbert and R. J. Fiorito

11 June 1969

THE MARQUARDT COMPANY
CCI Aerospace Corporation



Prepared for

NATIONAL AERONAUTICS AND SPACE ADMINISTRATION

NASA Lewis Research Center
Contract NAS 3-11215
Paul Herr, Project Manager

NOTICE

This report was prepared as an account of Government-sponsored work. Neither the United States, nor the National Aeronautics and Space Administration (NASA), nor any person acting on behalf of NASA:

- A.) Makes any warranty or representation, expressed or implied, with respect to the accuracy, completeness, or usefulness of the information contained in this report, or that the use of any information, apparatus, method, or process disclosed in this report may not infringe privately-owned rights; or
- B.) Assumes any liabilities with respect to the use of, or for damages resulting from the use of, any information, apparatus, method or process disclosed in this report.

As used above, "person acting on behalf of NASA" includes any employee or contractor of NASA, or employee of such contractor, to the extent that such employee or contractor of NASA or employee of such contractor prepares, disseminates, or provides access to any information pursuant to his employment or contract with NASA, or his employment with such contractor.

Requests for copies of this report should be referred to

National Aeronautics and Space Administration
Scientific and Technical Information Facility
P. O. Box 33
College Park, Md. 20740

FINAL REPORT

SPACE STORABLE THRUSTOR INVESTIGATION

by

C. D. Coulbert and R. J. FioRito

THE MARQUARDT COMPANY
CCI Aerospace Corporation
Van Nuys, California

Prepared for

NATIONAL AERONAUTICS AND SPACE ADMINISTRATION

11 June 1969

CONTRACT NAS 3-11215

NASA Lewis Research Center
Cleveland, Ohio
Paul Herr, Project Manager
Liquid Rocket Technology Branch

This page intentionally left blank

FOREWORD

This report was prepared by the Rocket Systems Division of The Marquardt Company under Contract NAS 3-11215, "Space Storable Thrustor Investigation". It is the final report on the subject contract.

Contract NAS 3-11215 was administered by the Lewis Research Center, Liquid Rocket Technology Branch, of the National Aeronautics and Space Administration, Cleveland, Ohio. The NASA Project Manager was Mr. Paul Herr.

A coordinated concurrent test firing program with the FLOX/Methane propellant combination using some of the same test hardware to evaluate new material concepts was conducted under NASA Contract NAS 7-555, "Advanced Pyrolytic Spacecraft Thrust Chamber Materials". All test results are summarized in this report. However, complete details of the advanced thrust chamber materials investigation will be reported under Contract NAS 7-555.

The following Rocket Systems Division personnel at Marquardt contributed to the technical effort and preparation of this report: C.D. Coulbert (Program Manager), R.J. Fiorito (Project Engineer), M. Wilson (Analysis), and J.G. Campbell (Materials and Design).

This page intentionally left blank

ABSTRACT

A design, fabrication, and experimental test firing program was conducted to demonstrate the feasibility of a radiation cooled, 100-pound thrust, liquid FLOX/Methane, reaction control thruster of advanced pyrolytic refractory composite materials. A matching high performance FLOX/Methane injector was developed and long duration demonstration firings with chambers of pyrolytic refractory composites, pure copper, and high density graphite established the feasibility of the thruster and injector design approaches which were selected. Data are presented on injector performance, thruster material erosion rates, and carbon deposition characteristics.

This page intentionally left blank

CONTENTS

<u>Section</u>		<u>Page</u>
I	SUMMARY	1
II	INTRODUCTION	2
III	INJECTOR DEVELOPMENT	3
	A. Phase I Program	3
	B. Injector Design	3
	C. Injector Fabrication	5
	D. Cold Flow Tests and Results	9
	E. Summary of Phase I Firing Tests	17
	F. Chamber Erosion and Deposition	21
	G. Injector Modifications	28
IV	THRUST CHAMBER DEVELOPMENT	39
	A. Thrust Chamber Design	39
	B. Thrust Chamber Materials	39
	C. Chamber Contraction Ratios and Internal Configuration	41
	D. Injector/Chamber Joint Design	43
	E. Chamber Length	43
	F. Streak Chamber Design	43
	G. Composite Chamber Fabrication Techniques	48
	H. Thrust Chamber Fabrication	50
V	PHASE II -- FINAL THRUSTOR TESTS	57
VI	THERMAL ANALYSES	67
	A. Free Standing PG Chambers	67
	B. POCO Graphite Chambers	73
	C. PG/Carbitex Chambers	74
	D. Copper Chamber	74
VII	DESIGN RE-EVALUATION AND CONCLUSIONS	78
VIII	REFERENCES	79
--	APPENDIX A -- Injector Design Criteria for Hypergolic Bipropellant Rocket Thrusters	93
--	APPENDIX B -- Structural Properties of Carbitex	115
--	APPENDIX C -- Bifluid Spray Tests of Injectors	123
--	APPENDIX D -- Description of Firing Test Facility	139
--	APPENDIX E -- Measurement of High Surface Temperatures Using a Photographic Technique	147
--	DISTRIBUTION	165

This page intentionally left blank

ILLUSTRATIONS

<u>Figure</u>	<u>Page</u>
1. Program Plan for Space Storable Thrustor Investigation	4
2. Assembly Drawing for the 100-pound Thrust FLOX/Methane Injector	6
3. View of Face of the 100-pound Thrust FLOX/Methane Injector . . .	7
4. Single Element Oxidizer Spray Pattern	8
5. 100-pound Thrust FLOX/Methane Injector	10
6. Cold Flow Test Data for the Serial No. 001 FLOX/Methane Injector	11
7. Cold Flow Test Data for the Serial No. 002 FLOX/Methane Injector	12
8. Flow Distribution from Cold Flow Tests of the Serial No. 001 FLOX/Methane Injector	13
9. Flow Distribution from Cold Flow Tests of the Serial No. 002 FLOX/Methane Injector	14
10. Total Spray Pattern from Water Flow Tests of the Serial No. 001 FLOX/Methane Injector	15
11. Mixing Excellence Parameter from Cold Flow Bifluid Mixing Tests with the Serial No. 002 Injector	16
12. Effect of Chamber L* Geometry on Combustion Performance	18
13. Effect of Mixture Ratio on Combustion Performance	19
14. Wall Thicknesses of PG Streak Chambers Prior to Firing	22
15. Side View of Thin Wall PG Chamber after Test Run 45	23
16. Erosion Pattern of the Serial No. 006 PG Chamber after Test Run 45	24
17. Radially Magnified View and Location of Erosion of the POCO Chamber Throat after Run 46	25
18. Radially Magnified View and Location of Erosion of the Serial No. 002 PG Chamber Throat after Run 25	26

ILLUSTRATIONS (Continued)

<u>Figure</u>	<u>Page</u>
19. Radially Magnified View and Location of Erosion of the Serial No. 004 PG Chamber Throat after Run 47	27
20. End View of Thin Wall PG Chamber Inlet after Run 45	29
21. End View of Thin Wall PG Chamber Exit after Run 45	30
22. Distribution of PG Chamber Temperatures, Run 47	31
23. Distribution of PG Chamber Temperatures, Run 25	32
24. Final Configuration of the 100-pound Thrust FLOX/Methane Injector	33
25. Final Configuration, Serial No. 002 Injector	34
26. Spray Pattern from Cold Flow Tests of the 100-pound Thrust FLOX/Methane Injector with 18 Fuel Film Holes	35
27. Distribution Pattern with Only the Fuel Film Jets Flowing	36
28. Erosion Pattern of Chamber No. SL-11 at Plane of Injector after Run 13	37
29. Wall Thicknesses of Chamber No. SL-11 at 0.75 inch from Injector Face after Run 13	38
30. Wall Thicknesses of Chamber No. SL-1 at 0.75 inch from Injector Face after Run 14	40
31. Layout of 100-pound Thrust PG/Carbitex Altitude Chamber with Nozzle Extension	42
32. Tapered Seat Design for Free Standing PG and Composite Chambers	44
33. Pyrolytic Graphite Streak Chambers	46
34. POCO-AXF-5Q Machined Graphite Heat Sink Thrust Chamber	47
35. Completed Carbitex Thrust Chamber Shells	49
36. Tool Used for Lapping the Injector End of a Pyrolytic Graphite Chamber	51

ILLUSTRATIONS (Continued)

<u>Figure</u>	<u>Page</u>
37. Test Fixture Used for Pressure Tests of Pyrolytic Graphite Combustion Chambers	52
38. Pressure Test Fixture Installed on Pyrolytic Graphite Combustion Chamber	53
39. Layout of FLOX/Methane Thrust Chamber	55
40. 100-pound Thrust FLOX/Methane Engine with Copper Thrust Chamber, Showing Thermocouple Installation	56
41. 100-pound Thrust FLOX/Methane Engine Assembly with PG/Carbitex Thrust Chamber and RPG Nozzle Extension	58
42. X-Ray Photograph of PG/Carbitex Thrust Chamber with RPG Nozzle Extension	59
43. Injector after 170 seconds of Firing with FLOX/Methane	60
44. PG/Carbitex Sea Level Chamber (SL-1) after 40 seconds of Firing	62
45. PG/Carbitex Chamber (SL-3) after 322 seconds of Firing	63
46. Sectioned PG/Carbitex Chamber (SL-3) after 322 seconds of Firing	64
47. Erosion Pattern of the POCO Graphite Chamber after Runs 10, 11, and 18	65
48. Sectioned POCO Graphite Chamber after FLOX/Methane Firing, Runs 10, 11, and 18	66
49. Thermal Test Data from Copper Heat Sink Chamber, Run 20	68
50. Erosion Pattern of the Copper Heat Sink Chamber after Runs 20 and 21	69
51. Sectioned Copper Thrust Chamber after 141 seconds of Firing	70
52. Comparison of Throat Temperatures from Firing Tests of the 100-pound Thrust Copper Heat Sink Chamber	71
53. Theoretical Transient Throat Wall Temperatures of Free Standing PG Chambers for the Conditions of Run 47	72

ILLUSTRATIONS (Continued)

<u>Figure</u>		<u>Page</u>
54.	Theoretical Throat Wall Temperatures of PG/Carbitex Chambers	75
55.	Thermal Model Used for Temperature Analysis of the Copper Thrust Chamber	76
56.	Flow Chart for Heat Transfer Analytical Techniques	77
A-1.	Model of Hypergolic Bipropellant Rocket Thrustor	102
A-2.	Effect of Mixture Ratio Distribution on Specific Impulse Efficiency	103
A-3.	Effect of Mixing Factor on Characteristic Velocity Efficiency	104
A-4.	Effect of Rupe Cold Flow Mixing Parameter on Mixing Excellence Parameter for an Impinging Doublet Injector Element	105
A-5.	Impinging Jet Stream Separation Criteria	106
A-6.	Effect of Propellant Atomization on Combustion Performance	107
A-7.	Effect of Thrust per Injector Element on Specific Impulse Efficiency for Various Injector Types	108
A-8.	Variation of Mixing Parameters with Doublet Location	109
A-9.	Film Cooling Performance	110
A-10.	Thermal Effects of Film Cooling, Comparison of Analytical and Test Data	111
A-11.	Temperature Characteristics of the 1000-pound Thrust Engine	112
A-12.	Tangential Stability Limit Characteristics	113
B-1.	Typical Carbitex Cones, 60° and 75° Wrap Angle	119
B-2.	Variation of Circumferential Modulus of Elasticity of Carbitex with Wrap Angle	120
B-3.	Variation of Axial Strength of Carbitex Cones with Wrap Angle	121

ILLUSTRATIONS (Continued)

<u>Figure</u>	<u>Page</u>
C-1. Schematic of Nonreactive Fluids Flow Bench System	129
C-2. Spray Booth Used for Bifluid Flow Test of Injector	130
C-3. View of Injector During Bifluid Spray Test	131
C-4. Collection Cylinder Rack No. 3, Run No. 13	132
C-5. Collection Cylinder Rack No. 4, Run No. 13	133
C-6. Injector Cold Flow Distribution, Run No. 13	134
C-7. Distribution of Injector Cold Flow in Center Row Cross Section, Run No. 13	135
C-8. Definition of Mixing Excellence Factor	136
C-9. Spray Characteristics of the Serial No. 002 Injector	137
C-10. Correlation of Impulse Efficiency with Propellant Distribution Index for CR F ₃ /N ₂ H ₄ Injectors	138
D-1. Test Cell M-2 of The Marquardt Magic Mountain Rocket Test Laboratory	143
D-2. Firing Position of Test Cell M-2	144
D-3. Schematic of Test Setup in Cell M-2	145
E-1. Apparatus Used for Temperature Calibration	157
E-2. Temperature vs. Density for Various Phenolics	158
E-3. Effect of Filter Color on Density vs. Temperature for Pyrographite	159
E-4. Temperature Density for Various Lighting Conditions Using a Standard Tungsten Calibration Lamp	160
E-5. Bellows Extension vs. Density at 2200°F (1478°K) for M ₀ Si ₂ . .	161
E-6. Temperature Profile of Pyrolytic Graphite	162
E-7. Typical Chamber (Columbium) Evaluation Using XR Film	163

This page intentionally left blank

TABLES

<u>Table</u>		<u>Page</u>
I.	Injector Design Parameters, 100-pound Thrust FLOX/Methane Engine	81
II.	Summary of the Phase I Injector Evaluation Firing Tests	82
III.	Gaseous Methane Peak Ignition Pressures for Runs 30 through 33	84
IV.	Summary of the Phase I Chamber Erosion Tests	85
V.	Summary of the Phase II Thrust Chamber Firing Tests	86
VI.	Summary of Average Thrust Chamber Throat Erosion Data, Phase II Tests	91
VII.	Extended Range Film Temperature Data, Phase II Tests	92

This page intentionally left blank

SPACE STORABLE THRUSTOR INVESTIGATION

SECTION I SUMMARY

A design, fabrication, and experimental test firing program was conducted to demonstrate the feasibility of a radiation cooled, 100-pound (445-newton*) thrust, liquid FLOX/Methane, reaction control thruster of advanced pyrolytic refractory composite materials.

This program included the design, fabrication, and evaluation of a matching 100-pound thrust, FLOX/Methane injector which provided fuel film injection for cooling and chemical protection of the thrust chamber wall. The goal of the program was to demonstrate a radiation/film cooled thruster life of 1800 seconds with multiple starts at a performance level of 92% of theoretical C* or better.

The thrust chamber material approach selected for this program was use of a pyrolytic graphite composite structure with an inner wall of pyrolytic graphite deposited on a structural shell of a fibrous graphite composite (Carbitex 713).

The program was conducted in two phases. In Phase I, a multiple like-on-like doublet injector with separate fuel film injection holes was evaluated for performance and erosion/carbon deposition characteristics as a function of chamber length, chamber material, mixture ratio, and fuel film cooling injection pattern and amount.

In Phase II, demonstration firings were conducted with FLOX/Methane using the modified injector and several chamber materials with the following significant results:

1. Two consecutive test runs of 64 and 68 seconds duration, respectively, using a copper heat sink chamber with resulting minimum throat erosion
2. Five test runs with a high density graphite chamber accumulating 194 seconds of operation with negligible throat erosion
3. Six test runs with a PG/Carbitex composite chamber accumulating 322 seconds prior to burn through

* The term "100-pound thrust" is a nominal engine designation and the conversion to 445 newtons will not be repeated where the units refer only to the nominal designation.

4. Over 900 seconds of firing with one injector with no plugging or overheating during operation at efficiencies between 89 to 98% (for chamber L^* values of 10 inches and 18 inches, respectively)

During these tests, both chamber erosion and carbon deposition were evident and varied locally in the chamber from the injector to the nozzle throat as a function of fuel film flow, wall material, O/F, L^* , and duty cycle.

It was concluded that the injector design approach was successful and, with additional optimization, the design should be capable of providing high performance and control of erosion and carbon deposition. Both the high density graphite and the pyrolytic carbon composite materials demonstrated high temperature structural integrity in the FLOX/Methane combustion environment. An optimized graphite chamber design may utilize film cooling -- along with axial conduction, radiation, and heat sink effects -- to minimize both erosion and carbon deposits.

SECTION II INTRODUCTION

The primary objective of this program was to conduct a feasibility demonstration of a 100-pound thrust, reaction control, radiation cooled, pyrolytic refractory composite thruster using the FLOX/Methane propellant combination. The technical effort included the design, fabrication, and evaluation of a matching FLOX/Methane injector to meet the performance and durability goals of the program. The design goals for the engine were an 1800-second life in multiple firings with a combustion performance of greater than 92% of theoretical C^* with no duty cycle limitations and minimum thermal soakback to the injector.

The thrust chamber material approach selected for this program was use of a pyrolytic graphite composite structure with an inner wall of pyrolytic graphite in contact with the combustion environment and with a fibrous graphite outer structural shell to resist the thrust, thermal, and pressure loads. Graphitic materials have demonstrated the greatest resistance to fluorinated propellants and combustion products at very high temperatures (above 4500°F) (2760°K) (Reference 1). Pyrolytic graphite is the most resistant of the graphites. However, all graphites are subject to oxidation and reaction with the propellants and oxidizer rich products and must be either cooled or chemically protected.

Theoretical and experimental studies (Reference 2) indicated that graphitic materials could operate at temperatures up to 6000°F (3600°K) if a carbon rich boundary environment were maintained. These same studies and NASA experience, as well as the criteria for pyrolytic carbon deposition, indicated the probable deposition of carbon on hot chamber walls under some conditions. Therefore, it was apparent that the propellant injector design and film injection provisions would be critical in achieving very long run

durations with limited erosion and deposition. The high wall temperature approach with chemical film protection is attractive for the FLOX/Methane propellant combination because of the small amount of fuel available ($O/F \sim 5.0$) and the narrow liquidus range of methane.

The primary chamber material system candidate was pyrolytic graphite deposited on a structural shell of fibrous graphite (Carbitex). This material system has been developed and evaluated under NASA Contract NAS 7-555. The characteristics of this material are summarized in Appendix B.

This space storable thruster investigation was carried out in two phases: Phase I -- injector design, fabrication, test evaluation, and injector modification; and Phase II -- thrust chamber design, fabrication, and test firing evaluation. The fabrication and test firing program was coordinated with work on the development and evaluation of advanced pyrolytic refractory materials under Contract NAS 7-555 (Reference 3). Under the coordinated program, additional injector hardware was fabricated and newer chamber materials and fabrication techniques were evaluated.

The program plan and the relationship between the two coordinated test firing programs is shown schematically in Figure 1.

SECTION III INJECTOR DEVELOPMENT

A. Phase I Program

The Phase I investigations included the analysis, design, and fabrication of one injector. A second injector assembly of the same design was fabricated under NASA Contract NAS 7-555. These programs were conducted in close coordination to reduce hardware duplication and test costs. In addition, heat sink and thin wall pyrolytic graphite test chambers were designed and fabricated for evaluation of injector performance and streaking characteristics.

Injector cold flow spray testing and analysis were performed prior to final injector selection. Hot firing tests of 5 to 30 seconds duration were subsequently conducted to evaluate the injector structural, performance, and chemical protection (streaking) characteristics. A determination of the injector modifications required to improve the overall performance was accomplished in Phase I and incorporated into the existing hardware prior to the Phase II program.

B. Injector Design

The primary considerations dictating the injector thermodynamic design are discussed in detail in Appendix A (Injector design criteria for hypergolic bipropellant rocket thrusters). Of prime importance for the design of the 100-pound thruster injector was the requirement to provide a chemically inert

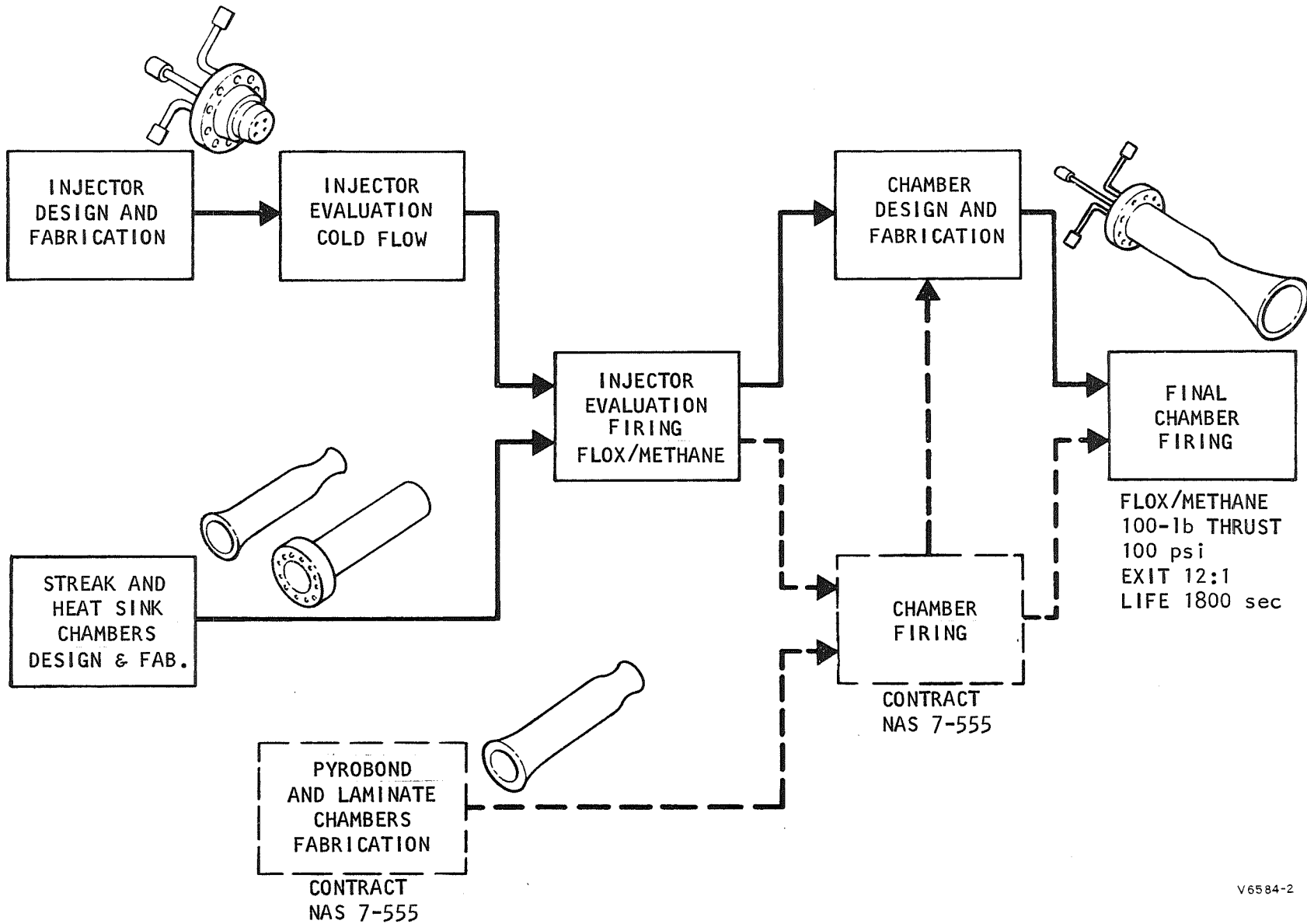


FIGURE 1. Program Plan for Space Storable Thruster Investigation

V6584-2

film at the boundary layer of the graphite chamber to prevent erosion of the hot surface of the graphite. Film protection was required with minimum compromise to C* performance (92% C* efficiency minimum). This requirement dictated a highly efficient primary combustor core element (good atomization and mixing) and minimal interaction of combustion products with the boundary layer film.

On this basis, a six-element, like doublet, edge impinging, spray fan, injector core design was selected. Film injection was initially accomplished by six equally spaced fuel jets located at the injector periphery and directed outward toward the chamber wall at an angle of 7° (0.122 rad). An assembly drawing of the injector is shown in Figure 2 and a close-up photograph of the injector face is illustrated in Figure 3. The chamber pressure tap is evident at the center of the injector face. The injector was constructed of Nickel 200 and 321 stainless steel for optimal structural characteristics and propellant compatibility.

This injection configuration was selected because of good atomization and mixing characteristics, insensitivity of doublet momentum angle to changes in mixture ratio, and minimal interaction between the primary injection core and the fuel film injection elements at the periphery of the injector face. A tabulation of the more important injection parameters is given in the first two lines of Table I for the Serial Nos. 001 and 002 injectors. It will be noted that these injectors were designed with small differences in injection momentum ratio and in proportion of fuel film injection for test evaluation.

The initial injector design favored high C* performance with minimal film injection. However, provisions were made to increase the film injection by enlarging the existing jets or increasing the number and distribution of the film injection jets. The last four lines of Table I show the variation in injection parameters with the addition of six and twelve film injection orifices to the basic six film jets.

A single like-doublet oxidizer and fuel test element was fabricated and water flow tested to establish the injection passage fabrication process and to determine hydraulic flow data for the injector metering orifices as a basis for the final injector design. A photograph of the single element spray rig is shown in Figure 4. The flow discharge coefficients listed in Table I were established.

C. Injector Fabrication

Three injector faceplate units containing the propellant distribution passages and injector core elements were fabricated and water flow tested in a flow fixture. This intermediate quality control step was performed to establish the proper injector hydraulic flow characteristics, doublet spray patterns, and mass distribution. This step in the injector assembly process allowed remedial action, if necessary, while the important metering orifice inlets were still accessible prior to the final closure welds. The three injector faceplates were flow checked satisfactorily and two were selected

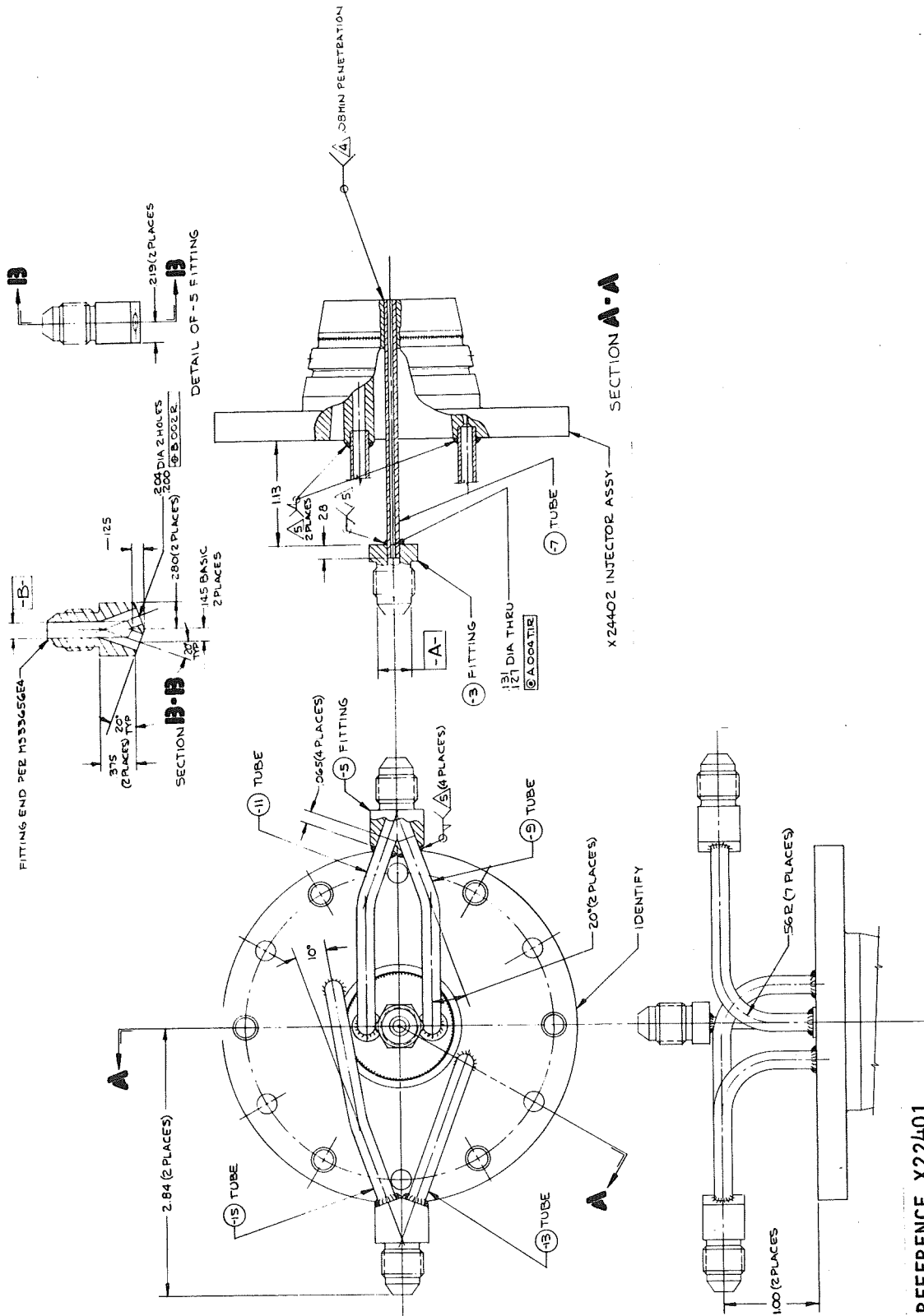


FIGURE 2. Assembly Drawing for the 100-pound Thrust FLOX/Methane Injector

REFERENCE X22401

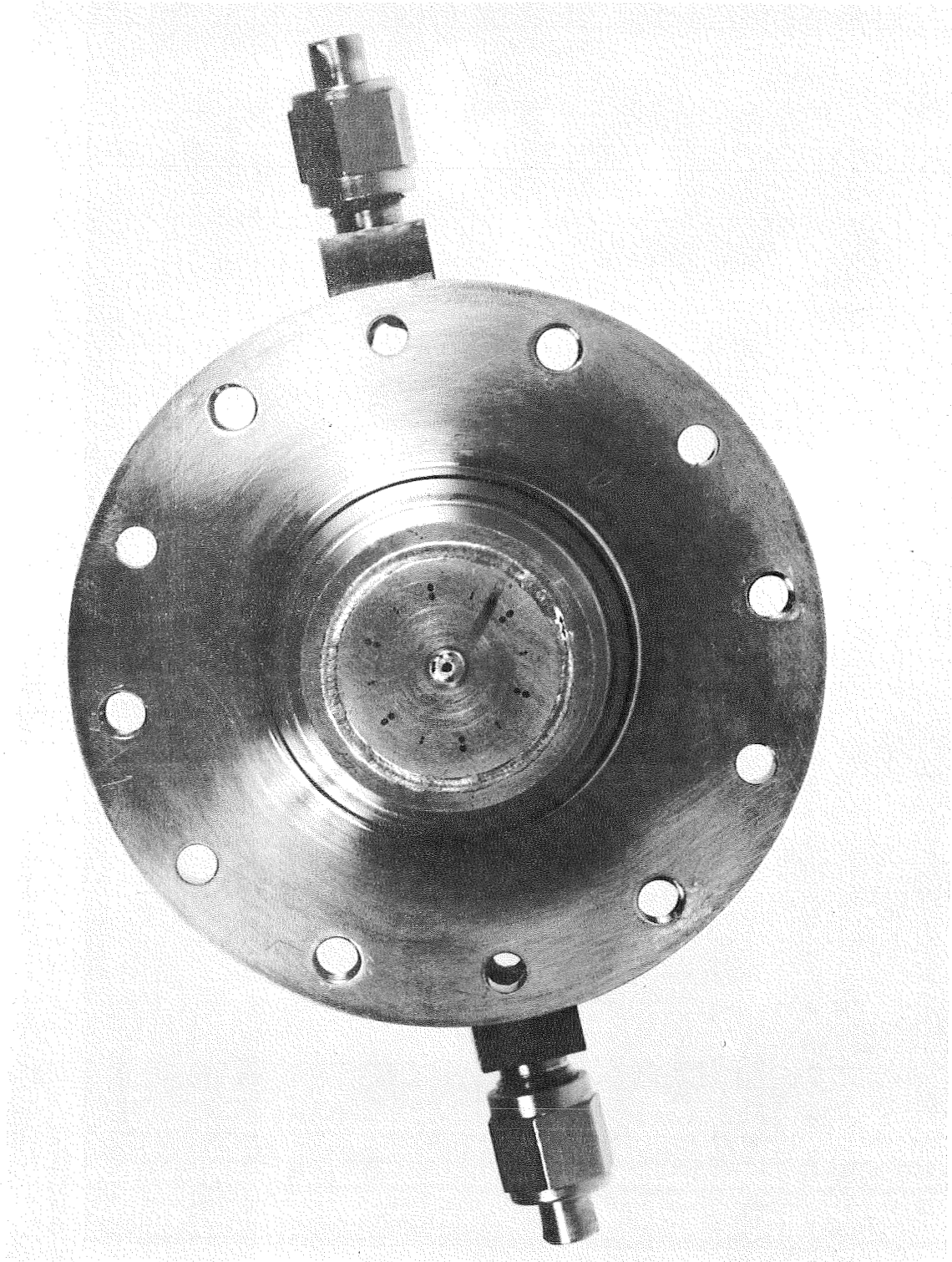


FIGURE 3. View of Face of the 100-pound Thrust FLOX/Methane Injector

9157-3

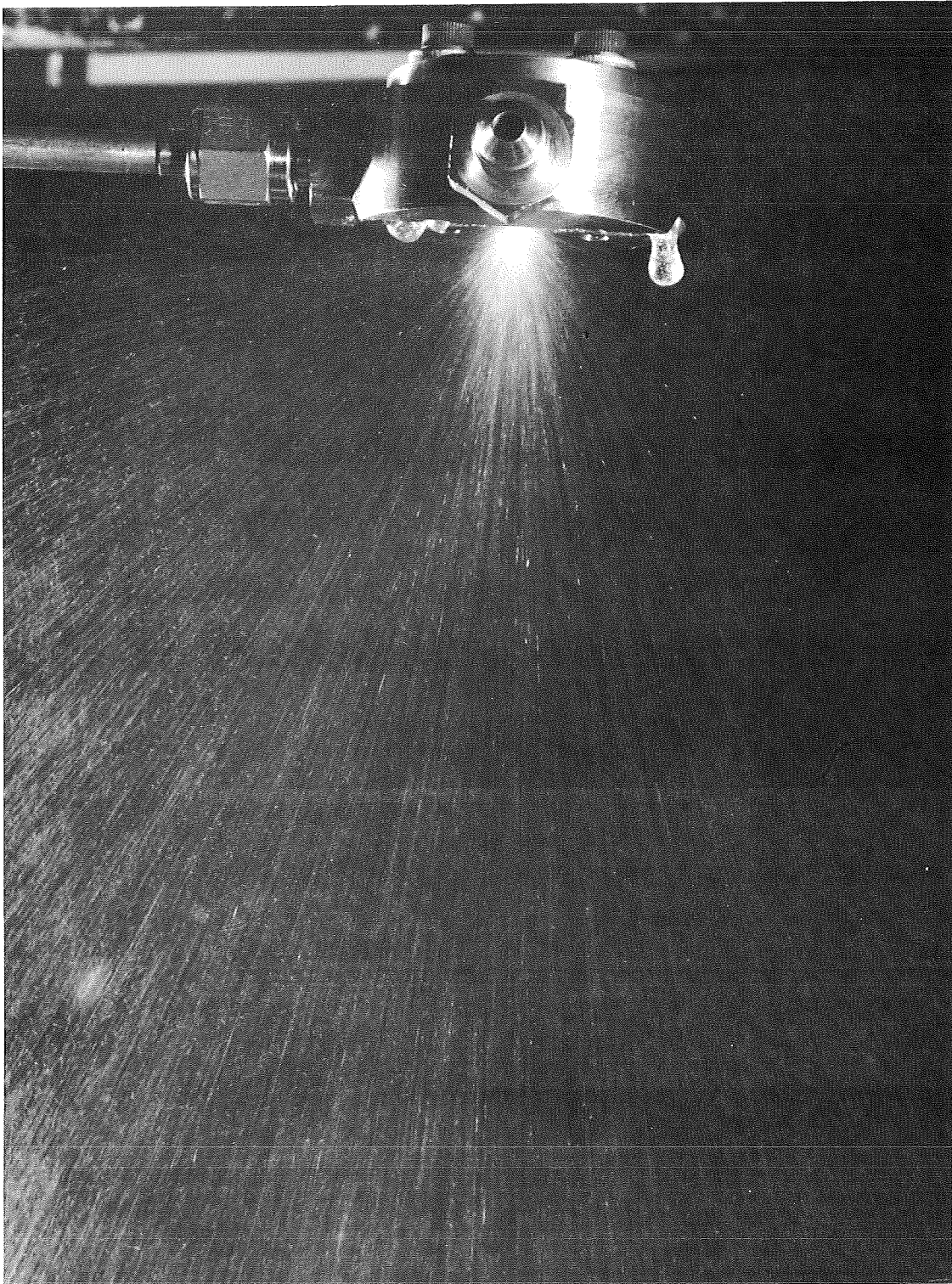


FIGURE 4. Single Element Oxidizer Spray Pattern.

T11362-1

for completion to the welded assembly as shown in Figure 5. Electron beam welding techniques were utilized in completing the assembly. The injector core injection orifices (doublets) were drilled by standard precision drilling and deburring techniques. The film injection orifices were formed by electrical discharge (Elox) methods. All welds were hydrostatically pressure tested during the assembly process. This injector was designed for use with separate facility type propellant valves, and accordingly, the inlet connections for both propellants are standard AN B-nut type connectors. Propellant flow balance to the injector internal flow distribution manifolds was accomplished by splitting the flow into two equal legs for each propellant from the facility valve outlet line connections to the injector manifold inlets.

D. Cold Flow Tests and Results

Nonreaction fluid flow tests of the injector assembly were performed in two categories, as follows:

1. Water flow calibration of both propellant injection systems to establish the flow versus pressure drop characteristics and the flow balance of the individual injection elements
2. Bifluid spray tests utilizing concurrent flow of nonreactive propellant simulants to evaluate the injector mixing and distribution characteristics

The results of the Category 1 tests of the Serial Nos. 001 and 002 injector assemblies are plotted in Figures 6 through 9. Figures 6 and 7 show the total pressure drop versus propellant flow (water flow data converted to propellant density). Also included in these data are the injector flow characteristics of the injector faceplates which did not include the film injection flow. Figures 8 and 9 are polar distribution plots showing the percentage of total flow for individual fuel and oxidizer doublets and the film injection jets (weepers) at design inlet conditions. The injection pattern orientation is referenced to the oxidizer line connector inlet. It is seen that both injectors show a flow balance within several percent for both the fuel and oxidizer circuit. Figure 10 is a photograph of the water flow spray pattern of the Serial No. 001 injector.

The results of the Category 2 cold flow bifluid mixing tests with the Serial No. 002 injector are summarized in Figure 11. The details of the test setup and testing procedures are presented in Appendix C. The mixing excellence parameter (E_m) shown in Figure 11 is a measure of the departure of the local mixture ratio from the overall mixture ratio. Values of E_m above 0.80 are required for C* efficiencies above 90%. All values of E_m for the S/N 002-injector were above 0.85 with 7% fuel film injection.

The Serial No. 001 injector was cold flow tested for pattern uniformity and impingement accuracy but it was not tested in the bifluid mixing test setup because of the similarity of the two injectors and the added cost of the testing and data reduction.

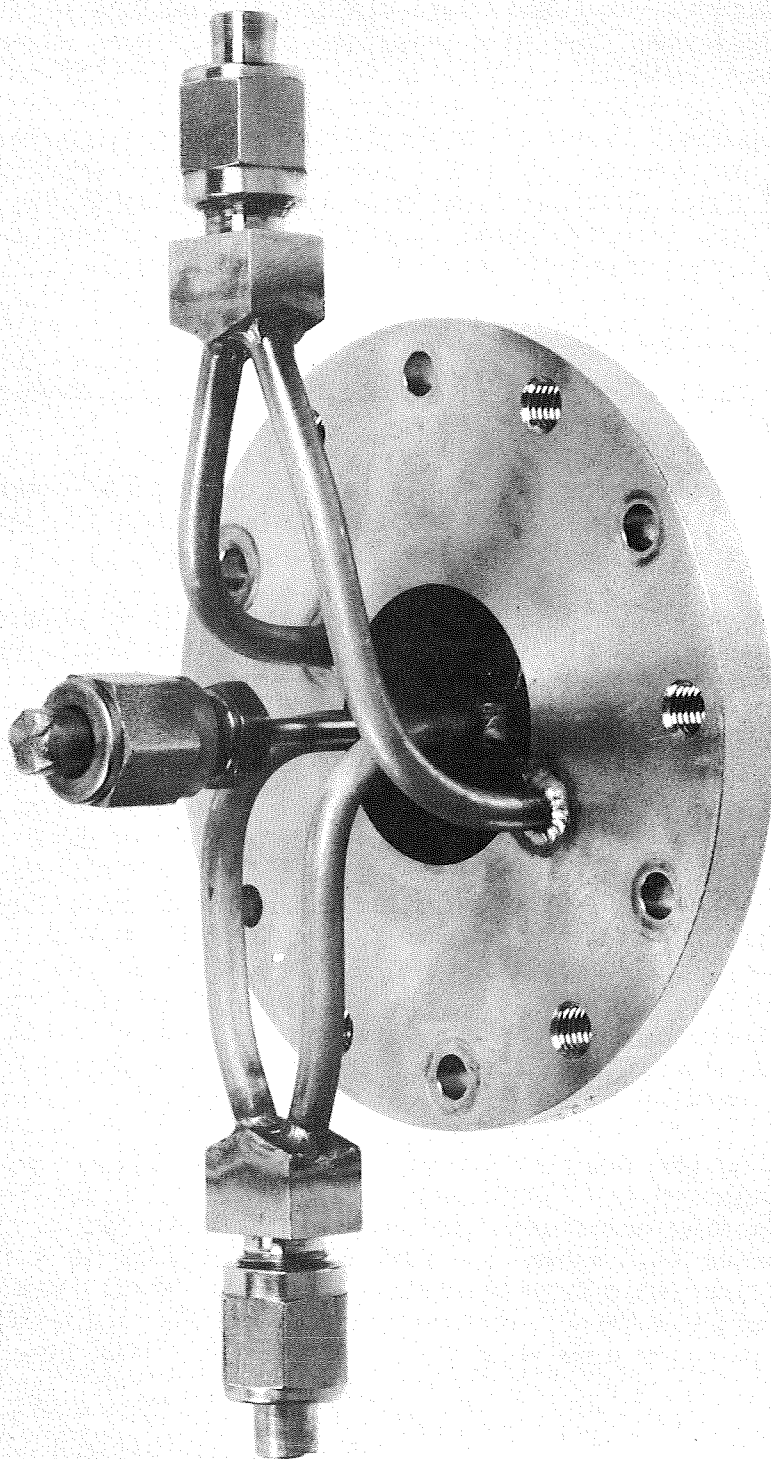


FIGURE 5. 100-pound Thrust FLOX/Methane Injector

9157-4

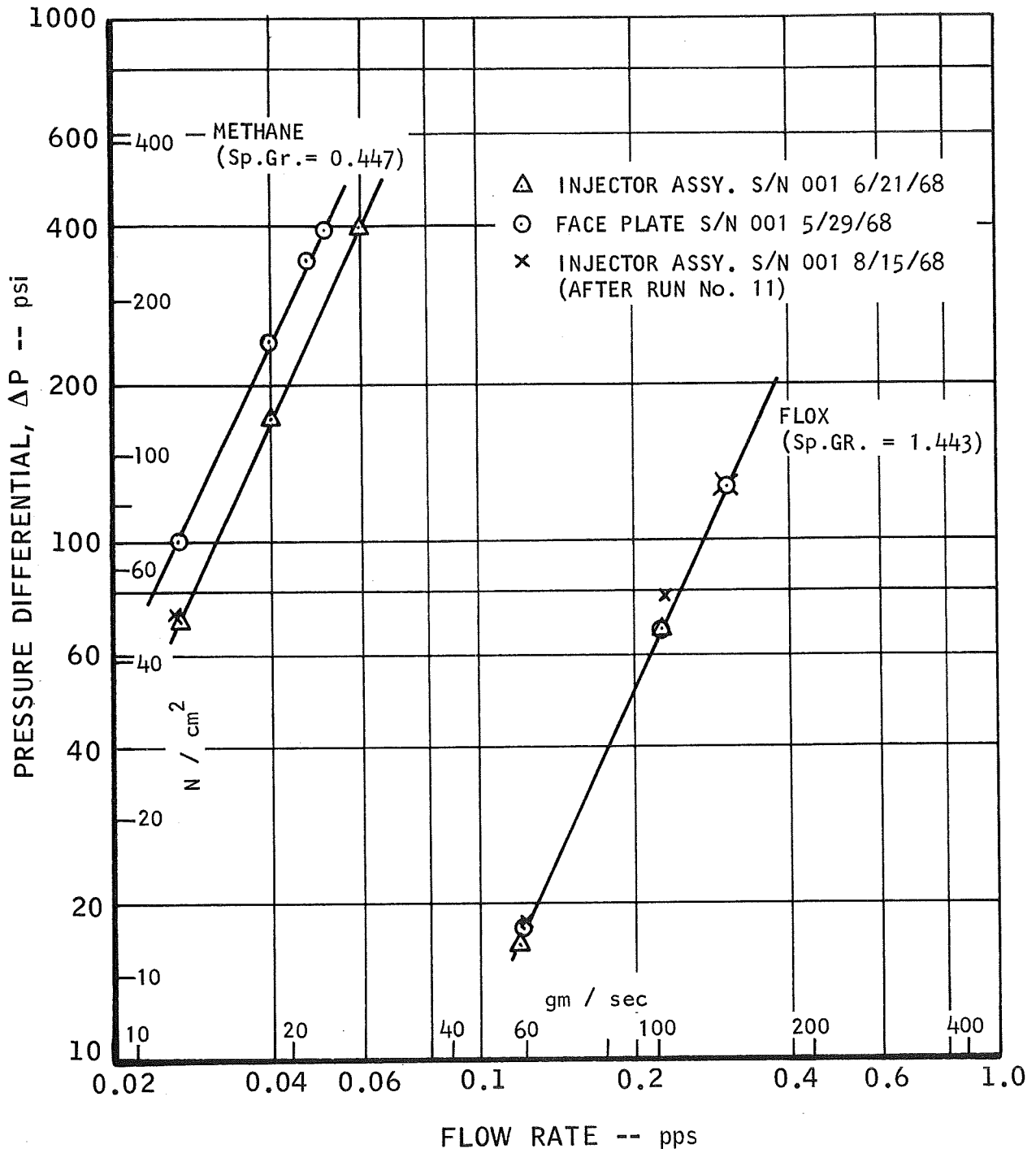


FIGURE 6. Cold Flow Test Data for the Serial No. 001 FLOX/Methane Injector

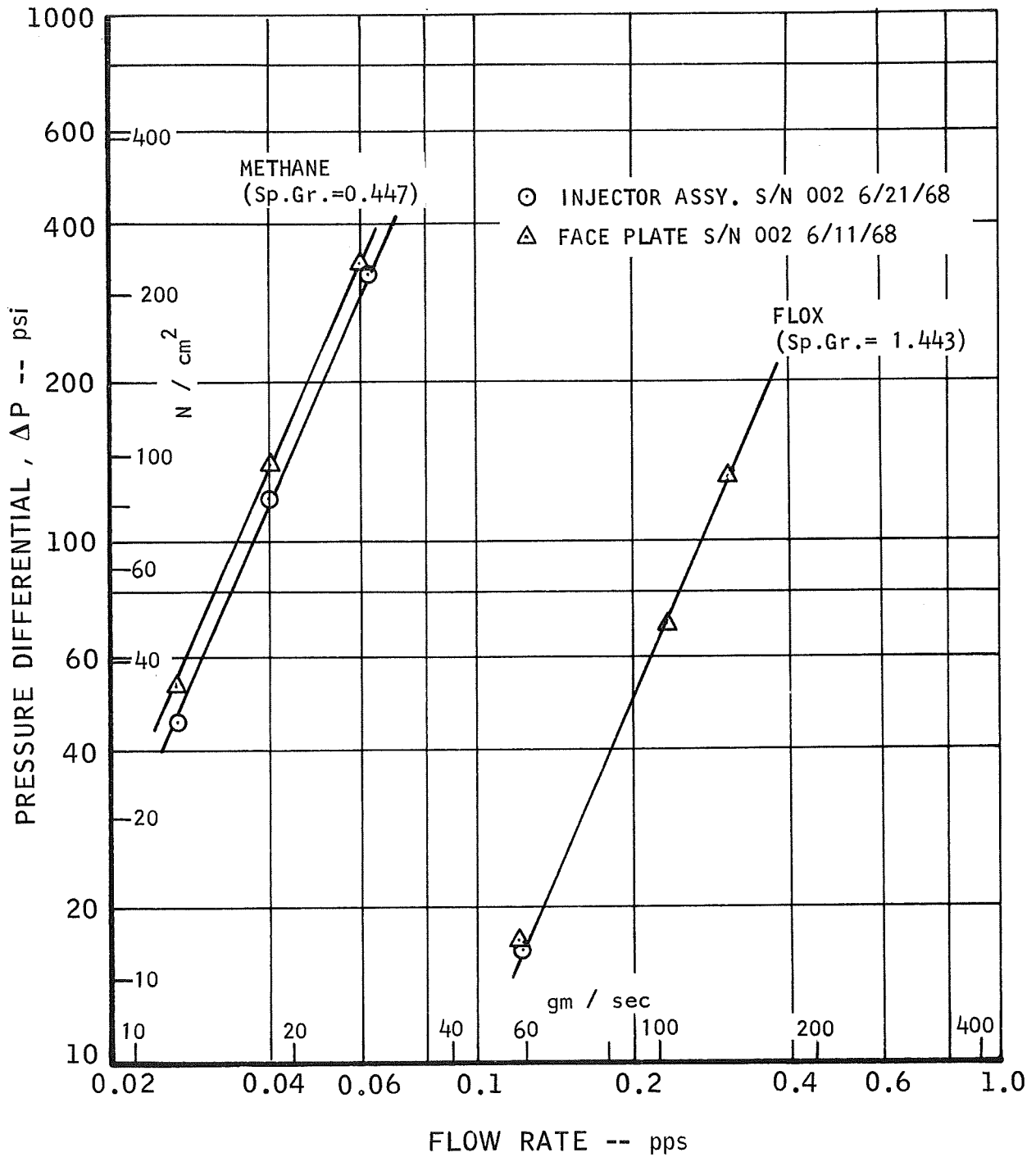


FIGURE 7. Cold Flow Test Data for the Serial No. 002 FLOX/Methane Injector

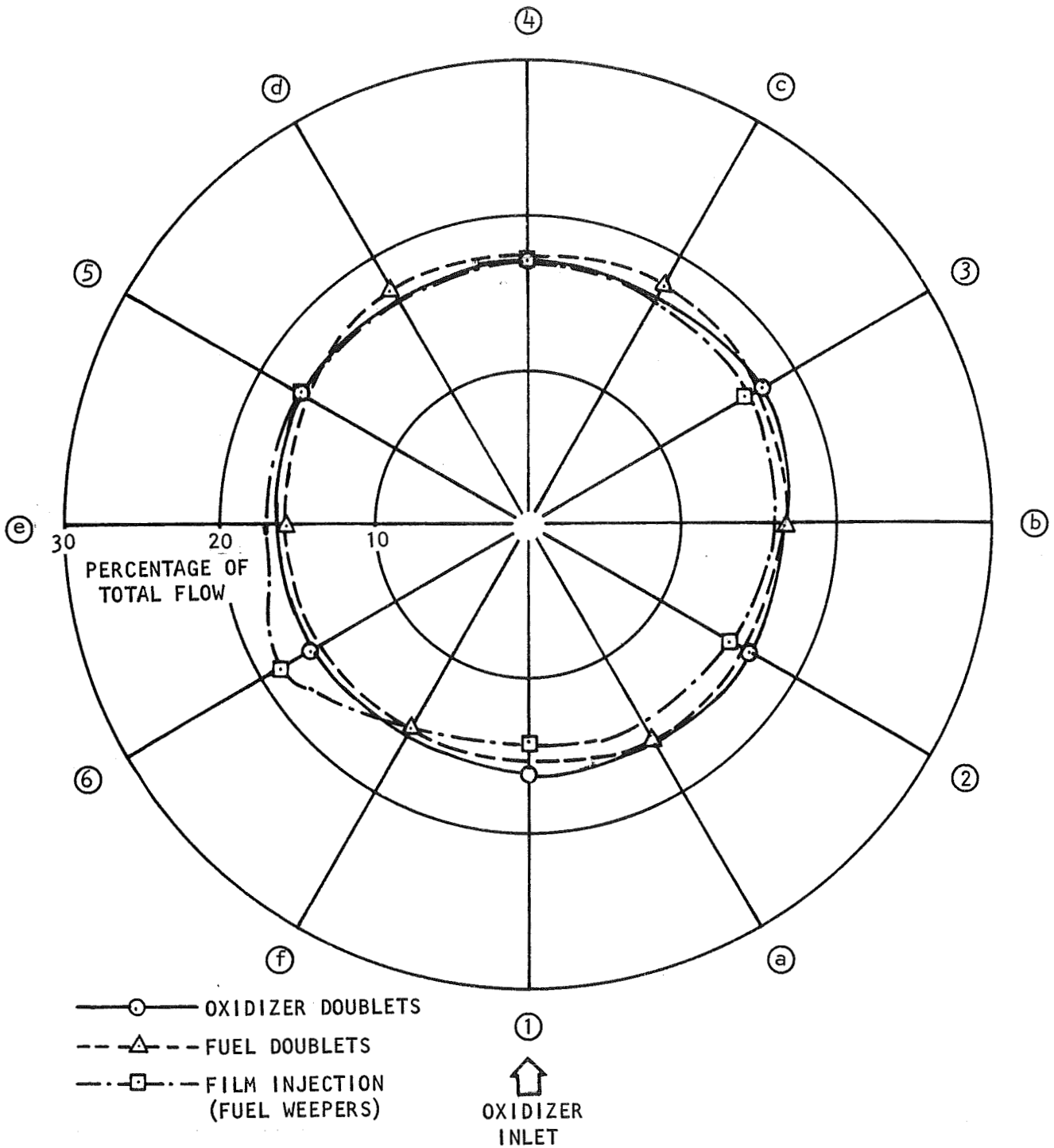


FIGURE 8. Flow Distribution from Cold Flow Tests of the Serial No. 001 FLOX/Methane Injector

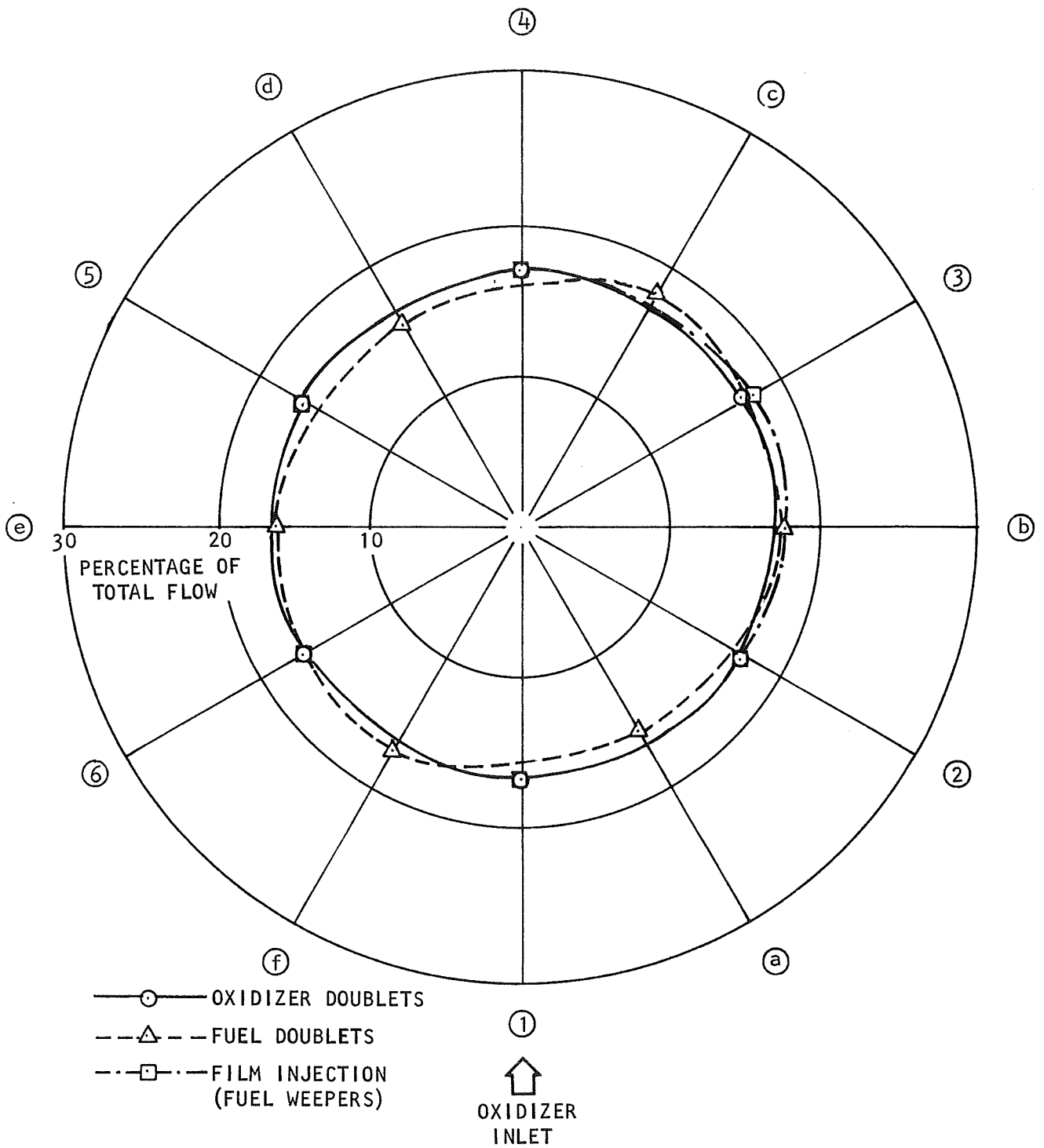


FIGURE 9. Flow Distribution from Cold Flow Tests of the Serial No. 002 FLOX/Methane Injector



T11370-3

FIGURE 10. Total Spray Pattern from Water Flow Tests of the Serial No. 001 FLOX/Methane Injector

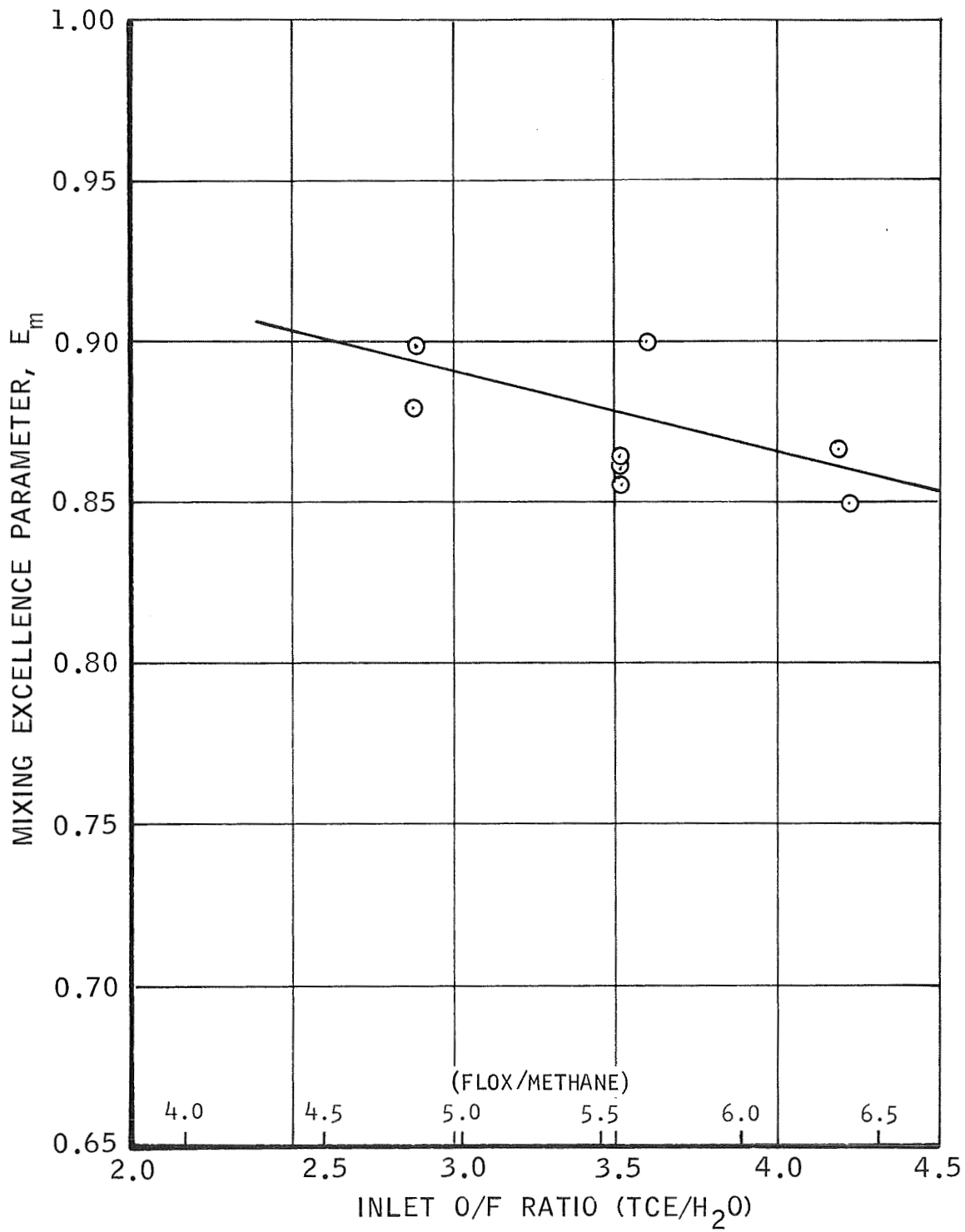


FIGURE 11. Mixing Excellence Parameter from Cold Flow Bifluid Mixing Tests with the Serial No. 002 Injector

E. Summary of Phase I Firing Tests

The injector firing evaluation tests were divided into three basic categories relative to primary test objectives, namely:

1. Combustion performance evaluation
2. Ignition compatibility evaluation
3. Influence of the injector upon the thermal and erosion characteristics of the chamber

The injector evaluation test firings were conducted in Cell M-2 of the Marquardt Magic Mountain Rocket Test Laboratory (see Appendix D) at ambient pressure exhaust conditions. The propellants used were liquid FLOX (82.5% F₂ + 17.5% O₂) and liquid commercial methane (87.5% CH₄ + 11.6% C₂H₆).

All of the thrust chamber designs used in this program, including the heat sink and streak chambers, are discussed in Section IV.

Table II summarizes the firing tests which were accomplished and some of the pertinent performance values which were obtained during the injector evaluation test phase.

Runs 1 through 10 were conducted to evaluate combustion performance, as well as to make the necessary improvements to the test facility, instrumentation, and run procedures as indicated by actual test operation. These tests were conducted with copper heat sink chambers. The effect of three chamber L* geometries (chamber length change only) upon combustion performance was evaluated (Figure 12). The effect of mixture ratio on combustion performance is shown in Figure 13.

Runs 11 and 12 were made with graphite chambers and they were intended to evaluate the streaking and erosion characteristics. However, it became apparent during these tests that ignition overpressures were being encountered which exceeded the structural limits of the graphite chambers. Consequently, Runs 13 through 43 were conducted to establish a reliable ignition approach which would eliminate or limit the overpressures to acceptable levels. The parameters chosen for investigation to decrease the ignition delay time were:

1. Propellant synchronization (oxidizer lead or lag) influencing the ignition O/F ratio
2. Propellant thermodynamic state at ignition (liquid phase versus gas phase, or combinations thereof)
3. Propellant reactivity (GF₂ lead ahead of FLOX)

Since the test engine configuration did not include close-coupled flight type valves, (Facility Annin valves located approximately 15 inches

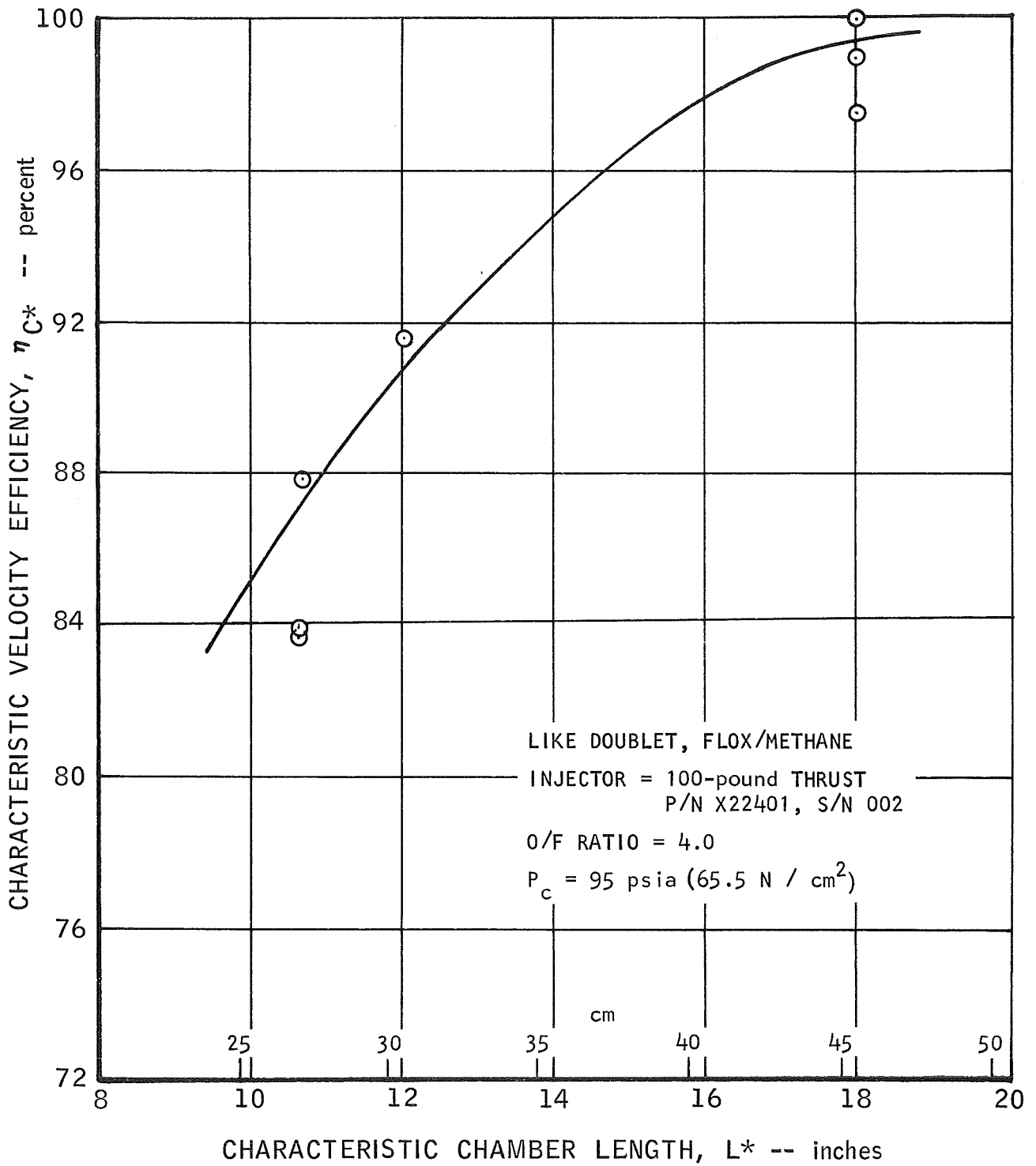


FIGURE 12. Effect of Chamber L^* Geometry on Combustion Performance

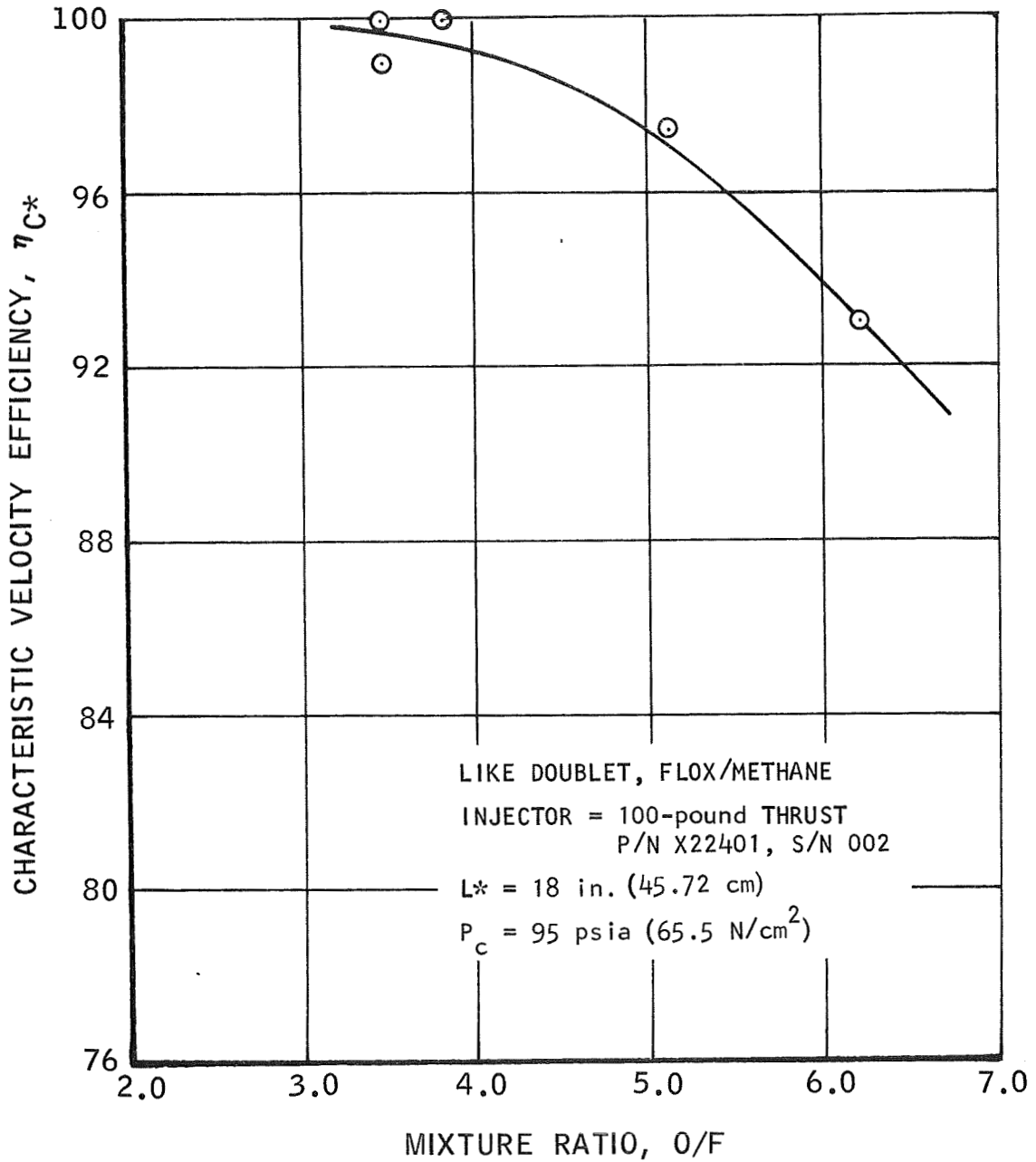


FIGURE 13. Effect of Mixture Ratio on Combustion Performance

(38 cm) upstream from the injector were utilized to control the propellant flow to the engine), it was not practical to obtain precise synchronization of propellant flows to the engine during the ignition cycle. Oxidizer lead, fuel lead, and simultaneous propellant valve opening were investigated.

It was established during Runs 13 through 17 that low energy (minimum overpressure) ignitions could be reliably accomplished by the introduction of gaseous propellants during the ignition cycle. This was accomplished by chilling the propellant system upstream from the propellant run valves to liquid conditions, but allowing the engine and propellant lines downstream from the run valves to remain at ambient temperature conditions. However, this procedure was not acceptable, as indicated by Run 18. The transition from saturated vapor to saturated liquid could not be accomplished in a reasonable time period. The engine performance was erratic and, generally, at a lower level during the period of variable propellant quality.

Runs 19 through 28 evaluated a revised ignition procedure which consisted of the following sequence of operations:

1. A 1 second oxidizer lead. The temperature of the oxidizer at the starting cycle was controlled to give partial vaporization of the oxidizer.
2. Minimum (saturated liquid) temperatures were maintained in the fuel system and cold N_2 purge was maintained through the engine.

This procedure resulted in partial success, but completely reliable ignitions could not be maintained due to the difficulty in achieving accurate control of the two-phase oxidizer lead.

Runs 29 through 37 were accomplished to evaluate a revised ignition procedure. This procedure was intended to reduce the energy level at ignition by minimizing the propellant flow rate through the introduction of vaporized fuel. Accordingly, the procedure which was evaluated was as follows:

1. A 1 second FLOX lead with the temperature of the complete oxidizer system and oxidizer side of the engine down to the saturated liquid temperature
2. A one-half second gaseous CH_4 flow at a regulated pressure of 400 psig (276 N/cm^2) introduced downstream from the propellant run valve
3. Introduction of CH_4 with the complete fuel system and fuel side of the engine at near-saturated liquid temperatures

The test results of Runs 29 through 37 (Table III) indicated marginal and nonrepeatable ignition characteristics which were unacceptable. Runs 38 through 44 were then performed to evaluate the reactivity (hypergolicity) of gaseous F_2 relative to FLOX. It was postulated that the higher reactivity of GF_2 would minimize the ignition delay and allow quick transition

to steady state liquid phase injection. Accordingly, the following ignition sequence was evaluated:

1. A 1 second GF_2 lead, at a supply pressure of approximately 240 psig (165.5 N/cm^2), introduced downstream from the facility valve
2. The introduction of liquid methane with the complete fuel system and fuel side of the injector at near-saturated liquid temperatures
3. Three seconds later, introduce FLOX and cut GF_2 . The complete oxidizer system and the oxidizer side of the injector were cooled to saturated liquid temperatures at the start of the run.

This approach resulted in reliable low pressure ignitions and minimal transition time to steady state liquid flow conditions and the procedure was utilized for the concluding tests in evaluating streaking and erosion in the PG and POCO thrust chambers.

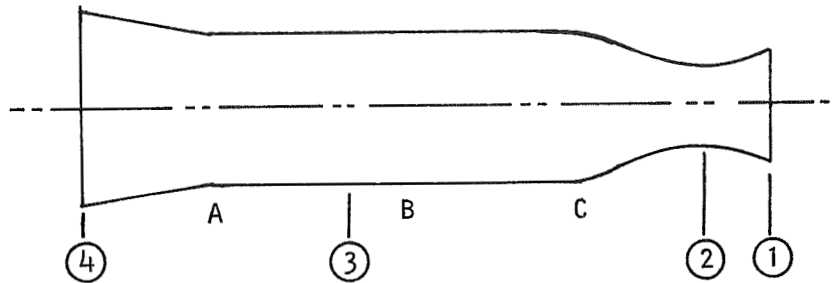
Runs 45 through 47 were conducted for long run durations with graphite chambers having L^* values varying from 10.6 to 18 inches (26.92 to 45.72 cm). The effect of $L^* = 10.6$ (26.92 cm) is noted for Run 46 during which the C^* efficiency was reduced to the 84 to 88% level, compared to C^* efficiencies of 93 to 100% for the $L^* = 18$ tests. Performance correlation data for Runs 29, 45, and 47 are listed in Table II.

F. Chamber Erosion and Deposition

Table IV summarizes the results of the Phase I erosion tests of the free standing PG streak chambers and the POCO chambers. The wall thicknesses of the PG streak chambers prior to firing (as received) are listed in Figure 14. After firing, the streak chambers had circumferential nonuniform erosion at both the injector chamber interface and the throat. The throat wall erosion rates were 0.0 to 0.00074 in./sec (0.00188 cm/sec). The injector chamber interface wall erosion rates were 0.0 to 0.00170 in./sec (0.00432 cm/sec) in line with the film orifices and 0.00075 to 0.0035 + in./sec (0.00191 to 0.00889 cm/sec) between the film orifices. The 0.0035 + in./sec (0.00889 cm/sec) rate occurred during Run 45 in which the chamber wall was eroded through (Figures 15 and 16).

Figure 17 represents a radially magnified view of the POCO chamber throat erosion and the locations. Similar enlargements of the erosion and deposition locations in the free standing PG chambers during Runs 25 and 47 are shown in Figures 18 and 19, respectively. It is also seen from these figures that the maximum erosion near the injector face occurred at circumferential locations between the oxidizer doublets.

It is hypothesized that this effect was caused by the local interaction of the oxidizer fans with the mating fuel doublets. The high release of combustion gases caused local high radial flow components which impinged upon and reacted with the hot chamber walls in the absence of adequate chemically protective film.



CHAMBER SERIAL No.	OUTSIDE DIAMETER in. (cm)				INSIDE DIAMETER in. (cm)	THICKNESS in. (cm)	
	①	②	③	④	②	③	②
001	1.176 (2.987)	0.928 (2.357)	1.529 (3.883)	2.035 (5.144)	0.821 (2.085)	0.064 (0.163)	0.053 (0.135)
002	1.176 (2.987)	0.931 (2.365)	1.528 (3.881)	2.013 (5.113)	0.814 (2.068)	0.066 (0.168)	0.057 (0.145)
003	1.168 (2.967)	0.932 (2.367)	1.525 (3.874)	2.022 (5.136)	0.827 (2.101)	0.062 (0.157)	0.051 (0.130)
004	1.177 (2.989)	0.931 (2.365)	1.531 (3.889)	2.022 (5.136)	0.827 (2.101)	0.062 (0.157)	0.052 (0.132)
005	1.171 (2.974)	0.928 (2.357)	1.528 (3.881)	2.014 (5.116)	0.827 (2.101)	0.063 (0.160)	0.053 (0.135)
006	1.173 (2.979)	0.929 (2.360)	1.528 (3.881)	2.021 (5.133)	0.826 (2.097)	0.066 (0.168)	0.053 (0.135)
007	1.174 (2.982)	0.937 (2.355)	1.529 (3.884)	2.010 (5.105)	0.822 (2.088)	0.063 (0.160)	0.053 (0.135)

* THICKNESS MEASUREMENTS AT STATIONS ③ and ②

FIGURE 14. Wall Thicknesses of PG Streak Chambers Prior to Firing

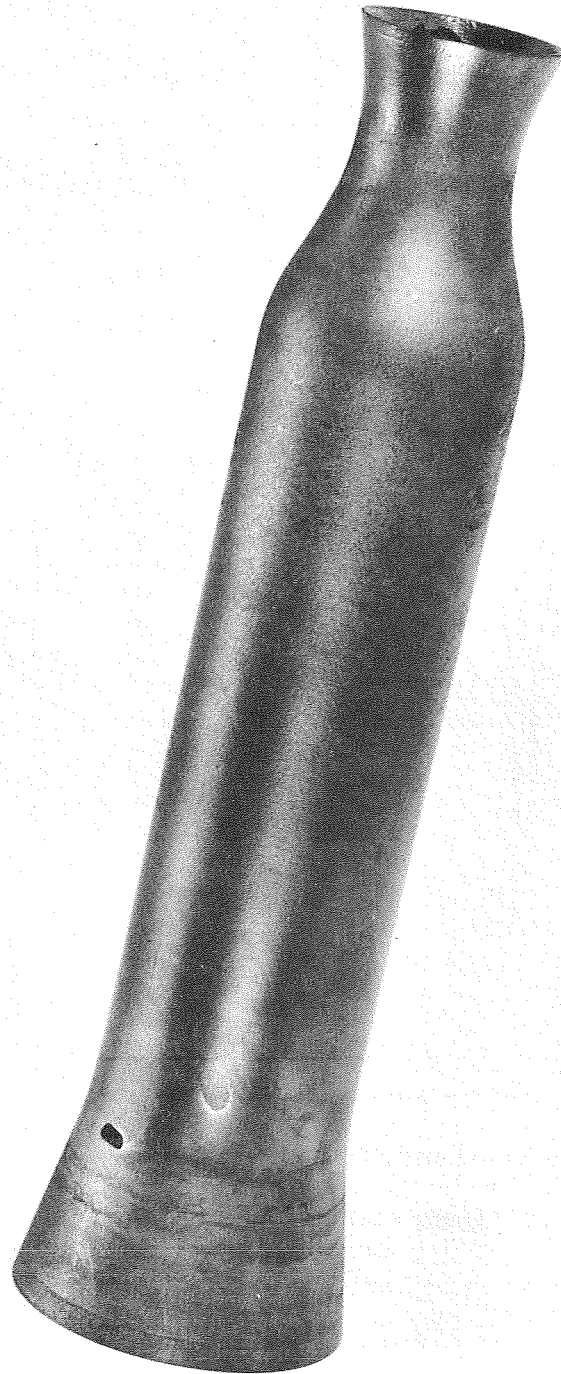


FIGURE 15. Side View of Thin Wall PG Chamber after Test Run 45

9189-20

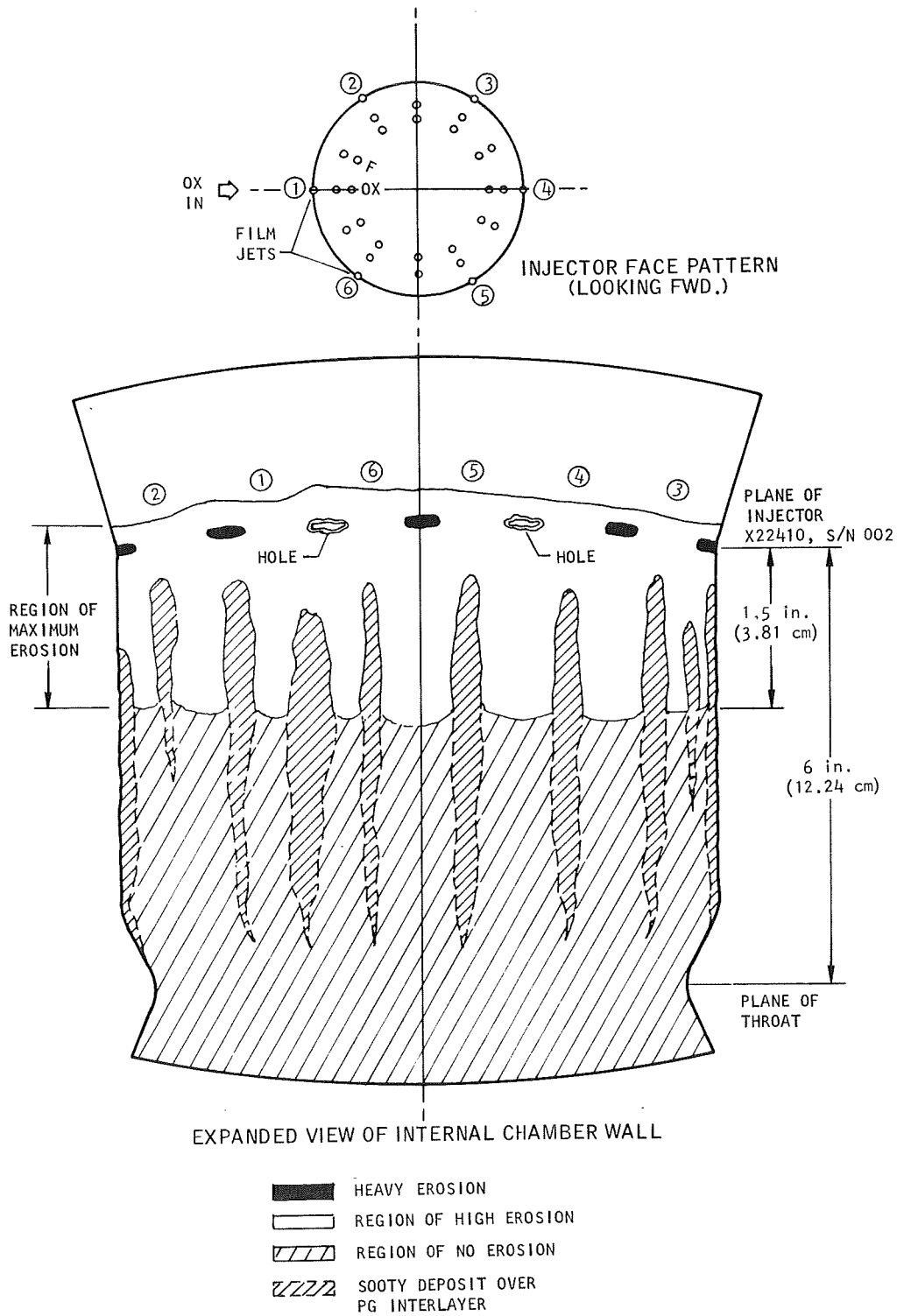
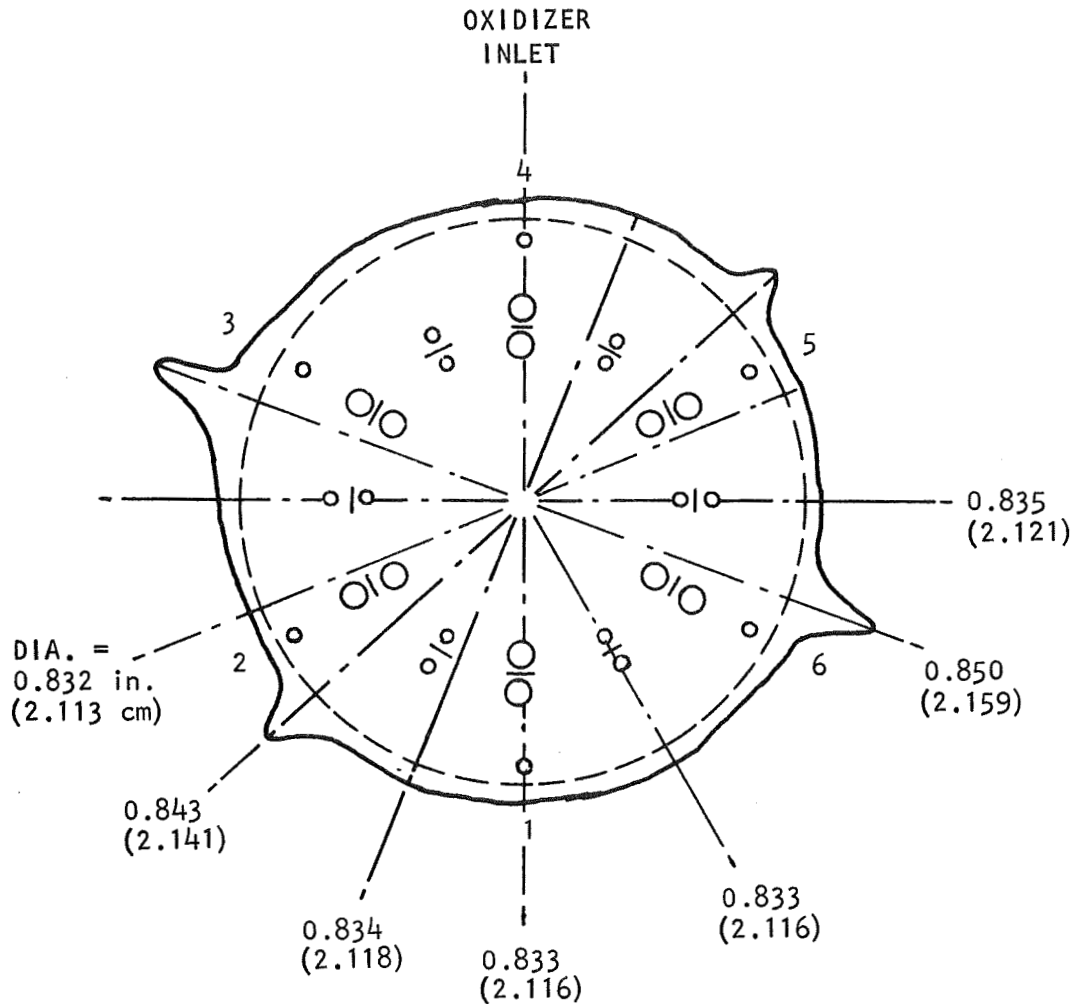
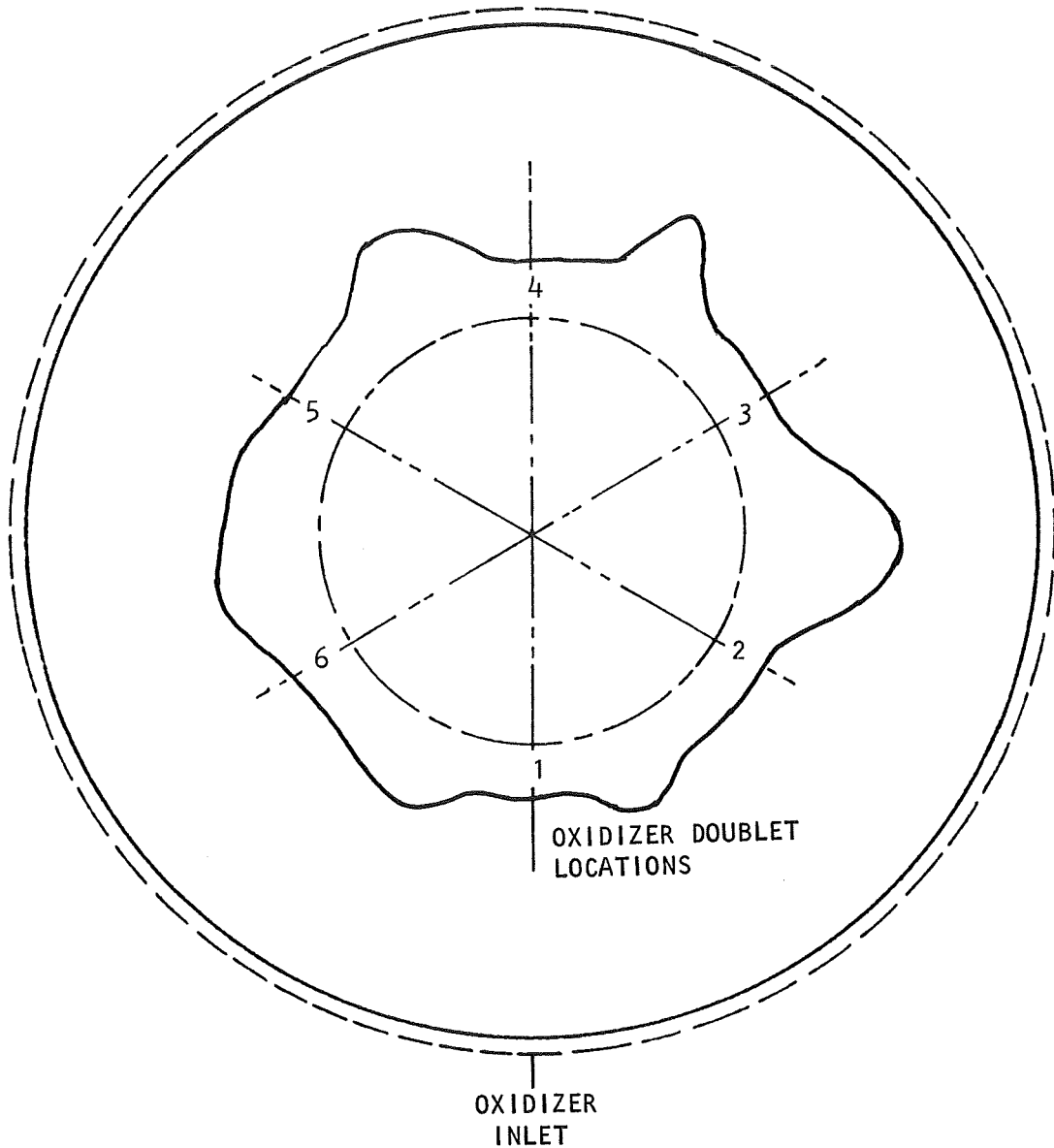


FIGURE 16. Erosion Pattern of the Serial No. 006 PG Chamber after Test Run 45



CHAMBER CROSS SECTION AT THROAT
 EXIT VIEW TOWARD INJECTOR
 EROSION SCALE 25 : 1
 INJECTOR SCALE 3 : 1
 X24401 INJECTOR S/N 002
 DURATION = 19.6 sec
 — — — ORIGINAL DIAMETER = 0.830 in.

FIGURE 17. Radially Magnified View and Location of Erosion of the POCO Chamber Throat after Run 46



CHAMBER CROSS SECTION AT INJECTOR FACE

VIEW AT INLET TOWARD EXIT

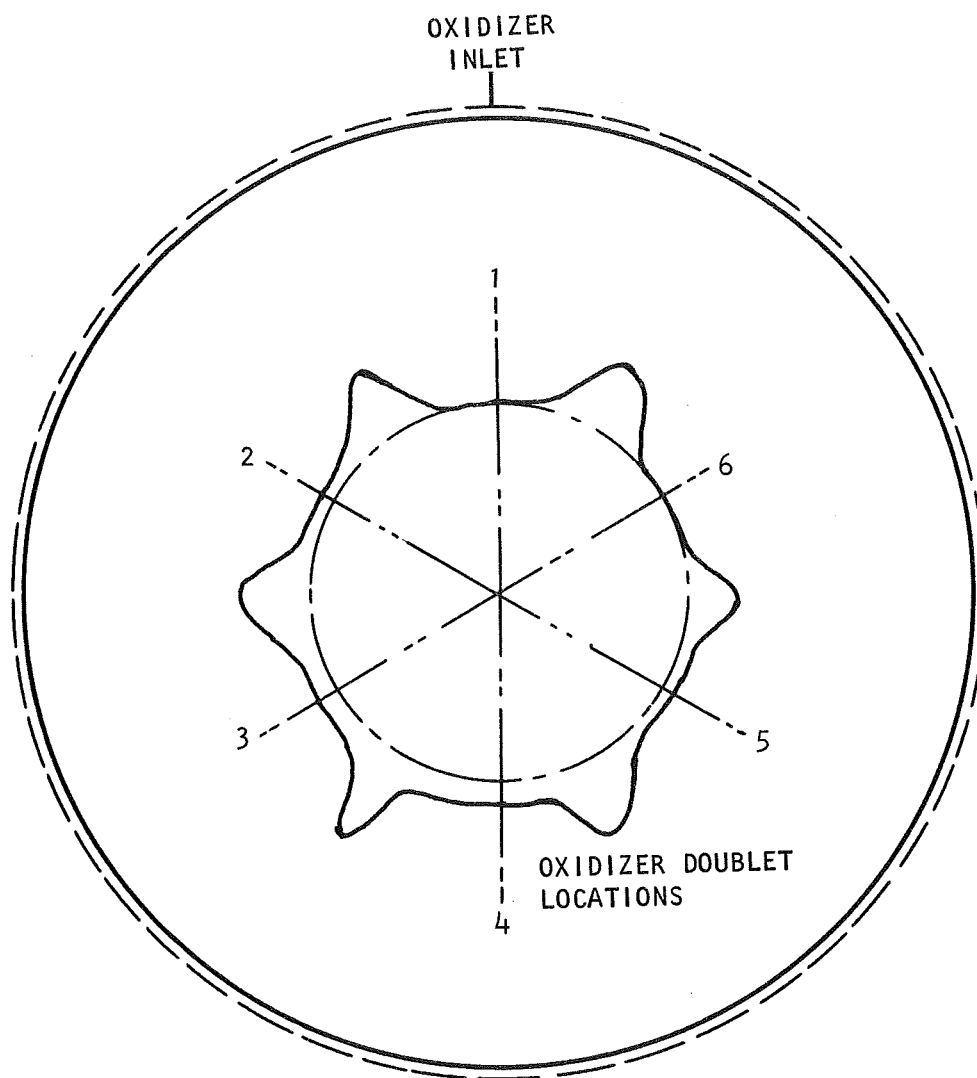
EROSION SCALE 25 : 1

X24401 INJECTOR S/N 001

— — — ORIGINAL OD = 1.528 in. (3.881 cm)

— · — · — ORIGINAL ID = 1.396 in. (3.546 cm)

FIGURE 18. Radially Magnified View and Location of Erosion of the Serial No. 002 PG Chamber Throat after Run 25



CHAMBER CROSS SECTION AT INJECTOR FACE

VIEW AT INLET TOWARD EXIT

EROSION SCALE 25 : 1

X24401 INJECTOR S/N 002

— — — ORIGINAL OD = 1.531 in. (3.889 cm)

— - - ORIGINAL ID = 1.407 in. (3.574 cm)

FIGURE 19. Radially Magnified View and Location of Erosion of the Serial No. 004 PG Chamber Throat after Run 47

Photographs of deposits in line with the film orifices are shown in Figures 20 and 21. The depositions and erosions indicated that redesign of the injector with new film orifices at the injector chamber interface would alleviate the erosion problem. These additional orifices were designed to impinge the film at the injector-chamber interface in line with and between the oxidizer orifices. This redesign was also made to increase the film mass flow from 10% to 25 and 35% of total fuel flow for the Serial Nos. 002 and 001 injectors, respectively. The chamber temperature distribution (determined from XR film for Run 47) is presented in Figure 22. Typical wall temperatures for the 20 second test runs were in the 2700° to 3000°F (1755° to 1922°K) range (Figure 23).

G. Injector Modifications

From the free standing PG streak chamber firing results of Phase I, it was obvious that maximum graphite erosion was occurring on the wall at the plane of the injector face and in line with the intersection of the impinging oxidizer fans (see Figure 16). The 0.005-inch (0.0127 cm) diameter fuel film jets were being bypassed because they impinged on the wall about one-half inch downstream from the injector face. Also, it was observed that maximum carbon deposition on the chamber wall occurred in line with the fuel film jets.

The final injector configuration (shown in Figures 24 and 25) contained 18 fuel film injection holes, each of 0.005-inch (0.0127 cm) diameter. This modification to the Serial No. 001 injector provided 35% fuel film flow. Six of the jets were the original jets which were directed 7° (0.122 rad) outward and located radially in line with the oxidizer doublets. The twelve additional holes were Eloxed into the fuel manifold from the outside wall of the injector and they were directed 26° (0.454 rad) outward to impinge on the chamber wall exactly in the plane of the injector face. These holes were located radially in line with each fuel and oxidizer doublet.

The fuel film injection streams are shown in the cold flow pattern of Figure 26. The film impingement pattern in a plastic chamber with only the cooling jets flowing with water is shown in Figure 27. The holes were accurate and clean and the impingement pattern was uniform. However, there were still unprotected areas at the plane of the injector face, as was borne out by subsequent firing tests. A typical erosion pattern is shown in Figure 28, showing small pits in the chamber wall near the plane of the injector face. The downstream erosion characteristics, however, were significantly improved as shown in Figure 29.

Accordingly, the final configuration also included the addition of a short deflection ring welded to the face of the injector just outside the circumference of the oxidizer doublets. This modification was very effective in reducing the local erosion of the wall near the injector face.

Intermediate injector modifications were made and test fired initially during the Phase II testing. The results are reported in Table V for Runs 1 through 15. The final configurations for the Serial Nos. 001 and 002 injectors were used for all test runs subsequent to Phase II Run 15. The intermediate

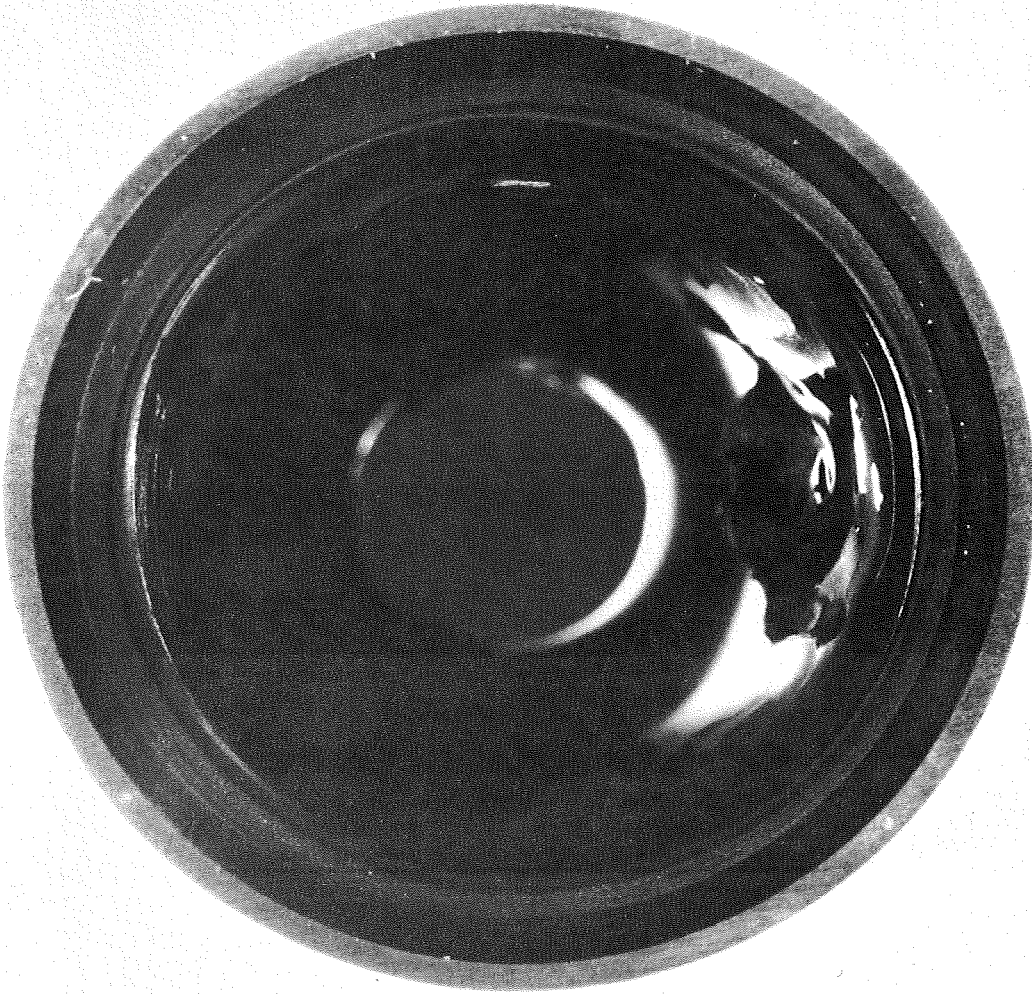


FIGURE 20. End View of Thin Wall PG Chamber Inlet after Run 45

9189-14

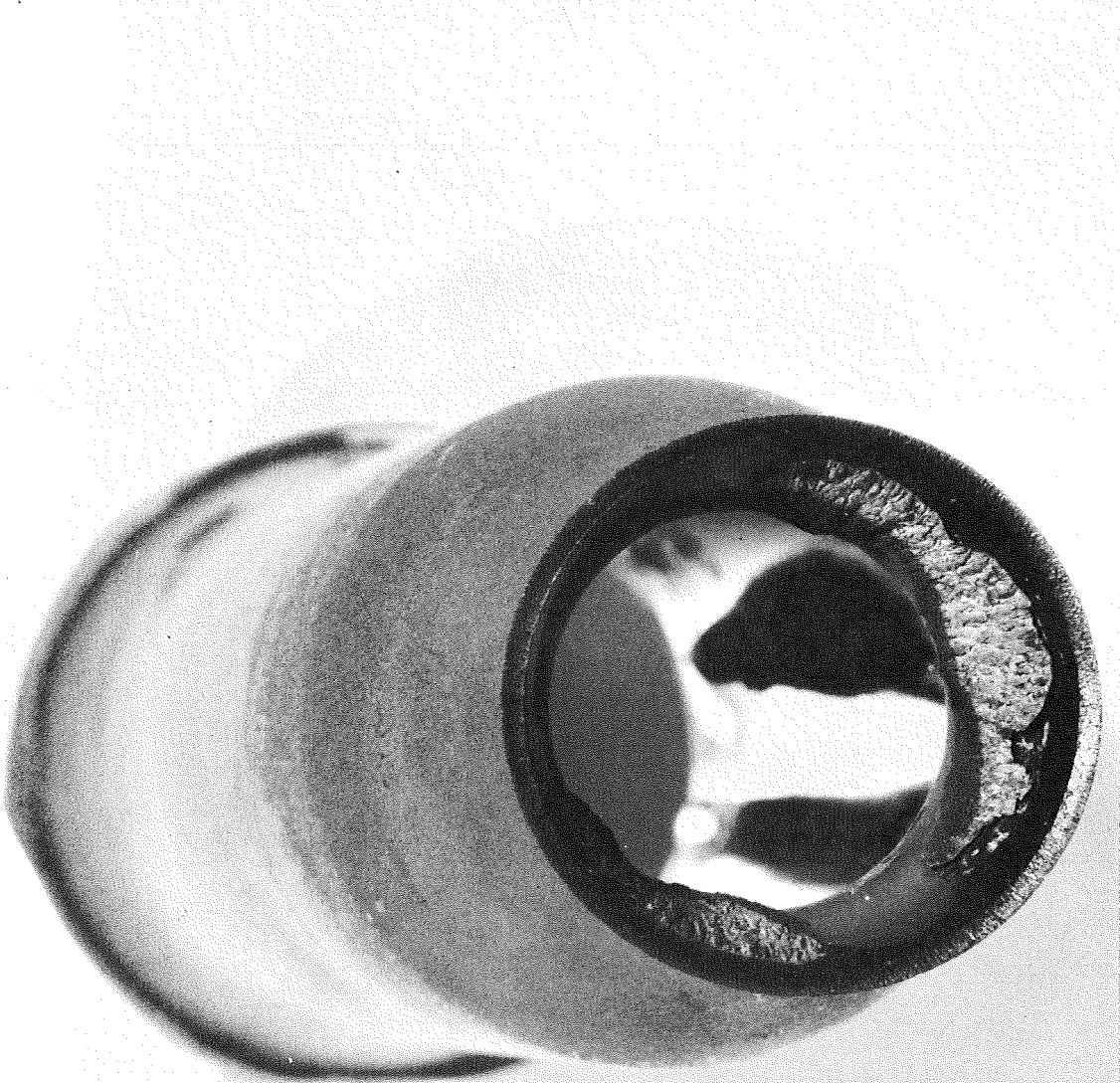
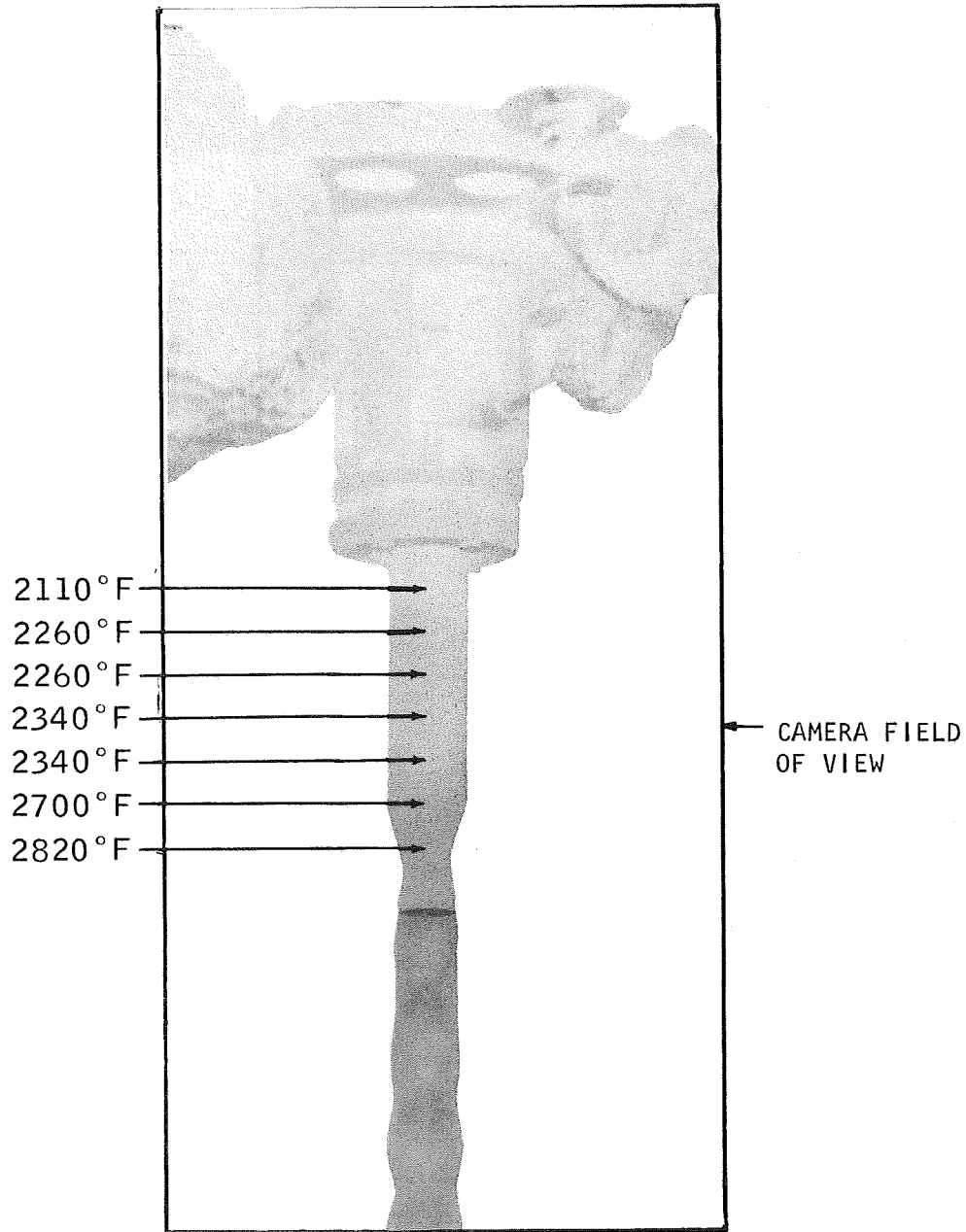


FIGURE 21. End View of Thin Wall PG Chamber Exit after Run 45

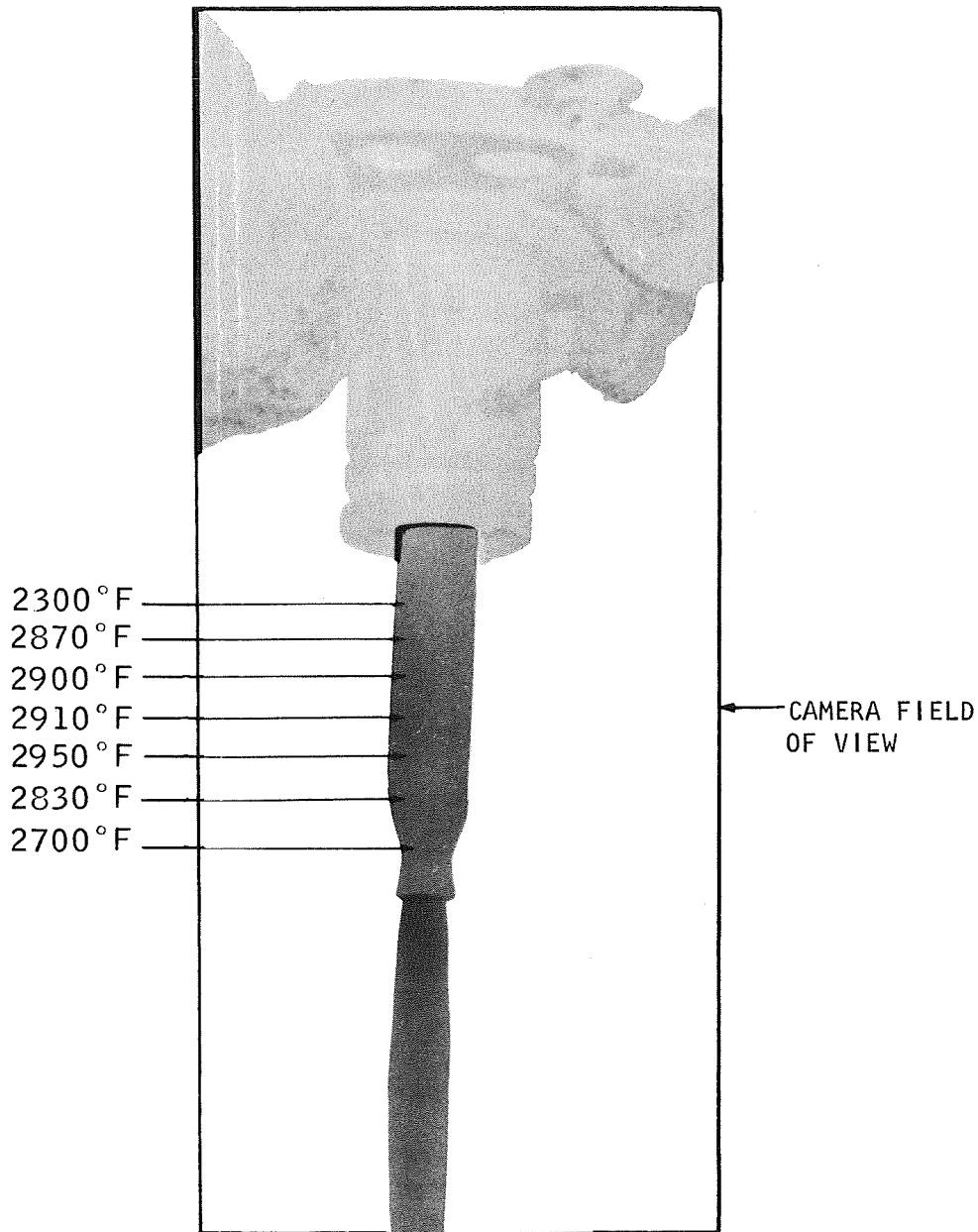
9189-17



CHAMBER S/N PG 004 O/F = 3.5
INJECTOR X24401 S/N 002 $P_c = 101.4$
RUN NO. 47 12 SEC. FROM FLOX VALVE ON
TEST NO. 6056 TEST DATE 9/9/68
MEASURED WITH XR FILM -- FLOX / METHANE

V6975-4

FIGURE 22. Distribution of PG Chamber Temperatures, Run 47



CHAMBER S/N PG 002 O/F = 5 - 13
INJECTOR X24401 S/N 001 $P_c = 77.4$
RUN NO. 25 6 SEC. AFTER FLOX VALVE ON
TEST NO. 6056 TEST DATE 8/22/68
MEASURED WITH XR FILM -- FLOX / METHANE

V6975-1

FIGURE 23. Distribution of PG Chamber Temperatures, Run 25

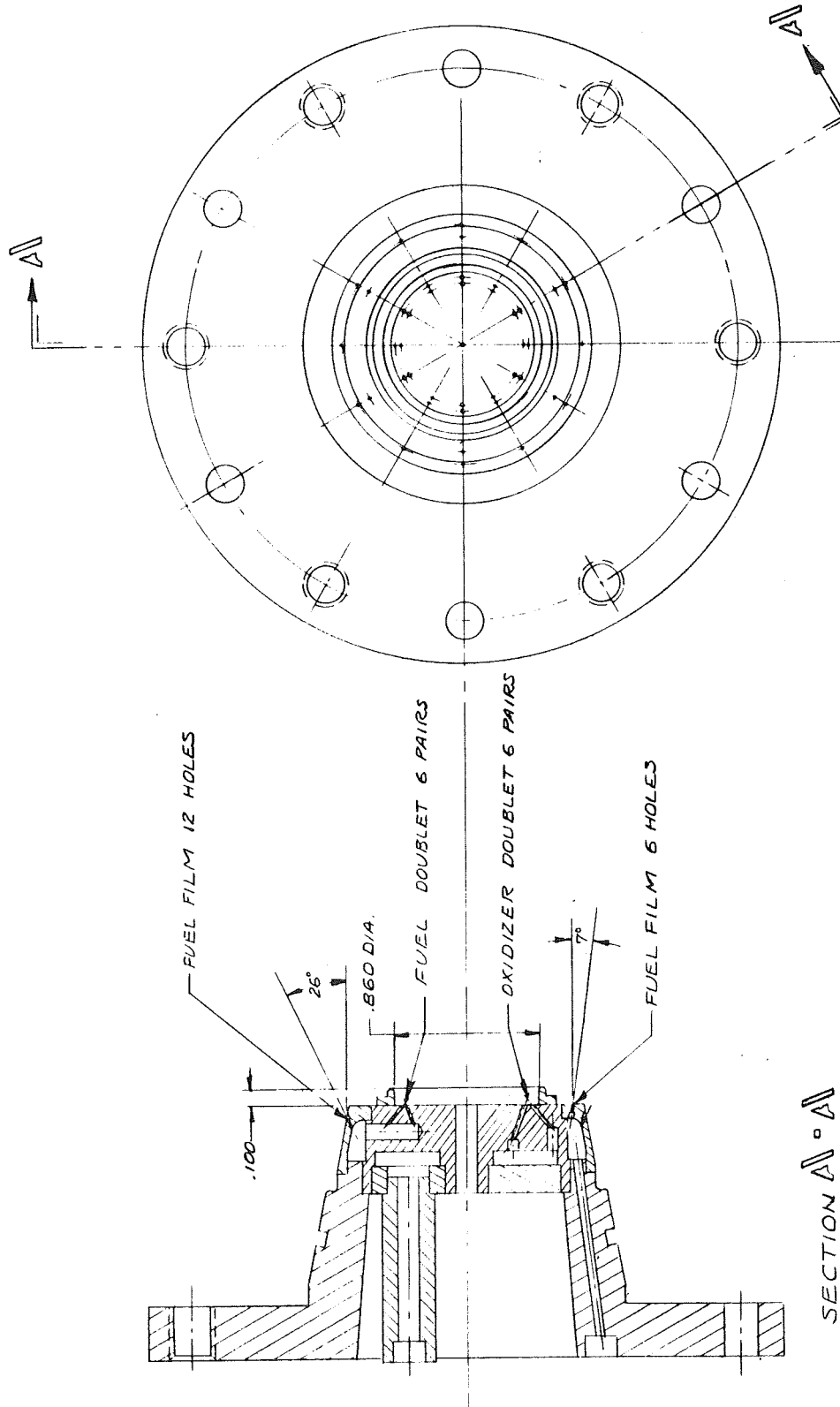


FIGURE 24. Final Configuration of the 100-pound Thrust FLOX/Methane Injector

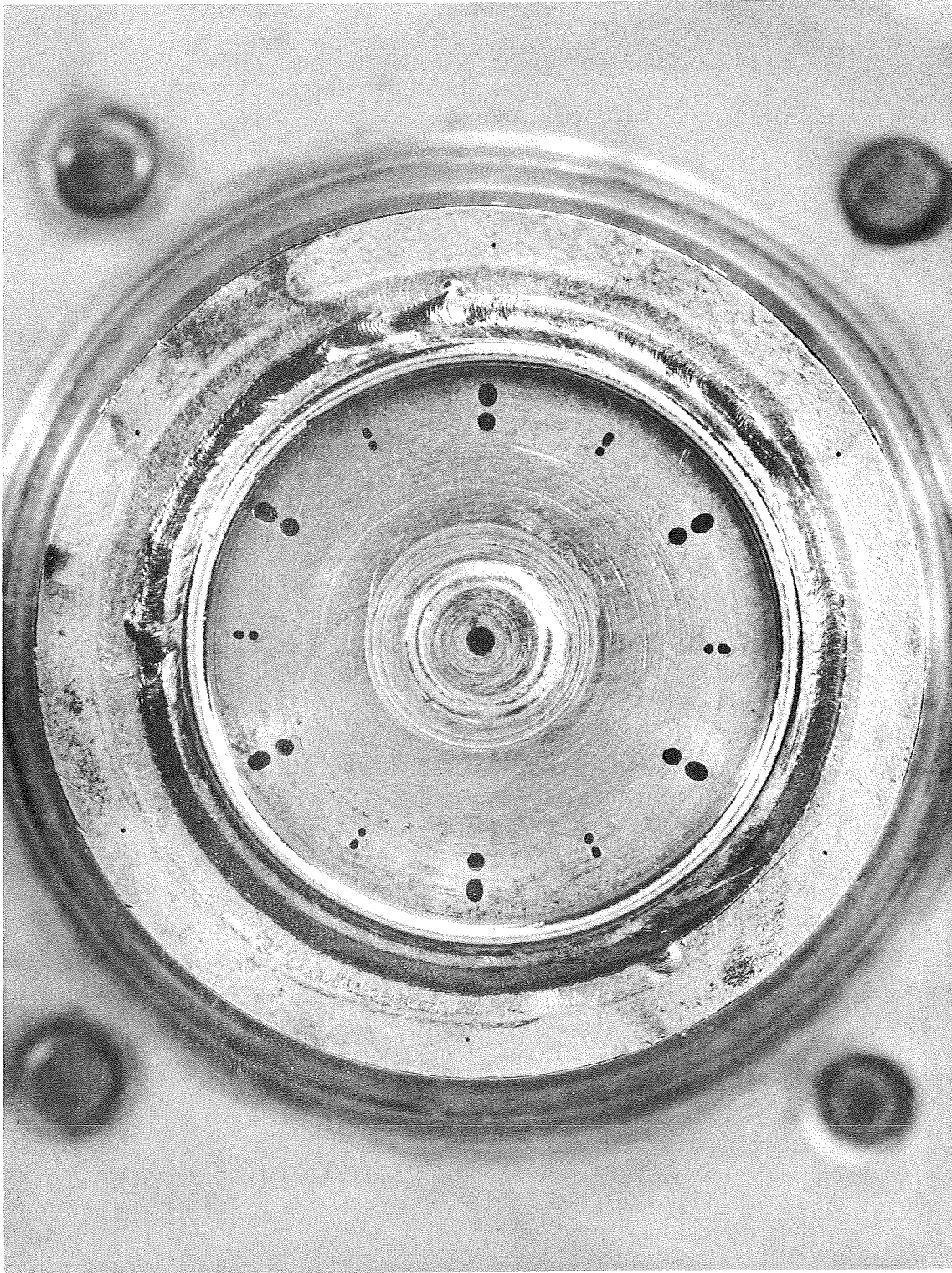
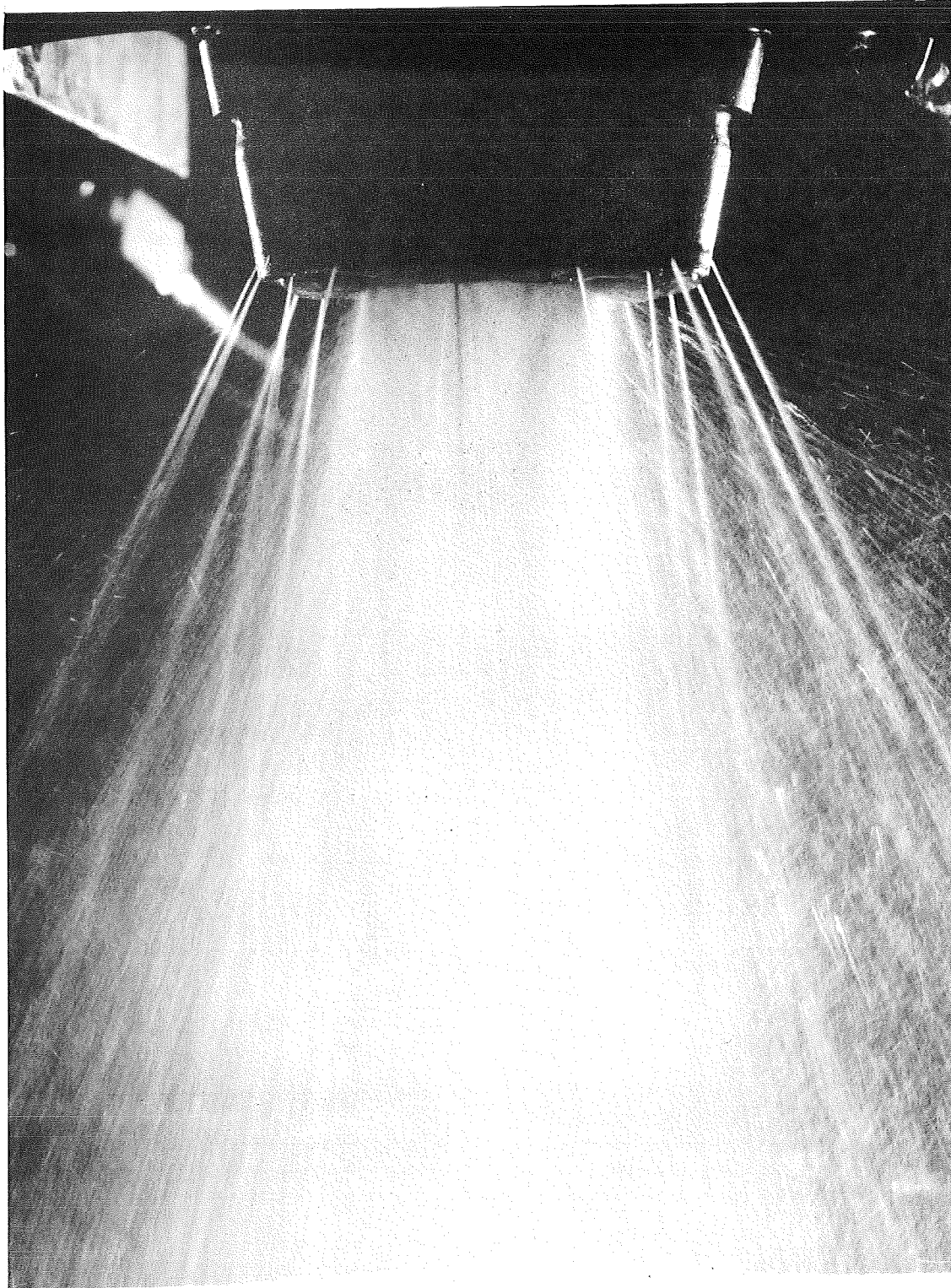


FIGURE 25. Final Configuration, Serial No. 002 Injector

9470-3



T11401-8

FIGURE 26. Spray Pattern from Cold Flow Tests of the 100-pound Thrust FIOX/Methane Injector with 18 Fuel Film Holes

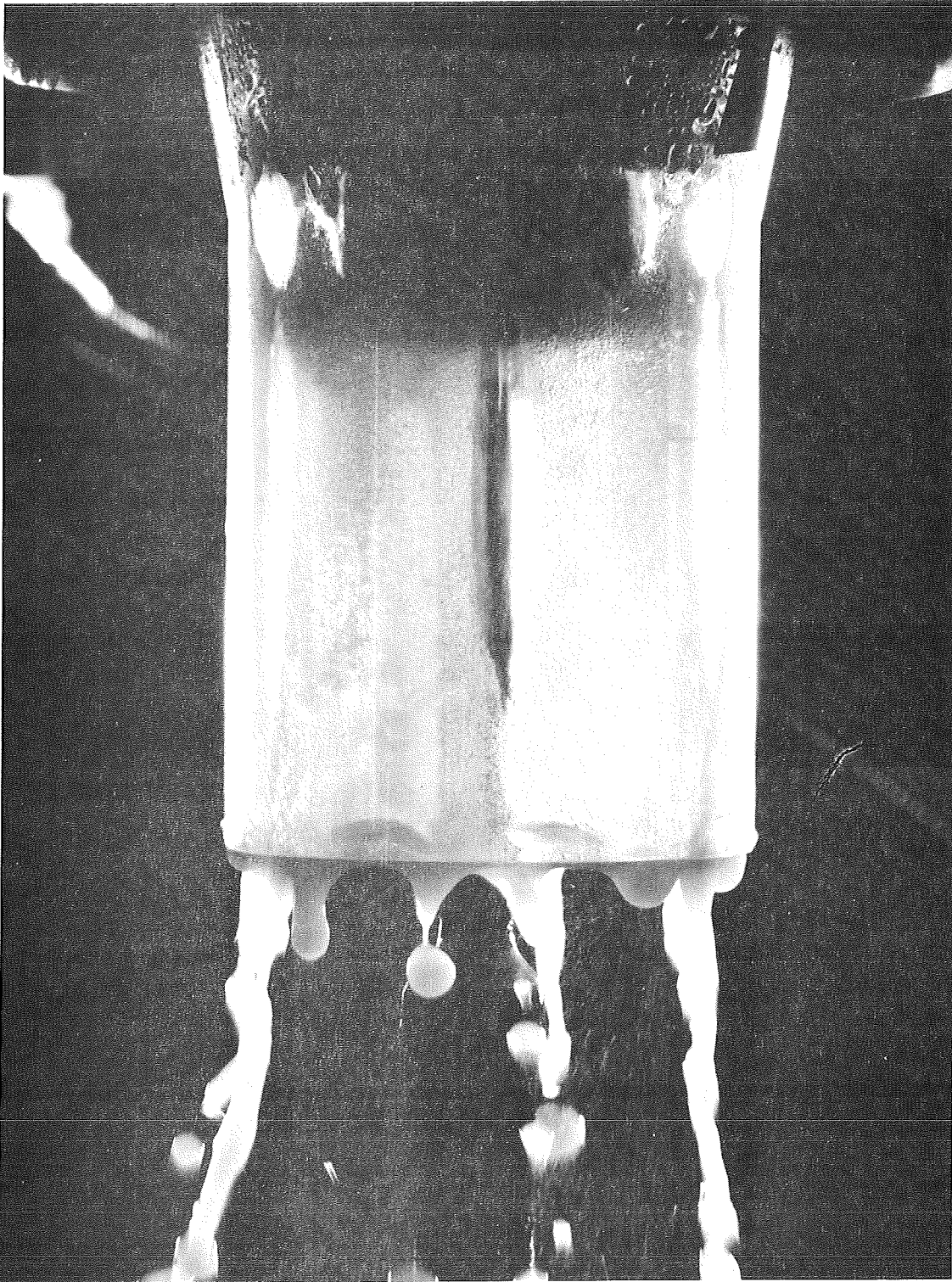
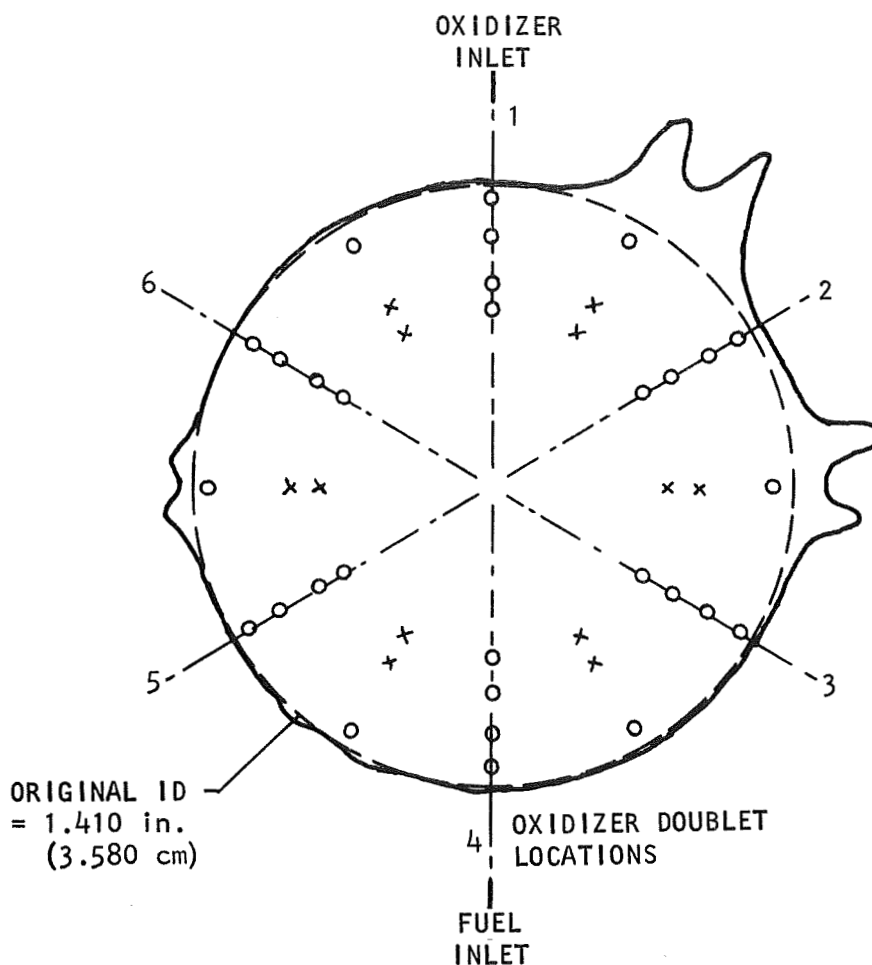


FIGURE 27. Distribution Pattern with Only the Fuel Film Jets Flowing

11401-5



VIEW LOOKING TOWARD INJECTOR FACE

X22401 INJECTOR S/N 001 (18 WEEPERS)

PG CHAMBER No. SL11

L^* = 14 in. (25.6 cm)

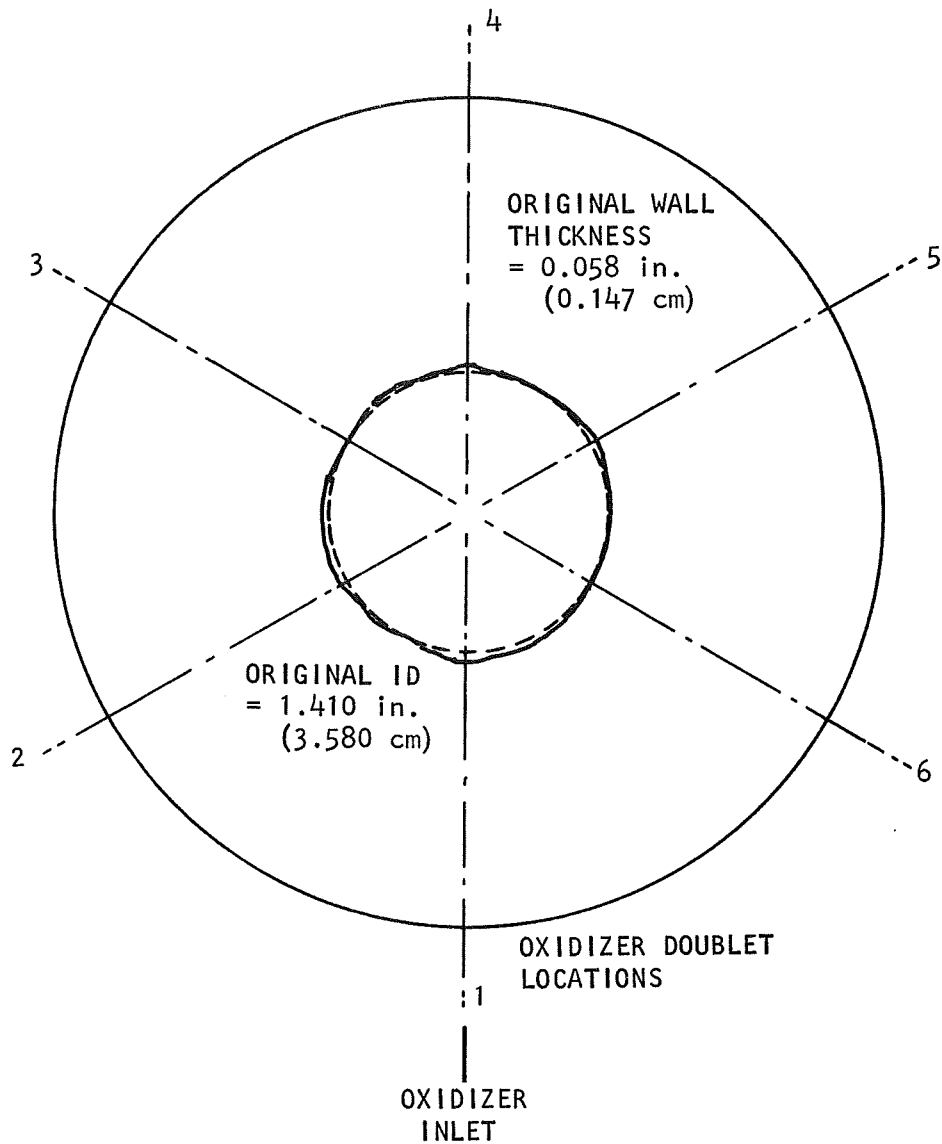
P_c = 97 to 141 psia (67 to 97.1 N/cm²)

η_c = 94 %

RUN DURATION = 20 sec

EROSION MAGNIFIED 25X

FIGURE 28. Erosion Pattern of Chamber No. SL-11 at Plane of Injector after Run 13



VIEW LOOKING TOWARD INJECTOR
X24401 INJECTOR S/N 001 MOD. (18 WEEPERS)
EROSION MAGNIFIED 25X

FIGURE 29. Wall Thickness of Chamber No. SL-11 at 0.75 inch from
Injector Face after Run 13

injector modifications included testing with the twelve new fuel film holes flowing and the original six film holes closed. Downstream PG chamber erosion increased (Run 14) as shown in Figure 30. Consequently, the downstream set of six film injection jets were included in the final injector configuration.

When the splash ring was originally welded on, the axial length was made 0.312 inch (0.792 cm). After Phase II Run 14, the length of the splash ring on each injector was cut back to 0.10 inch (0.254 cm) to eliminate overheating and burning of the ring. No overheating of the ring or injector was experienced on all subsequent test firings.

SECTION IV THRUST CHAMBER DEVELOPMENT

A. Thrust Chamber Design

The thrust chamber design evaluated during this program was based both on design criteria selected at the beginning of the program and on those criteria established as a result of the Phase I injector development tests. The criteria selected at the beginning of the program included:

1. Chamber materials and wall thickness
2. Chamber contraction ratio and internal configuration
3. Injector/chamber joint design

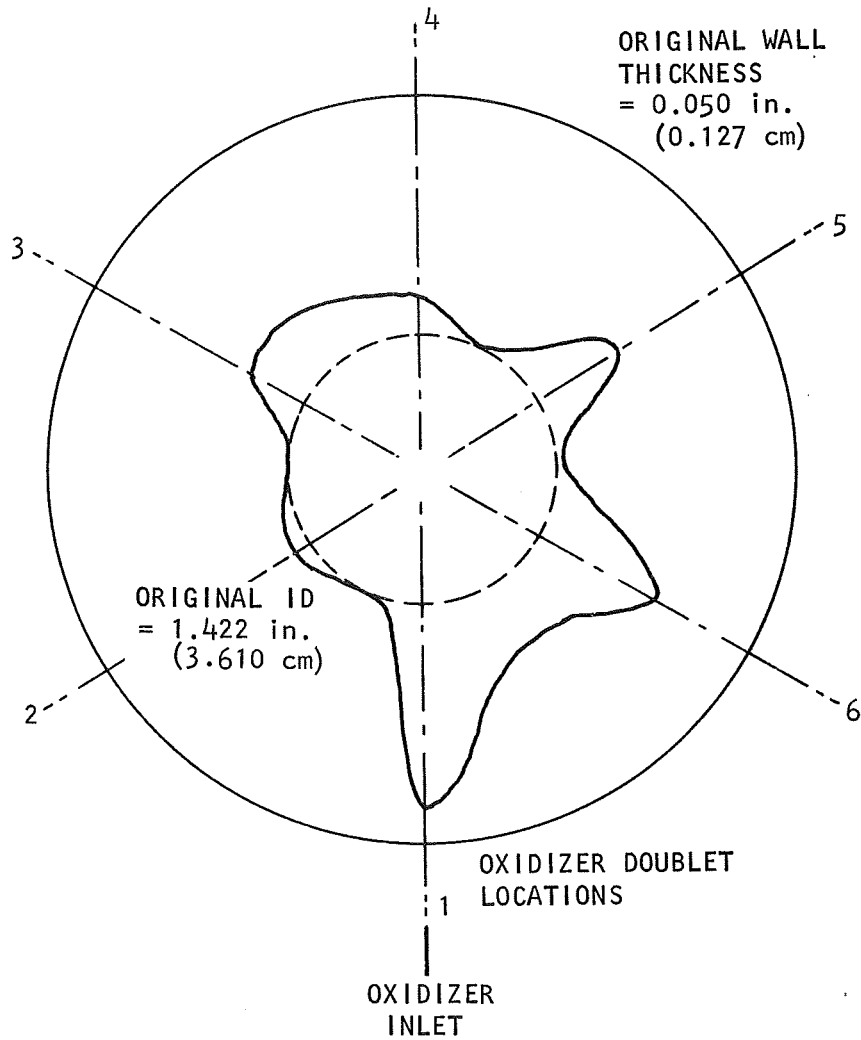
Chamber design criteria selected on the basis of injector development included:

1. Chamber length (L^*)
2. Film coolant flows and injection pattern

As a result of the final Phase II test firing program, recommendations for further optimization of the design criteria were defined. The various chamber design criteria are discussed below.

B. Thrust Chamber Materials

Two basic rocket thrust chamber material concepts which were available included the use of ductile metallic chamber materials, which must be cooled to safe operating temperatures, or refractory materials capable of operation at near the propellant flame temperatures but which must be chemically protected. The objective of this program was to evaluate the refractory material approach, specifically graphitic materials. Two recent developments in graphitic materials which hold promise of superior performance in thrust chambers are the high strength carbon fiber composites and pyrolytic graphite.



VIEW LOOKING TOWARD INJECTOR
X24401 INJECTOR S/N 001 MOD. (12 WEEPERS, HI ANGLE)
EROSION MAGNIFIED 25X

FIGURE 30. Wall Thickness of Chamber No. SL-1 at 0.75 inch from
Injector Face after Run 14

Under NASA Contract NAS 7-555 (Reference 3) and preceding programs (References 4, 5, and 6), the production, fabrication, characterization, and test evaluation of pyrolytic refractory materials were investigated. A material system which combines the strength and fabrication flexibility of the carbon fiber composites with the surface quality and erosion resistance of pyrolytic graphite was achieved by depositing pyrolytic graphite (PG) on the surface of a thrust chamber shell of a filament wound carbon fiber composite (Carbitex 713) developed by The Carborundum Company, Graphite Products Division. The strength and related physical properties of the material system obtained under Contract NAS 7-555 are summarized in Appendix B.

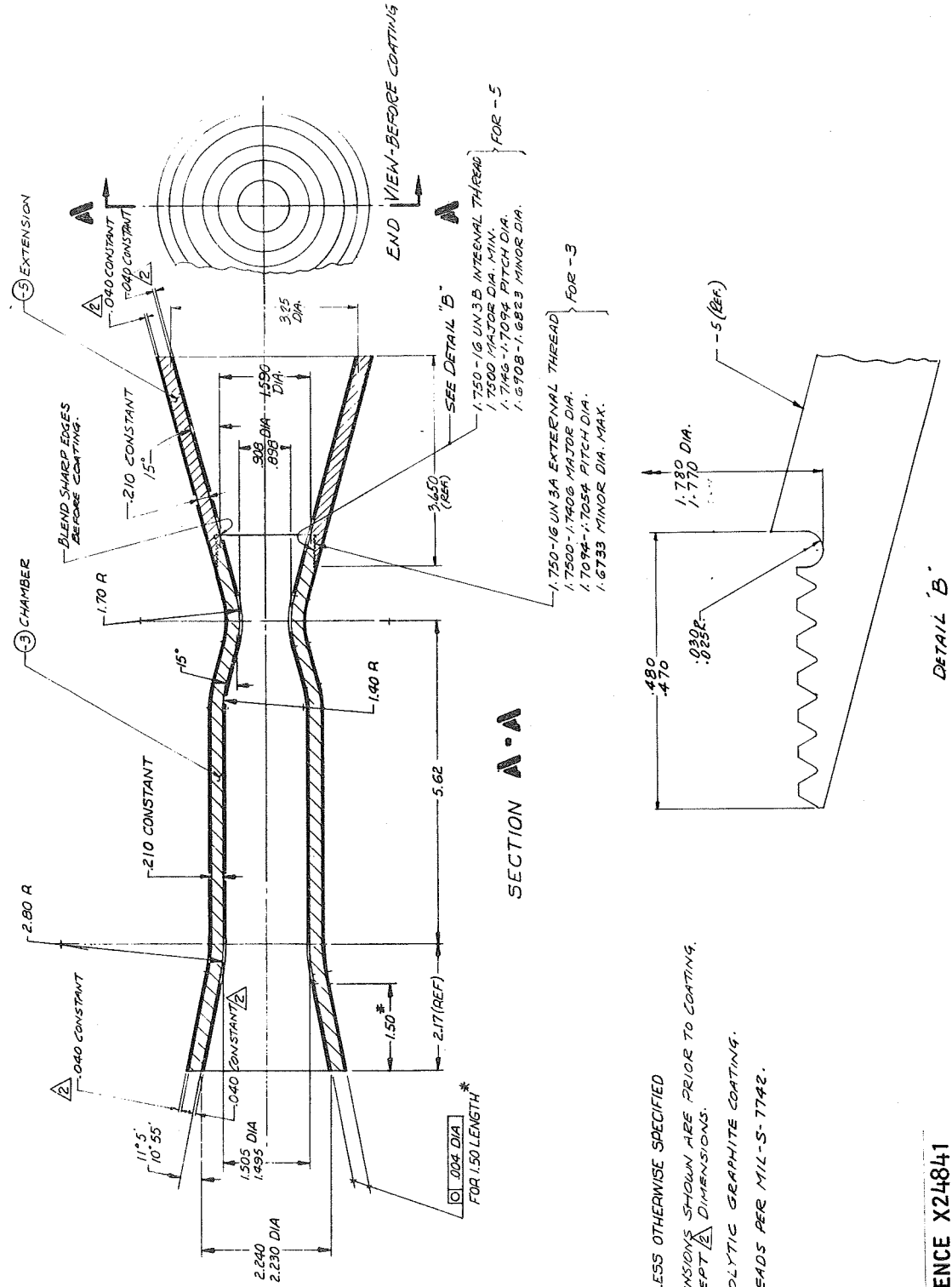
The selection of a Carbitex wall thickness and PG coating thickness in the chamber design shown in Figure 31 was based on the fabrication experience with this system. As the Carbitex wall thickness is increased much beyond one-quarter inch in small chamber sizes, the internal delaminations tend to increase. The Carbitex wall thickness and PG coating thickness were selected as the nominal maximum for a sound fiber composite structure. The operating hoop stresses in the Carbitex due to chamber pressure (at 100 psia (68.9 N/cm^2)) were less than 400 psi (275.8 N/cm^2). Thermal stresses in the Carbitex due to firing were calculated to be less than 800 psia (551.6 N/cm^2). Circumferential thermal stresses in the inner PG layer coating during firing would be compressive and were estimated to be between 4,000 and 8,000 psi (2758 and 5516 N/cm^2). These estimates were based on analyses made for similar designs used in other programs (Reference 7). Since these stresses were not critical, further analyses of this design layout were not made.

C. Chamber Contraction Ratios and Internal Configuration

The selection of contraction ratio was based on several considerations but the ratio was not necessarily optimized. The choice of a minimum contraction ratio was favored by the requirement to distribute the small amount of fuel coolant film uniformly over the chamber circumference through a limited number of small diameter injection holes. The minimum nominal injection hole diameter was 0.005 inch. A minimum contraction ratio also decreases the exposed injector face area subject to heat transfer from the hot gases and from the chamber walls after shutdown. A contraction ratio of 3.0 was selected on the basis of successful chamber designs at Marquardt (Reference 8) and Pratt and Whitney (Reference 9).

For a fixed value of chamber volume (L^*) and wall temperature, the total heat flux from the combustion gases in the chamber to the walls is almost inversely proportional to the contraction ratio, so that, for highly cooled walls typical of a film-conduction cooled (inter-regenerative) chamber, a larger contraction ratio and a shorter chamber length is advantageous. However, when the film is used only for chemical protection, a carbon rich boundary zone can be maintained over longer axial distances through the nozzle throat region by fuel injected into the boundary layer from the injector face. This has been borne out by the carbon deposition experience in this program.

The internal nozzle configuration (curvature) was based on criteria for minimum residual stress in the pyrolytic graphite coating. A throat radius



NOTES: UNLESS OTHERWISE SPECIFIED
 1- DIMENSIONS SHOWN ARE PRIOR TO COATING.
 EXCEPT \triangle DIMENSIONS.
 \triangle PYROLYTIC GRAPHITE COATING.
 3- THREADS PER MIL-S-7742.

REFERENCE X24841

FIGURE 31. Layout of 100-pound Thrust PG/Carbitex Altitude Chamber with Nozzle Extension

of curvature of twice the throat diameter was found satisfactory in an Air Force supported study of this parameter (Reference 8).

D. Injector/Chamber Joint Design

A tapered and lapped seat joint design (Figure 32) was selected for this chamber design because it was found to be completely satisfactory in two previous programs (References 8 and 3) for use with pyrolytic graphite chambers. In cases where the injector can be designed to match the chamber, the problems of leakage, heat soakback, and film injection optimization are readily resolved. Several alternate seal designs could have been used in this program, but the tapered seat was selected for convenience in accommodating the PG/Carbitex design along with free standing PG and multilamina pyrocarbide chamber configurations to be evaluated under Contract NAS 7-555. The possibility of chamber axial misalignment using the tapered seat should be evaluated in greater detail, but no indications of chamber cocking on the seat were encountered during this program.

E. Chamber Length

For the copper heat sink chamber, an L^* range of 12 to 18 inches (30.48 to 45.72 cm) was selected to cover a chamber length predicted to yield at least 92% C^* efficiency. As indicated by the test firing results, these two chamber lengths did bracket the performance goal of the program. An L^* of 15 inches (38.1 cm) was selected as the minimum value capable of meeting the performance goal with the increased fuel film protection incorporated in the final injector configuration.

F. Streak Chamber Design

The primary purpose of the streak chambers was to reveal streaking visually after a short firing run with the FLOX/Methane propellants. The streaking due to the injector characteristics could cause either local overheating of the chamber walls or excess erosion due to oxidizer rich zones. Inasmuch as graphite is subject to erosion by oxidation and the oxidation rate is a function of surface temperature, the streak chambers should be of graphite and should heat up rapidly. Further, the chambers should be relatively inexpensive.

Candidate streak chamber materials considered in this program included the following:

Free Standing PG - Fast temperature response, good temperature simulation, local temperature response visible from outside for XR film temperature documentation (see Appendix E).

Stainless Steel - Fast temperature response, streaking visible during firing for XR film documentation, streaking visible in temperature stains for posttest observation, easy to install thermocouples for transient temperature documentation, operating temperature limited to less than 2500°F (1644°K).

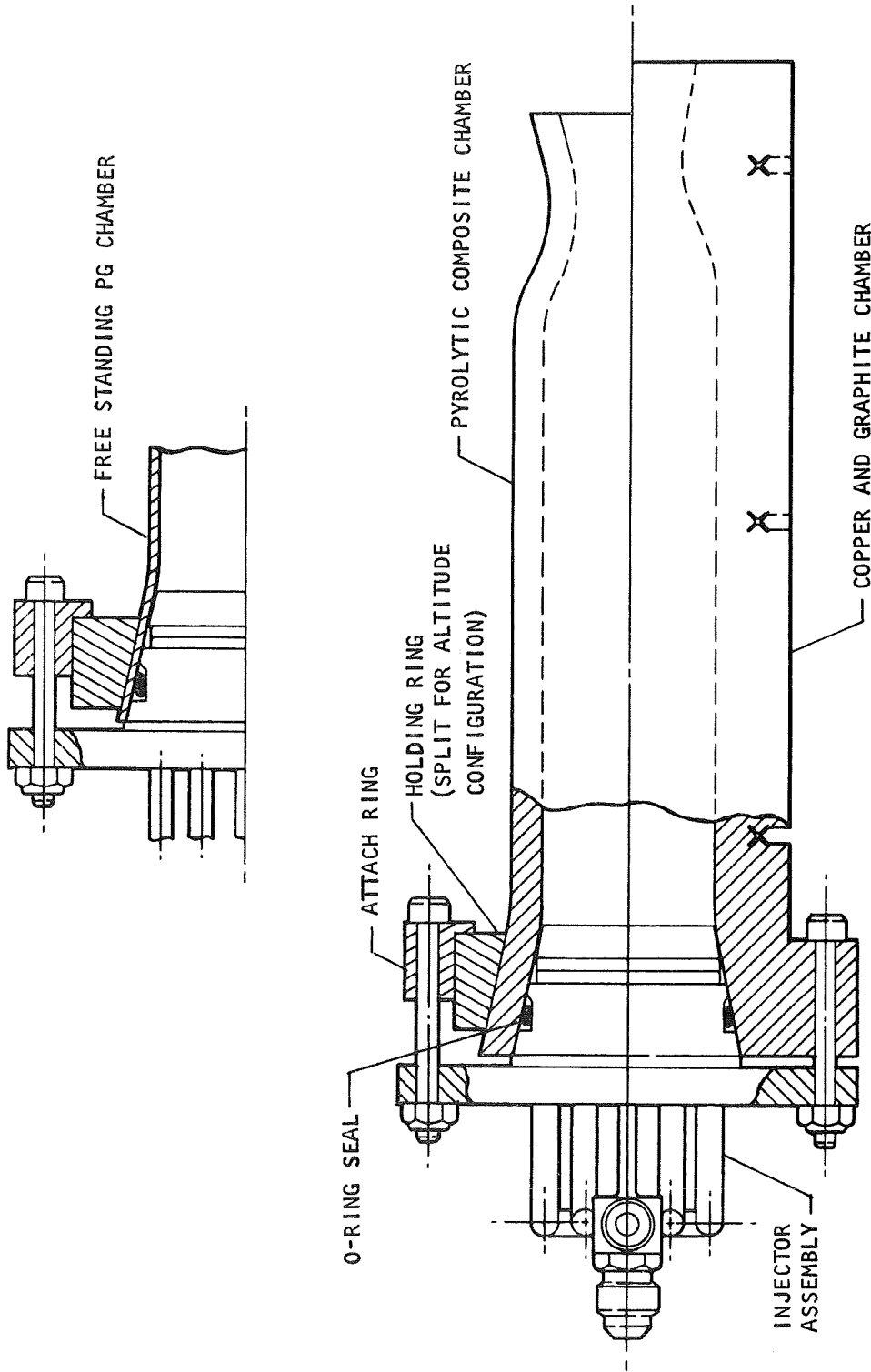


FIGURE 32. Tapered Seat Design for Free Standing PG and Composite Chambers

Pyrolytic Graphite Sleeves in Heat Sink Chamber - PG sleeves can be installed in graphite or copper chambers, good temperature response simulation, erosion and deposition characteristics well simulated, readily replaced low cost sleeves, film impingement pattern visible after run, difficult to measure transient temperatures, not suitable for pulsing or restarts if propellant can seep between liner and chamber.

Carbon/Phenolic Ablative - In the form of an insert in a structural shell, erodes more readily than PG, good temperature response, thermocouples can be installed in limited fashion, geometry changes can be readily incorporated in partially finished inserts, excessive erosion may mask carbon deposition effects.

Asbestos/Phenolic Ablative - High erosion rates may define streaking characteristics but not be related to relative oxidation and temperature response of a PG lined chamber.

Machined Graphite Chamber - Low cost, easy to install thermocouples, easy to alter configurations in partially machined chambers, heat sink effect slows temperature response, high strength graphite (POCO-AXF-5Q) may be used in free standing concepts at high temperatures.

Grooved Thick Wall Copper - Low cost, readily machined, easy to install thermocouples, can be used to measure local heat flux distribution, does not reveal chemical composition streaking, film impingement pattern revealed in chamber stains, limited to low wall temperatures.

For this program, the free standing PG chambers (Figure 33) and the POCO-AXF-5Q chambers (Figure 34) were selected because the high temperature streak effects were of specific interest. The POCO heat sink chambers allowed longer run times for evaluation of injector durability and the effect of deposit buildup. However, the high thermal conductivity of the POCO/graphite and its inherent erosion resistance made it less sensitive to streaking than the PG material.

In the Phase I tests, the longer L^* value (18 inches (45.72 cm)) was selected for the PG chambers to provide maximum chamber length for streak development. In the Phase II tests, the final L^* of 15 inches (38.10 cm) was selected to better simulate the throat heating and streaking condition. POCO chamber L^* values of 10 and 15 inches (25.40 and 38.10 cm) were used to provide additional L^* range for injector performance.

For future streak chamber testing, consideration may be given to the use of low conductivity castable carbon/phenolic replaceable inserts in a POCO-AXF-5Q structure shell in order to evaluate the high temperature streak effects and to achieve a faster surface temperature rise and higher erosion rates.



FIGURE 33. Pyrolytic Graphite Streak Chambers

9189-3

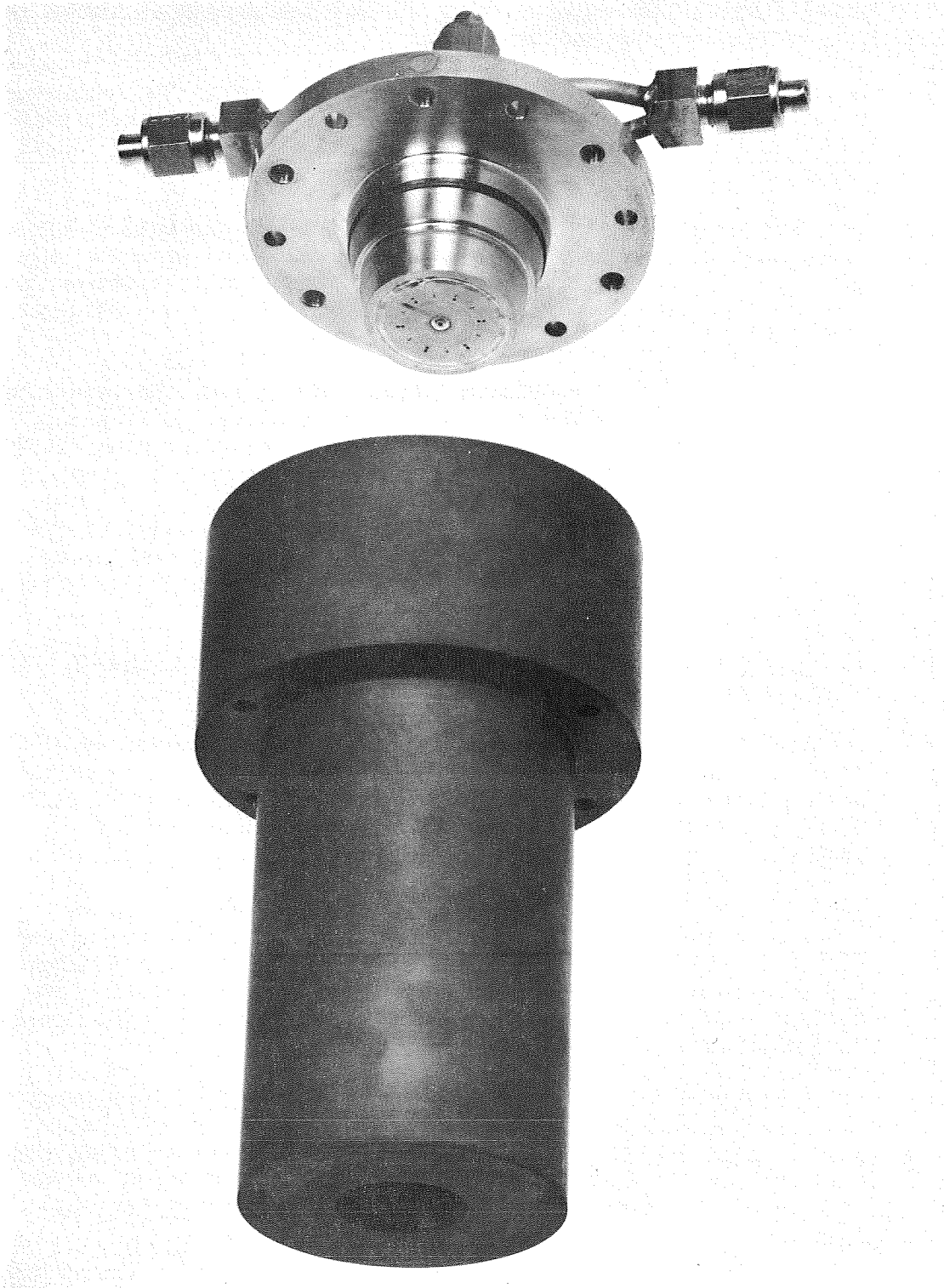


FIGURE 34. POCO-AFX-5Q Machined Graphite Heat Sink Thrust Chamber

9157-2

G. Composite Chamber Fabrication Techniques

The normal fabrication sequence for a PG/Carbitex composite thrust chamber as applicable to this program was as follows:

1. Detailed chamber fabrication drawings were sent to The Carborundum Company, Graphite Products Division at Niagara Falls, N.Y. with the Carbitex wall thickness shown and surplus inlet and exit length indicated for final trimming after PG deposition.
2. The Carborundum Company filament wound the chamber wall thickness with graphite yarn (dry) over a chamber contoured graphite male mandrel. Sufficient excess graphite filament wall thickness is provided for inside and outside final machining to the required dimensions.
3. After winding, The Carborundum Company impregnated the yarn with a proprietary resin system and subjected the part to a curing, pyrolyzing, and graphitizing furnace cycle requiring some thirty days.
4. Following the furnace processing, the chamber was machined internally and externally. The graphite mandrel was removed by machining and a final machined surface was produced by grinding (Figure 35).
5. The Carbitex thrust chamber shell was returned to Marquardt where it was inspected, X-rayed, and pressure checked.
6. A detailed fabrication drawing and the Carbitex chamber were then shipped to the selected PG coating vendor. This capability resides with several companies. Super Temp Company of Santa Fe Springs, California was selected as the PG vendor for this program.
7. The Carbitex chamber was set up and processed within the PG deposition furnace with proper manifolding to direct the methane source gas through the chamber to produce the required PG coating thickness on the surface of the Carbitex. The coating may be deposited all on the inside or both inside and outside simultaneously with a desired thickness ratio.
8. After coating, the chamber was returned to Marquardt for final trimming, inspection, lapping of the injector sealing surface, and pressure checking. The inside surface and throat dimensions were left in the as-deposited condition. In production, these dimensions can be held to satisfactory tolerances without machining.

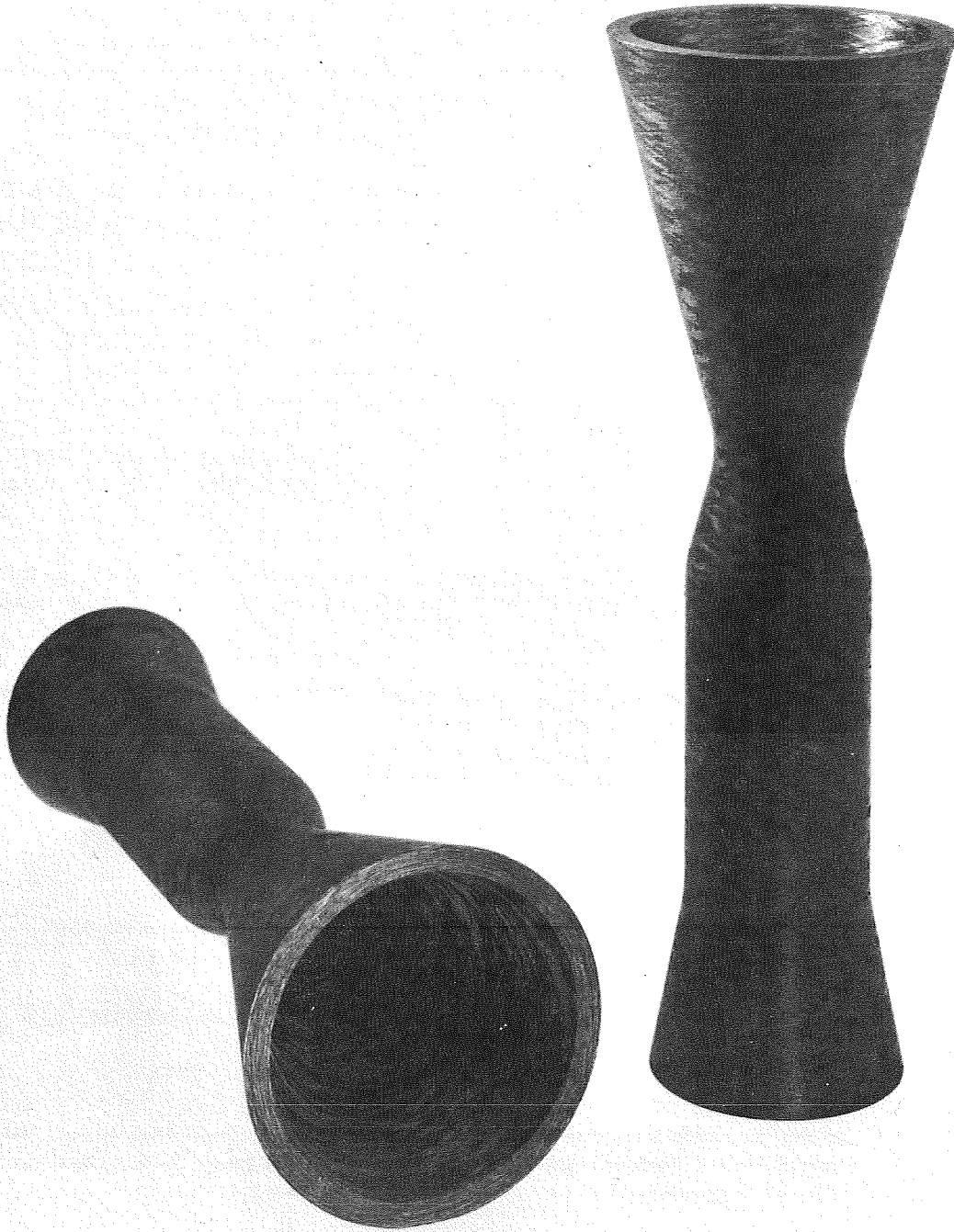


FIGURE 35. Completed Carbitex Thrust Chamber Shells

9529-2

H. Thrust Chamber Fabrication

1. Free Standing Streak Chambers

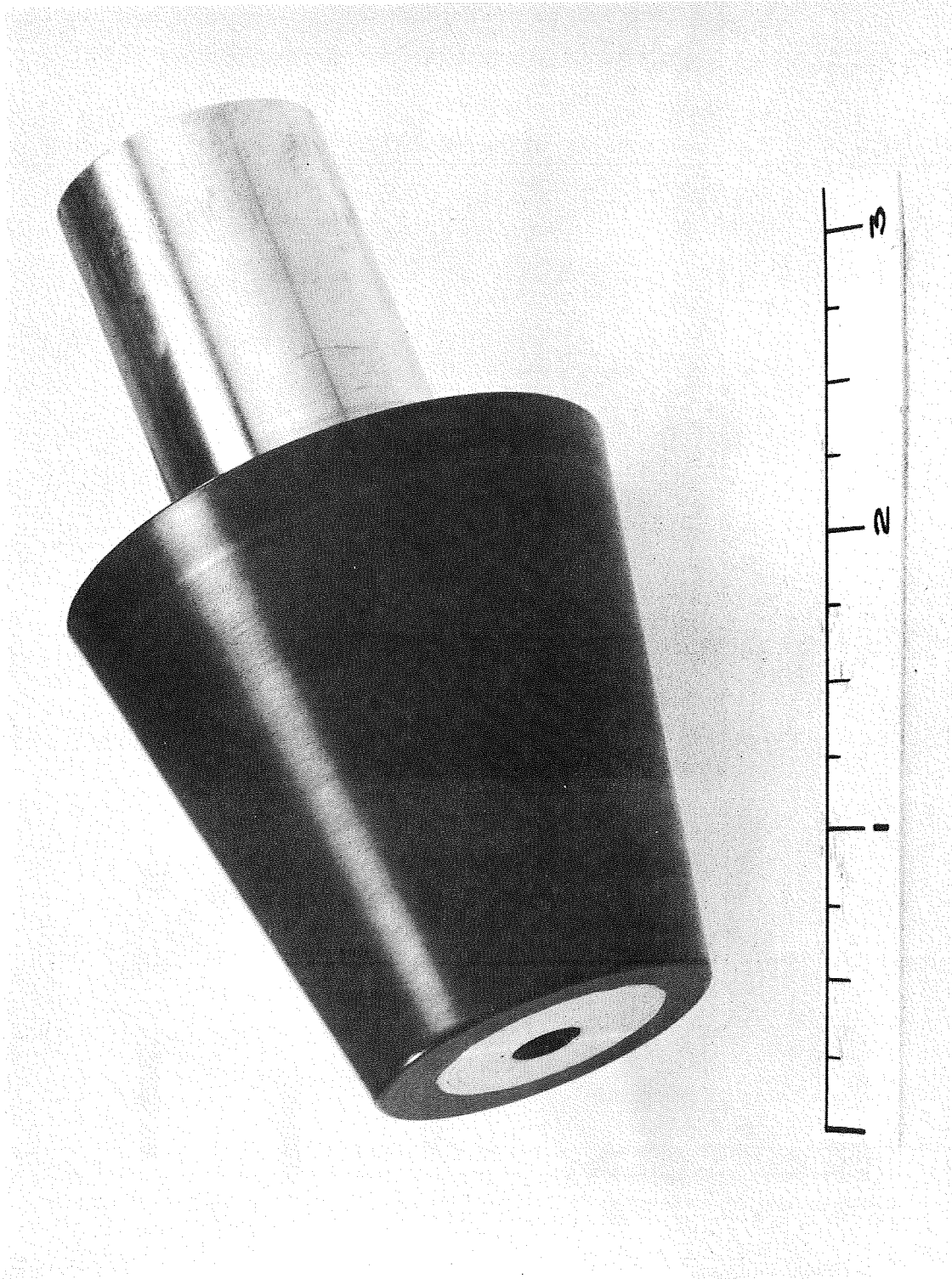
Free standing pyrolytic graphite streak chambers (Figure 33) were fabricated by the Super Temp Company of Santa Fe Springs, California. The nominal wall thickness of these vapor deposited PG chambers was 0.050 inch (0.127 cm). The actual wall thickness and chamber diameters measured prior to Phase I test firing are listed in Figure 14. The nominal L^* of these chambers was 18 inches (45.72 cm), the value selected to achieve maximum injector performance and exposure of the chamber to the highest temperature gases.

After the streak chambers were received at Marquardt, the sealing surface of the PG at the injector end of the chamber was lapped using the tool shown in Figure 36.

All of the streak chambers were Zygllo-inspected for cracks except the Serial No. 001 chamber, which had structurally failed in Test Run 11. No defects were detected in Serial No. 002 and Serial No. 005 chambers. Visually perceptible surface defects detected on the Serial Nos. 003 and 006 chambers were surface blemishes. Cracks detected on the Serial Nos. 004 and 007 chambers were not observed on the inner wall of these chambers, and it was concluded that the defects on the Serial Nos. 003, 004, 006, and 007 chambers were only surface defects.

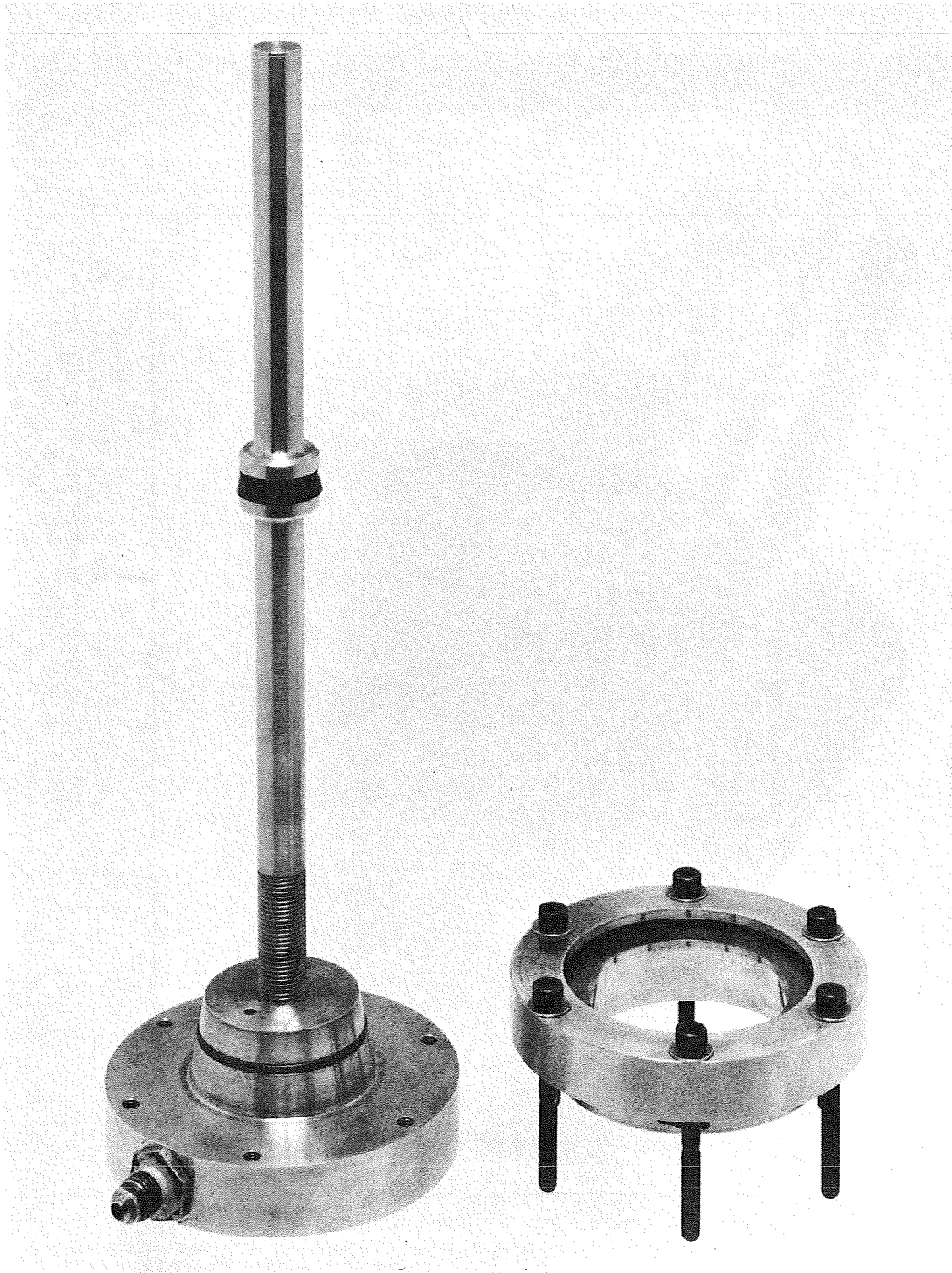
The test fixture used for pressure tests of the pyrolytic graphite chambers is shown in Figures 37 and 38. The following procedure was used for making the pressure tests:

1. The chamber was positioned on the stand and the bolts were tightened to a torque of 2 to 3 in.-lb (22.6 to 33.9 cm-N). The bolts were tightened in a 360° (6.283 rad) sequence to assure an even distribution of stress on the O-ring.
2. The water and nitrogen lines were attached to the AN fitting on the bottom of the fixture.
3. The long shaft was adjusted so the throat plug and the throat O-ring were on the exit side of the throat.
4. The chamber was filled with water, carefully purging all air from the chamber as a safety precaution.
5. The throat was then sealed by turning the plug into it and, when no leaks occurred, the chamber was pressurized to 90 psig (62.1 N/cm^2) at a rate of approximately 1 psi/sec ($0.69 \text{ N/cm}^2/\text{sec}$).
6. Nitrogen was used to pressurize the water in the chambers to the desired check value. Tests to 120 psig and 200 psig (82.7 and 137.9 N/cm^2) were obtained by using increments of approximately 1 psi/sec ($0.69 \text{ N/cm}^2/\text{sec}$).



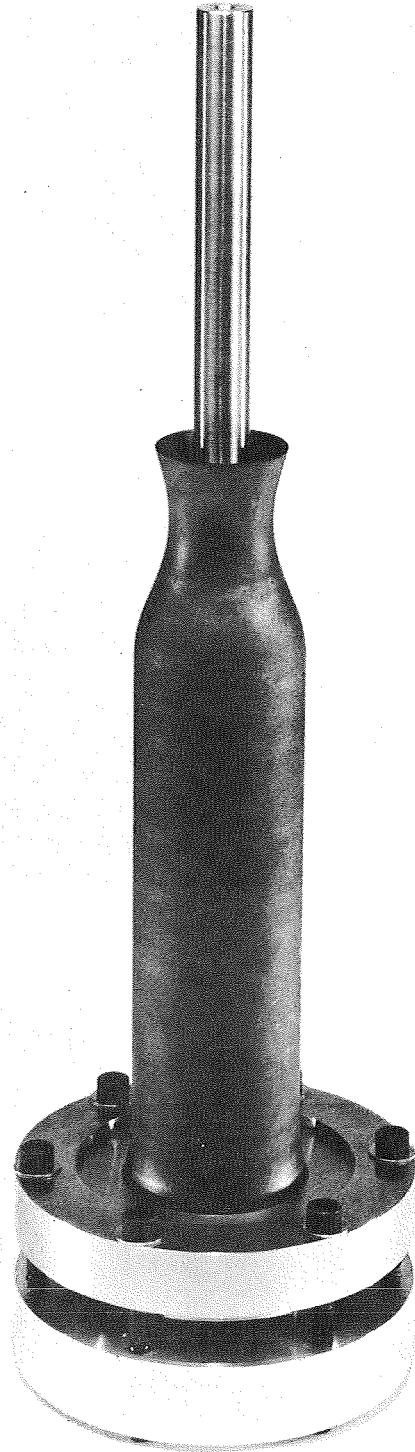
9189-7

FIGURE 36. Tool Used for Lapping the Injector End of a Pyrolytic Graphite Chamber



9189-5

FIGURE 37. Test Fixture Used for Pressure Tests of Pyrolytic Graphite Combustion Chambers



9209-1

FIGURE 38. Pressure Test Fixture Installed on Pyrolytic Graphite Combustion Chamber

The seven PG streak chambers were proof pressure tested to the following pressures:

Chamber Serial No.	Pressure	
	psig	N/cm ²
001	120	82.7
002	120, 200	82.7, 137.9
003	120, 200	82.7, 137.9
004	120, 200	82.7, 137.9
005	120, 200	82.7, 137.9
006	120, 200	82.7, 137.9
007	120, 200	82.7, 137.9

2. POCO Graphite Chamber

Two POCO graphite chambers (Figure 34) were machined from billets of POCO-AXF-5Q graphite in accordance with design drawing X24488 (Figure 39) as follows:

Serial No. 001 -- L = 4 inch (10.2 cm)

Serial No. 002 -- L = 2.8 inch (7.11 cm)

Each chamber was proof pressure checked to a pressure of 500 psia before testing.

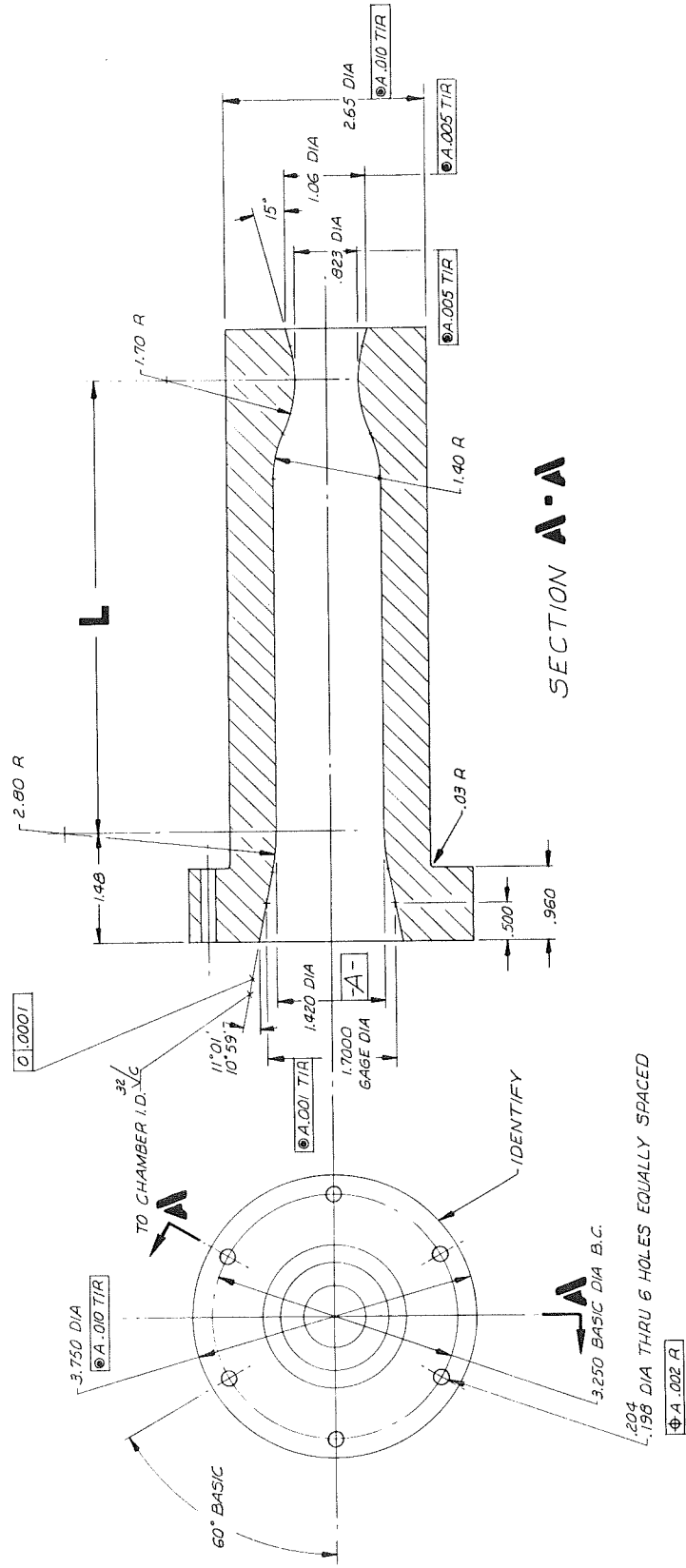
3. Copper Chambers

Two copper thrust chambers (L* = 12 in. (30.48 cm) and L* = 18 in. (45.72 cm)) in accordance with design drawing X24488 (Figure 39) were used for the initial FLOX/Methane performance tests. Three Cr-Al thermocouples were installed along the wall of each chamber (Figure 40). The L* = 18 inch (45.72 cm) copper chamber had a Kistler pressure transducer tap installed to permit evaluation of the ignition spike.

4. PG/Carbitex Chambers

The original program schedule provided for the final design and ordering of an altitude configuration (12:1 exit) Carbitex chamber from The Carborundum Company after review of the Phase I injector evaluation tests. The initial projected fabrication time for the filament wound Carbitex chamber was 12 weeks with a 4-week additional period scheduled for coating the chamber inner wall with an 0.040-inch (0.102 cm) layer of PG. Delays in ordering the chamber and an extended delivery schedule precluded on-time fabrication

DASH NO	L
-1	4.00
-501	6.00



SECTION A-A

FIGURE 39. Layout of FIOX/Methane Thrust Chamber

REFERENCE X24488

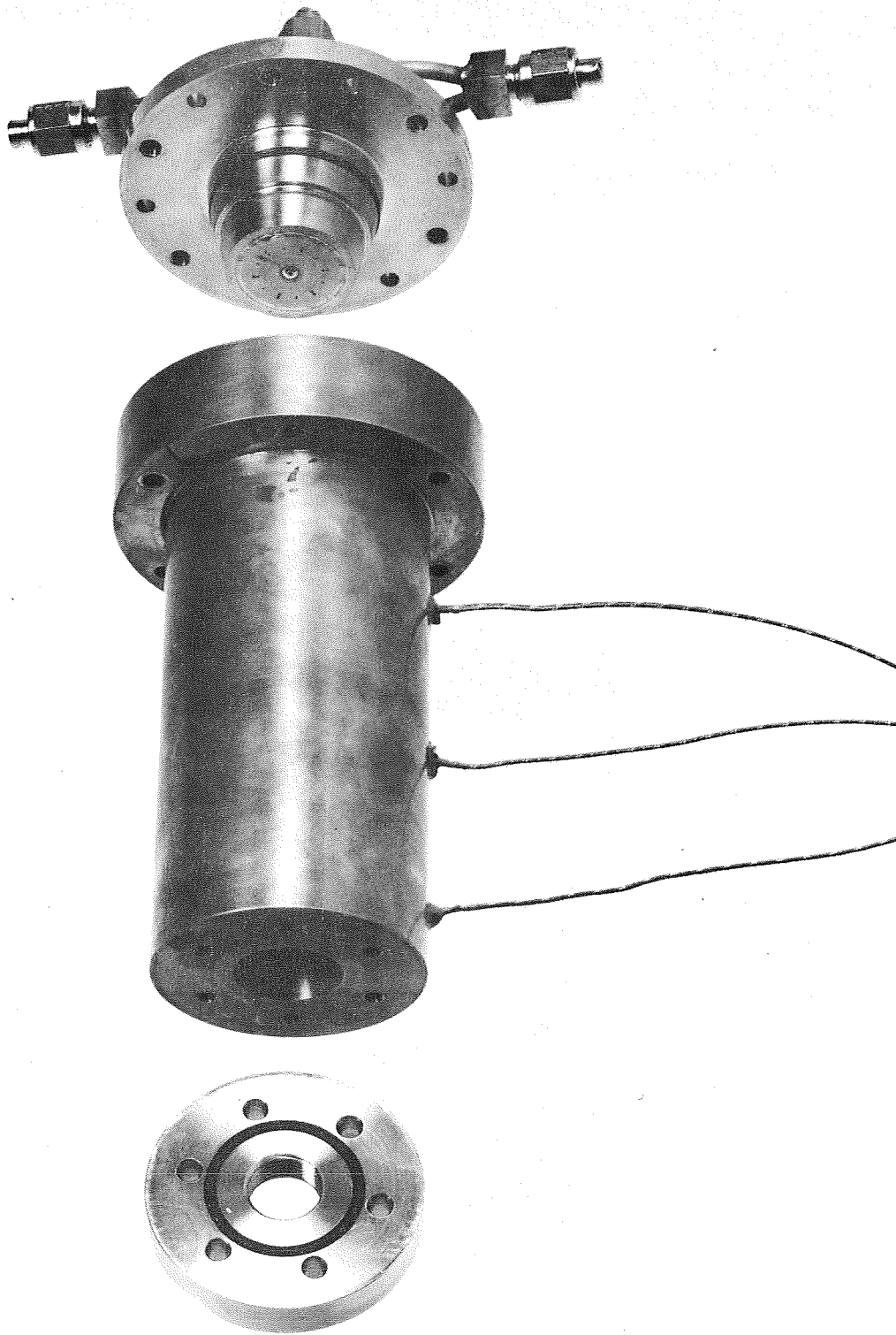


FIGURE 40. 100-pound Thrust FLOX/Methane Engine with Copper Thrust Chamber, Showing Thermocouple Installation

9157-1

of the final PG/Carbitex composite chamber within the program schedule. Therefore, an alternate plan to meet the program objectives was initiated.

Three PG/Carbitex thrust chambers with sea level exit nozzles and an L^* of 18 inches (45.72 cm) were being fabricated for structural evaluation under Contract NAS 7-555. A revised test chamber configuration was designed in which a 12:1 exit nozzle extension fabricated of a PG/carbon felt composite (RPG) was added to the sea level Carbitex chamber (Figure 31). The RPG exit cone was attached to the Carbitex chamber by a threaded joint. The chamber and nozzle were then coated inside and outside with an 0.040-inch (0.102 cm) layer of PG. The chamber is shown as tested in Figure 41 connected to the injector and a Marquardt valve assembly. Figure 42 is an X-ray photograph which shows the threaded joint and also reveals a separation between the outer PG layer and the Carbitex. The inner PG layer was well bonded to the Carbitex.

The outside of the exit nozzle downstream from the threaded joint was trimmed to remove the loose PG layer and to fit the no-flow exit diffuser used to provide the test altitude simulation.

SECTION V PHASE II -- FINAL THRUSTOR TESTS

During the period 28 December 1968 through 11 February 1969, thirty hot firing runs were made with FLOX/Methane in Cell M-2 of The Marquardt Magic Mountain Rocket Test Laboratory. The test runs are summarized in Table V. Briefly, the test items and firing durations were as follows:

1. Heat sink copper -- two chambers, No. 1 ; 8 runs, 45 seconds
No. 2 ; 3 runs, 141 seconds
2. Free standing PG -- three chambers; 3 runs, 58 seconds
3. POCO graphite -- one chamber; 5 runs, 194 seconds
4. Multilamina pyrocarbide -- one chamber; 1 run, 60 seconds
5. PG/Carbitex (sea level) -- one chamber; 1 run, 40 seconds
6. PG/Carbitex (with 12:1 exit) -- one chamber; 6 runs, 322 seconds

Essentially all of the 860 seconds of run time listed above was accumulated with one injector with no indication of injector plugging or overheating during operation (Figure 43).

The PG/Carbitex chamber (SL-3) with an L^* of 18 inches (45.72 cm), which was fired for 322 seconds, had been modified by attaching a 12:1 exit nozzle of a PG/carbon felt composite (RPG). The joint was formed by threading the exit nozzle and chamber. The inside and outside of the assembly were coated with a 0.040-inch (0.102 cm), layer of PG.

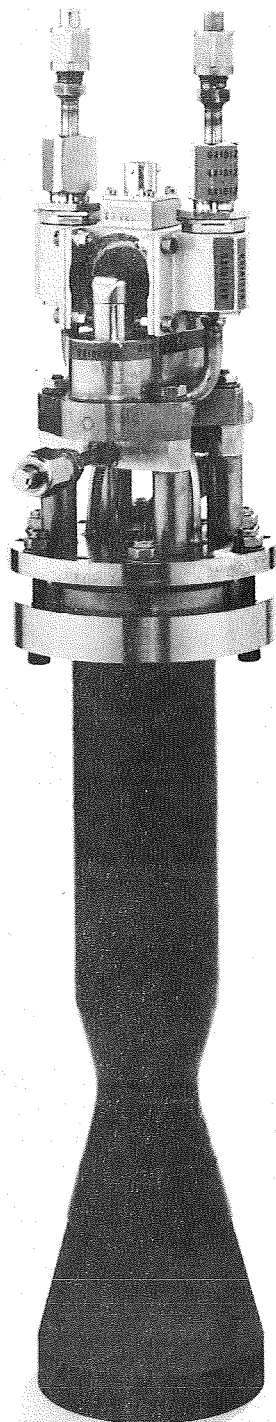


FIGURE 41. 100-pound Thrust FLOX/Methane Engine Assembly with PG/Carbitex Thrust Chamber and RPG Nozzle Extension

9432-2



FIGURE 42. X-Ray Photograph of PG/Carbitex Thrust Chamber with RPG Nozzle Extension

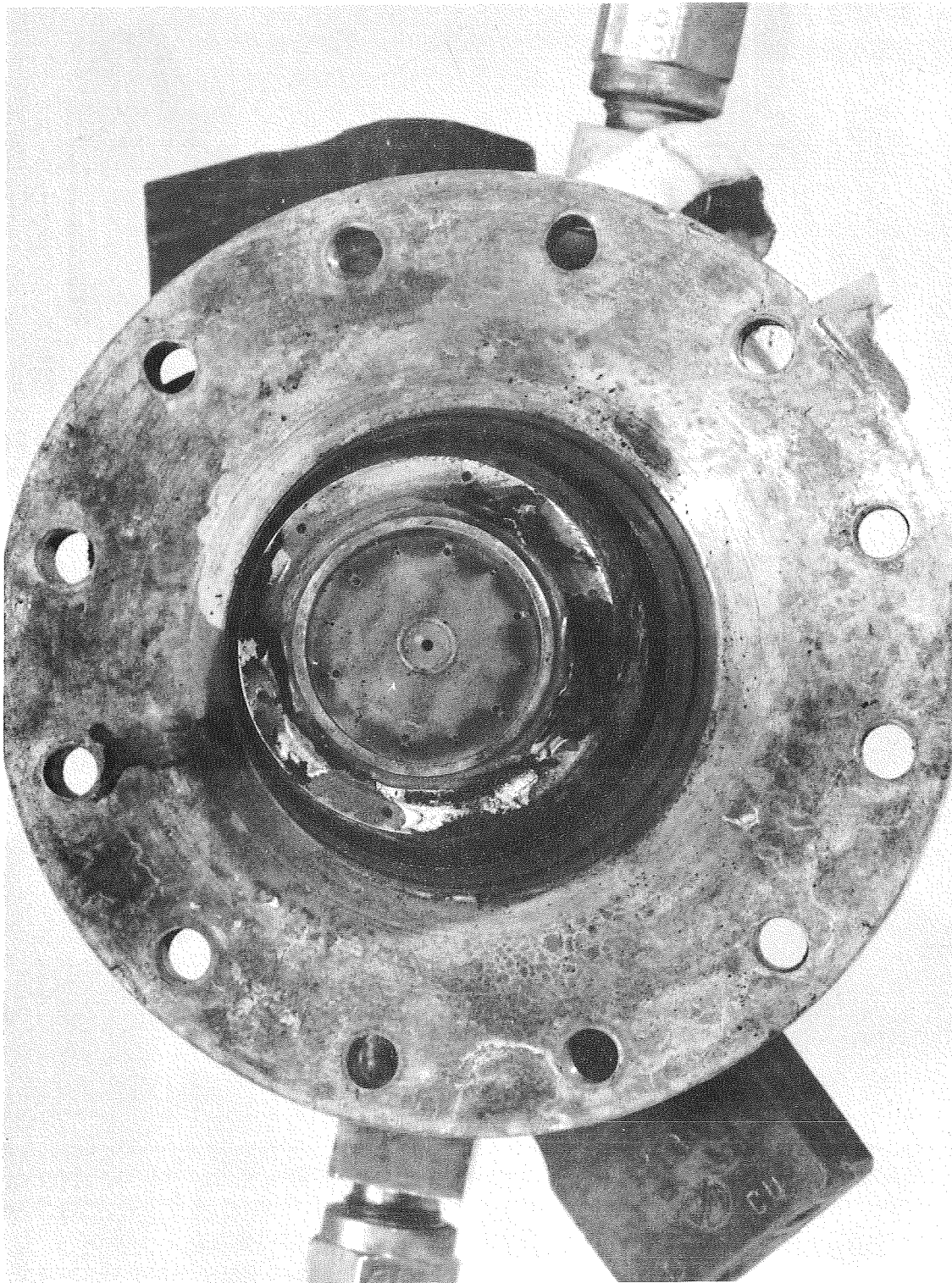


FIGURE 43. Injector after 170 seconds of Firing with FLOX/Methane

9424-7

During the first 60 second firing run with the above chamber at altitude conditions using the no-flow ejector, the exit nozzle extension apparently failed early in the run. The mode of failure of the exit cone is not known since the parts of the cone were ejected sideways into the altitude bell rather than downstream. There was no sign of burning or erosion on the cone pieces. One possible explanation is that a lateral deflection of the chamber assembly against the diffuser inlet occurred during the start transient and cracked the exit cone.

After the first firing, the chamber was removed from the cell and examined. There was very little throat erosion. There was carbon deposit build-up within the chamber and throat. There was some minor local erosion at the injector end of the chamber. There did appear to be several hairline cracks in the PG inner wall. The appearance of the chamber was similar to that of the first PG/Carbitex chamber (SL-1) (Figure 44) which had been fired for 40 seconds.

The first PG/Carbitex chamber (Figure 44) (which also developed hairline cracks) was pressurized after the 40 second firing run. At 50 psi (34.5 N/cm^2), pressure did leak through the wall at the throat. It should be noted that all the uncoated 100-lb Carbitex chambers leaked gas at all pressures when they were pressurized to 100 psig (68.9 N/cm^2) prior to coating.

Test firing of PG/Carbitex chamber SL-3 with FLOX/Methane was continued for five more runs. The maximum firing durations were limited by the pressure drop increases across the FLOX line filter. It is postulated that this was due to solid crystals of HF, since after each run, when the filter was allowed to heat up, the blockage disappeared. It was the objective of this firing series to run until some definite failure occurred in the chamber. At the beginning of the sixth run, after successful runs of 60, 47, 60, 71, and 68 seconds, there was an apparent burn through. Examination of the chamber after the run showed failure due to gradual erosion through the PG coating on the wall ahead of the throat and then a more rapid burn through in the Carbitex. The PG inner wall in the throat region showed nearly uniform circumferential erosion. At local areas, where a very thin coating of PG remained, the PG/Carbitex bond remained intact. There was no tendency for the PG to separate from the inner wall of the Carbitex. The hairline cracks did not initiate any local erosion or failure (Figures 45 and 46).

The estimated PG erosion rate over the total burn time (0.040/322) is about 0.12 mil/second at the pressure, temperatures, and mixture ratios involved.

Also noteworthy were the results of long firing runs with both the copper and the POCO graphite heavy walled chambers. Runs of 30, 60, and 90 seconds were obtained with the POCO graphite chamber. The erosion pattern at the completion of these runs is shown in Figure 47. Throat erosion was almost negligible during these runs. The carbon deposition was much less than in the PG lined chambers, due primarily to the lower transient wall temperatures (Figure 48).

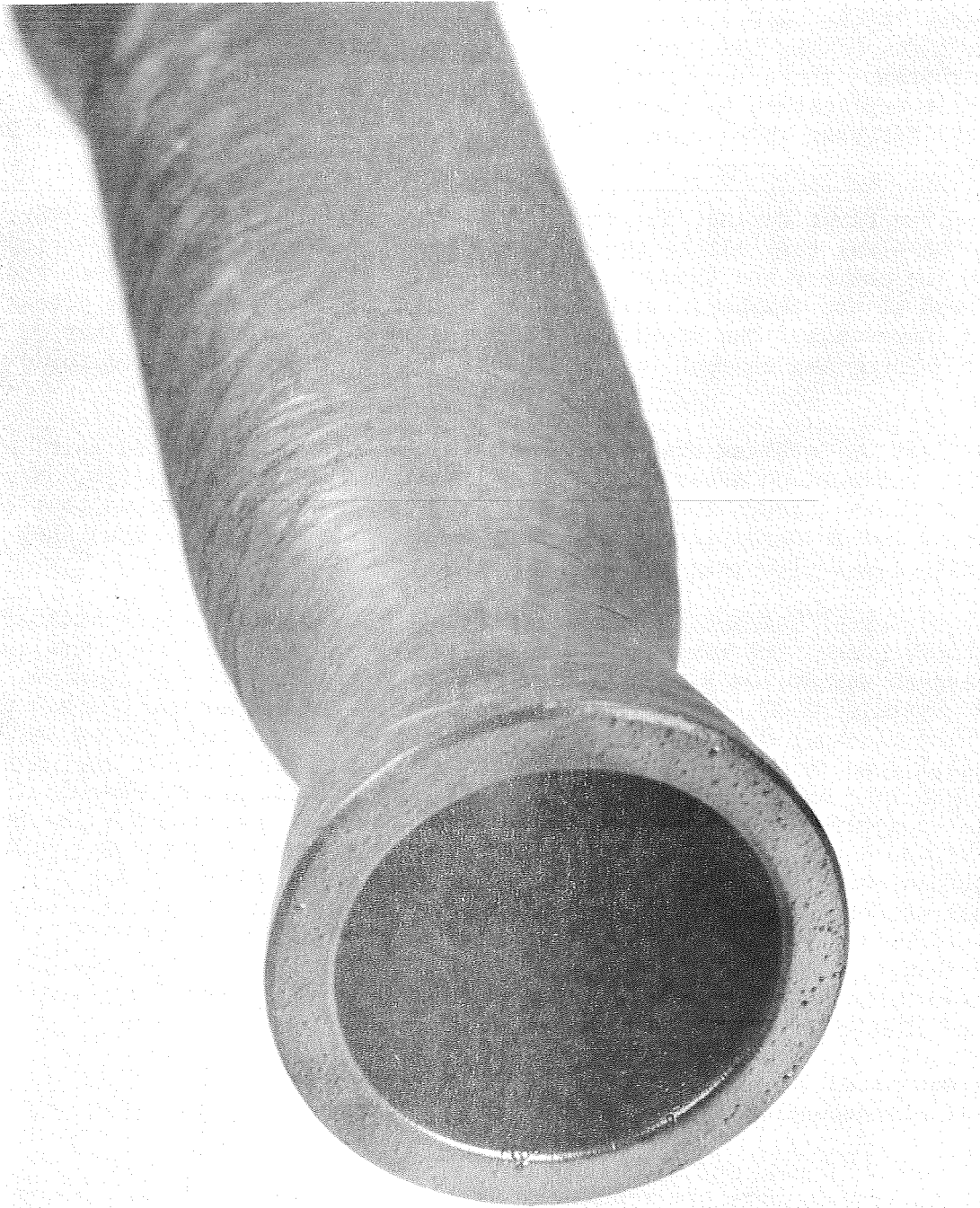


FIGURE 44. PG/Carbitex Sea Level Chamber (SL-1) after 40 seconds of Firing

9424-4

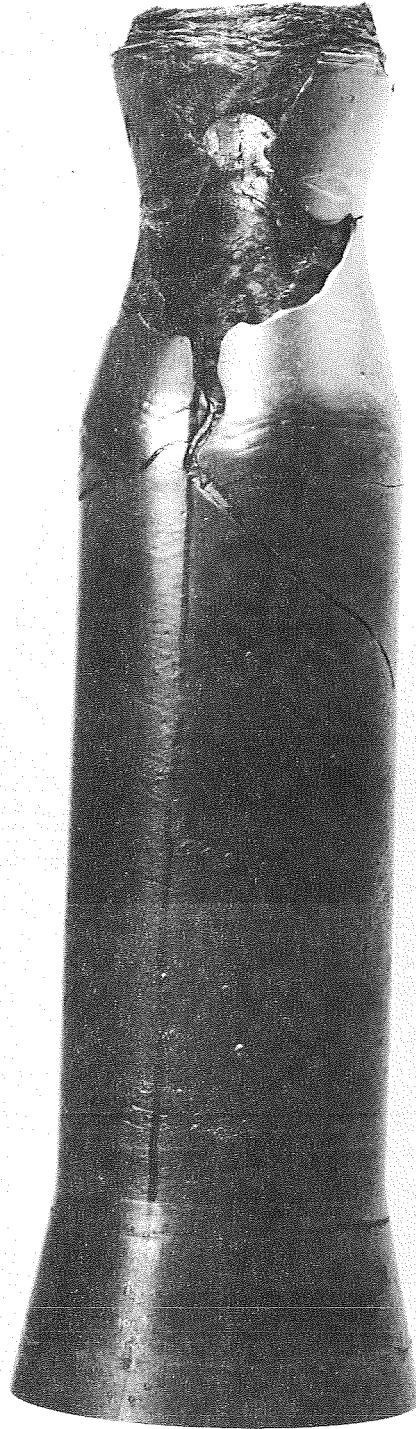
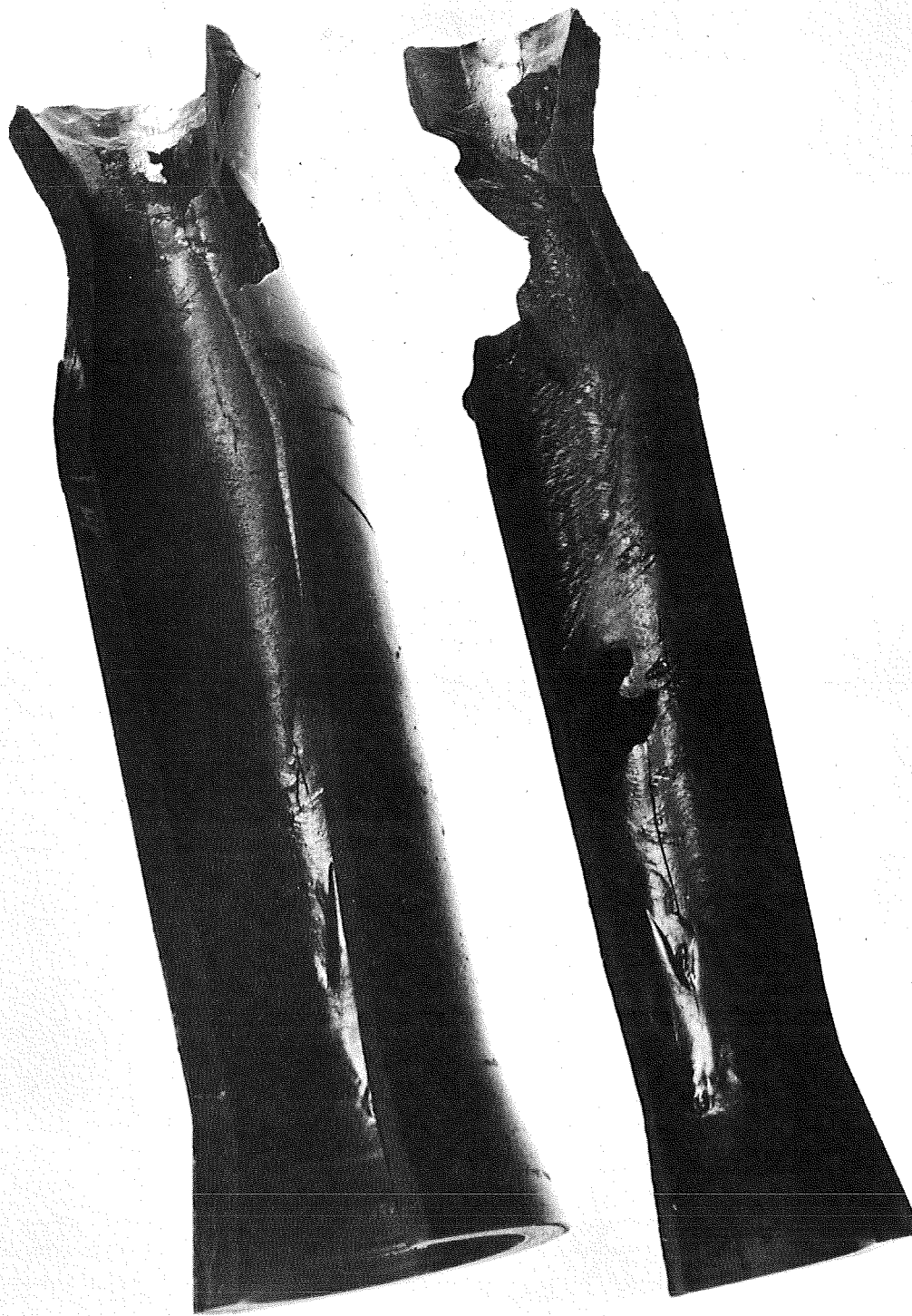


FIGURE 45. PG/Carbitex Chamber (SL-3) after 322 seconds of Firing

9453-1



9472-2
FIGURE 46. Sectioned PG/Carbitex Chamber (SL-3) after 322 seconds of Firing

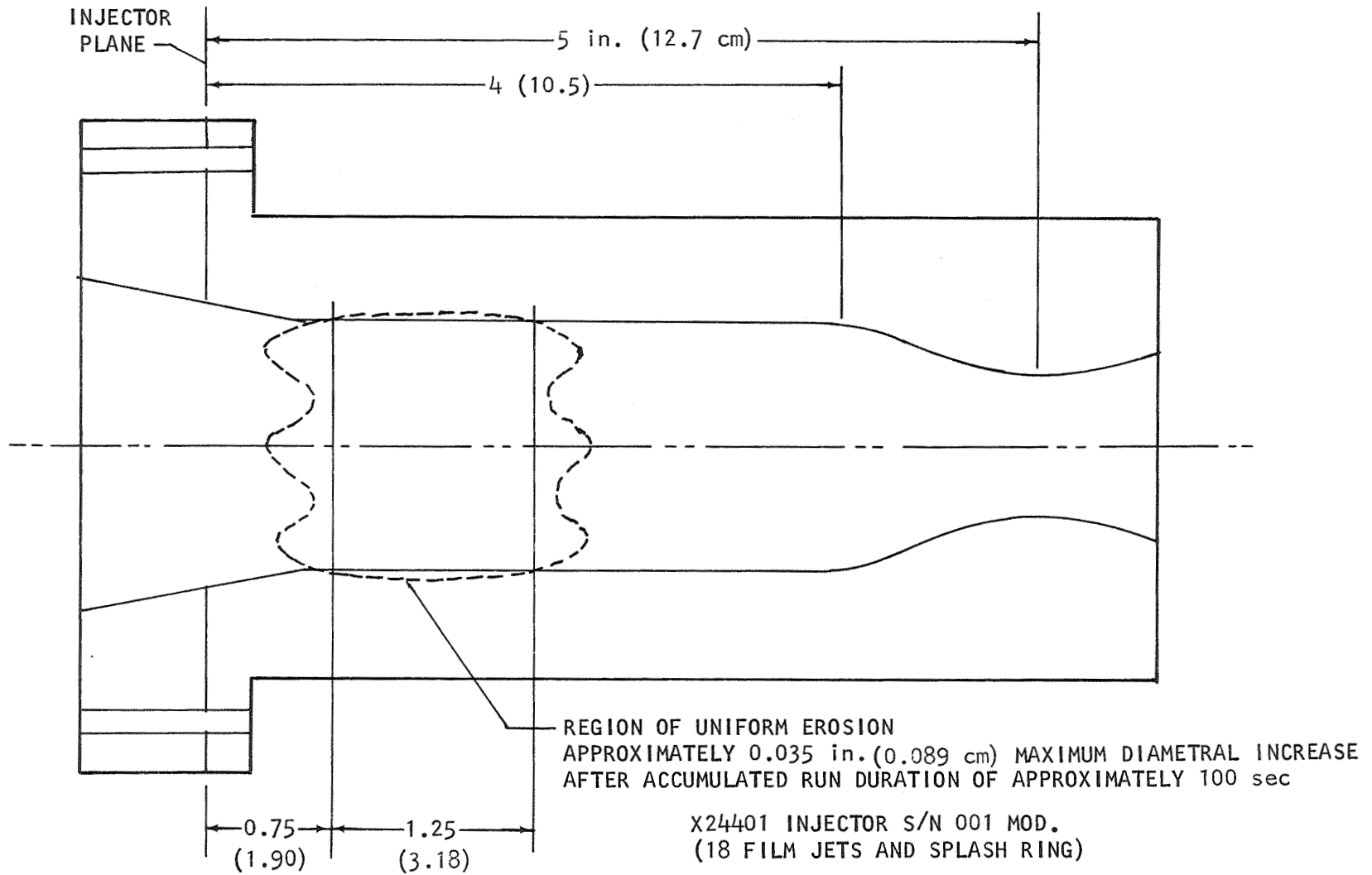
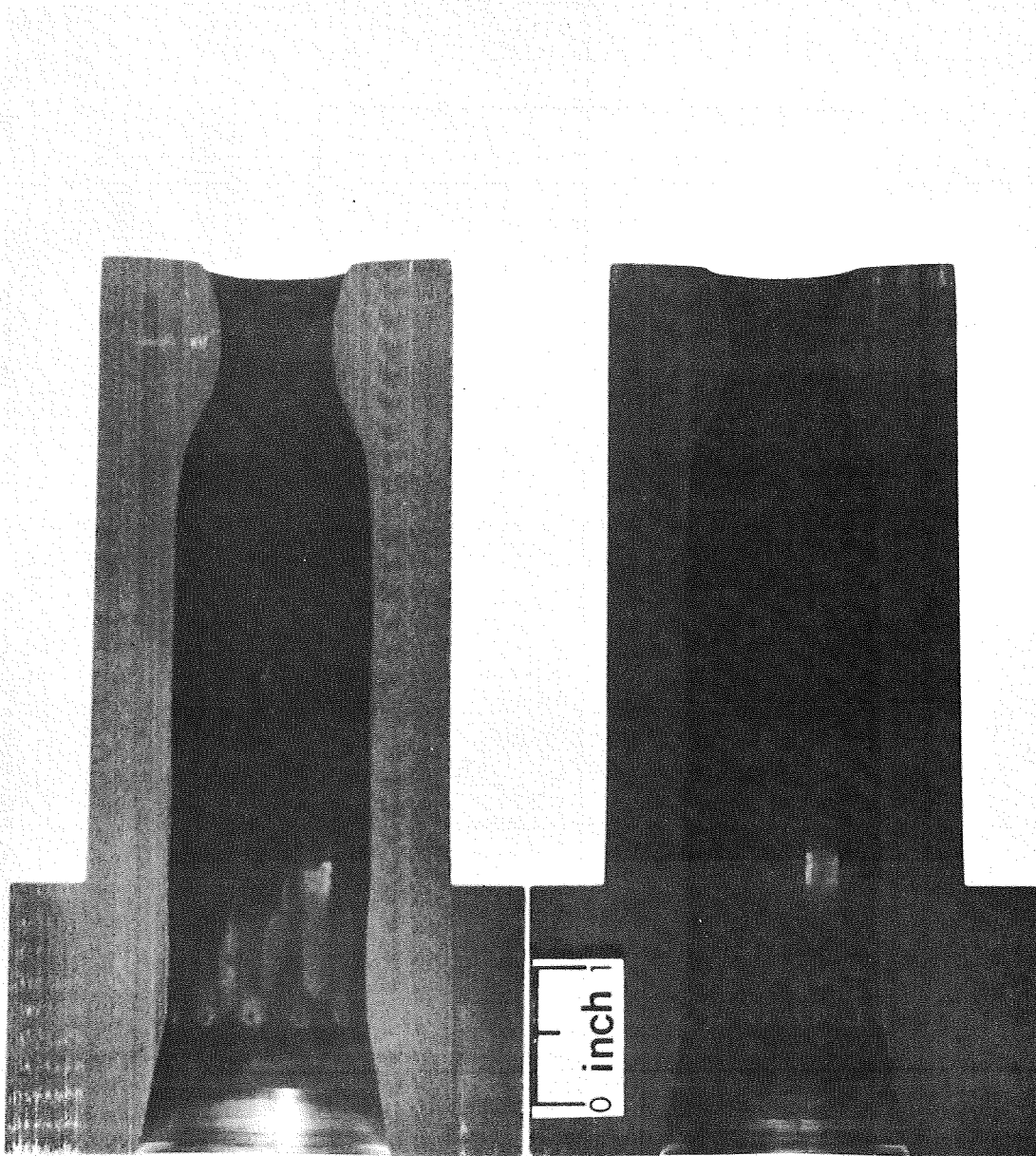


FIGURE 47. Erosion Pattern of the POCO Graphite Chamber after Runs 10, 11, and 18



9523-1
FIGURE 48. Sectioned POCO Graphite Chamber after FLOX/Methane Firing, Runs 10, 11, and 18

Two 65 second firing runs were made with the copper heat sink ($L^* = 12$ in. (30.48 cm)) chamber to evaluate the heat transfer characteristics of the injector. The throat wall temperature at the end of each firing run was about 1450°F (1061°K) but still increasing (Figure 49). Some uniform throat erosion did occur at these temperatures as shown in Figure 50. Minor localized carbon deposition occurred (Figure 51). These data were further analyzed for comparison with analytical predictions and to evaluate the effectiveness of the fuel film cooling and conduction effects (Figure 52).

Average throat erosion rates for the Phase II tests -- obtained by dividing the throat radius change by run time -- are summarized in Table VI.

SECTION VI THERMAL ANALYSES

A. Free Standing PG Chambers

The test results obtained during Run 47, Phase I, Test No. 6056 were analytically verified. This test utilized a free standing PG chamber with a wall thickness of 0.052 inch (0.132 cm) at the throat. The extended range (XR) film for that run is shown in Figure 22. The only other data available was an XR photo from Run 25 (Figure 23). During part of Run 25, however, an oxidizer valve was only partly open and the temperature results from the run are not meaningful. It is interesting to note, however, that wall temperatures indicated on the XR film for Run 25 were higher than those from Run 47, despite the shorter run time, greater percentage film cooling, and lower chamber pressure. This effect is due to the fact that the mixture ratio of Run 25 was close to stoichiometric whereas the mixture ratio of Run 47 was considerably below the stoichiometric ratio.

Figure 53 shows theoretical transient temperatures for the inner and outer walls at the throat for the conditions of Run 47 with and without carbon deposits. It can be seen that steady state conditions had been reached when the XR photo was taken (12 seconds into the run).

The assumed run conditions were as follows:

$$P_c = 101.4 \text{ psi } (69.9 \text{ N/cm}^2)$$

$$T_o = 5700^\circ\text{F } (3422^\circ\text{K}) \text{ (Taken from Reference 10 for } O/F = 3.5 \text{ and assuming } \eta_{c*} = 0.975 \text{ as measured)}$$

$$h_g = 0.0004 \text{ Btu/in.}^2 \text{ sec } ^\circ\text{F } (0.1178 \text{ Joules/cm}^2 \text{ sec } ^\circ\text{K}) \text{ for laminar flow at the throat}$$

The thermal properties of PG were taken from Reference 8. The outside surface emissivity was taken as 0.8. Since only about 7% of the total fuel flow was used for film cooling in Run 47, the effect of the cooling film at the throat was assumed to be negligible.

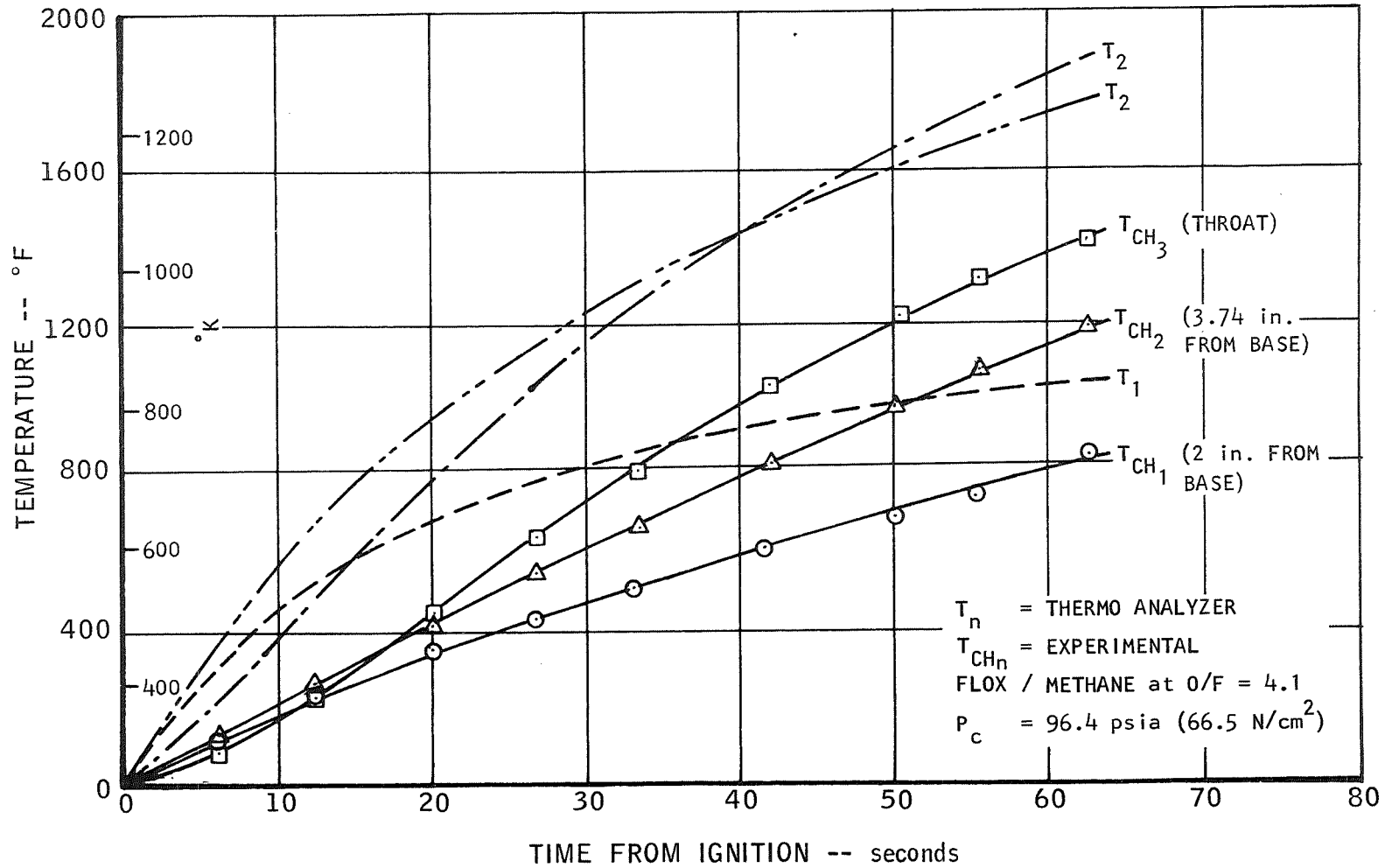
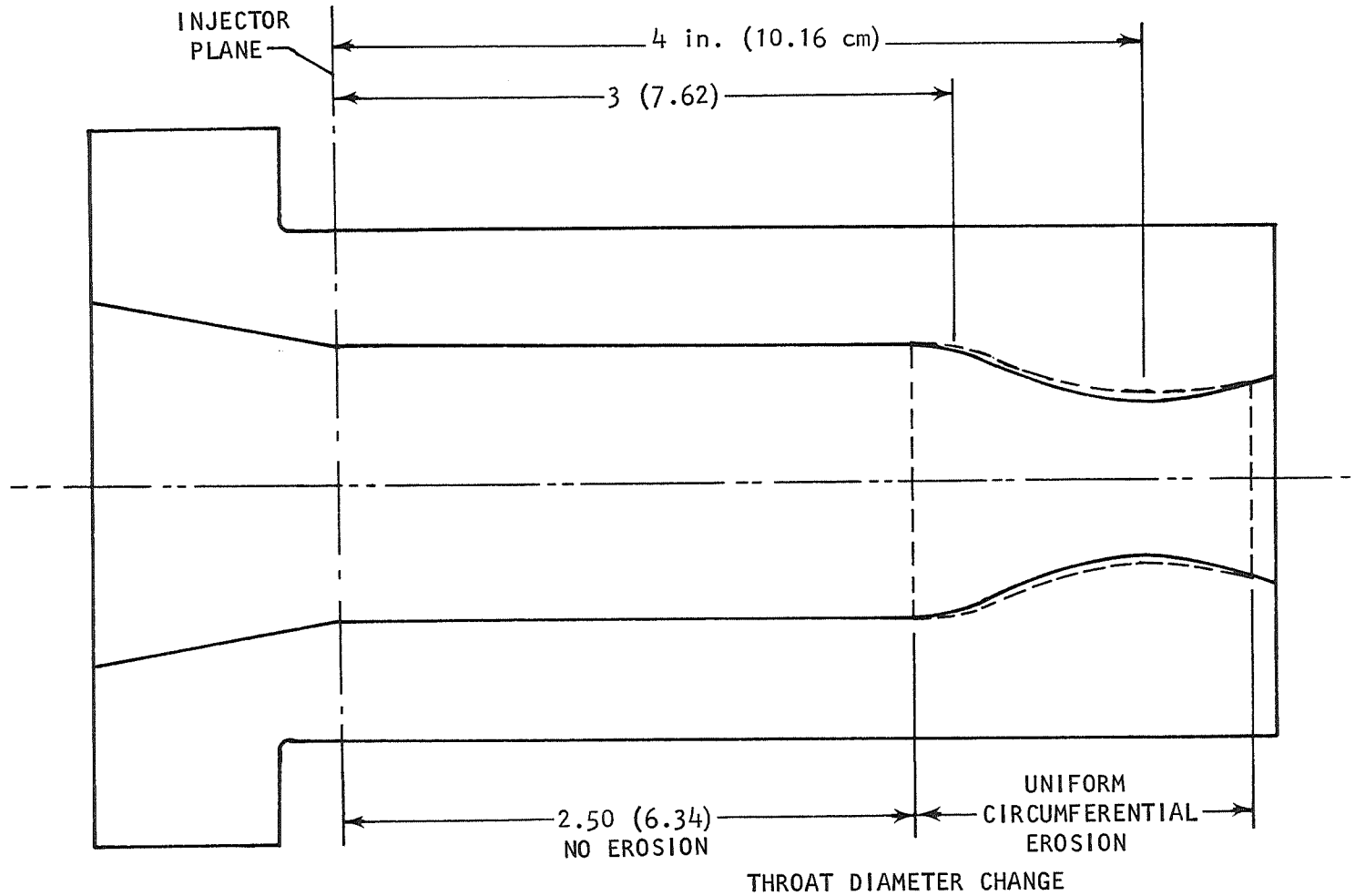


FIGURE 49. Thermal Test Data from Copper Heat Sink Chamber, Run 20



RUN 20
0.0248 in. (0.0630 cm); 63.7 sec

RUN 21
0.0400 in. (0.1016 cm); 67.5 sec

FIGURE 50. Erosion Pattern of the Copper Heat Sink Chamber after Runs 20 and 21

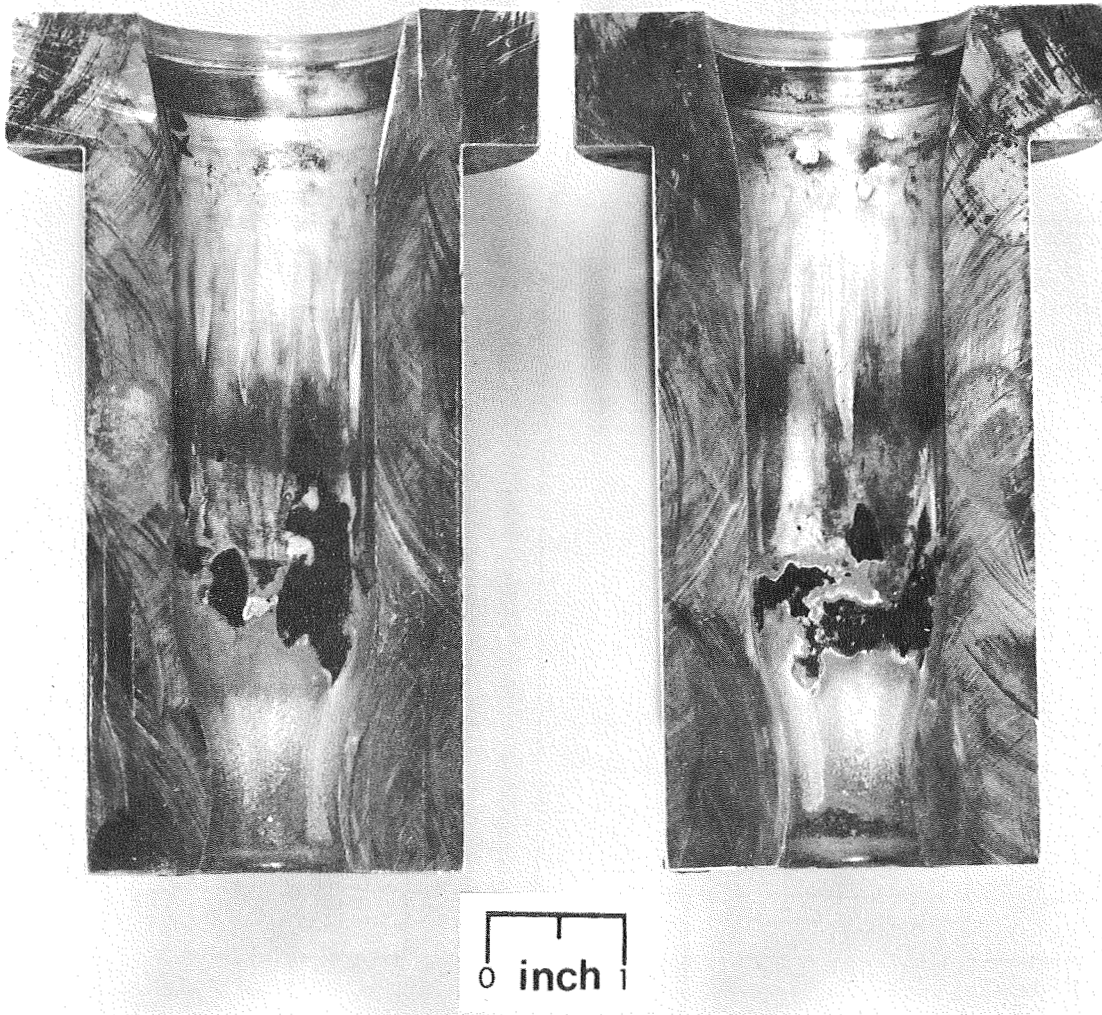


FIGURE 51. Sectioned Copper Thrust Chamber after 141 seconds of Firing

9512-1

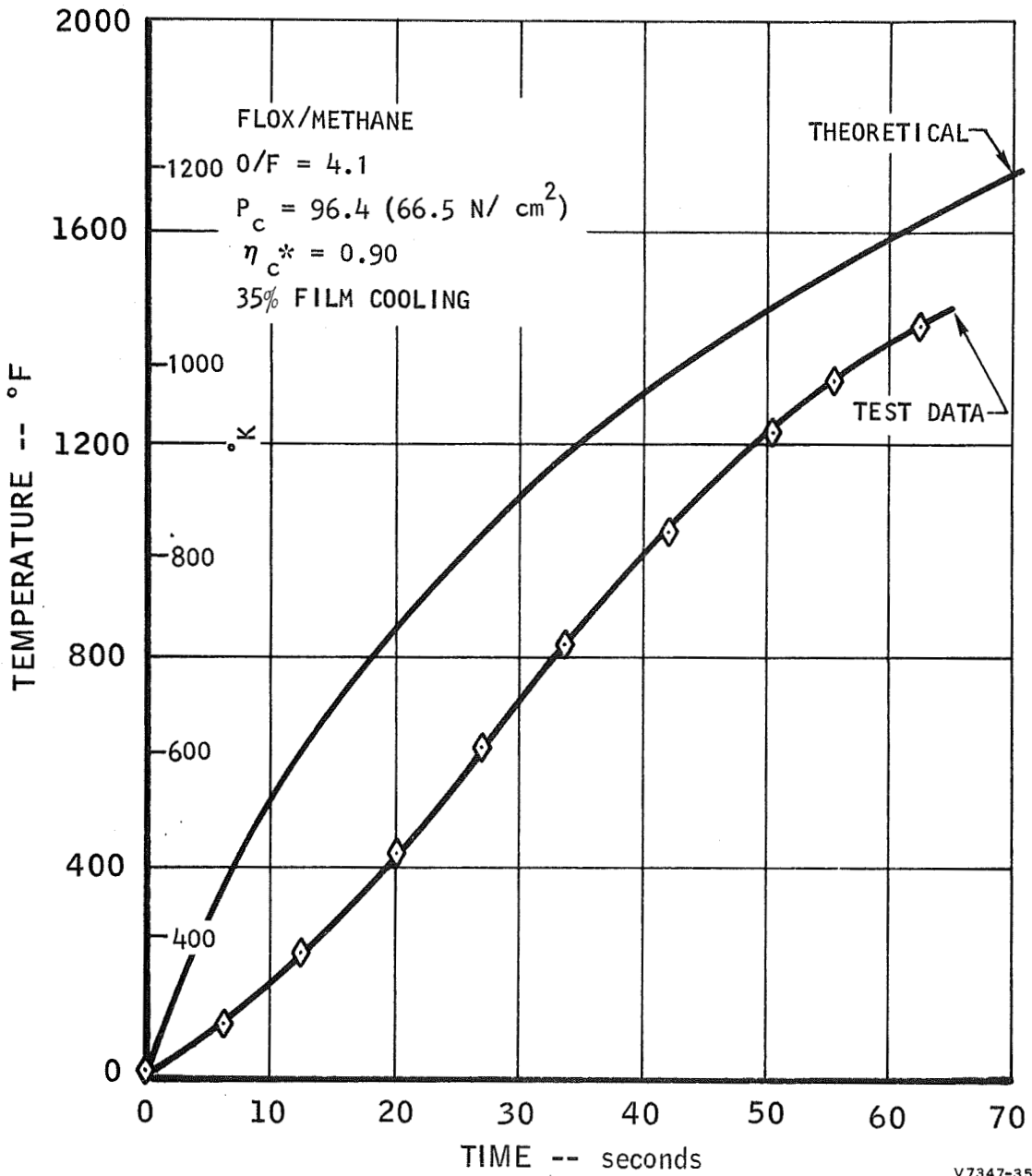


FIGURE 52. Comparison of Throat Temperatures from Firing Tests of the 100-pound Thrust Copper Heat Sink Chamber

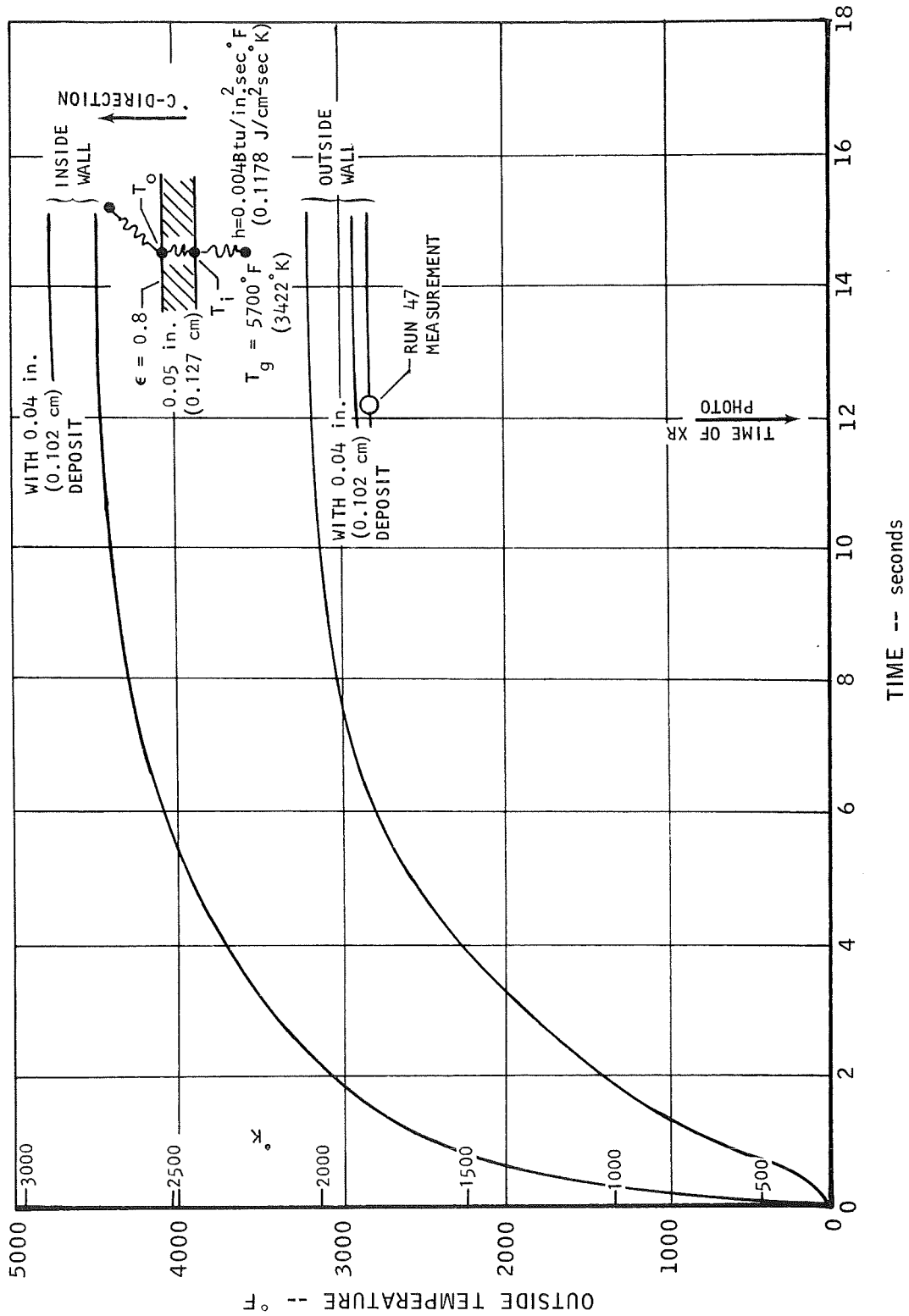


FIGURE 53. Theoretical Transient Throat Wall Temperatures of Free Standing PG Chambers for the Conditions of Run 47

The flame temperature was determined assuming the film to be at the same temperature as the core temperature and assuming $\eta_{C*} = 0.88$ as measured for Run 11.

The analytical result is in very good agreement with test results, especially in consideration of the run-to-run variation in the test data. As an example of the variation, a higher exit temperature was recorded for Run 11 than for Run 18 even though the firing duration of Run 11 was shorter, the chamber pressure was somewhat lower, and the measured η_{C*} was lower.

Though the highest visible temperature was 2700° to 2800°F (1755° to 1811°K), the inside wall further upstream would be expected to run about 400° (478°K) hotter. The exit surface is cooler because the heat transfer coefficient is lower, it is radiating to ambient air, and it is in close proximity to the large radiating surface at the end of the nozzle.

C. PG/Carbitex Chambers

No useful temperature data were obtained for PG/Carbitex chambers from the FLOX/Methane test program. However, an analysis was made to determine the inside and outside throat wall temperatures for various flame temperatures. Axial conduction was ignored, a simplification which is more valid for free standing chambers than for the composite chambers. The axial thermal resistance at operating temperatures for the free standing chambers is about 2 1/2 times that of the PG/Carbitex chambers.

Figure 54 shows the inside and outside throat wall temperatures for the PG/Carbitex chamber as a function of flame temperature. At close to stoichiometric mixture ratio, the inside wall temperature will exceed 5000°F (3033°K).

D. Copper Chamber

A thermal analysis was carried out to attempt to match thermocouple data obtained in Phase II Runs 20 and 21 using a copper thrust chamber. A thermal network as shown in Figure 55 was established for the chamber, considering in detail the convection, conduction, and radiation processes occurring during the firing. The thermal analysis was made using a combination of existing Marquardt IBM 360 computer programs. The two principle computer programs used were the following:

1. Thermal Analyzer (Electric Analog) Program P4000
2. Film Cooling Program (Iterative Film Heat Balance)

Other auxiliary programs used in this type of thermal analysis are the Radiation Configuration Program (P4031) and the Rocket Performance Program (P4004). The interaction of these programs in the prediction of transient and steady state temperatures is illustrated by the flow chart of Figure 56.

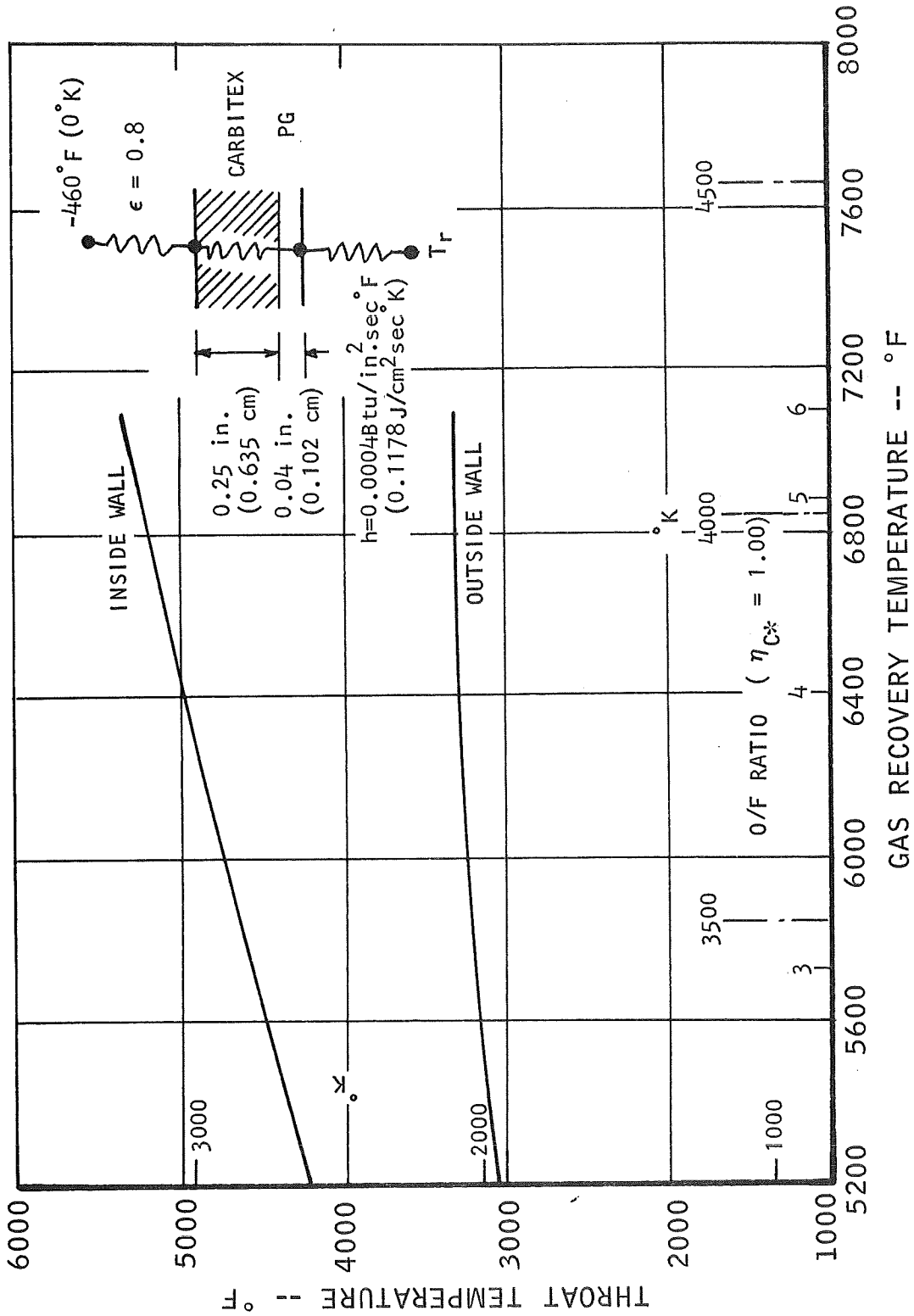


FIGURE 54. Theoretical Throat Wall Temperatures of PG/Carbitex Chambers

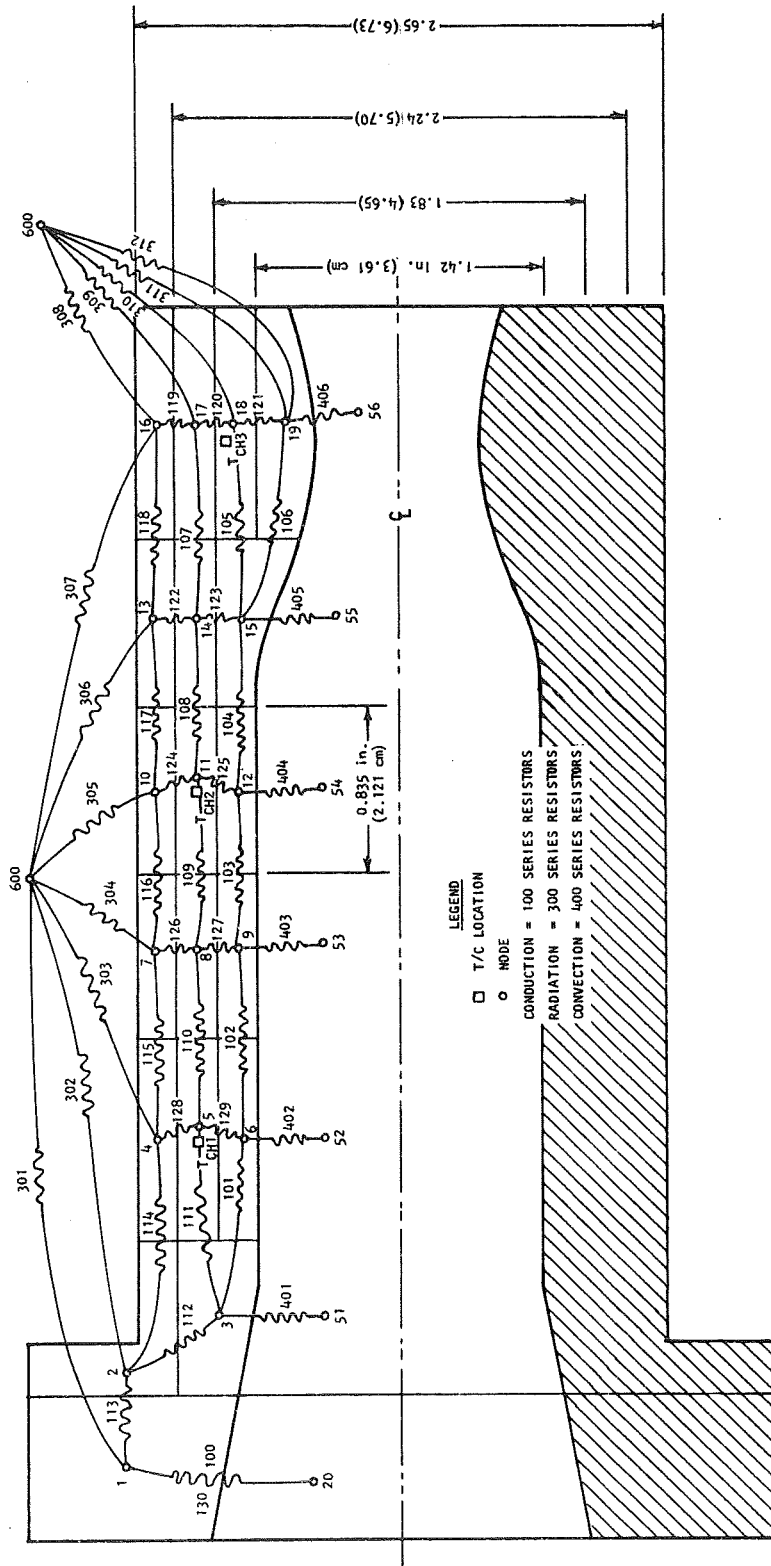
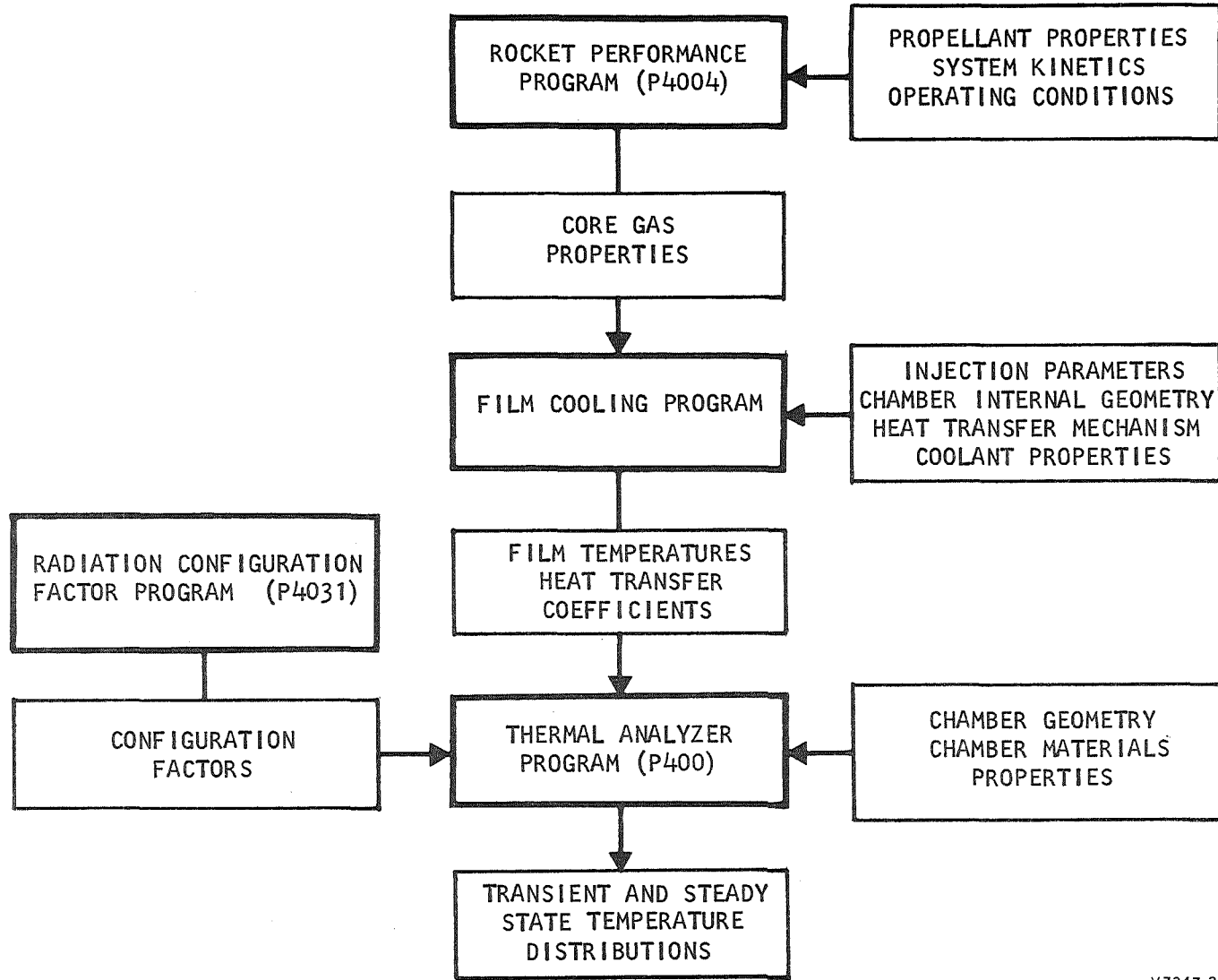


FIGURE 55. Thermal Model Used for Temperature Analysis of the Copper Thrust Chamber



V 7347-22

FIGURE 56. Flow Chart for Heat Transfer Analytical Techniques

The results of this analysis are shown in Figure 49. The test data showed heating rates slower than those predicted analytically. Most of the discrepancy occurred in the first 10 seconds of firing. This observation leads to the suspicion that thermocouple lag accounts for the difference. Such a lag is certainly possible. The thermocouples were glued in holes in the chamber and were not in direct contact with the metal. After about 10 seconds, the theoretical and test curves matched well in slope (rate of temperature rise) except near the injector. Errors are not surprising near the injector because the thermal conditions are least well known in that area. The stability and spreading characteristics of the liquid film are not well known, and the magnitude of heat conduction into the cold injector is not well known. Both of these conditions can significantly affect the temperature at T_{CH_1} (2 inches (5.08 cm) from the base).

In order to isolate the effects of the injector, a sophisticated analysis of the throat region was performed. The throat was isolated by using the test temperatures at T_{CH_2} (3.74 inches (9.50 cm) from the base) as boundary conditions. The thermal capacity, thermal conductivity, emissivity, and heat transfer coefficients were all assumed to be functions of wall temperature. Laminar flow was assumed to exist near the throat. The results of this analysis are shown in Figure 52. After about 30 seconds of firing, the heat flux rates were almost identical. Again, the difference between the two curves is indicative of thermocouple lag.

It is expected that local melting would begin under the conditions of Runs 20 and 21 about 100 seconds after ignition. Certainly, the chamber could not be operated under steady state conditions under those conditions.

SECTION VII DESIGN RE-EVALUATION AND CONCLUSIONS

The results of test firings with FLOX/Methane during this program have provided several clear design criteria and potential problem areas which provide guidelines and a basis for the continuing development of space storable engine technology.

An assessment of the results of this program provides the following design criteria and conclusions:

1. The injector performance of the like-doublet design with fuel film protection was satisfactory and the C^* efficiency ranged between 89 and 98% as a function of chamber L^* and O/F . Good correlation was obtained between the cold flow mixing criteria and test C^* performance.
2. Under the test firing conditions run with FLOX/Methane, injector face overheating or erosion were not encountered.

3. The achievement of adequate fuel film protection of the chamber near the injector face is more sensitive to the film injection pattern and core interaction than to the amount of film flow. There were no indications from qualitative observations of combustion instabilities during any of the test runs. Ignition overpressures can be experienced at sea level ambient pressure when propellant is allowed to accumulate in the chamber.
4. Both chamber erosion and carbon deposition vary over a wide range locally in the chamber from the injector face to the throat as a function of fuel film flow, O/F , and L^* .
5. Carbon deposition and erosion rates are also very sensitive to wall temperatures as indicated by the different results of firings with copper, POCO graphite, and PG chambers.
6. During the Phase II 322 second test firing of the PG/Carbitex chamber, the final mode of failure was gradual erosion through the PG inner wall in the throat region. After erosion through the PG at a rate of about 0.12 mil/sec (0.000305 cm/sec) erosion through the Carbitex wall proceeded several times faster until burn through.
7. The structural bond between the PG inner wall and the Carbitex shell remained intact under all conditions of test firing and resultant pressure and thermal cycling. Axial hairline cracks in the PG inner wall did not cause failure nor increase the rate of chamber degradation.
8. The relationships observed between throat wall temperatures for different chamber materials, and the erosion rates and combustion efficiencies in the range of L^* values from 12 to 18 inches (30.48 to 45.72 cm), indicate that both film cooling and conduction cooling (inter-regenerative) were effective in controlling wall temperatures. An optimized graphite chamber design of promise may utilize film cooling along with axial conduction, radiation, and heat sink effects to minimize both erosion and carbon deposits.

SECTION VIII REFERENCES

1. II TRI-B6058-26 "Protective Coatings for Refractory Metals in Rocket Engines", dated 15 March 1968, NASA Contract NAS 7-431. UNCLASSIFIED.
2. Marquardt Report 6069, "(U) Spacecraft Engine Thrust Chamber Cooling", Contract NAS 7-103, Amendment 2, 22 July 1964. UNCLASSIFIED.

3. Marquardt Report 6142, "(U) Pyrolytic Refractory Materials for Spacecraft Thrust Chambers, Composite Fabrication Investigation", 4 October 1968, Contract NAS 7-555. UNCLASSIFIED.
4. Marquardt Report 6086, "(U) Refractory Thrust Chambers for Spacecraft Engines, Final Report", Contract NAS 7-262, 22 March 1965. UNCLASSIFIED.
5. Marquardt Report 6106, "(U) Free Standing Pyrolytic Graphite Thrust Chambers for Space Operation and Attitude Control. Phase I: Analysis and Preliminary Design", (AFRPL-TR-66-95), Contract AF 04(611)-10790, 15 June 1966. UNCLASSIFIED.
6. Marquardt Report 6115, "(U) Pyrolytic Refractory Materials for Spacecraft Thrust Chambers, Final Report. Pyrolytic Composites of Hafnium and Zirconium Carbides in Graphite for the Period 20 May 1965 to 20 September 1966", Contract NAS 7-373, 15 December 1966. UNCLASSIFIED.
7. Marquardt Report PR 5033-5Q, "Fifth Quarterly Progress Report, Advanced Pyrolytic Spacecraft Thrust Chamber Materials", Contract NAS 7-555, 22 November 1968. UNCLASSIFIED.
8. Marquardt Report 6135 "Free Standing Pyrolytic Graphite Thrust Chambers for Space Operation and Attitude Control", Contract AF 04(611)-10790, September 1968. CONFIDENTIAL.
9. NASA CR-72147, "Investigation of Light Hydrocarbons with Fluorine Oxygen Mixtures as Liquid Rocket Propellants", 15 September 1967. UNCLASSIFIED.
10. NASA CR-54445, "Investigation of Light Hydrocarbons with Fluorine Oxygen Mixtures as Liquid Rocket Propellants", September 1965. UNCLASSIFIED.

TABLE I
INJECTOR DESIGN PARAMETERS
100-POUND THRUST FLOX/METHANE ENGINE

Dwg. X22401

$$\rho_{\text{FLOX}} = 90.0 \text{ lb/cu ft} \quad \rho_{\text{CH}_4} = 27.6 \text{ lb/cu ft}$$

$$= 1.442 \text{ gr/cm}^3 \quad = 0.442 \text{ gr/cm}^3$$

Injector S/N	O/F	D _o in. (cm)	D _f in. (cm)	D _{Film} in. (cm)	α _F °F (°K)	α _o °F (°K)	(C _D) _F	(C _D) _o	$\frac{\dot{w}_f V_f}{\dot{w}_o V_o}$	V _f fps (m/sec)	V _o fps (m/sec)	% (Fuel) B.L.Film
001	5.0	0.026 (0.066) (6 Doublet)	0.0110 (0.0279) (6 Doublet)	0.005 (0.013) (6 Jets)	-10 (249.8)	-11 (249.3)	0.645	0.678	0.65	190 (57.9)	59 (18.0)	10
002	5.0	0.026 (0.066) (6 Doublet)	0.0125 (0.0318) (6 Doublet)	0.005 (0.013) (6 Jets)	-10 (249.8)	-11 (249.3)	0.64	0.68	0.50	147 (44.8)	59 (18.0)	7
FOR S/N 001 MODIFICATION TO ADD FILM RING NO. 2 (6 JETS)												
001 (Mod) ₁	5.0	0.026 (0.066) (6 Doublet)	0.0110 (0.0279) (6 Doublet)	0.005 (0.013) (12 Jets)	-10 (249.8)	-11 (249.3)	0.645	0.678	0.59	174 (53.0)	59 (18.0)	20
FOR S/N 001 MODIFICATION TO ADD FILM RINGS NO. 2 AND 3 (12 JETS)												
001 (Mod) ₂	5.0	0.026 (0.066) (6 Doublet)	0.0110 (0.0279) (6 Doublet)	0.005 (0.013) (18 Jets)	-10 (249.8)	-11 (249.3)	0.645	0.678	0.54	160 (48.8)	59 (18.0)	30
FOR S/N 002 MODIFICATION TO ADD FILM RING NO. 2 (6 JETS)												
002 (Mod) ₁	5.0	0.026 (0.066) (6 Doublet)	0.0125 (0.0318) (6 Doublet)	0.005 (0.013) (12 Jets)	-10 (249.8)	-11 (249.3)	0.64	0.68	0.465	137 (41.8)	59 (18.0)	14
FOR S/N 002 MODIFICATION TO ADD FILM RINGS NO. 2 AND 3 (12 JETS)												
002 (Mod) ₂	5.0	0.026 (0.066) (6 Doublet)	0.0125 (0.0318) (6 Doublet)	0.005 (0.013) (18 Jets)	-10 (249.8)	-11 (249.3)	0.64	0.68	0.43	128 (39.0)	59 (18.0)	21

NOMENCLATURE:

Oxidizer (Flox) flow
O/F Fuel (LPG) flow
D_o Diameter of oxidizer orifices
D_f Diameter of fuel orifices
D_{Film} Diameter of fuel film orifices
α_F Resultant momentum angle of fuel stream tube relative to chamber centerline
α_o Resultant momentum angle of oxidizer stream tube relative to chamber centerline
(C_D)_f Fuel orifice discharge coefficient
(C_D)_o Oxidizer orifice discharge coefficient

$\frac{\dot{w}_f V_f}{\dot{w}_o V_o}$ Fuel-to-oxidizer momentum ratio
V_f Fuel injection velocity
V_o Oxidizer injection velocity
% (Fuel) $\frac{\text{Film fuel flow}}{\text{Total fuel flow}}$
B.L.Film

TABLE II
SUMMARY OF THE PHASE I INJECTOR EVALUATION FIRING TESTS

Run No.	Date (1968)	Configuration			Injector S/N	Duration sec	Category*	t _{data} ** sec	0/F	P _c		F _N		η _{ck}	Remarks	
		Chamber	L*							Kistler Used	psia	N/cm ²	lbf			N
			in.	cm												
1	2 Aug.	Copper	18	45.72	No	001	4	1	-4	8.02	107	73.8	--	--	Facility shakedown and combustion performance. Instrumentation and propellant conditioning discrepancies resolved.	
2	2 Aug.	Copper	18	45.72	No	001	4	1	-4	7.62	100	68.9	--	--		
3	6 Aug.	Copper	18	45.72	No	001	10	1	-4	6.26	102	70.3	59	262.4		
4	6 Aug.	Copper	18	45.72	No	001	10	1	-4	6.13	102	70.3	58	258.0		
5	6 Aug.	Copper	18	45.72	No	001	10	1	-4	4.36	88	60.7	48	213.5		
6	6 Aug.	Copper	18	45.72	No	001	10	1	-4	4.15	84	57.9	46	204.6		
7	8 Aug.	Copper	12	30.48	No	001	5	1	-4	5.40	88	60.7	49	218.0		
8	8 Aug.	Copper	12	30.48	No	001	5	1	-4	5.17	92	63.4	50	222.4		
9	8 Aug.	Copper	12	30.48	No	001	5	1	-4	6.57	102	70.3	56	249.1		
10	8 Aug.	Copper	12	30.48	No	001	5	1	-4	6.06	101	69.6	56	249.1		
11	13 Aug.	PG 001	18	45.72	No	001	Ign.	3	--	--	--	--	--	--		Chamber shattered, hard start
12	15 Aug.	POCO	18	45.72	No	001	Ign.	3	--	--	--	--	--	--		
13	19 Aug.	Copper	18	45.72	Yes	001	0.5	2	Ignition data only					High response P _c instrumentation installed to monitor effect of ignition sequence and thermodynamic state.		
14	20 Aug.	Copper	18	45.72	Yes	001	0.5	2								
15	20 Aug.	Copper	18	45.72	Yes	001	0.5	2								
16	20 Aug.	Copper	18	45.72	Yes	001	0.5	2								
17	20 Aug.	Copper	18	45.72	Yes	001	0.5	2								
18	20 Aug.	Copper	18	45.72	No	001	10.0	1, 2	5.3	5.3	80.4	55.4	40	177.9	84	Steady state run to evaluate effect of propellant thermodynamic state.
19	21 Aug.	Copper	18	45.72	Yes	001	0.5	2	Ignition data only					Ignition sequence and propellant thermodynamic state revised to achieve steady state transition.		
20	22 Aug.	Copper	18	45.72	Yes	001	0.5	2								
21	22 Aug.	Copper	18	45.72	Yes	001	0.5	2								
22	22 Aug.	Copper	18	45.72	Yes	001	0.5	2								
23	22 Aug.	Copper	18	45.72	Yes	001	0.5	2								
24	22 Aug.	Copper	18	45.72	No	001	6.0	1, 2	5.8	6.1	95	65.5	54	240.2	95	Steady state run to evaluate effect of propellant thermodynamic state.
25	22 Aug.	PG 002	18	45.72	No	001	20.0	3	6.1	13.1	77.4	53.4	39	173.5	80	Oxidizer valve inadvertently closed during run.
26	26 Aug.	PG 005	18	45.72	No	001	Ign.	3	--	--	--	--	--	--	--	Chamber shattered at ignition, hard start, ignition marginal.
27	29 Aug.	PG 007	18	45.72	No	001	-3	3	Data not stabilized					Run cut prematurely, smooth start.		
28	29 Aug.	PG 007	18	45.72	No	001	Ign.	3	--	--	--	--	--	--	--	Chamber failed at ignition, hard start, marginal ignition.

TABLE II (Continued)

Run No.	DATE (1968)	Configuration				Injector S/N	Duration sec	Category*	t _{data} ** sec	O/F	P _c		F _N		η _{cr}	Remarks
		Chamber	L*		Kistler Used						psia	N/cm ²	lbf	N		
			in.	cm												
29	29 Aug.	Copper	18	45.72	No	002	5	5.6	87	60	--	--	100	GCH ₄ system installed. Revised ignition sequence		
30	29 Aug.	Copper	18	45.72	No	002	0.5	Ignition data only							Hard start	
31	29 Aug.	Copper	18	45.72	No	002	0.5									
32	30 Aug.	Copper	18	45.72	Yes	002	0.76									
33	30 Aug.	Copper	18	45.72	Yes	002	1.76									
34	30 Aug.	Copper	18	45.72	Yes	002	1.65									
35	30 Aug.	Copper	18	45.72	Yes	002	2.3									
36	30 Aug.	Copper	18	45.72	Yes	002	5.2									
37	30 Aug.	Copper	18	45.72	No	002	8.0									Hard start
38	4 Sept.	Copper	18	45.72	Yes	002	0.5	Ignition data only							GF ₂ system installed. Revised ignition sequence. Soft starts.	
39	4 Sept.	Copper	18	45.72	Yes	002	0.5									
40	4 Sept.	Copper	18	45.72	Yes	002	0.5	GF ₂ off prematurely. (Steady state. Evaluate effect of propellant thermodynamic state. Good transition from ignition transient to steady state.								
41	4 Sept.	Copper	18	45.72	No	002	4.0		--	--	--	--	--	--		
42	4 Sept.	Copper	18	45.72	No	002	9.7		9	6.5	87	60	45	200.2	99	
43	4 Sept.	Copper	18	45.72	No	002	9.2		8.7	6.1	83.4	57.5	43	191.3	94	
44	5 Sept.	PG 003	18	45.72	No	002	Ign.		3	--	--	--	--	--	--	--
45	5 Sept.	PG 006	18	45.72	No	002	23	3	2.5	3.8	92.4	63.7	53	238.8	100	Revised fuel start sequence--soft start Thermal performance and erosion -- Final data Pin hole in side of chamber
									12.4	5.1	87.4	60.3	43.5	193.5	99	
									19.0	6.2	80.4	55.4	39.5	175.7	97.5	
46	9 Sept.	POCO	10.65	27.05	No	002	20	3	3.3	4.0	74.4	51.3	--	--	84	Thick wall graphite heat sink (POCO), minimum L*
									13.4	3.7	76.4	52.7	--	--	88	
									20.6	3.6	75.4	52.0	--	--	84	
47	9 Sept.	PG 004	18	45.72	No	002	19	3	4.5	3.5	94.4	65.1	52	231.3	97	Thin wall PG chamber, maximum L*
									8.6	3.45	102.4	70.6	53	235.8	100	
									16.0	5.22	96.4	66.5	49	218.0	100	

* Category:

1. Combustion performance
2. Ignition compatibility
3. Thermal and erosion characteristics

** t_{data} = Time (sec) from both propellants on to performance point

PG = Pyrolytic graphite

OXIDIZER:

FLOX -- 82.5% LF₂/17.5% LO₂ Mixture (by weight)

FUEL:

Liquified natural gas (weight %)

Methane 87.5
Ethane 11.6
Propane 0.5
Nitrogen 0.4

TABLE III

GASEOUS METHANE PEAK IGNITION PRESSURES

Prerun Conditions for Runs 30 through 33

T_{O_i} = -330°F (72°K)
 T_{m_o} = -270°F (105°K)
 $T_{inj_{ox}}$ = -250°F (116°K)
 T_{f_i} = -280 to -330°F (100 to 72°K)
 T_{m_f} = -260°F (111°K)
 T_{inj_f} = -130°F (183°K)
 T_{tank_f} = -230°F (128°K)

Run No.	T_{m_f}		T_{inj_f}		$P_{Kistler}$ Peak Meter		$P_{Kistler}$ O'graph		Remarks
	°F	(°K)	°F	(°K)	psi	(N/cm ²)	psi	(N/cm ²)	
30	-278	(101)	-133	(181)	--	--	80	(55.2)	Simultaneous on
31	-266	(108)	-138	(179)	--	--	1100	(758.4)	Simultaneous on
32	-272	(104)	-120	(189)	700	(482.6)	675	(465.4)	Simultaneous on
33	-254	(114)	-128	(184)	450	(310.3)	--	--	1 sec ox lead

NOTES:

Injector S/N 002

Runs 30 and 31: pressure regulator installed. Low volume capacity gave very large O/F values at ignition.

Runs 32 and 33: larger volume pressure regulator installed.

Simultaneous on gave fuel lead due to slower responding oxidizer valve.

TABLE IV
SUMMARY OF THE PHASE I CHAMBER EROSION TESTS

Run No.	Run Time sec	Chamber at Injector Face						Mid-Chamber				Throat							
		Initial		Final Wall Thickness				Initial		Final		Initial				Final			
		ID in. (cm)	Wall Thickness in. (cm)	Between Film Orifices		In Line with Film Orifices		ID in. (cm)	Wall Thickness in. (cm)	Wall Thickness		ID in. (cm)	OD in. (cm)	Wall Thickness in. (cm)	OD in. (cm)	Wall Thickness		Internal Erosion Rate	
				in.	(cm)	in.	(cm)			in.	(cm)					in.	(cm)	in./sec	(cm/sec)
25	21.1	1.396 (3.546)	0.066 (0.168)	0.029 to 0.041	(0.074 to 0.104)	0.050 to 0.053	(0.127 to 0.135)	1.396 (3.546)	0.066 (0.168)	0.042 to deposit	(0.107 to deposit)	0.814 (2.068)	0.931 (2.365)	0.057 (0.145)	0.928 (2.357)	0.043 to 0.052	(0.109 to 0.132)	0.00060 to 0.00016	(0.00152 to 0.00041)
45	19	1.396 (3.546)	0.066 (0.168)	0.000 to 0.026	(0.000 to 0.026)	0.034 to 0.048	(0.086 to 0.122)	1.396 (3.546)	0.066 (0.168)	0.043 to deposit	(0.109 to deposit)	0.826 (2.098)	0.929 (2.360)	0.053 (0.135)	0.926 (2.352)	0.044 to deposit	(0.112 to deposit)	0.00040 to 0	(0.00102 to 0)
47	16	1.407 (3.574)	0.062 (0.157)	0.047 to 0.050	(0.119 to 0.127)	0.056 to 0.050	(0.142 to 0.127)	1.407 (3.574)	0.062 (0.157)	0.043 to deposit	(0.104 to deposit)	0.827 (2.101)	0.931 (2.365)	0.052 (0.132)	0.925 to deposit (2.350 to deposit)	0.038 to deposit	(0.097 to deposit)	0.00188 to 0	(0.00188 to 0)
46	19.6	POCO Chamber										Initial ID		Final ID		Throat Internal Erosion Rate			
												in.	(cm)	in.	(cm)	in./sec	(cm/sec)		
												0.830	(2.108)	0.832 to 0.850	(2.113 to 2.159)	0.00005 to 0.0005	(0.000127 to 0.00127)		

TABLE V

SUMMARY OF THE PHASE II THRUST CHAMBER FIRING TESTS
CELL M-2, MARQUARDT MAGIC MOUNTAIN ROCKET TEST LABORATORY

28 December 1968 to 2 February 1969, Test No. 6060

Run No.	Date	Configuration		Duration (sec)	O/F Ratio	P _c psia (N/cm ²)	C* fps (m/sec)	η _c (%)	Run Objectives (Note 1)	Remarks
		Chamber	Injector							
1.	28 Dec. 1968	Cu L* = 18 in. (45.72 cm)	X24401, S/N 001 18 weep holes (12 Hi Angle 6 Lo Angle)	7.52	5.07	98.3 (67.8)	6340 (1932)	92	(2), (4)	GF ₂ /LCH ₄ Ignition
2.	28 Dec.	Cu L* = 18 in. (45.72 cm)	X24401, S/N 001 18 weep holes (12 Hi Angle 6 Lo Angle)	12.18	4.98	100.4 (69.2)	6460 (1969)	93	(2), (4)	GF ₂ /LCH ₄ Ignition
3.	28 Dec.	Cu L* = 18 in. (45.72 cm)	X24401, S/N 001 18 weep holes (12 Hi Angle 6 Lo Angle)	10.5	3.55	88.4 (60.9)	6620 (2018)	98	(2), (4)	FLOX flow decay due to tank near empty
4.	28 Dec.	Cu L* = 18 in. (45.72 cm)	X24401, S/N 001 18 weep holes (12 Hi Angle 6 Lo Angle)	10.13	2.48	66.4 (45.8)	6450 (1966)	99	(2), (4)	FLOX flow decay due to tank near empty
5.	31 Dec.	PG, SL-6	X24401, S/N 001 18 weep holes (12 Hi Angle 6 Lo Angle)	--	--	--	--	--	(3)	Chamber shattered at ignition
6.	6 Jan. 1969	Cu L* = 18 in. (45.72 cm) Kistler P _c	X24401, S/N 001 18 weep holes (12 Hi Angle 6 Lo Angle)	0.5	--	--	--	--	(1)	Ambient purge prior to ignition GF ₂ /LCH ₄ Max. P _c spike = 75 psia (51.7 N/cm ²)
7.	6 Jan.	Cu L* = 18 in. (45.72 cm) Kistler P _c	X24401, S/N 001 18 weep holes (12 Hi Angle 6 Lo Angle)	0.5	--	--	--	--	(1)	Ambient purge prior to ignition GF ₂ /LCH ₄ Max. P _c spike = 75 psia (51.7 N/cm ²)

TABLE V (Continued)

Run No.	Date	Configuration		Duration (sec)	O/F Ratio	P _c psia (N/cm ²)	C* fps (m/sec)	η _c (%)	Run Objectives (Note 1)	Remarks
		Chamber	Injector							
8.	6 Jan.	Cu L* = 18 in. (45.72 cm) Kistler P _c	X24401, S/N 001 18 weep holes (12 Hi Angle 6 Lo Angle)	0.5	--	--	--	--	(1)	Max. P _c spike = 100 psia (68.9 N/cm ²)
9.	6 Jan.	Cu L* = 18 in. (45.72 cm) without Kistler	X24401, S/N 001 18 weep holes (12 Hi Angle 6 Lo Angle)	7.02	4.12	99.4 (68.5)	6100 (1859)	90	(1), (2)	Data not stabilized
10.	7 Jan.	POCO No. 2 L* = 14 in. (35.56 cm)	X24401, S/N 001 18 weep holes (12 Hi Angle 6 Lo Angle)	31.52	4.5	99.9 (68.9)	6260 (1908)	91	(2), (3)	Erosion nil
11.	7 Jan.	POCO No. 2 L* = 14 in. (35.56 cm)	X24401, S/N 001 18 weep holes (12 Hi Angle 6 Lo Angle)	65.0	4.27	97.4 (67.2)	6000 (1829)	88	(2), (3)	Erosion nil
12.	8 Jan.	PG, SL-7 L* = 14 in. (35.56 cm)	X24401, S/N 001 18 weep holes (12 Hi Angle 6 Lo Angle)	--	--	--	--	--	(1), (3)	Chamber shattered at ignition
13.	8 Jan.	PG, SL-11 L* = 14 in. (35.56 cm)	X24401, S/N 001 18 weep holes (12 Hi Angle 6 Lo Angle)	22.9	4.18	97.4 (67.2)	6550 (1996)	95	(3)	GF ₂ /GCH ₄ Ignition procedure Upstream chamber
14.	13 Jan.	PG, SL-1 L* = 14 in. (35.56 cm)	X24401, S/N 001 12 weep holes (Hi Angle) Long splash ring	20.9	4.56	95.9 (66.1)	6400 (1951)	93	(3)	Upstream erosion nil Erosion at mid-chamber in line with oxidizer doublets
15.	14 Jan.	PG, SL-9 L* = 14 in. (35.56 cm)	Same, with short splash ring	15.5	3.9	93.4 (64.4)	6080 (1853)	90	(3)	Upstream erosion nil Erosion at mid-chamber in line with oxidizer doublets

TABLE V (Continued)

Run No.	Date	Configuration		Duration (sec)	O/F Ratio	P _c psia (N/cm ²)	C* fps (m/sec)	η _c (%)	Run Objectives (Note 1)	Remarks
		Chamber	Injector							
16.	15 Jan.	PG, SL-2 L* = 14 in. (35.56 cm)	X24401, S/N 002 18 weep holes Short splash ring. Biprop valve modified with blank plate	--	--	--	--	--	--	Hard start caused by defective Teflon seal at biprop blank plate
17.	16 Jan.	MRS-58 Pyrocarbide multilaminate L* = 14 in. (35.56 cm)	X24401, S/N 001 with 18 weep holes Short splash ring	60	4.27	106.9 (73.7)	6400 (1951)	94	(3)	One axial streak in line with fuel doublet (Note 2)
18.	23 Jan.	P0C0 No. 2 L* = 14 in. (35.56 cm)	X24401, S/N 001 with 18 weep holes Short splash ring	81.1	4.29	100.9 (69.6)	6300 (1920)	92.5	(3)	Erosion nil
19.	23 Jan.	P0C0 No. 2 L* = 14 in. (35.56 cm)	X24401, S/N 001 with 18 weep holes Short splash ring	6.1	--	32.4 (22.3)	--	--	(3)	Restart without engine disassembly after Run 18. Facility FLOX valve did not open.
20.	1 Feb.	Cu L* = 12 (30.48 cm)	X24401, S/N 001 Short splash 18 weep	63.7	4.10	96.4 (66.5)	6100 (1859)	89.5	(6)	Good run Throat dia. change 0.8232 to 0.8480 in. (2.0909 to 2.2555 cm)
21.	1 Feb.	Cu L* = 12 (30.48 cm)	X24401, S/N 001 Short splash 18 weep	67.5	4.43	94.9 (65.4)	6000 (1829)	87	(6)	Good run Throat dia. change 0.8480 to 0.8880 in. (2.1539 to 2.2555 cm)
22.	1 Feb.	PG/Carbitex SL-1	X24401, S/N 001 Short splash 18 weep	36.7	4.42	101.4 (69.9)	6850 (2088)	99	(3)	Good run Erosion nil

TABLE V (Continued)

Run No.	Date	Configuration		Duration (sec)	O/F Ratio	P _c psia (N/cm ²)	C* fps (m/sec)	η _c (%)	Run Objectives (Note 1)	Remarks
		Chamber	Injector							
23.	4 Feb.	POCO No. 2	X24401, S/N 002 Biprop valve blank plate	10.7	--	--	--	--	(2)	P _c tap failure
24.	6 Feb.	Cu Ch L* = 12 (30.48 cm) ε = 12	X24401, S/N 001 Short splash 18 weep	10.2	4.27	101.9 (70.3)	6400 (1951)	93	(5)	Good run Cell transient ~ 20 sec
25.	7 Feb.	PG/Carbitex SL-3 ε = 12	X24401, S/N 001 Short splash 18 weep	59.8	4.22	107.4 (74.0)	6470 (1972)	94.4	(5)	Good run Min. P _{cell} = 3.12 psia (2.15 N/cm ²) - Chamber bell failure at ~ 12 sec
26.	10 Feb.	Same without nozzle expansion	X24401, S/N 001 Short splash 18 weep	47.5	4.18	97.4 (67.2)	6350 (1935)	92.6	(3)	Good run Throat erosion rate 0.221 mil/sec (0.00561 cm/sec)
27.	10 Feb.	Same without nozzle expansion	X24401, S/N 001 Short splash 18 weep	59.5	4.23	96.4 (66.5)	6500 (1981)	94.9	(3)	Good run
28.	11 Feb.	Same without nozzle expansion	X24401, S/N 001 Short splash 18 weep	71.3	4.67	98.4 (67.8)	6690 (2039)	96.5	(3)	Good run Throat erosion rate 0.129 mil/sec (0.00328 cm/sec)
29.	11 Feb.	Same without nozzle expansion	X24401, S/N 001 Short splash 18 weep	68.2	4.50	92.4 (63.7)	6500 (1981)	94.3	(3)	Good run
30.	11 Feb.	Same without nozzle expansion	X24401, S/N 001 Short splash 18 weep	15.7	--	--	--	--	(3)	Chamber failed at throat

TABLE V (Continued)

TOTAL ACCUMULATED RUN TIME:

1. Test Phase I	213.4 sec
2. Test Phase II	862.7 sec
3. Total Time on One Injector (Phase II) (X24401, Mod. S/N 001)	852.0 sec
4. Total Time on One Chamber (Phase II) (PG/Carbitex SL-3)	322.0 sec

Notes:

1. Run objectives: (1) = Ignition, (2) = Performance, (3) = Streaking and life, (4) = Facility check, (5) Altitude test, (6) Film conduction cooling investigation
2. Caused by misaligned film jet, which occurred when low angle weeper jets were reopened from 12 weeper configuration.
3. All data points taken at stabilized conditions 6 to 16 seconds from engine ignition
4. Oxidizer: FLOX - 82.5% LF_2 /17.5% LO_2 (by weight)
Fuel: Methane (LCH_4)

TABLE VI

SUMMARY OF AVERAGE THRUST CHAMBER THROAT EROSION DATA,
PHASE II TESTS -- DECEMBER 1968 TO FEBRUARY 1969

Chamber Type	Chamber Number	Run Number	Run Duration sec	Throat Diameter Before Run in. (cm)	Throat Diameter After Run in. (cm)	Erosion Rate mil/sec (cm/sec)
Copper, L* = 12 in. = 30.48 cm	--	20	63.7	0.8232 (2.0909)	0.8428 (2.1407)	0.154 (0.000391)
Copper, L* = 12 in. = 30.48 cm	--	21	67.5	0.8428 (2.1407)	0.8845 (2.2466)	0.309 (0.000785)
POCO Graphite	POCO 2	10, 11, 18	180 ⁽¹⁾	0.8188 (2.0798)	0.8150 (2.0701)	0 (0)
PG Streak	SL 11	13	22.9	0.8258 (2.0975)	0.8278 (2.1026)	0.044 (0.000712)
PG Streak	SL 1	14	20.	0.8345 (2.1196)	0.8440 (2.1428)	0.238 (0.000605)
PG Streak	SL 9	15	15.	0.8277 (2.1024)	0.8365 (2.1247)	0.25 (0.000635)
Multilamina	MRS 58	17	60.	0.7907 (2.0084)	0.8135 (2.0663)	0.19 (0.000482)
PG/Carbitex	Carbitex SL-1	22	40.	0.8553 (2.1724)	0.8572 (2.1773)	0.024 (0.000061)
PG/Carbitex/ RPG Altitude	Carbitex SL-3	25	59.8	0.8042 (2.0427)	0.8333 (2.1166)	0.243 (0.000617)
PG/Carbitex/ RPG Altitude	Carbitex SL-3	26, 27	107. ⁽²⁾	0.8333 (2.1166)	0.8609 (2.1867)	0.129 (0.000328)
PG/Carbitex/ RPG Altitude	Carbitex SL-3	28, 29, 30	155.2 ⁽³⁾	0.8609 (2.1867)	0.906 ⁽⁴⁾ (2.3012)	0.145 ⁽⁴⁾ (0.000368)

NOTES:

- (1) Run 10 (30 sec), Run 11 (60 sec), Run 18 (90 sec)
- (2) Run 26 (47.5 sec), Run 27 (59.5 sec)
- (3) Run 28 (71.3 sec), Run 29 (68.2 sec), Run 30 (15.7 sec)
- (4) Hole burned in vicinity of throat

TABLE VII

EXTENDED RANGE FILM TEMPERATURE DATA, PHASE II TESTS

Run No.	Max. Temp.		Run Duration sec	Chamber	Remarks
	°F	(°K)			
11	2760	(1789)	65	POCO No. 2	Measurement taken at internal surface of exit
13	2730	(1772)	22.9	FG SL-11	External surface at throat
14	2880	(1855)	20.9	FG SL-1	External surface at throat
17	3150	(2005)	60	Pyrocarbide Multilaminar MRS-58	External surface at throat (See Note 1)
18	2700	(1755)	81.1	POCO No. 2	Same as Run 11

NOTES:

1. Temperature measurement questionable due to fogging of camera window.
2. Tests of the 100-pound FLOX/Methane engine.

APPENDIX A

INJECTOR DESIGN CRITERIA FOR
HYPERGOLIC BIPROPELLANT ROCKET THRUSTORS

By R. J. FioRito

This page intentionally left blank

APPENDIX A

INJECTOR DESIGN CRITERIA FOR HYPERGOLIC BI-PROPELLANT ROCKET THRUSTORS

By R. J. Fiorito

SECTION A-I INTRODUCTION

The information contained in this Appendix A is presented for the purpose of delineating the more important considerations in the design of the injector system for space restartable bipropellant rocket engines. A large body of substantiating data now exists for earth storable (noncryogenic) hypergolic propellants and work is increasing in evaluating similar design criteria for the higher performing, space storable (fluorinated) propellants.

SECTION A-II SUMMARY

This presentation includes brief discussions and substantiating data charts from Marquardt and industry investigations of the following important design considerations: Space ignition, Propellant mixing, Hypergolic stream separation, Atomization and distribution, Film cooling, and Combustion stability.

The important factors affecting both the pulsing and steady state characteristics of injectors for hypergolic space thrusters are summarized in Table A-I.

SECTION A-III INJECTOR/COMBUSTOR MODEL

A model of an idealized injector and its resultant combustion zone is shown in Figure A-1. Primary combustion is initiated by the injection elements which provide the required mixing, atomization, and mixture ratio profile (O/F ratio distribution). A fuel-rich mixture ratio is provided at the injector periphery by injection and by film formation on the internal walls of the chamber. Depending on the propellant system and chamber material system, the primary combustion core is O/F ratio-profiled to react the film propellant to achieve maximum C* performance.

SECTION A-IV DESIGN CONSIDERATIONS

A. Space Ignition

Ignition transient studies by Marquardt and other investigators of storable hypergolic propellants have indicated the possibility that the observed large ignition overpressures might be related to the high energy accumulations of propellant residues on the internal surfaces of the chamber. Similar possibilities exist with the fluorinated space storable propellants and ignition studies are continuing in this area. Propellant deposits are materially influenced by the following considerations:

1. Ignition delay
2. Propellant thermodynamic properties -- Evaporation rates and condensed phase constituents
3. Injection characteristics
 - a. Uniform liquid phase mixing
 - b. Propellant synchronization
 - c. Dribble volume (Injector emptying and filling time)
4. Temperature of chamber walls
5. Engine duty cycle -- It is desirable to operate in a temperature-duty cycle regime which prevents accumulation of residual propellants between ignition cycles.

Marquardt has developed a pulse operation model computer program to study the effect of ignition delay, initial combustor wall temperature, and pulsing duty cycle on the amount of propellant which can be collected on the walls of the combustor. This computer program accounts for the thermodynamic heat balance influencing combustor wall temperature and the mass rates of propellant accumulated during any pulse train. Extensive ignition testing using specialized dynamic measurement techniques (pressure, accelerometers, temperature, and ultra-high speed photography of the ignition process) have demonstrated the usefulness of the analytical pulse operation model in predicting ignition overpressures. More detailed information regarding this program is presented in Reference A-I.

B. Propellant Mixing Criteria

A mixing excellence parameter (E_m) for bipropellant rocket engines has been developed by Jack Rupe of JPL. This parameter permits quantitative characterization of an injector from nonreactive fluid spray testing. A

correlation of the cold flow mixing parameter with engine firing specific impulse performance is shown in Figures A-2 and A-3. The data of Figure A-2 were developed using two types of injection elements in multi-element injectors for $\text{ClF}_5/\text{N}_2\text{H}_4$ propellants. Figure A-3 shows the effect of mixing excellence upon C^* efficiency for a 100-pound thrust, multi-like doublet injector with FLOX/Methane propellants.

Rupe also developed a cold flow mixing factor for unlike impinging jet type injection elements which serves as an aid in the design and sizing of injection elements. The relationship of the Rupe parameter to the mixing excellence factor is shown in Figure A-4. It is seen that optimal mixing for a given injector element (in this case a doublet) is obtained at a Rupe parameter value of 0.5. Similar relationships hold for other injection elements such as triplets, quadruplets, etc.

C. Hypergolic Stream Separation

Evidence has been found by various investigators which leads to the belief that when two streams of highly reactive propellants impinge the sudden release of gaseous products at the impingement interface can drive the streams apart and prevent adequate mixing.

Analytical models have been formulated for the quantizing of this effect for the earth storable propellants and additional work is being conducted in evaluating this effect for the fluorinated space storable combinations.

The salient results of the analytical studies are shown in Figure A-5. This graph presents a map of regions where stream separation can occur in terms of propellant reactivity (reaction rates) and stream contact time which is a function of injection geometry. The analysis of Figure A-5 applies to the $\text{N}_2\text{O}_4/\text{N}_2\text{H}_4$ propellant combination and tends to show that the region of no stream separation occurs for higher injection velocity and smaller jet diameters. Also, stream separation is more likely to occur at conditions fostering higher reaction rates such as increased chamber pressure and propellant injection temperature. Additional details on this subject are presented in Reference A-2.

D. Atomization and Distribution Criteria

The effect of propellant atomization on combustion performance is shown in Figure A-6. Firing specific impulse performance is related to a mean propellant droplet size D_{30} as defined by the empirical equation developed by Ingebo for impinging streams of fluid. It is seen that the mean droplet diameter is influenced by injection diameter and velocity. The combustion performance with the hypergolic propellant combination improves with decreasing droplet size. Figure A-7 shows firing data for various injector types related to the sizing and interaction of injection elements. It is seen that improved thruster performance is attained with decreasing mass flow per injection element (or increased number of elements for a given overall propellant mass flow rate).

Figure A-8 illustrates a common situation in practical injector design relating to the influence upon propellant distribution within the combustor by the manifolding system which delivers propellant to the injection elements. Figure A-8 shows the distribution variation in an eight unlike-doublet engine which can lead to sizeable variation from one doublet to another of the important mixing parameters.

E. Film Cooling Performance

Chamber thermal and chemical protection through boundary layer film control has been shown to be a practical approach to small hypergolic thruster design. The cooling and protective film is produced by direct injection of one of the propellants having the more desirable thermal and chemical properties (usually fuel) into the chamber boundary layer. The effectiveness of this method depends upon:

1. The effective conversion of the jet to a liquid film which uniformly covers the chamber wall with minimum momentum and mass losses
2. The retention of the liquid film mass by the chamber wall to maximize the heat sink capability

An example of the advancements in film cooling technology is shown in Figure A-9. This chart shows the effect of improved film cooling techniques with the N_2O_4 /Aerozine 50 propellant combination upon maximum chamber wall temperature and specific impulse performance. These data apply to radiation refractory metal combustors.

This development was aided by a film cooling model computer program which permits the theoretical evaluation of film cooling effectiveness in terms of chamber wall temperatures and combustion efficiency. Empirical data substantiation of the computer analysis has been obtained with the higher energy fluorinated propellant combinations as shown in Figures A-10 and A-11.

Additional film cooling performance information is presented in Reference A-3.

F. Combustion Stability

High performance rocket combustors designed for extremely high heat release and gas flow per unit chamber volume are subject to three basic types of combustion induced instabilities. The three types of combustion instability are:

1. Low frequency "chugging" in which the interaction is between the feed system and the combustion chamber pressures. The characteristic frequencies are 100 cps (100 Hz) or less.

2. Intermediate frequency instabilities occur at or near the injector face. This type of instability can critically affect injection mixture ratio and propellant mass distribution, but does not result in the severe heat transfer rates associated with the third instability type. The frequency range is in the hundreds of cycles per second.
3. High frequency acoustic instability in which the interaction is between the combustion process as influenced by injection parameters, propellant chemical kinetics, and the chamber geometry.

The latter type of instability can be the most harmful to the chamber structure by imposing severely abnormal local heat transfer rates. The high frequency acoustic instability may consist of longitudinal or transverse modes. The transverse mode may incorporate tangential, radial, or mixed type oscillations. The frequency range for this type of instability can vary from 500 Hz to 20K Hz depending upon the size of the chamber. For small (1 inch (2.54 cm) or less) diameter chambers under consideration, the first instability modes will be in the 100 Hz to 200 Hz frequency range.

The development of analytical methods to describe and predict acoustic combustion instabilities in liquid bipropellant rockets has been an extremely difficult problem. The most successful basic approach has been developed by Priem and Guentert of NASA-Lewis. The Priem instability model considers the nonlinear conservation equations (with mass addition) for two-phase flow (liquid droplets in a combustion gas stream) through an annular combustion zone of very small length (ΔZ) and thickness (ΔR).

A summary map of the tangential instability limits as derived from the Priem theory is shown in Figure A-12. The pressure amplitude ratio shown is the pressure disturbance required to initiate sustained instability.

It is seen that as the Reynolds number of the droplet (or droplet size) decreases, the combustion stability improves. Also, minimum stability exists for constant droplet Reynolds numbers between burning rate parameter values of approximately 0.1 to 1.0. The burning rate parameter is a function of chamber diameter, contraction ratio, and fraction of total propellant vaporized per inch of chamber length. The theory also considers that the condition for maximum instability occurs at a region in which the droplet velocity is nearly equal to the combustion gas velocity. This condition exists generally within one inch (2.54 cm) of the injector face.

More detailed information regarding the combustion instability theory and correlation with experimental data is given in Reference A-4.

SECTION A-V REFERENCES

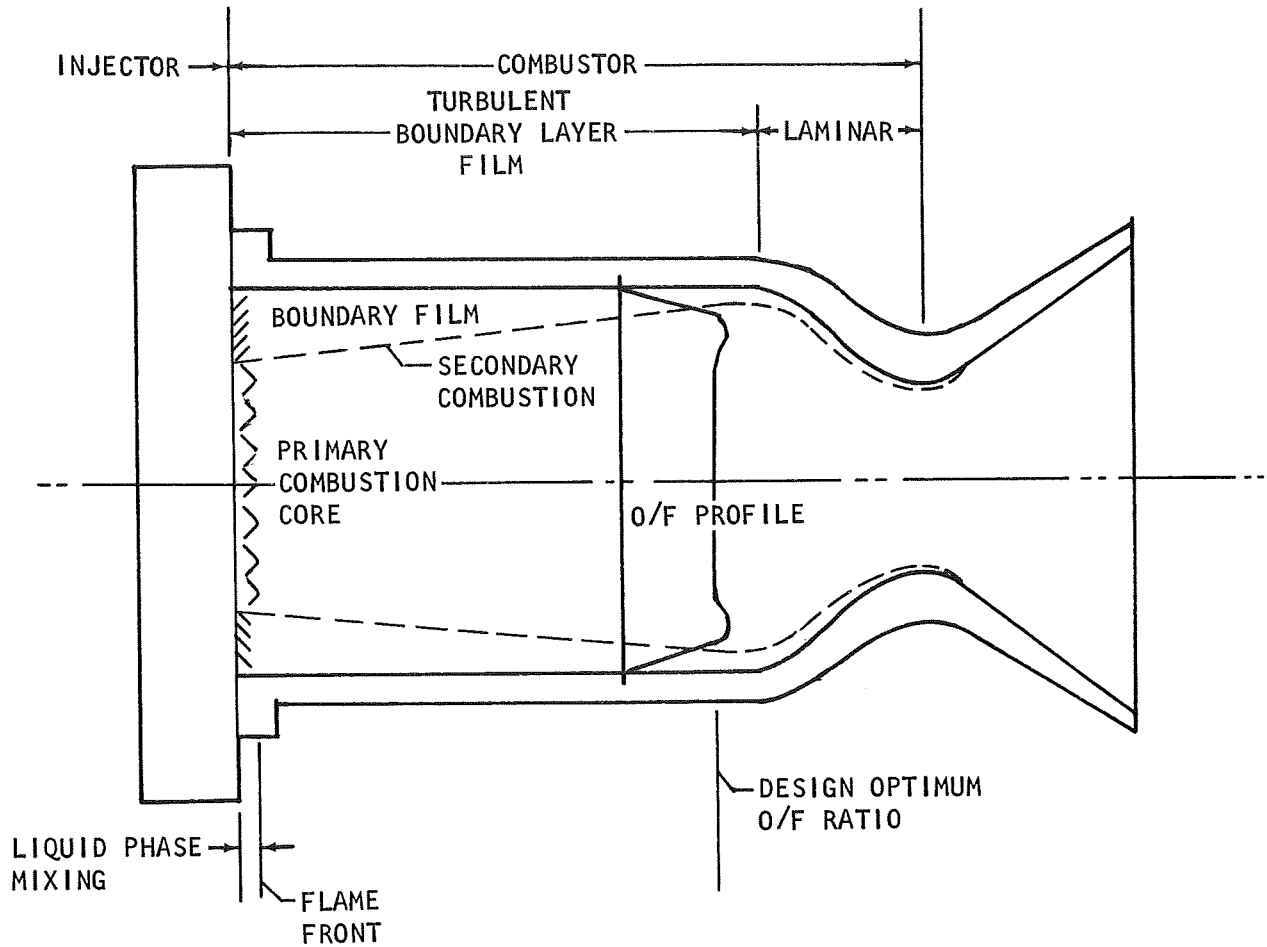
- A-1. Juran, W. and R.C. Stechman, Jr., "Ignition Transients in Small Hypergolic Rockets", AIAA Paper No. 67-515.

- A-2. Kushida, Raymond and John Houseman, "Criteria for Separation of Impinging Streams of Hypergolic Propellants", Western Section Combustion Institute, AIAA Paper No. 67-38.
- A-3. Stechman, R.C., Jr., Joelee Oberstone, and J.C. Howell, "Film Cooling Design Criteria for Small Rocket Engines", AIAA Paper No. 68-617, 4th Propulsion Joint Specialist Conference, Cleveland, Ohio, June 10-14, 1968.
- A-4. Weiss, R.R., C.J. Abbe, and C.W. McLaughlin, "Influence of Storable Propellant Liquid Rocket Design Parameters on Combustion Instability", AIAA Paper No. 67-474.

TABLE A-I

DESIGN FACTORS AFFECTING INJECTORS FOR SPACE THRUSTORS

Design Factor	Remarks
<u>Pulse Mode Operation</u>	
1. Minimal injector dribble volume and propellant injection synchronization	1. To optimize start and stop thrust transient and minimize propellant residues in chamber
2. Good liquid and vapor phase mixing. Large number of reaction sites	2. For optimal ignition reliability and minimal ignition delay
3. Optimum O/F during ignition transient	3. Influenced by system pressure dynamics and propellant valve synchronization
<u>Steady State Operation</u>	
4. Mixing	4. Optimum O/F ratio and mass distribution
5. Atomization	5. Maximum inter-propellant contact area
6. Mixture ratio profile (Film cooling)	6. Chamber wall cooling and chemical protection
7. Injector face cooling	7. Structural
8. Stream separation	8. Propellant blow apart at contact which impedes good mixing and complete combustion
9. Combustion stability	9. High frequency combustion oscillations can lead to catastrophic heat transfer rates and structural failure.



STEADY STATE PERFORMANCE MODEL
PRIMARY INFLUENCES ON PERFORMANCE

1. DISTRIBUTION OF O/F RATIO
2. ATOMIZATION
3. MASS DISTRIBUTION

FIGURE A-1. Model of Hypergolic Bipropellant Rocket Thrustor

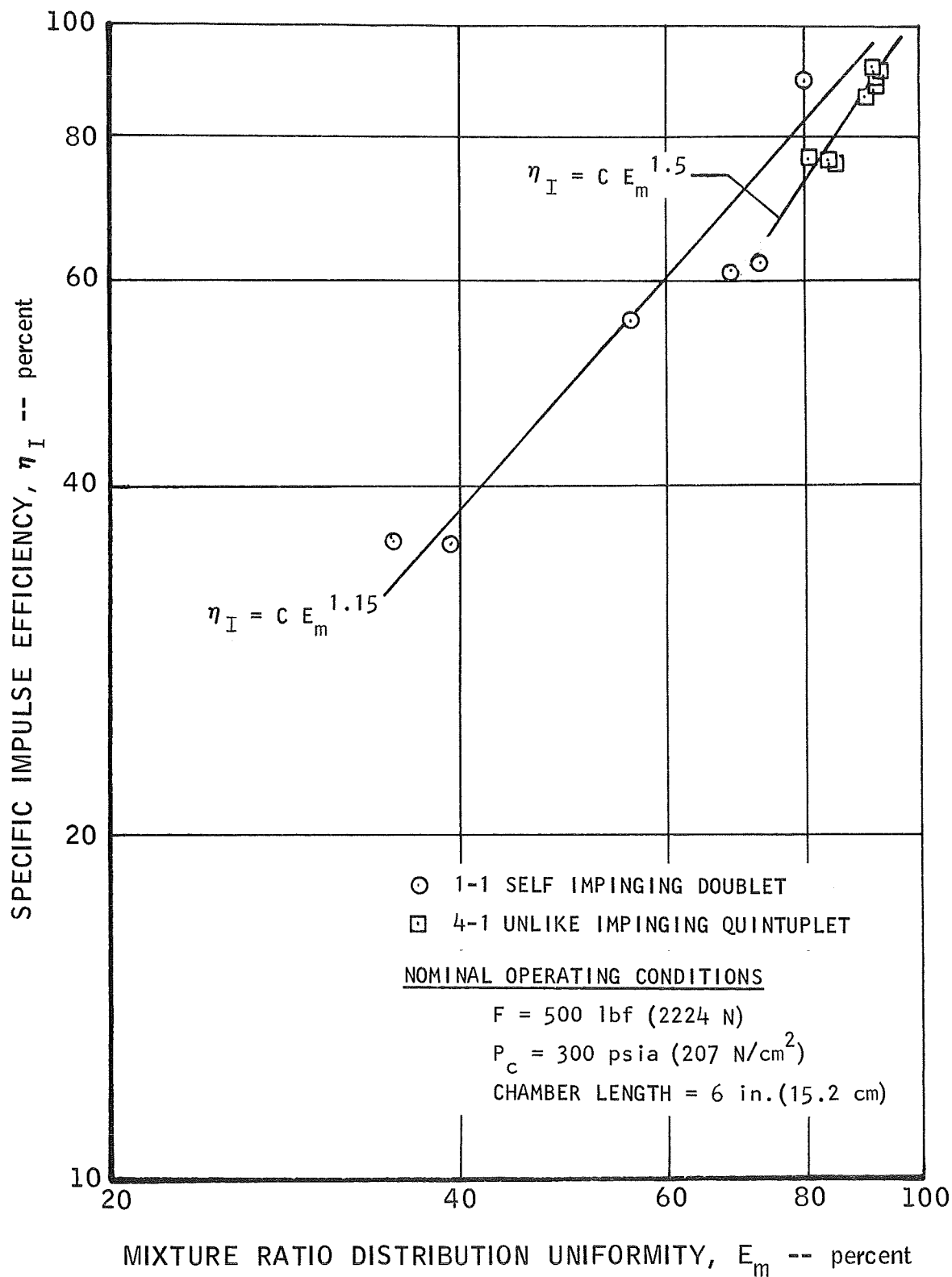


FIGURE A-2 Effect of Mixture Ratio Distribution on Specific Impulse Efficiency

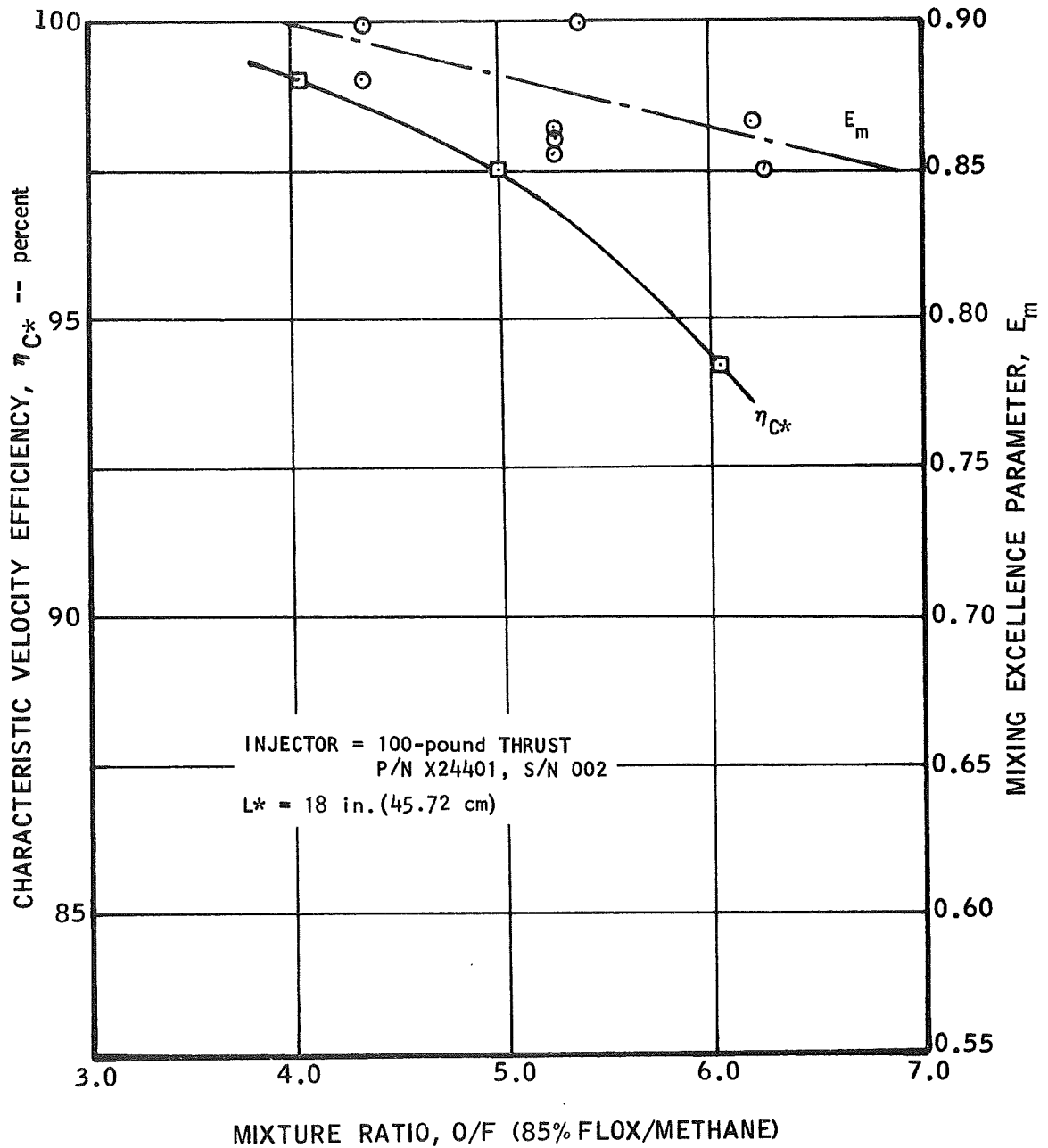


FIGURE A-3 Effect of Mixing Factor on Characteristic Velocity Efficiency

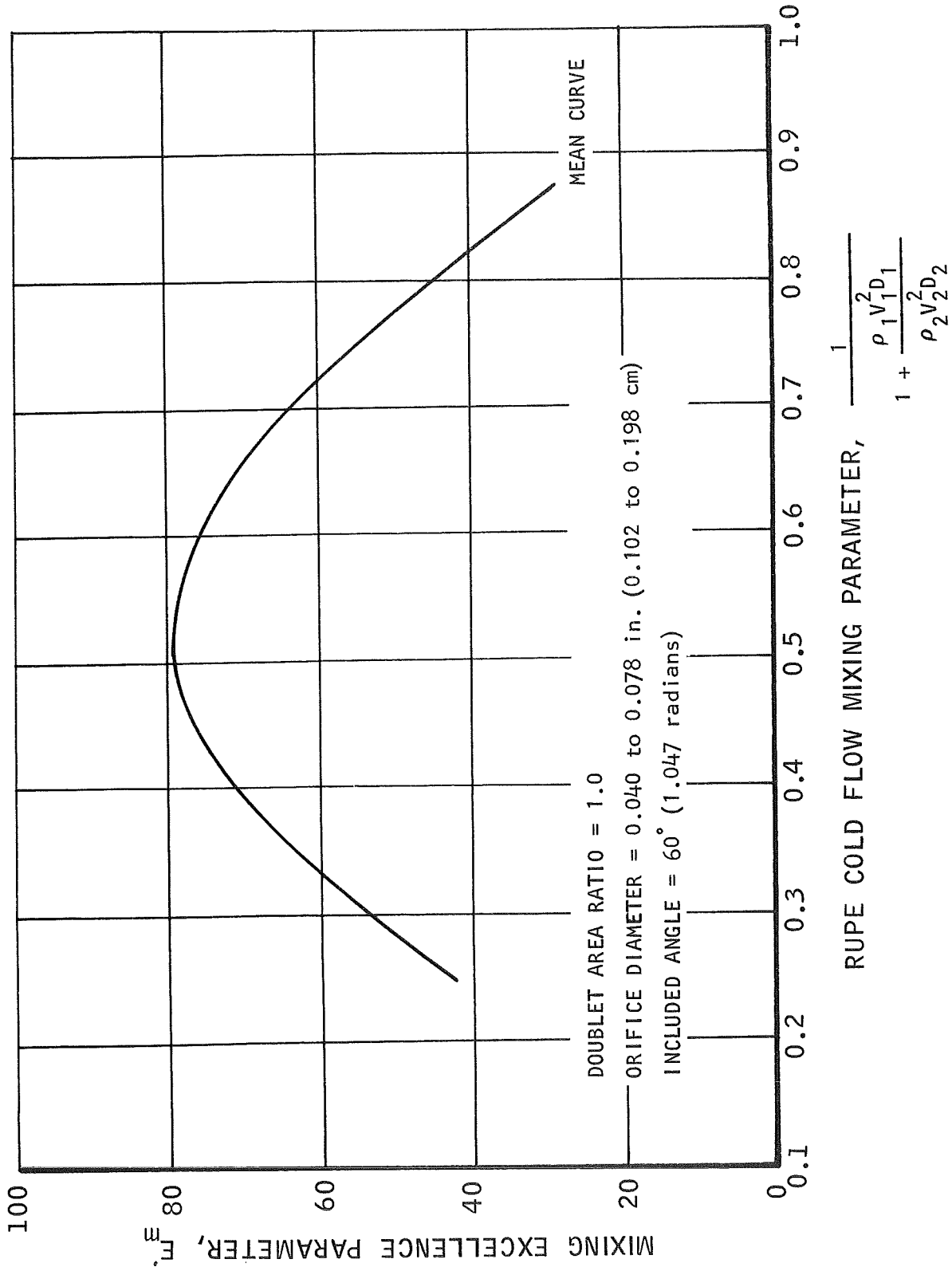


FIGURE A-4. Effect of Rupe Cold Flow Mixing Parameter on Mixing Excellence Parameter for an Impinging Doublet Injector Element

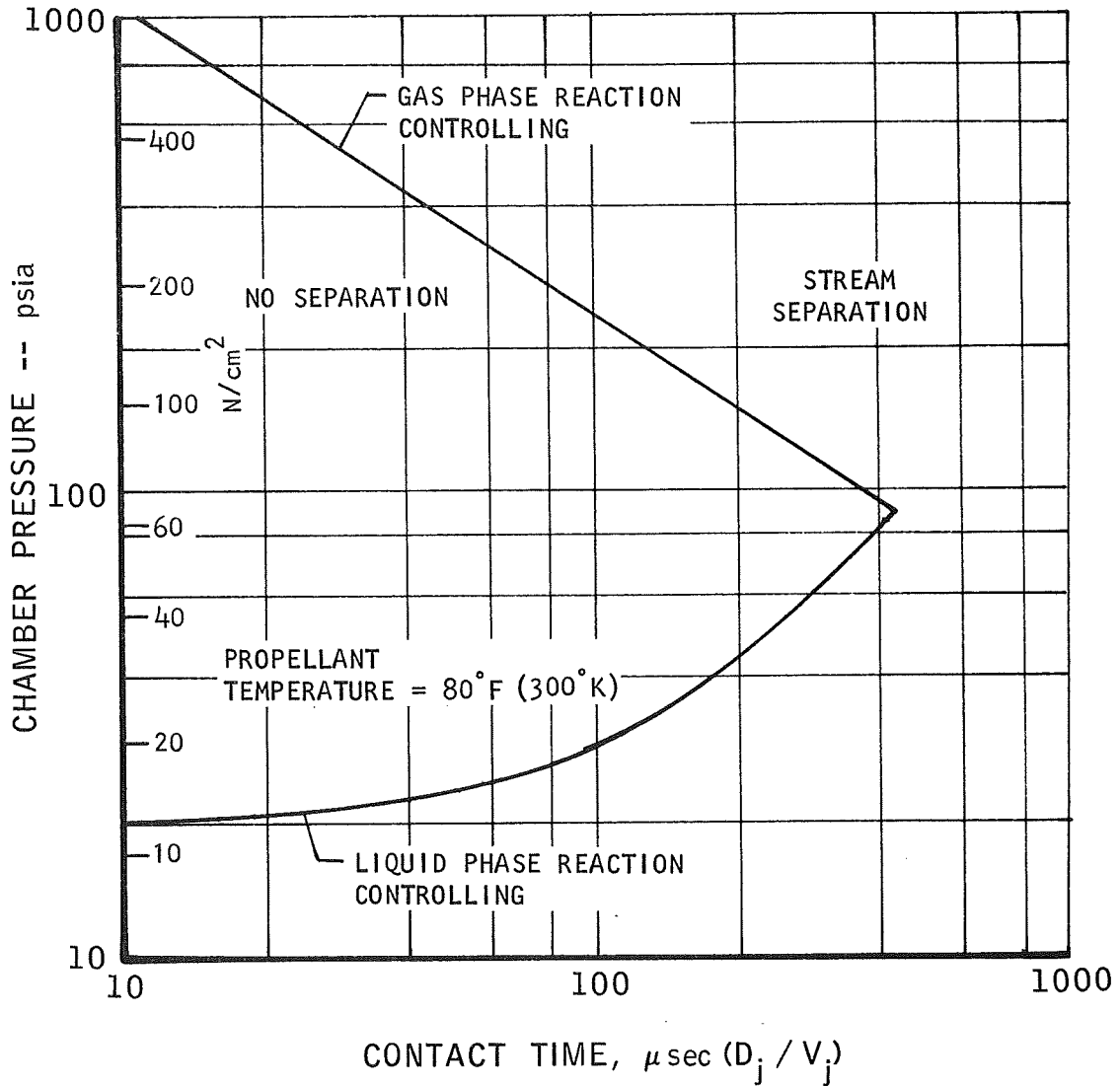


FIGURE A-5. Impinging Jet Stream Separation Criteria

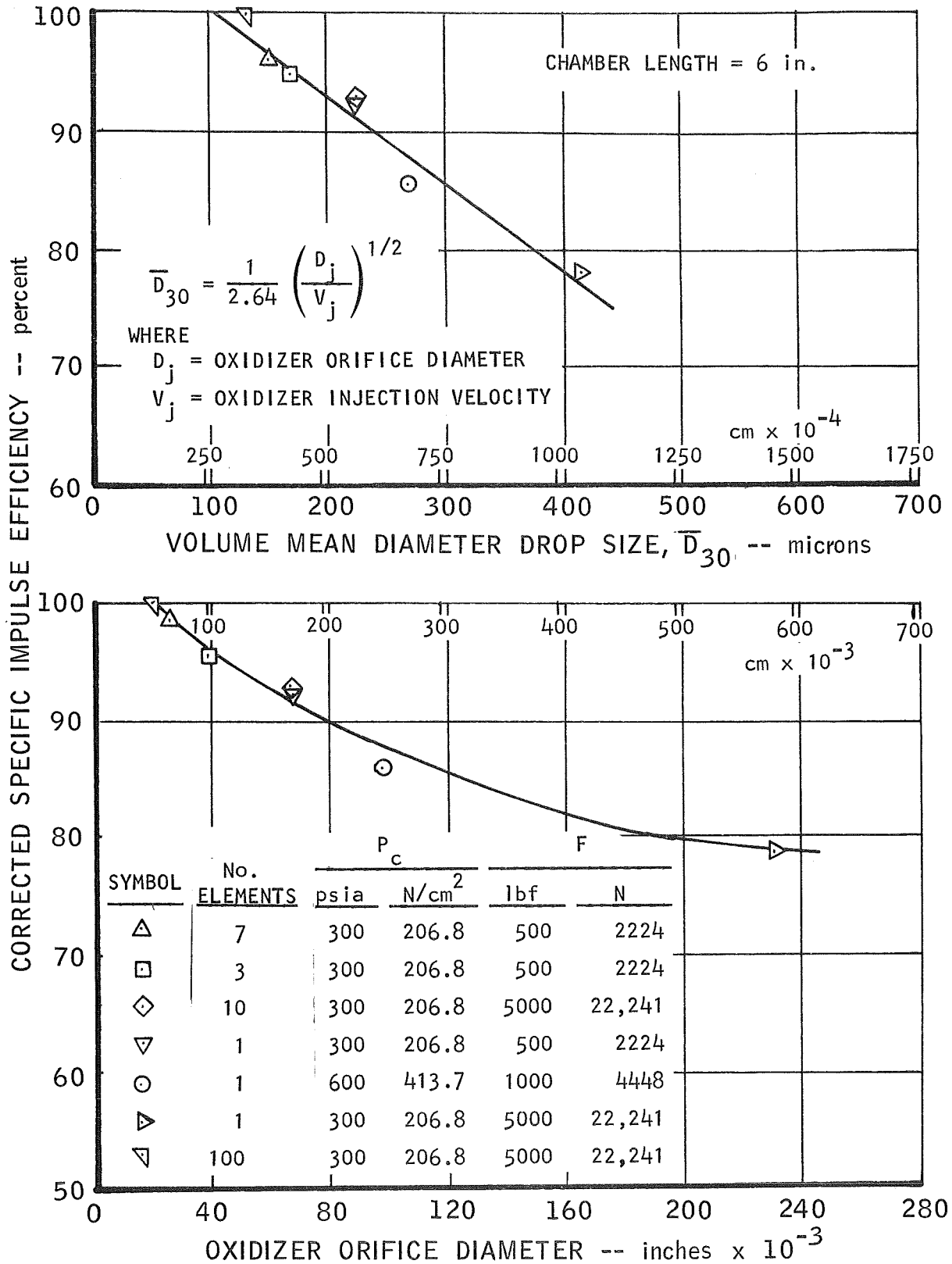


FIGURE A-6. Effect of Propellant Atomization on Combustion Performance

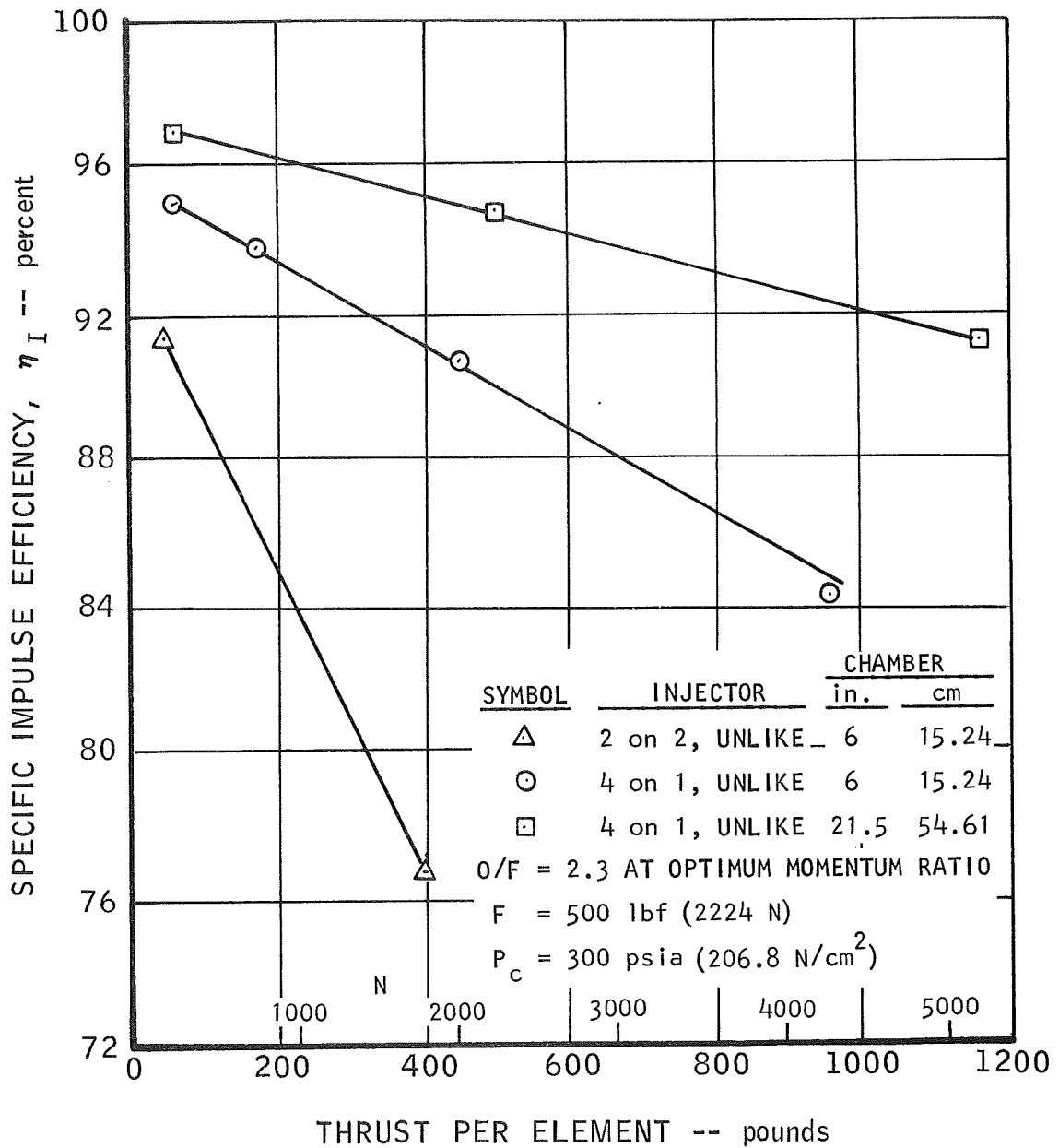


FIGURE A-7. Effect of Thrust per Injector Element on Specific Impulse Efficiency for Various Injector Types

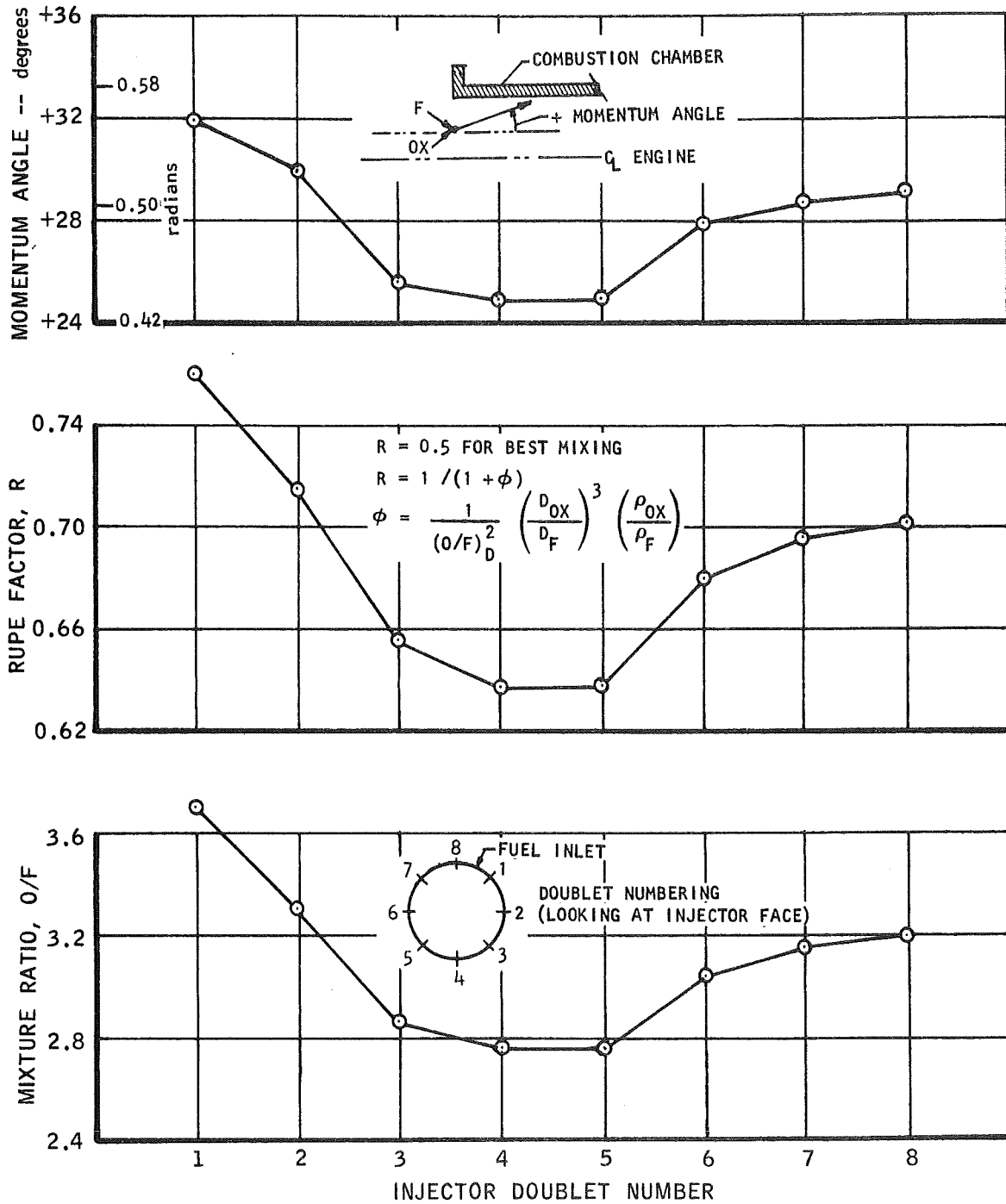


FIGURE A-8. Variation of Mixing Parameters with Doublet Location

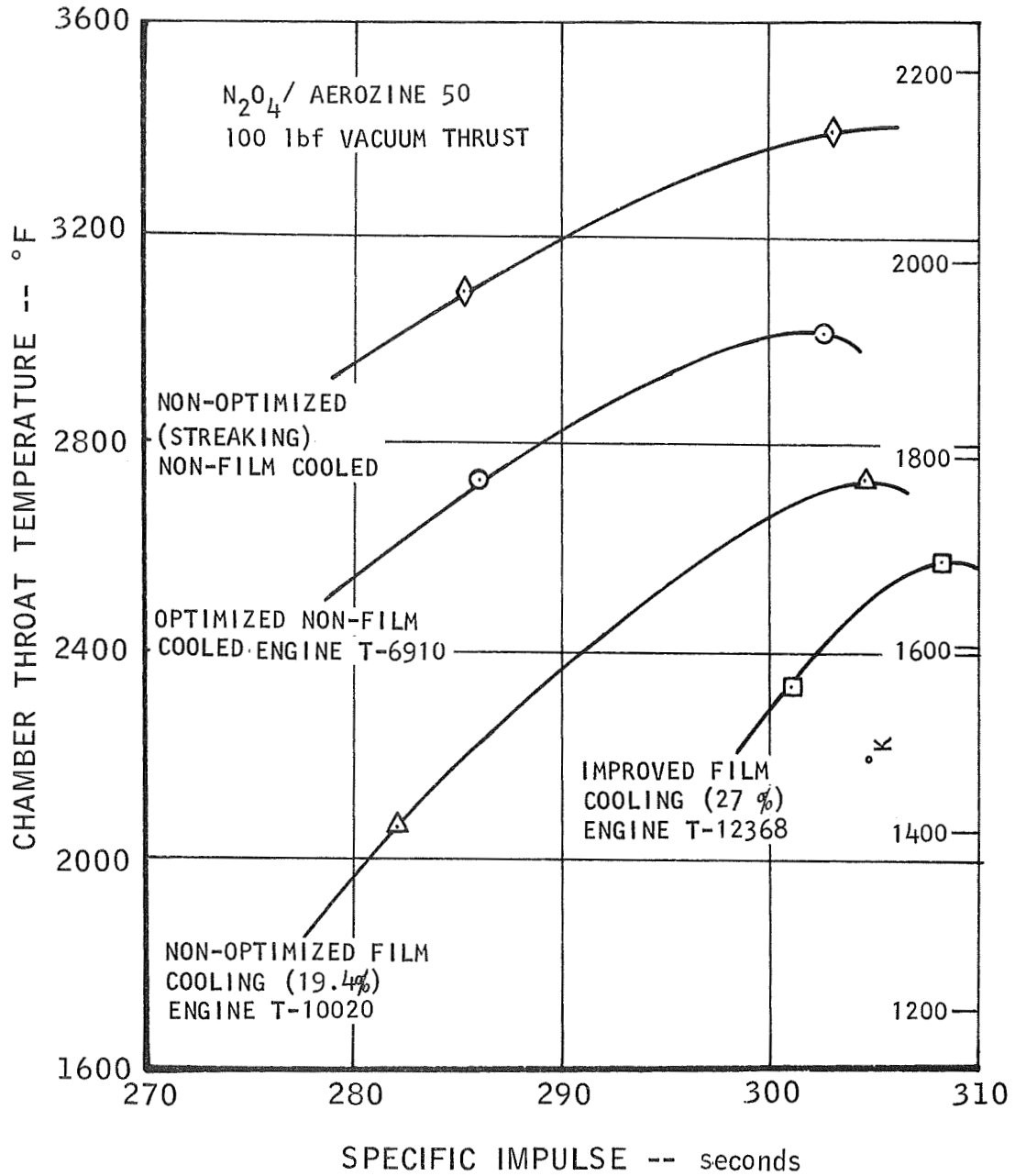


FIGURE A-9. Film Cooling Performance

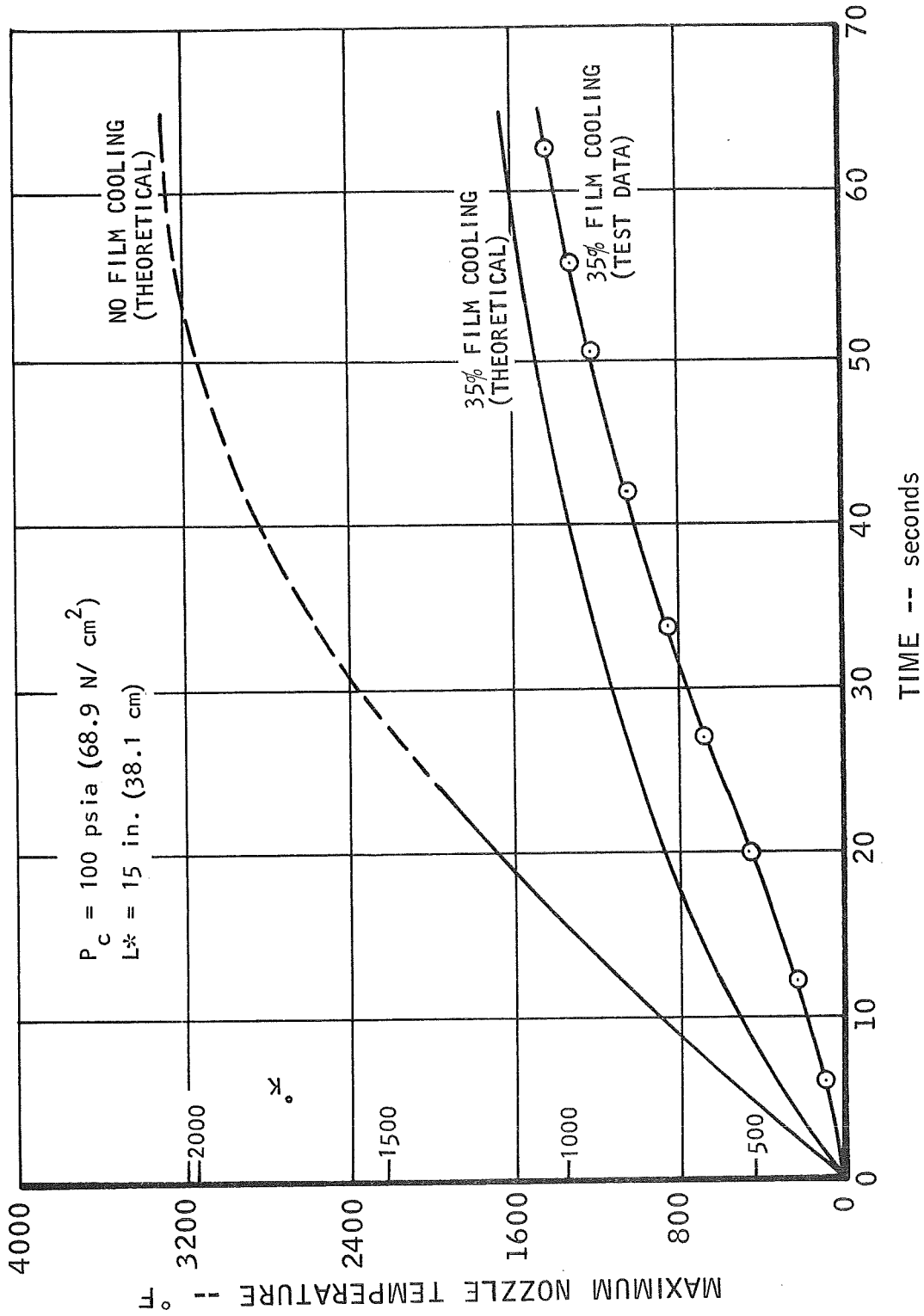
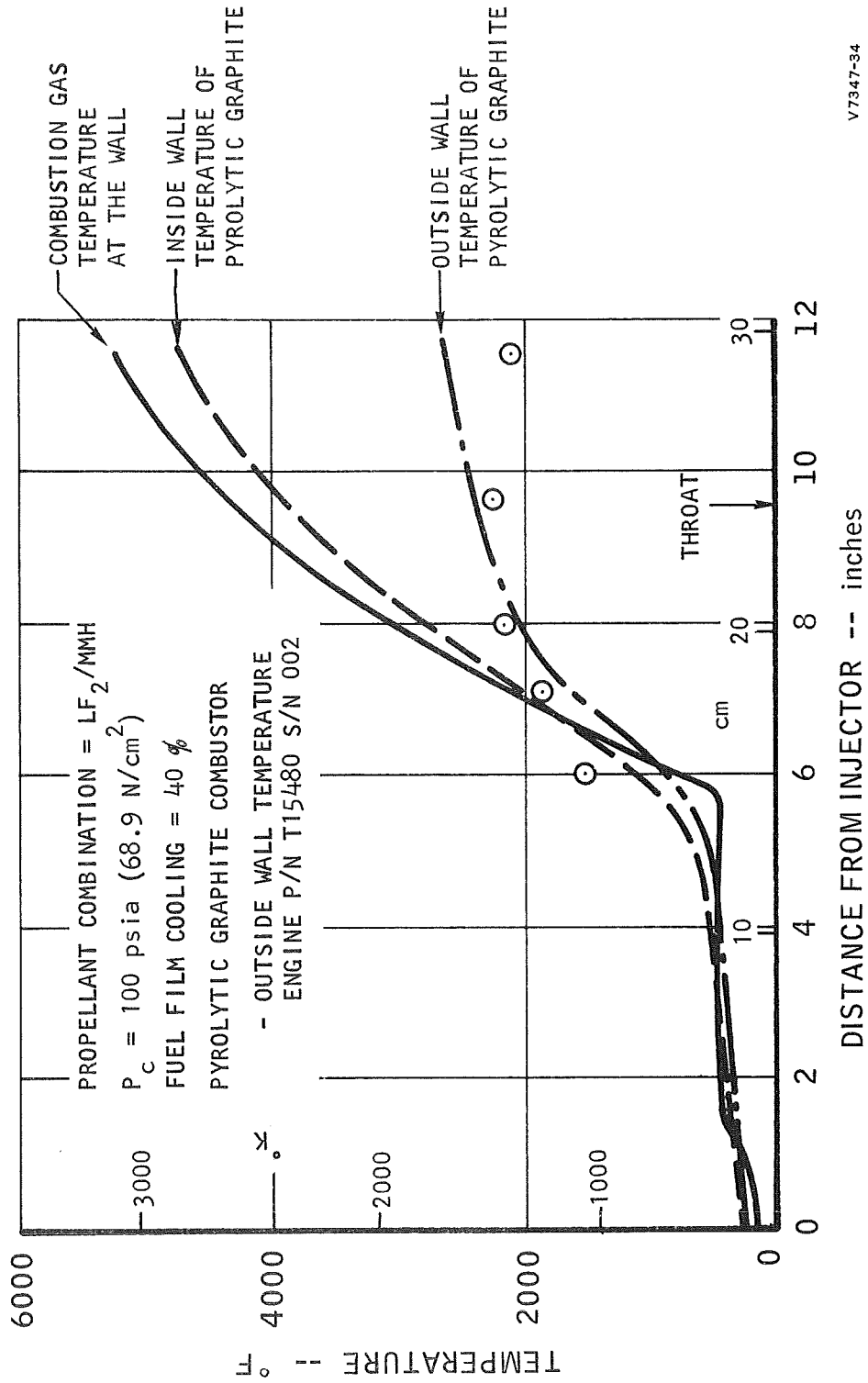


FIGURE A-10. Thermal Effects of Film Cooling, Comparison of Analytical and Test Data



V7347-34

FIGURE A-11. Temperature Characteristics of the 1000-pound Thrust Engine

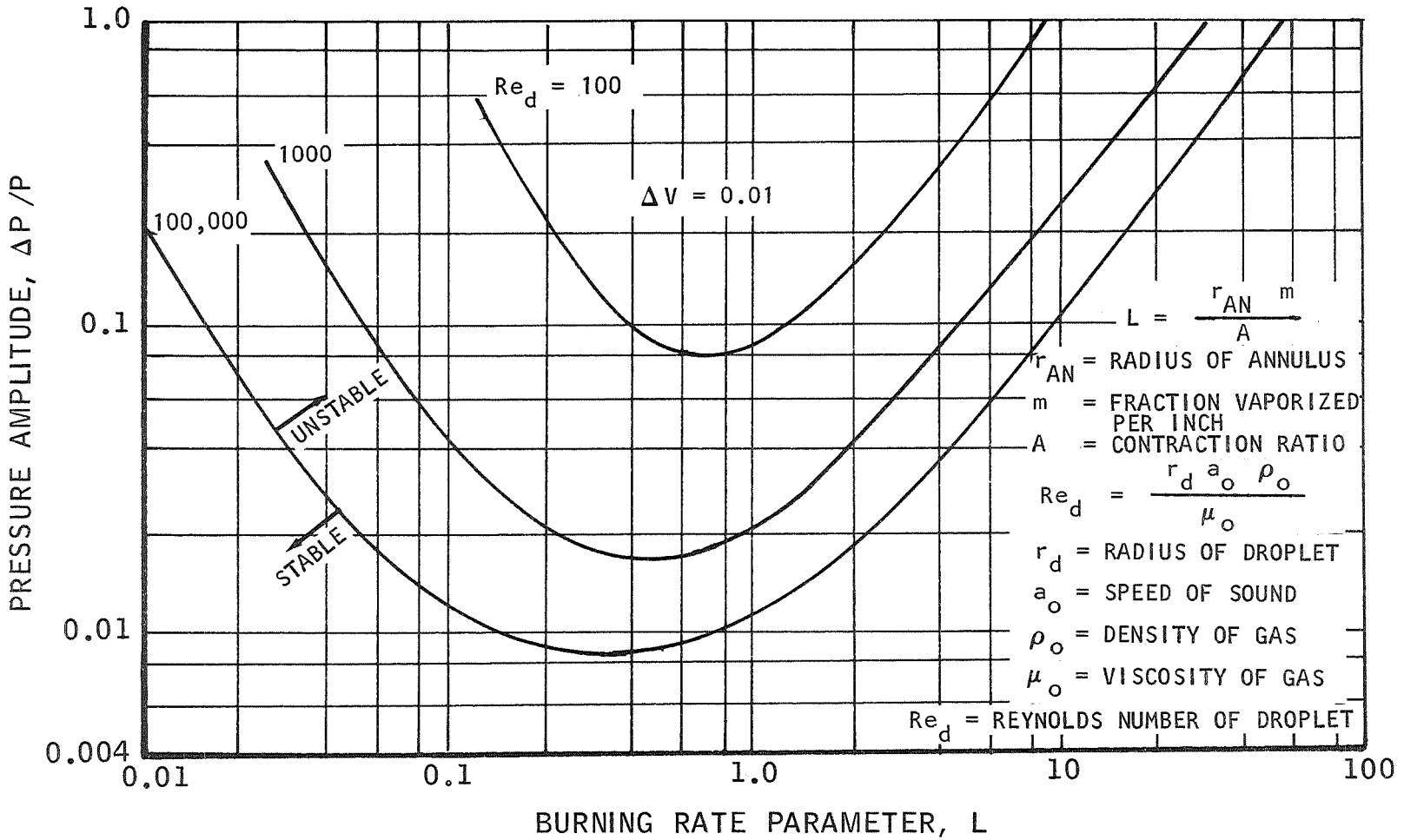


FIGURE A-12. Tangential Stability Limit Characteristics

This page intentionally left blank

APPENDIX B

STRUCTURAL PROPERTIES OF CARBITEX

This page intentionally left blank

APPENDIX B
STRUCTURAL PROPERTIES OF CARBITEX

SECTION B-I
GRADE NUMBERING SYSTEM

Carbitex is the brand designation of a family of carbon or graphite fiber base materials bonded together with carbon or graphite, exhibiting superior physical properties. Grade numbers are used to distinguish specific constructions as outlined below:

A. First Three Numbers in Grade Designations

First Number -- Fibrous Base Composition/Bond Composition

- 1 -- Carbon base/carbon bond
- 5 -- Graphite base/carbon bond
- 7 -- Graphite base/graphite bond

Second Number -- Form of Fibrous Base

- 0 -- Cloth of standard square weave
- 1 -- Yarn (all constructions)
- 2 -- Multiple base materials

Third Number -- Type of Construction

- 0 -- Layered flat construction
- 1 -- Angled construction
- 2 -- Tape wound
- 3 -- Filament wound
- 4 -- Multiple base constructions

B. Additional Letters

A through ZZZ -- Used for designation of customized grades, such as compositions containing chemical additives, having controlled porosity, density, or other physical properties.

C. Example

Grade 100 -- Carbon base/carbon bond - cloth of standard square weave - layered flat construction.

D. Carbitex Structures

Carbitex layered cloth structures are composed of standard square weave carbon or graphite cloth stacked in layers and bonded together with carbon or graphite to form a solid homogenous material. This construction is available in flat plate, rod, heavy wall tubing, solid and cored billet, and some formed shapes.

Figure B-1 illustrates typical Carbitex cones. Figures B-2 and B-3 are graphs of variations in physical properties of this material. The physical properties of standard layered cloth Carbitex are tabulated below.

PHYSICAL PROPERTIES OF STANDARD LAYERED CLOTH CARBITEX
Typical Values at 68° to 212°F

Property	Grade		
	100	500	700
Structure			
Bond Material	Carbon	Carbon	Graphite
Base Material	Carbon	Graphite	Graphite
Purity (% elemental carbon content)	99.5	99.7	99.9
Density (gm/cc)	1.38	1.40	1.44
Flexural Strength (psi)			
With grain	14,000	17,600	11,000
Compressive Strength (psi)			
With grain	8,000	10,200	7,600
Against grain	45,000	40,000	21,000
Tensile Strength (calculated psi)			
With grain	7,000	8,800	5,500
Young's Modulus (psi x 10 ⁵)			
With grain	16	27	13
Coefficient of Thermal Expansion (in./in./°F) x 10 ⁻⁷			
With grain	8.9	6.1	5.9
Against grain	8.3	14.1	18.0
Electrical Resistivity (ohm-inch)			
With grain	0.0025	0.0020	0.0006
Against grain	0.055	0.0035	0.0017
Coefficient of Thermal Conductivity (Btu/ft ² /°F/hr/ft) based on calculations from electrical resistivity			
With grain	12	--	--
Against grain	3	--	--
Scleroscope Hardness			
With grain	90	76	30
Against grain	57	59	32

(These properties do not indicate values or characteristics of other than layered cloth Carbitex structures)



9312-1

FIGURE B-1. Typical Carbitex Cones, 60° and 75° Wrap Angle

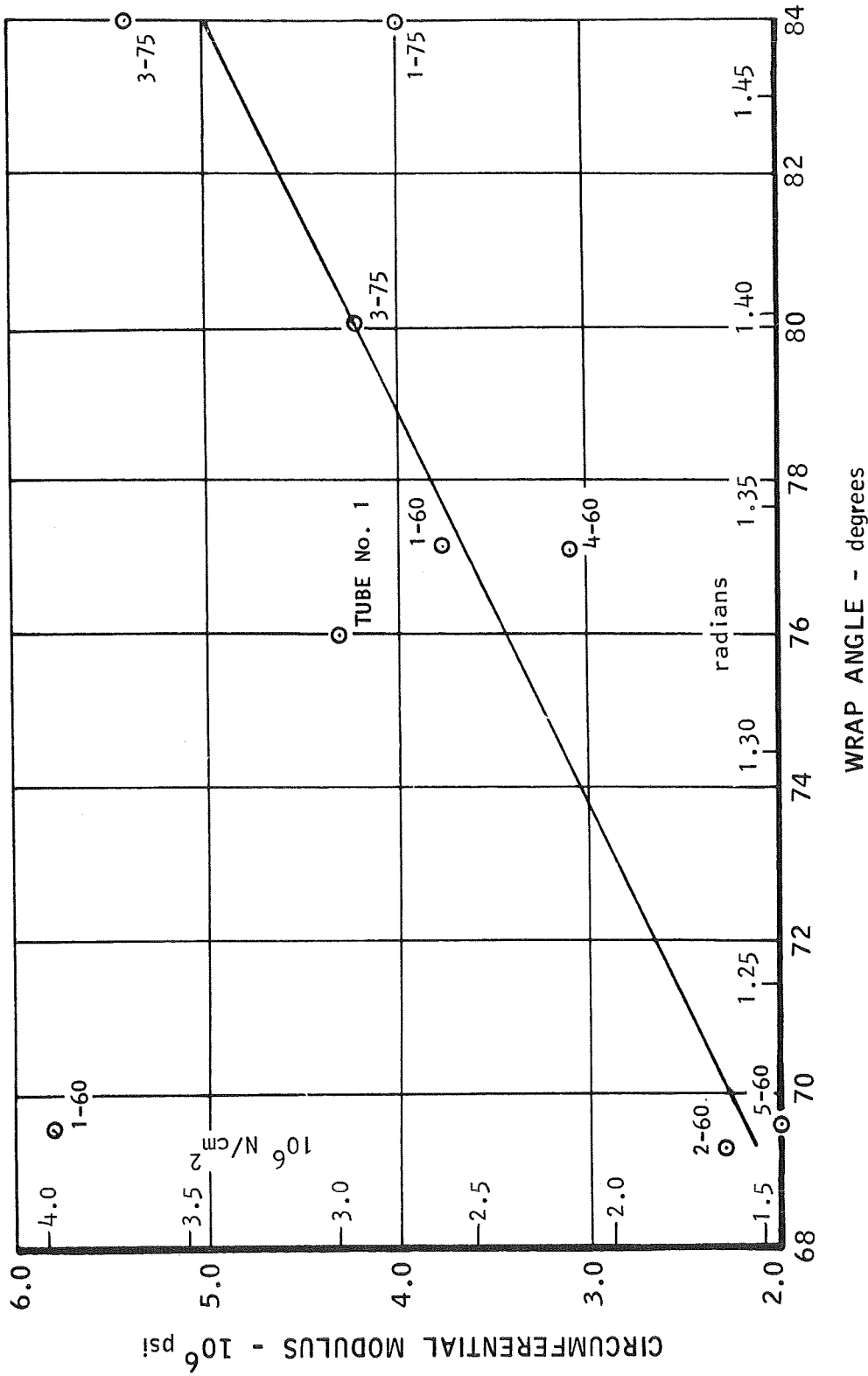


FIGURE B-2. Variation of Circumferential Modulus of Elasticity of Carbitex with Wrap Angle

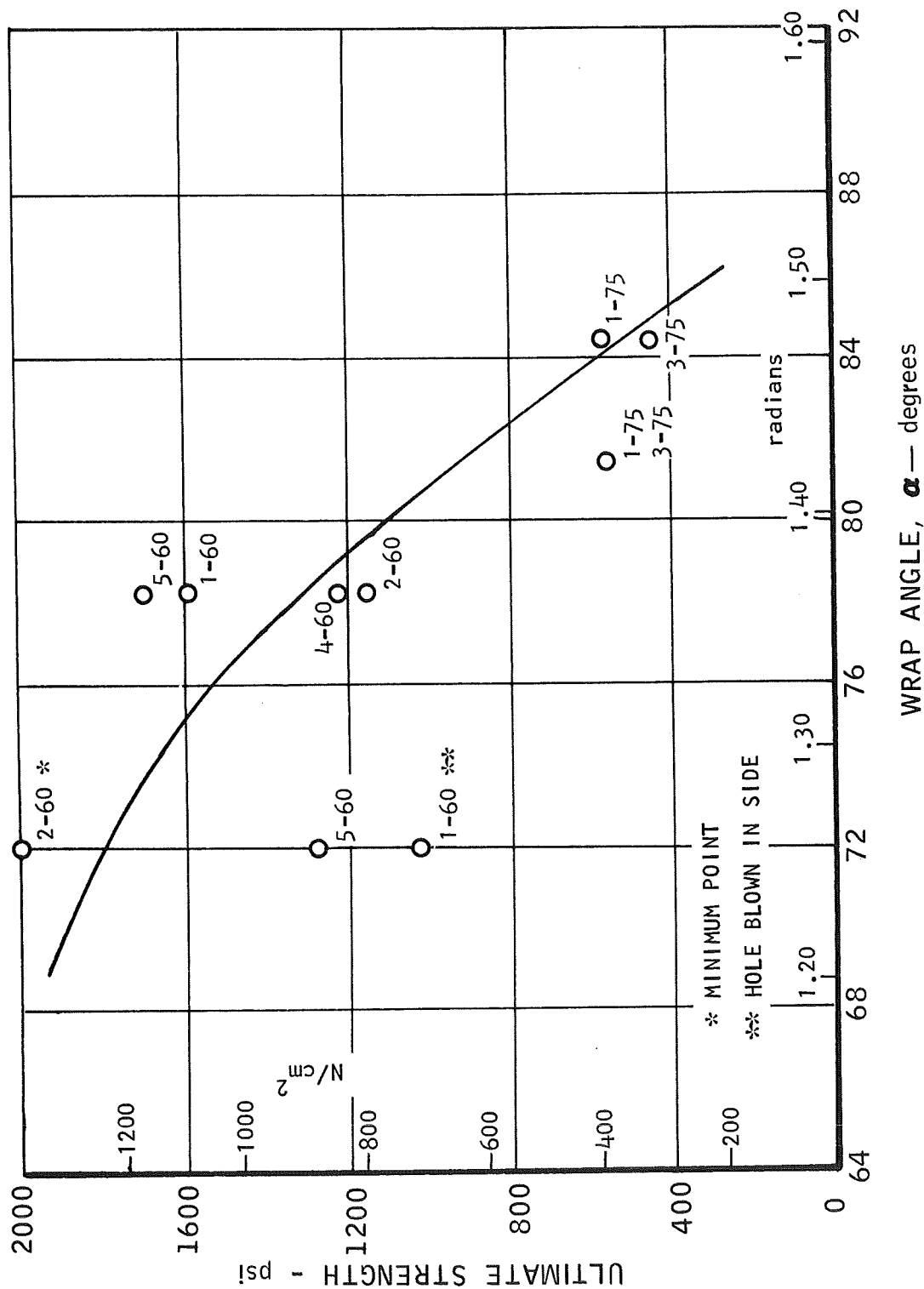


FIGURE B-3. Variation of Axial Strength of Carbitex Cones with Wrap Angle

This page intentionally left blank

APPENDIX C

BIFLUID SPRAY TESTS OF INJECTORS

By R. J. FioRito

This page intentionally left blank

APPENDIX C

BIFLUID SPRAY TESTS OF INJECTORS

By R. J. Fio Rito

This Appendix C presents the results of bifluid (water/trichlorethylene) flow characterization of the X24401 Serial No. 002 injector assembly. These bifluid spray tests were performed in the MJL Hydraulics Laboratory. A schematic diagram of the nonreactive fluid flow bench system is shown in Figure C-1. Photographs of the spray booth and a view of the injector during a test are shown in Figures C-2 and C-3.

The spray collector grid consisted of a 7 by 7 matrix of 3/8-inch (0.929 cm) ID tubes on 1/2-inch (1.27 cm) centers covering a 3 1/4-inch (8.26 cm) square (Figure C-2). The individual matrix tubes were drained to four racks of graduated collection cylinders, as shown in Figures C-4 and C-5. These photographs show the collected samples from a typical run (Run No. 13). The darker colored fluid at the top of the cylinder is dyed water which is the fuel simulant and the more dense fluid at the bottom is trichlorethylene which was used to simulate the oxidizer. It is apparent that the fluids are immiscible, thus allowing the volumetric measurement of each fluid in the collecting cylinders.

The tests were conducted by setting an inlet mixture ratio and total mass flow of the fluid simulants and collecting the flow for a timed interval. A typical run collection pattern is shown in Figure C-6. Each square of the matrix represents a collection tube and the total mass collected per tube is given with the corresponding trichlorethylene-to-water mixture ratio. The approximate zone locations of the film injection jets is also indicated. It will be noted that the mixture ratio tends to be lower in these regions.

A mixture ratio and mass profile bar graph taken from the center row cross section of the data from Run 13 (Figure C-6) is shown in Figure C-7. The profile follows the desired design contour except at the low mass flow extremities which are more subject to collection errors.

The spray run data were evaluated in terms of an empirical mixing excellence parameter (E_m) developed by J. Rupe of the Jet Propulsion Laboratory. As defined in Figure C-8, E_m is a value representing the departure of the local spray samples from the nominal inlet mixture ratio value on a percentage basis. The empirical equation accounts for the deviation of the mixture ratio from the nominal ratio as weighted by the spatial mass flow distribution of the spray. An IBM program was formulated to convert the data from the collection matrix to the E_m factor. This factor was used to compare the spray characteristics for the Serial No. 002 injector as a function of injection momentum ratio (fuel-to-oxidizer ratio). Thirteen runs were made. The results are presented in Figure C-9 and Table C-I. It is seen that the mixing factor for this injector configuration tends to increase with decreasing mixture ratio (or increasing fuel-to-oxidizer momentum ratio).

The mixing factor has been used to correlate injector combustion performance as shown in Figure C-10 using data for ClF_5/N_2H_4 injectors from Rocketdyne Report R-6028-2. The data of Figure C-10 indicate combustion efficiencies above 90% (neglecting nozzle losses) for all E_m values above 80%.

In general, the injectors meet hydraulic flow requirements with a high degree of excellence. The Serial No. 002 injector demonstrated a bifluid liquid phase mixing factor of from 86 to 90% at the design O/F (TCE/H_2O) of 3.5 and mass flows corresponding to the 100-pound thrust level.

Figure C-9 indicates the like-doublet injector element trend of increasing mixing factor with decreasing mixture ratio. The lower mixture ratios correspond to higher fuel-to-oxidizer momentum ratio which appears to produce the more optimal mixing characteristics.

Table C-II gives the pertinent properties of potential nonreactive propellant simulants.

TABLE C-I

SUMMARY OF BIFLUID SPRAY TESTS OF THE SERIAL NO. 002 INJECTOR
 100-lb Flox/LPG Injector
 X24410 S/N 002

Run No.	\dot{w}_{H_2O}		\dot{w}_{TCE}		O/F	O/F	E_m
	pps	(gm/sec)	pps	(gm/sec)	TCE/H ₂ O*	FLOX/Methane**	
6	0.1024	(46.45)	0.3607	(162.61)	3.52	5.22	0.855
7	0.1023	(46.40)	0.3607	(163.61)	3.52	5.22	0.865
8	0.1024	(46.45)	0.3607	(163.61)	3.52	5.22	0.862
9	0.0891	(40.42)	0.3722	(168.83)	4.18	6.21	0.866
10	0.0895	(40.60)	0.3765	(170.78)	4.22	6.25	0.8495
11	0.1145	(51.94)	0.3280	(148.78)	2.87	4.26	0.880
12	0.1148	(52.07)	0.3280	(148.78)	2.87	4.26	0.8988
13	0.1017	(46.13)	0.3645	(165.34)	3.59	5.33	0.901

NOTE: Runs 1 through 5 were facility and procedural check runs.

* Sp. Gr. of TCE = 1.46; Sp. Gr. of H₂O = 1.0

** Sp. Gr. of FLOX = 1.442; Sp. Gr. of Methane = 0.447

TABLE C-II
SUMMARY OF PROPERTIES OF NONREACTIVE PROPELLANT SIMULANTS

Fluid	Density		Boiling Point °F (°K)	Freezing Point °F (°K)	Surface Tension Dynes/cm	Flash Point °F (°K)	Toxicity TLV PPM	Viscosity Centipoise	Solubility	
	lb/gal (kg/m ³)	at Temp.							In. H ₂ O % by wt.	Hexane
Methane	3.68 (0.0491)	-280°F (100°K)	-159 (167)	-299 (89)	0.134	--	--	0.111	--	--
Propane	5.88 (0.1050)	-260°F (111°K)	-44 (231)	-306 (85)	--	--	--	--	--	--
82.5% Flox	12.6 (0.1050)	-300°F (89°K)	-305 (86)	-362 (54)	0.126 at -300°F (89°K)	--	--	0.218	--	--
Fuel Simulants										
Water	8.336 (0.0696)	--	212 (373)	32 (273)	72.75	None	None	1.0	100	Nil
Hexane	5.51 (0.460)	--	155 (341)	-139 (178)	18.4	-7 (251)	500*	--	0.014 at 60°F (289°K)	100
Oxidizer Simulants										
Trichlorethylene	12.22 (0.1020)	68°F (293°K)	192 362	-124 (186)	32 at 72°F (295°F)	None	100*	--	0.11 at 68°F (293°K)	--
Freon MF	12.42 (0.1037)	--	74.8 (296.9)	-168 (162)	18.7 at 70°F (294°K)	None	1000*	0.461 at 60°F (289°K)	0.14 at 68°F (293°K)	Miscible

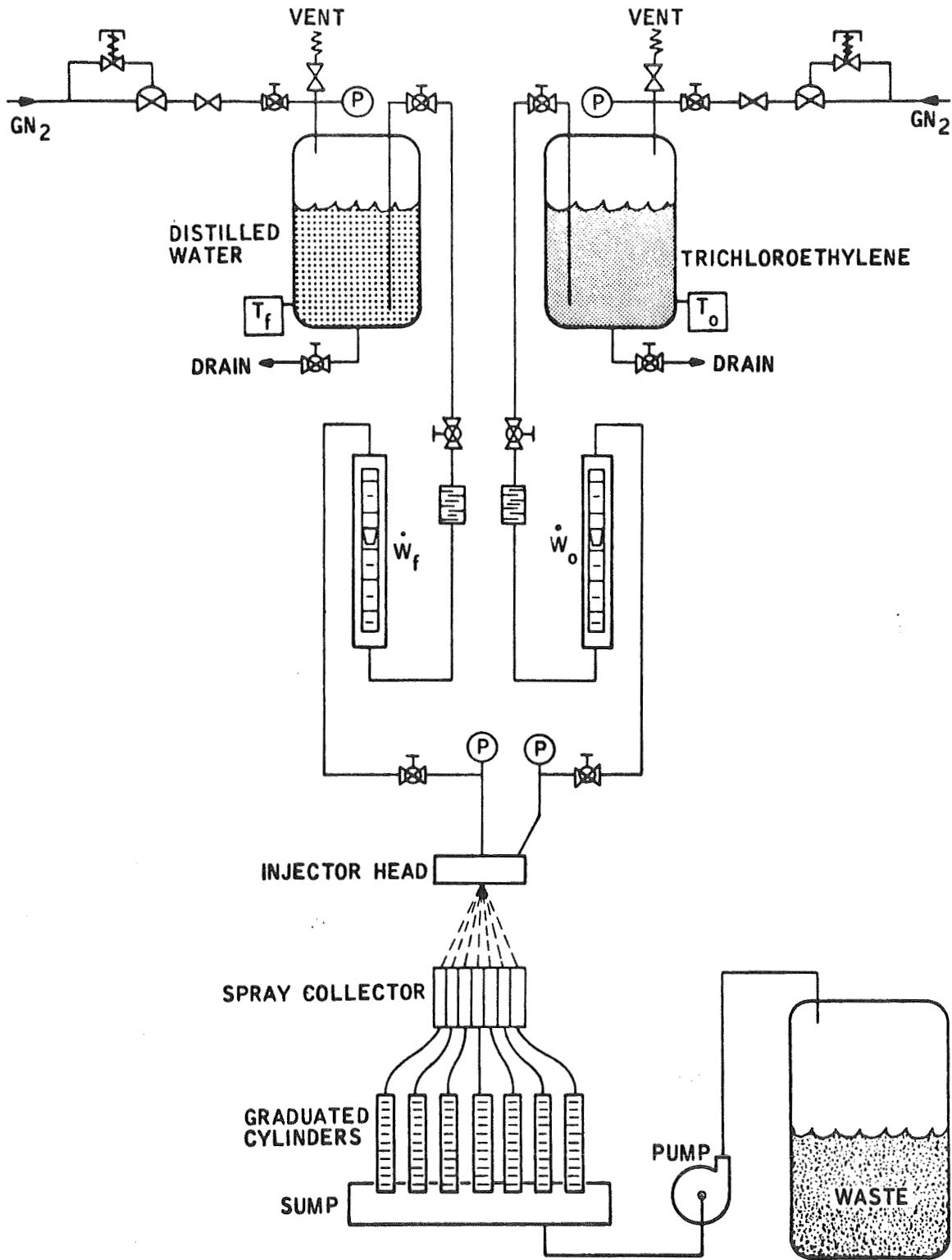
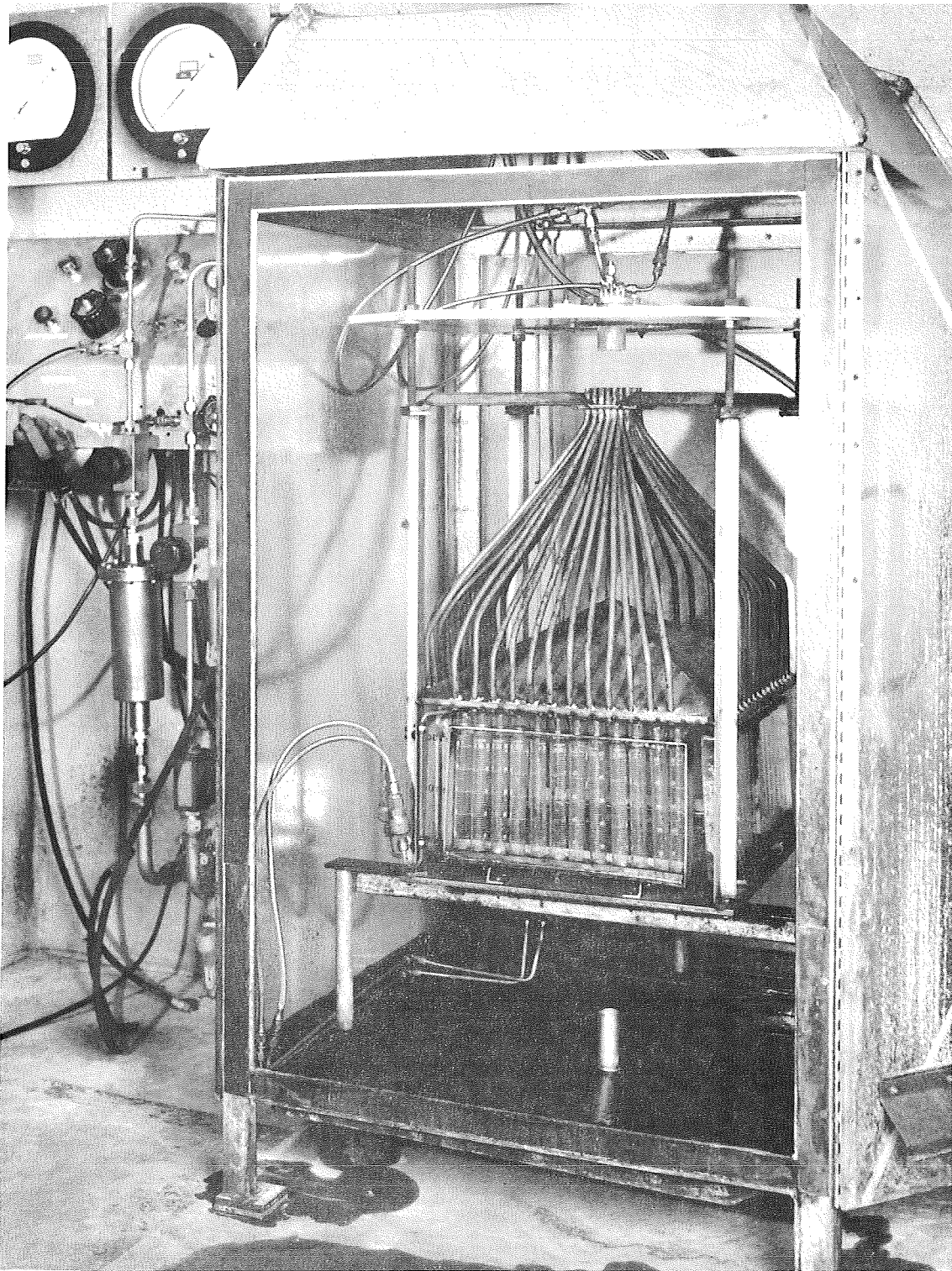
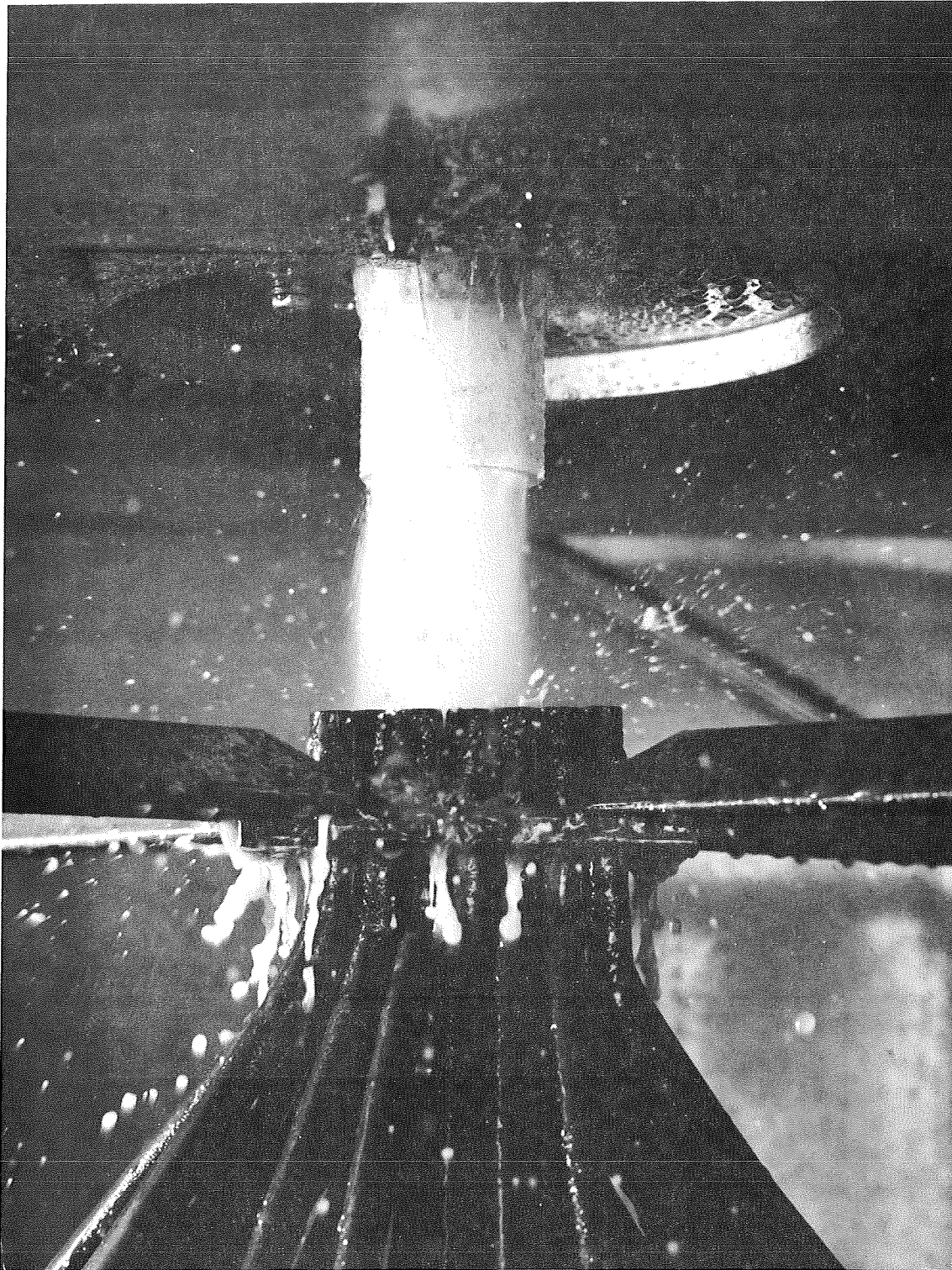


FIGURE C-1. Schematic of Nonreactive Fluids Flow Bench System



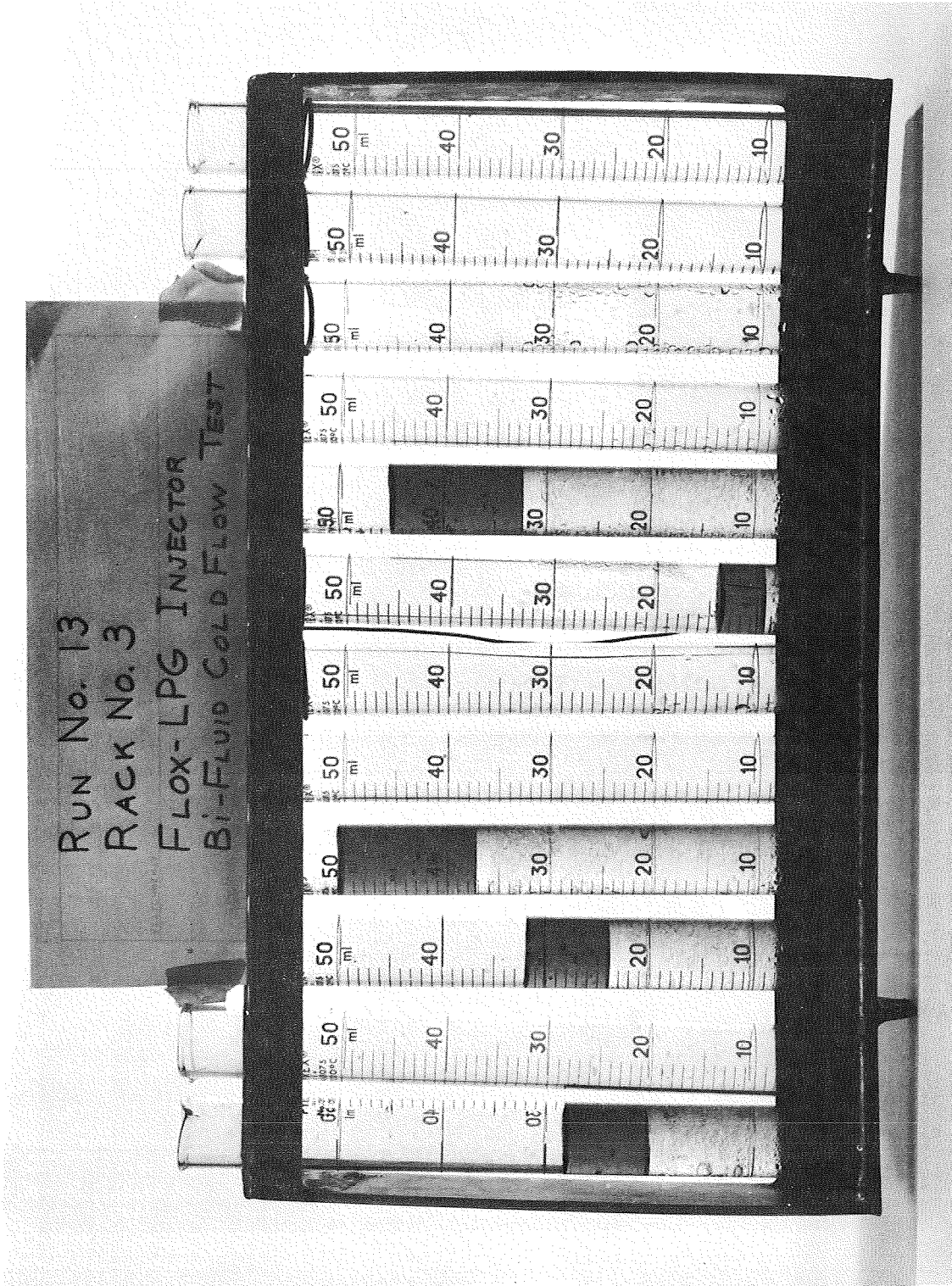
T11370-12

FIGURE C-2. Spray Booth Used for Bifluoride Flow Test of Injector



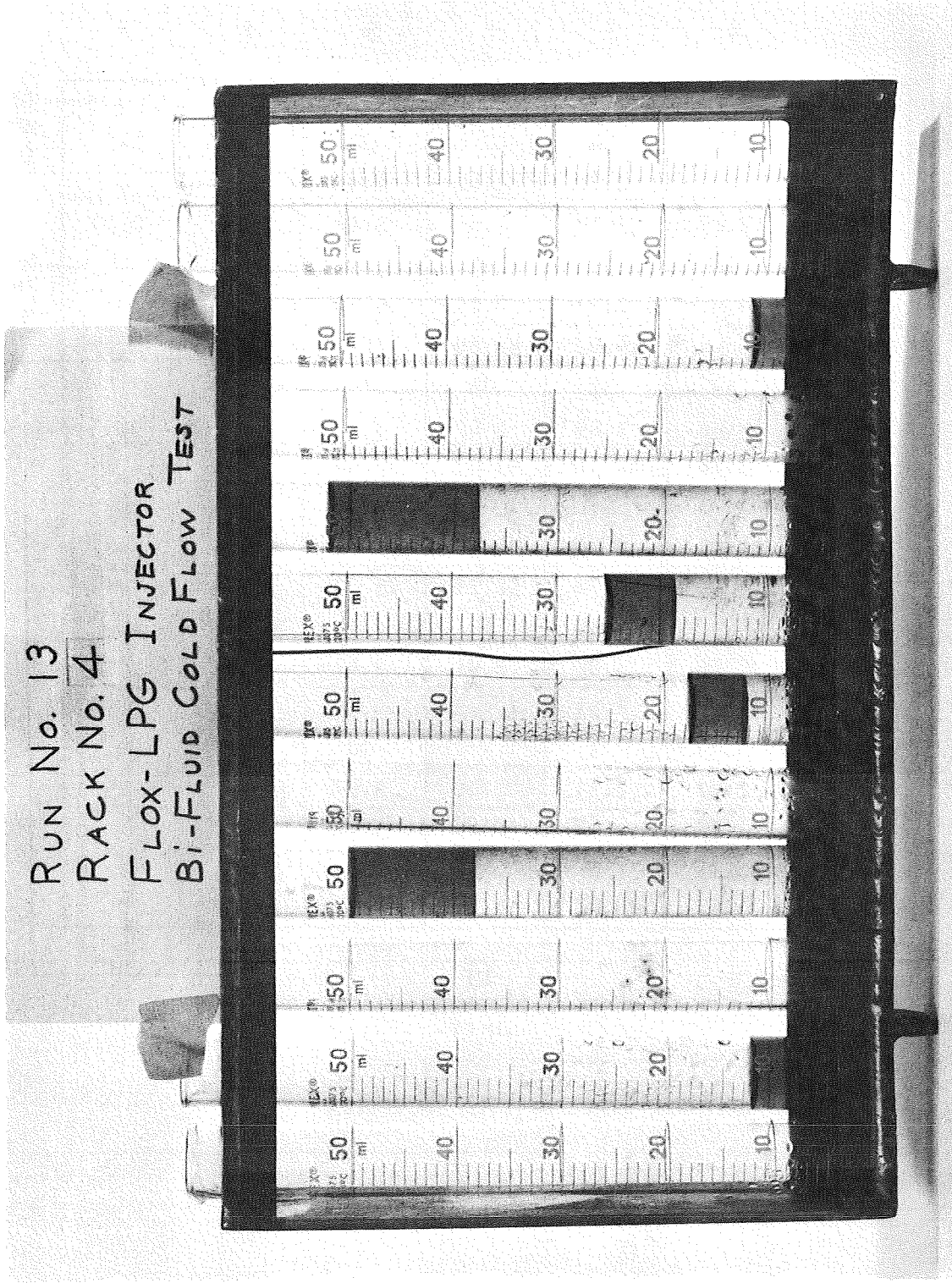
T11370-11

FIGURE C-3. View of Injector During Bifluid Spray Test



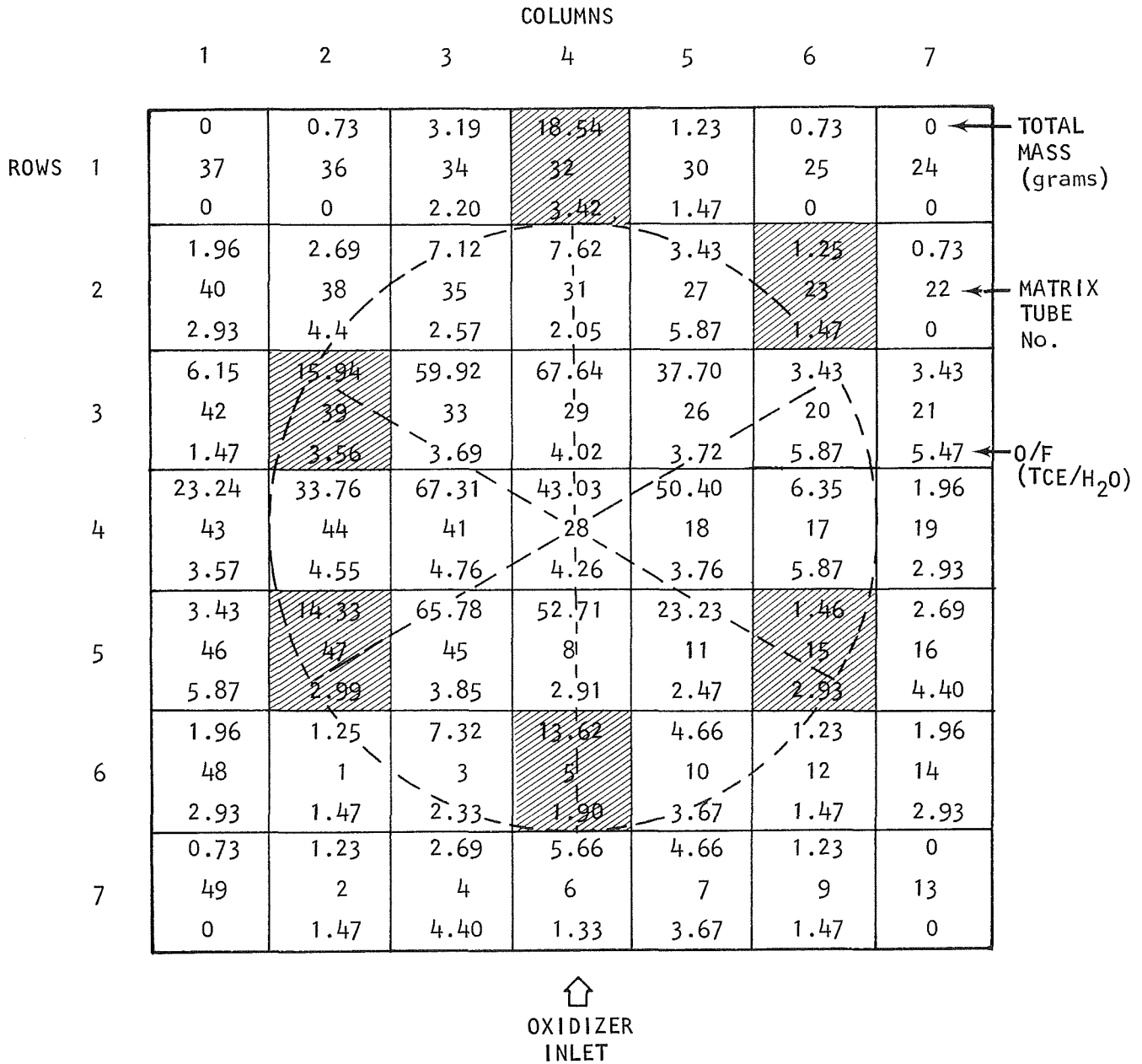
T11370-7


FIGURE C-4. Collection Cylinder Rack No. 3, Run No. 13



TEL1370-8

FIGURE C-5. Collection Cylinder No. 4, Run No. 13



 APPROXIMATE ZONES OF FILM INJECTION

X24401 INJECTOR S/N 002

FIGURE C-6. Injector Cold Flow Distribution, Run No. 13

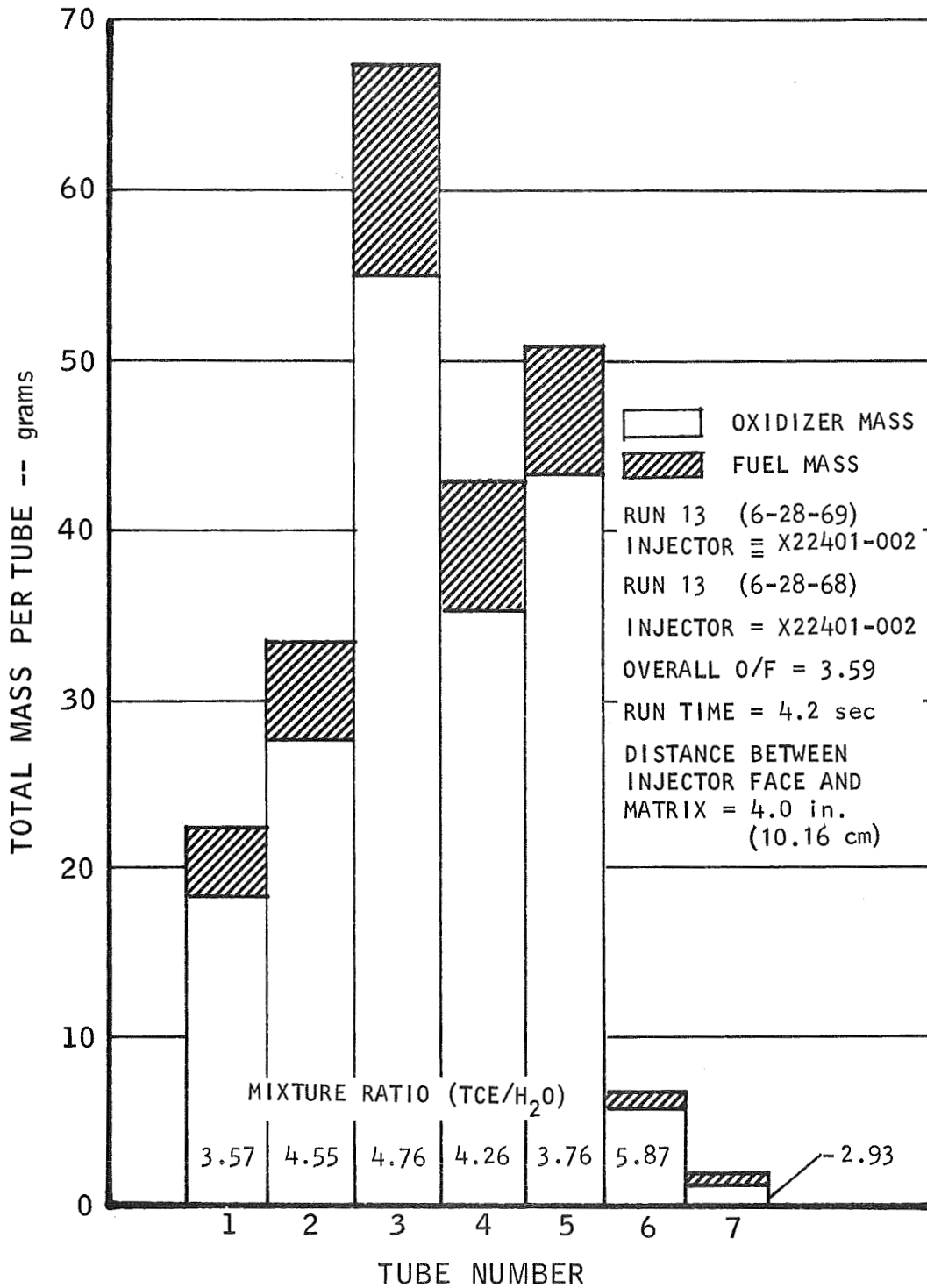


FIGURE C-7. Distribution of Injector Cold Flow in Center Row Cross Section, Run No. 13

FOR EMPIRICAL DETERMINATION OF LIQUID PHASE MIXING EXCELLENCE

$$E_m = 100 \left[1 - \left(\sum_0^n \frac{C \omega (R-r)}{WR} + \sum_0^{\bar{n}} \frac{C \omega (R-\bar{r})}{R (R-1)} \right) \right]$$

Where

- E_m = Mixing excellence, percent
- r = Local Mixture ratio for $r < R$
- \bar{r} = Local mixture ratio for $r > R$
- R = Nominal mixture ratio
- n = Number of samples with $r < R$
- \bar{n} = Number of samples with $r > R$
- A_t = Cross-sectional area of sampling tube
- A_s = Portion of spherical surface represented by sample
- C = Area correction factor = A_s / A_t
- ω = Total local weight flow rate of spray
- W = Total nominal weight flow rate of spray

FIGURE C-8. Definition of Mixing Excellence Factor

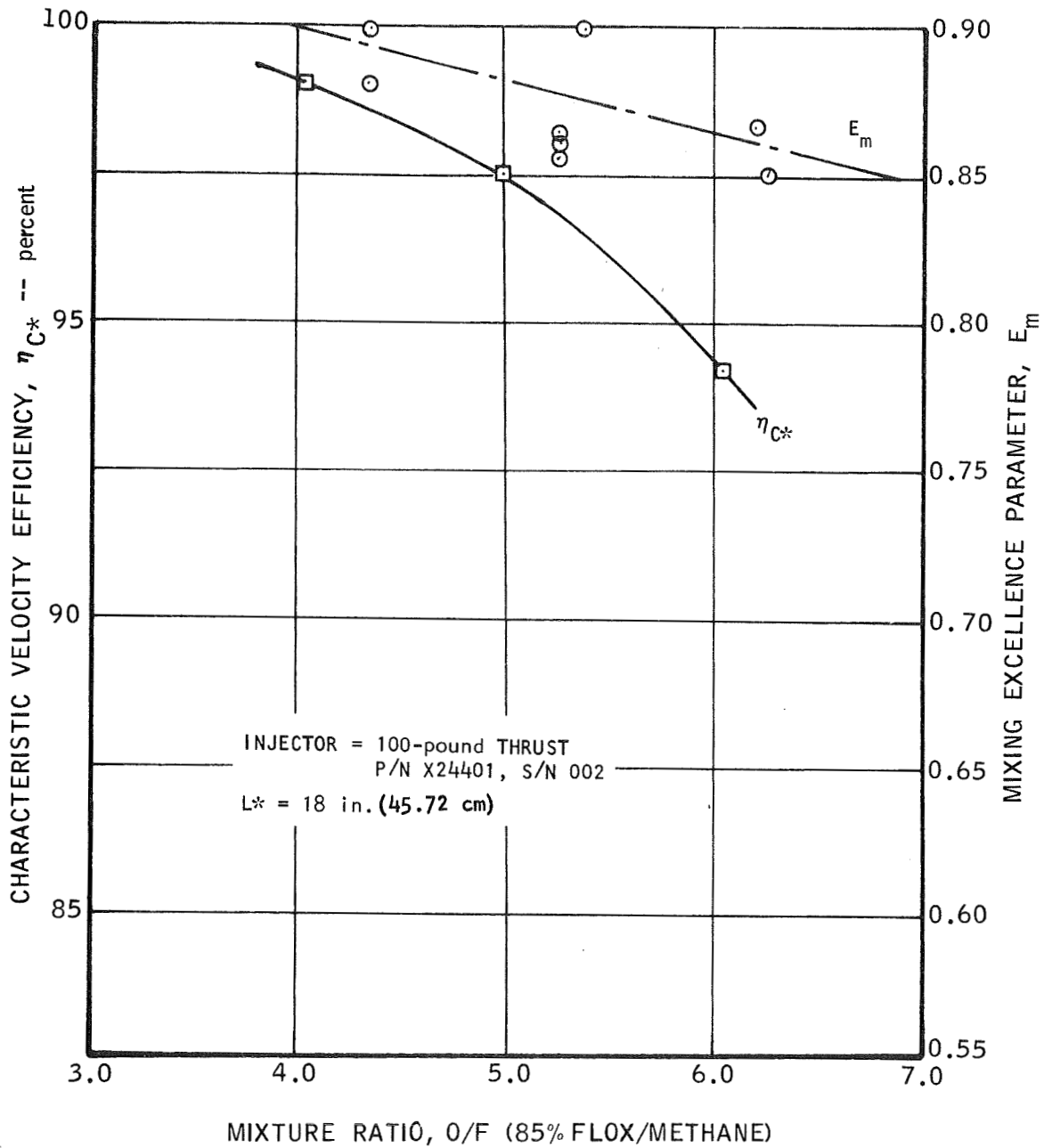


FIGURE C-9. Spray Characteristics of the Serial 002 Injector

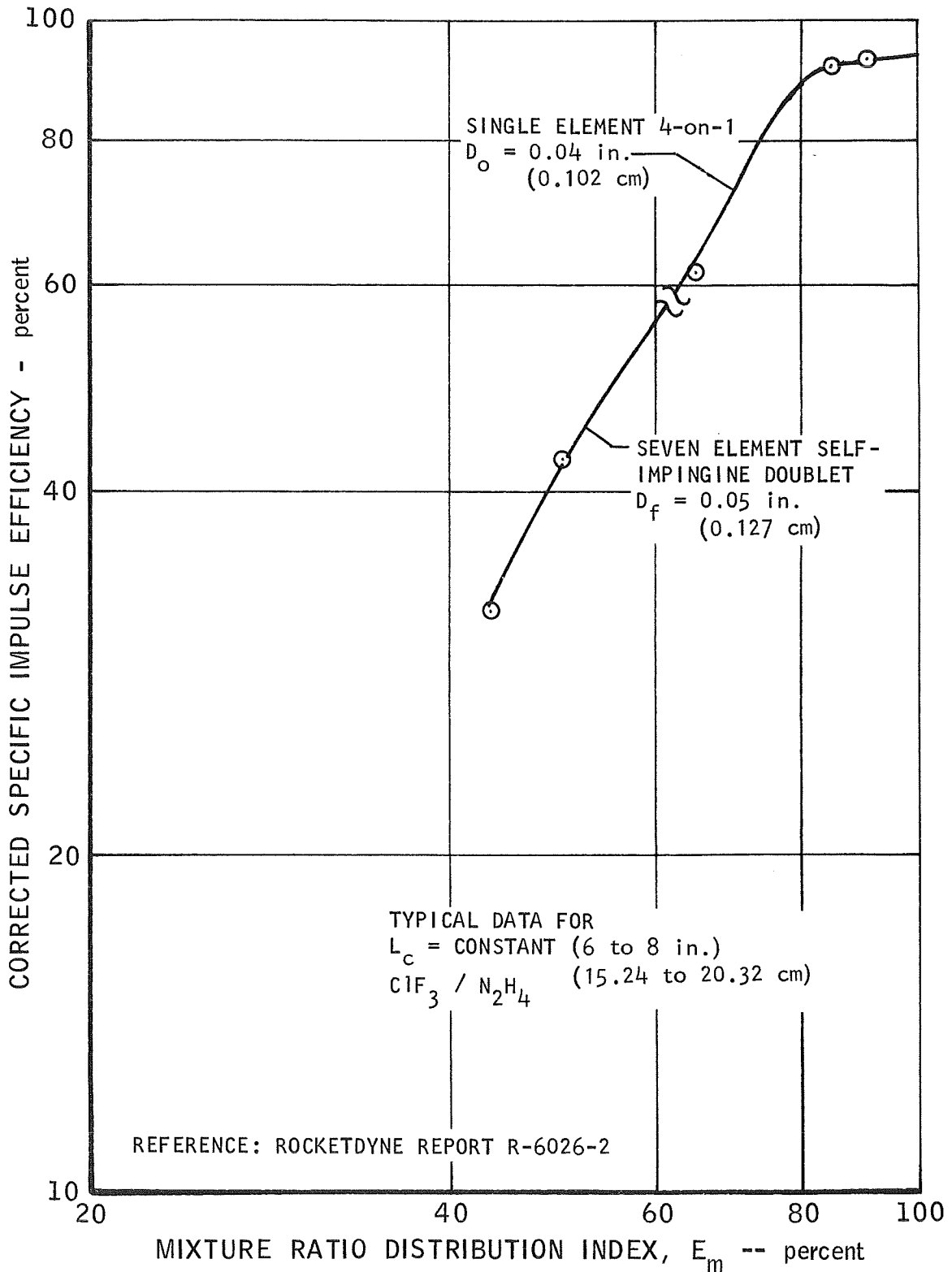


FIGURE C-10. Correlation of Impulse Efficiency with Propellant Distribution Index for ClF_3/N_2H_4 Injectors

APPENDIX D

DESCRIPTION OF
FIRING TEST FACILITY

This page intentionally left blank

APPENDIX D
DESCRIPTION OF FIRING TEST FACILITY

SECTION D-I
GENERAL DESCRIPTION

The hot test firings of the rocket engine during this program utilized the existing facilities at The Marquardt Rocket Test Laboratory. This laboratory is located at an elevation of 4860 feet (1481 m), on the top of Magic Mountain in the San Gabriel Range, 31 miles (49.9 Km) from Van Nuys, California. It was established by The Marquardt Company for rocket testing with highly reactive or toxic propellants that could not be easily handled in the more populated Van Nuys and Saugus Test Laboratories. The property is leased from the U.S. Department of Agriculture Forestry Service and has been improved with a capital acquisition of over a million dollars.

This facility has three rocket engine firing test areas. Cell M-1A is designed for firing rocket engines of up to 10,000-pound (44,482 N) thrust size in a vertical down position. Cell M-1B is a horizontal firing cell with thrust capability of up to 15,000 pounds (67,723 N). Test Cell M-2 is arranged to fire vertically downward and it is presently used for low thrust research and development rockets. This complex was used for the subject program because it contains high pressure fluorinated oxidizer and light hydrocarbon propellant systems. In addition, there is a reaction control system test area, Cell M-3, a Chemistry and Propellants Mixing Laboratory, and a combined General Purpose and Control Room Building. Figure D-1 shows the arrangement of Cell M-2 and Figure D-2 shows the firing position of this cell.

SECTION D-II
DETAIL DESCRIPTION

A. Fluorinated Oxidizer System

The 960 psi (662 N/cm²) 30 gallon (0.1136 m³) fluorinated oxidizer system in Cell M-2 was utilized in this program. FLOX was received in gaseous cylinders and cryopumped into the liquid nitrogen jacketed run tank for the Phase I tests. For the Phase II tests, which required long run durations, a liquid FLOX delivery of 1000 pounds (453.6 Kg) was received and stored as liquid in the shipping trailer. The run quantities were transferred to the 30 gallon (0.1136 m³) run tank periodically as required.

B. Fuel System

The temperature controlled methane (or propane) fuel system in Cell M-2 was utilized in this program. Methane and propane were received in liquid form

and temperature conditioned to meet the program requirements. Temperature conditioning was accomplished by blending ambient temperature gaseous nitrogen with liquid nitrogen in heat exchanger sections to achieve the desired run conditions.

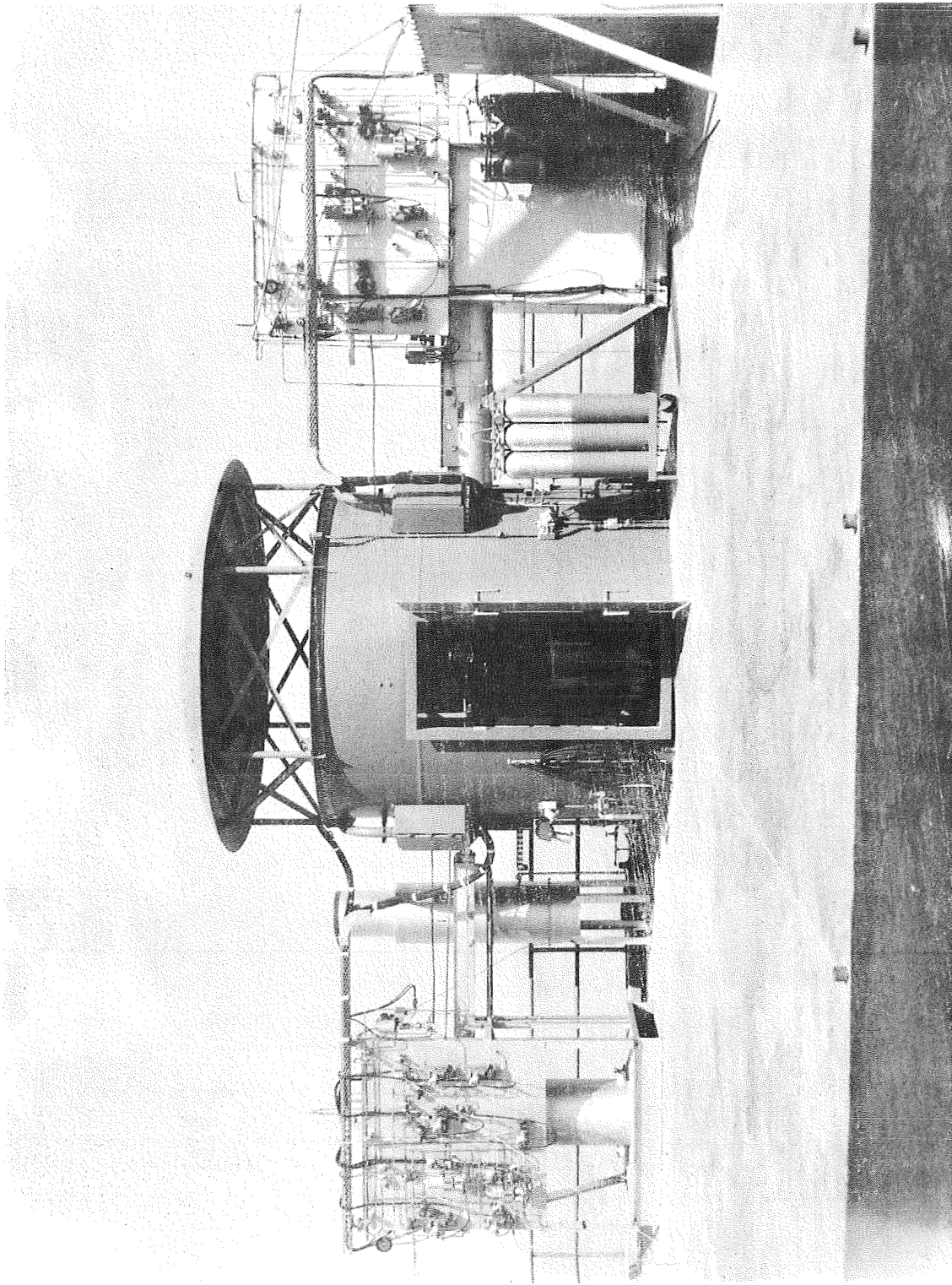
The propellant system lines and control instrumentation are shown in Figure D-3.

C. Instrumentation and Recording System

Cell M-2 is equipped with a 48 channel S.E.L. digital data system with appropriate front end signal conditioning equipment such as thermocouple reference junctions, bridge balance units, power supplies, and calibration equipment. This recording system is supplemented by a variety of portable equipment such as oscilloscopes, oscillographs, pen type recorders, gages, etc.

D. Altitude Simulation System

The altitude simulation system of Cell M-2 consists of a straight tube no flow diffuser capable of fully expanding a 12:1 rocket engine nozzle in thrust ranges up to 100 pounds.



6393-4
FIGURE D-1. Test Cell M-2 of the Marquardt Magic Mountain Rocket Test Laboratory

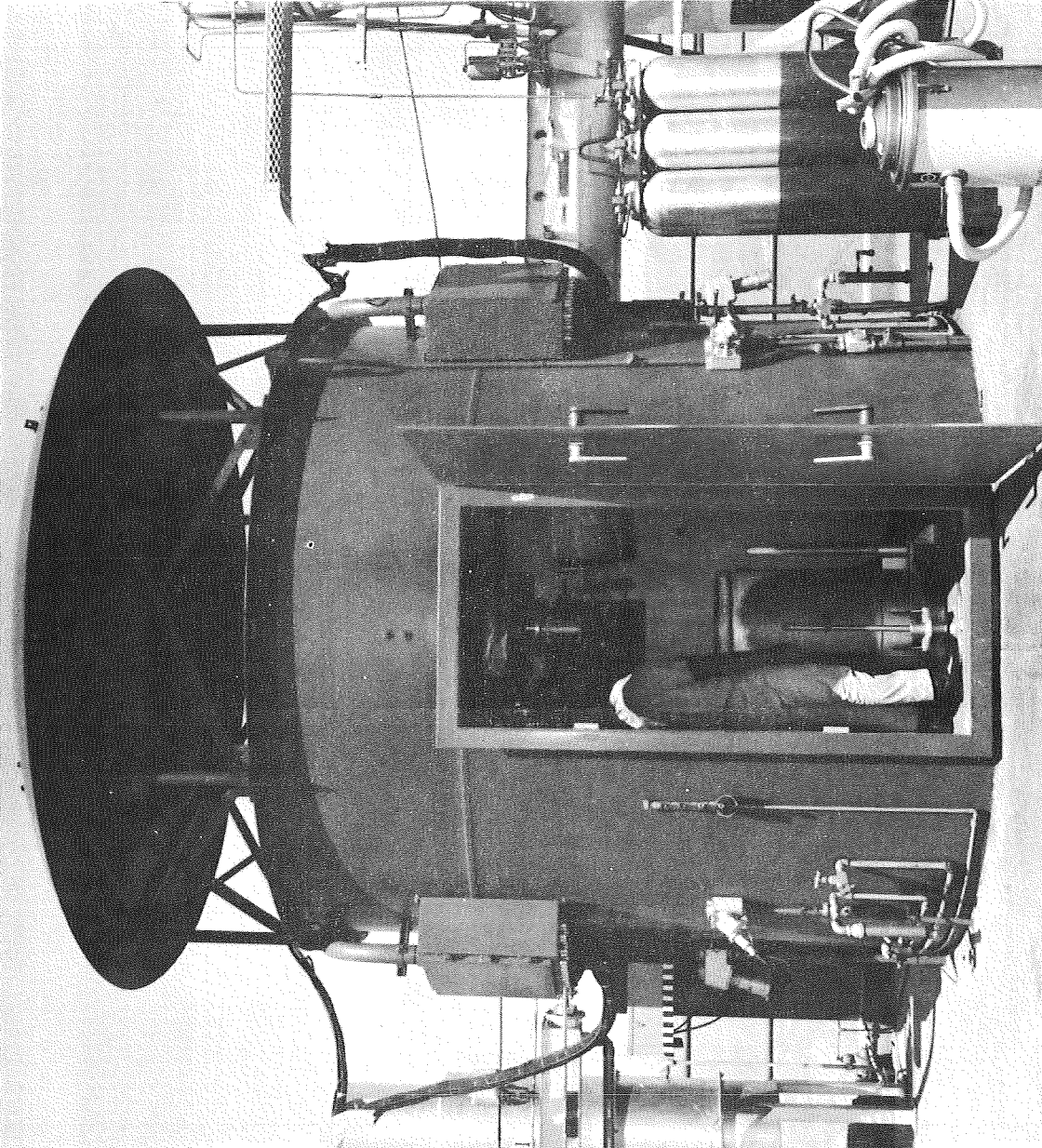


FIGURE D-2. Firing Position of Test Cell M-2

6354-43CN

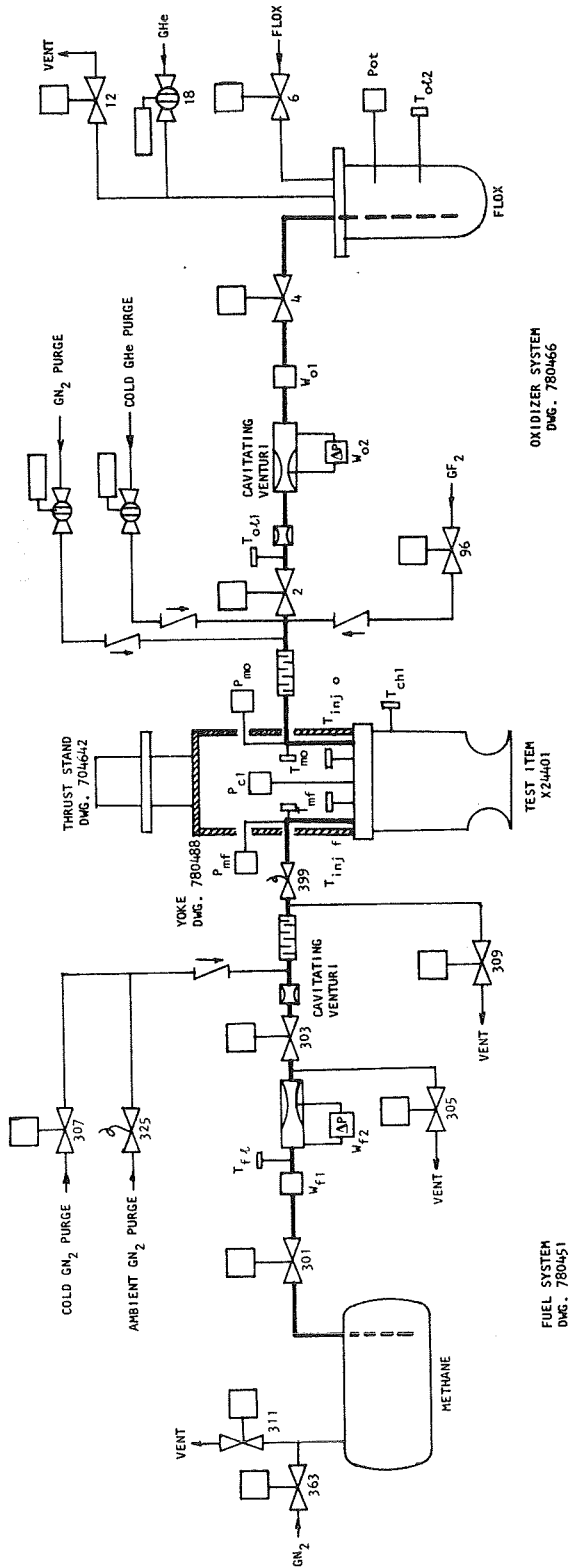


FIGURE D-3. Schematic of Test Setup in Cell M-2

This page intentionally left blank

APPENDIX E

MEASUREMENT OF HIGH SURFACE TEMPERATURES
USING A PHOTOGRAPHIC TECHNIQUE

By R. M. Davids and R. D. Lloyd

This page intentionally left blank

APPENDIX E

MEASUREMENT OF HIGH SURFACE TEMPERATURES USING A PHOTOGRAPHIC TECHNIQUE

By R. M. Davids and R. D. Lloyd

SECTION E-I INTRODUCTION

The measurement of temperatures under dynamic conditions encountered during engine firings has long been a problem in the aerospace industry and, for the most part, has not heretofore been solved. Extreme temperatures, high gas velocities, vibrational loads, and rotating parts have all but eliminated such mechanical techniques as thermocouples, high temperature paints, etc. Optical measurements have not been particularly accurate and like the mechanical methods, are single point focusing, hence, temperature spikes and gradients cannot be effectively measured.

The study described in this Appendix E was precipitated by the development of an "extended range film" (XR) manufactured by Edgerton, Germeshausen, & Grier, Inc. of Boston, Mass. (Reference E-1). This film was developed for scientific and industrial color photography for use over an extreme range of light conditions and it has the advantage of performing well under circumstances wherein exposures are unpredictable or where the brightness of the subject varies over enormous limits.

A preliminary investigation in which L-605, disilicide coated molybdenum, tungsten, and pyrolytic graphite were heated incrementally to known temperatures and photographed with the XR film indicated that the method was feasible. Subsequently, a program was initiated to establish the effect of several variables such as camera-to-object distance, bellows extension, and environmental light conditions on the color density of the projected image. The determination of the effects of these variables constitutes the subject matter of this appendix.

SECTION E-II SUMMARY

A novel method for measuring temperatures above 1600°F (1144°K) to well over 4000°F (2478°K) has been developed at Marquardt. The method incorporates a radiation sensitive color photographic film which virtually cannot be over exposed. By projecting the heated image on this film through a calibrated lens system and subsequently measuring the density of the projected color, an entire temperature profile can be obtained with an accuracy of $\pm 1\%$. Still or motion picture photography can be used as desired.

A detailed description of the method and its standardization is included in this appendix.

SECTION E-III PROCEDURE

In order to generate a reliable procedure for the measurement of elevated temperatures using photographic techniques, an investigation and calibration of those variables which could possibly affect the end result was necessary. Variables of particular concern were: 1. color density versus temperature conversion, 2. effect of densitometer filters on signal response, 3. camera-to-sample distance, 4. temperature versus density under various environmental light conditions, and 5. color density versus bellows extension.

A. Test Equipment

Testing was conducted in the laboratory using the following equipment:

1. 70 mm Camera, "Camerz" Model 35, Photo-Control Corp.
2. Potentiometer, Leeds and Northrup Type K-3 (accuracy > 0.01%)
3. Digital-Millivolt Meter, Cimron Model 7400A (checked before each test against a certified K-3 potentiometer)
4. Photomatic Automatic Optical Pyrometer (Transfer standard)
5. T-24 Pyrometer Calibration Lamp, NBS No. 176959

The test chamber (Figure E-1) consisted of an 18-inch (45.72 cm) diameter Pyrex bell jar situated on a metal platform. Glass arms, capped with 0.125-inch (0.318 cm) optical grade quartz, provided viewing ports in the jar for optical measurement. A vacuum pump attached to the system provided low pressure environments when it was necessary to reduce oxidation. Two water cooled copper electrodes, insulated from the metal base by Teflon washers, produced resistance heating of the tube.

Vacuum measurements were made with a thermocouple gage which was calibrated with a McLeod gage.

B. Specimen Design and Fabrication

Tubular specimens, each approximately 6 inches (15.24 cm) long, and of various diameters, depending upon the availability of material, were used in all tests. A hole was drilled through one wall of the tube in the center and normal to its longitudinal axis. The diameter of the hole varied in accordance with the tube diameter. This was necessary to produce the correct "black body" conditions (see References E-2, E-3, and E-4). The surface finish of the tubes was that of the received stock.

C. Experimental and Calibration Method

The tubular test specimen was placed between the copper electrodes in the test apparatus. Depending upon the test cell environmental conditions to be simulated, the specimen was either left exposed to the atmosphere or the bell jar was inserted in place so that one of its quartz windows was in line with the small hole in the tube. If vacuum was desired, it was produced to a 10^{-4} mm Hg level. The automatic pyrometer was next positioned so that it sighted through the quartz window into the hole in the tube. A 70 mm camera loaded with XR film was then positioned so that it was focused through the other quartz window on the outer tube wall 180° from the hole. The tube was then resistance heated and the true temperature (under black body conditions) was measured by the automatic pyrometer. The camera was actuated when the tube was at steady state temperature. The film was subsequently processed and the color density was measured with a densitometer.

A series of tests were conducted with this procedure to determine the effects of the aforementioned variables on the density and subsequent temperature conversion. These tests are outlined below:

1. Color density versus temperature conversion - Measurements were taken every 100°F (55°K) from 1600°F (1144°K) up on various materials such as phenolics, disilicide coated molybdenum, and pyrographite. A preliminary investigation involving L-605 and tungsten, was conducted to determine the feasibility of the test method.
2. Filter color versus signal response - The effect of a red and green filter in the densitometer lens system on the density signal response was determined for pyrolytic graphite at temperatures ranging from 1600° to 4500°F (1144° to 2755°K).
3. Camera-to-sample distance - Various tests were conducted varying the distance with the aid of a plus 2 lens. While maintaining a constant bellows extension of $3\frac{3}{4}$ inches (9.53 cm), tests were run with the camera lens at a fixed distance from the tube. A plus 2 lens effectively changed this distance while a 1-inch (2.54 cm) thick cell window placed in front of the normal lens simulated a test cell run.
4. Temperature versus color density under various lighting conditions - Three conditions of environmental light were investigated to determine their effect on the color density, using a green filter. (Experiments were conducted using a standard tungsten calibration lamp.) These conditions were black (no external lighting), shade, and, direct sunlight.
5. Color density versus bellows extension - Tests were conducted on a disilicide coated molybdenum sample where density was measured as a function of bellows extension. When the camera lens is

physically moved to or from the object a bellows adjustment becomes necessary. To determine the effect on the temperature measurement (by means of density), distances ranging from 1.0 to 4.5 inches (2.54 to 11.43 cm) were used at 2200°F (1476°K).

SECTION E-IV RESULTS AND DISCUSSION

The results obtained from the tests previously described showed definite effects of bellows extension, type of filter, and external light conditions on the color density. No effect was observed for various sample-to-camera distances at a fixed bellows extension. These results are detailed below:

1. Color density versus temperature conversion - The density-temperature calibrations for various materials are presented in Figures E-2 and E-3. The results showed that a somewhat linear relationship exists and appear to be dependent on the material emissivity as indicated in Figure E-2. Hence, duplication of the test material and surface condition is necessary for calibration.
2. Filter color versus signal response - The curves illustrated in Figure E-3 readily indicate the variance of film color density when red or green filters are used. Since the phenomenon is purely dependent on the color of the developed film the material photographed is not a variable and hence it holds true for all materials.

The desired situation for greatest accuracy when measuring density is to have a large density change over a small temperature range. It is evident from Figure E-3 that the green filter is better for calibration up to 3100°F (1978°K) but the red filter is superior from 3100° to 4500°F (1978° to 2255°K).

3. Camera-to-sample distance - Varying the distance of the lens to the sample while maintaining constant bellows extension, does not affect the color density, as reflected in Table E-I. Also, there is no definitive effect on density when the photograph is taken through a 1-inch (2.54 cm) cell window, representing actual operating conditions. This means that this procedure can be accomplished outside the test cell with no degradation of results.
4. Temperature versus color density under various lighting conditions - The data reflected in Figure E-4 point out that direct sunlight has a decided effect on the density at temperatures up to 2400°F (1589°K). The flatness of the initial portion of the curve would not effectively provide accurate measurements in that region. Whether the sample or engine part is photographed in complete darkness or in shaded sunlight is inconsequential, since the curves

fall on top of each other from 1600° to 3000°F (1144° to 1922°K). The data also suggest that there will be no additional variation at temperatures above 3000°F (1922°K).

5. Color density versus bellows extension - Changing the lens-to-film distance by bellows movement does not change the density. This is illustrated in Figure E-5. The test was run at a constant temperature of 2200°F (1478°K). It is easily seen that as the bellows is opened up the density decreases in intensity. This point is very important since it means that whatever extension is used for an engine run must be used during the subsequent calibration. When a bellows extension has been chosen, focusing should be done with the aid of plus lenses.

SECTION E-V RECOMMENDED CALIBRATION AND TEST PROCEDURE

The following calibration and test procedure was derived from the results of this investigation. It should be noted that some of the steps are conservative in nature due to lack of data, but they are functional.

A. Test Cell

1. Photograph the heated object using a 70 mm camera, loaded with XR film (Edgerton, Germeshausen & Grier, Inc.). If time dependent temperature profiles are desired, then lapse-time photography can be employed.
2. Note the bellows extension setting.
3. Photograph either in complete darkness or under shaded conditions. Photographing in direct sunlight can be accomplished if this same condition is reproduced during laboratory calibration. However, it must be realized that the minimum detectable temperature under these conditions is 1800°F (1255°K).
4. Note the material and coating of the part involved.

B. Laboratory

1. Obtain a tubular specimen of the same material and coating as the actual part.
2. Drill a hole, normal to the longitudinal axis, through one wall. The hole size is dependent on the tube diameter.
3. Place the tube between heating electrodes.

4. Depending upon the atmosphere or environment during the test, either place the bell jar over the assembly or omit it.
5. If reduced pressures are required, pull a vacuum at this time (make sure the bell jar is so positioned that one of the quartz windows is in line with the hole in the tube).
6. Focus the Photomatic Automatic Optical Pyrometer on this hole.
7. Focus the same 70 mm camera loaded with the same film that was used for the actual test, through the other quartz window on the side of the tube opposite the hole.
8. When all equipment is operational, heat the tube to known true temperatures (as read under black body conditions by the automatic pyrometer) and photograph the indicated surface temperature.
9. Process the film - The test and calibration will be on the same film, thus eliminating any process variables.
10. Measure the density for temperature calibration using a green filter for temperatures up to 3100°F (1978°K) and a red filter over that temperature.
11. Draw a calibration curve of color density versus true temperature.
12. Measure the color density on a test portion of film (see Figure E-6).
13. Referring to the calibration curve, calculate the operating temperature.
14. Make up a part overlay with temperatures indicated (optional).
15. Print the part and the overlay for a pictorial representation of the test (optional) (see Figure E-7).

NOTE: Laboratory test equipment should be calibrated periodically using a National Bureau of Standards tungsten lamp.

SECTION E- VI CONCLUSIONS

1. The photographic temperature measurement technique is a reliable method of obtaining temperature profiles above 1600°F (1144°K).
2. The accuracy of such a method is within 1%.

3. A clear permanent record of hot spots, cracks, etc., is an added advantage of this technique.
4. Test accuracy is poor below 2400°F (1589°K) when the heated object is photographed in direct sunlight.
5. Shade or total darkness provides the same desired result for photographing the test part.
6. A green filter on the densitometer is optimum up to temperatures of 3100°F (1978°K). A red filter is optimum above this value.
7. The camera bellows extension must be kept constant during a test sequence.
8. Color density is a function of the emissivity and temperature of the heated material.

SECTION E-VII REFERENCES

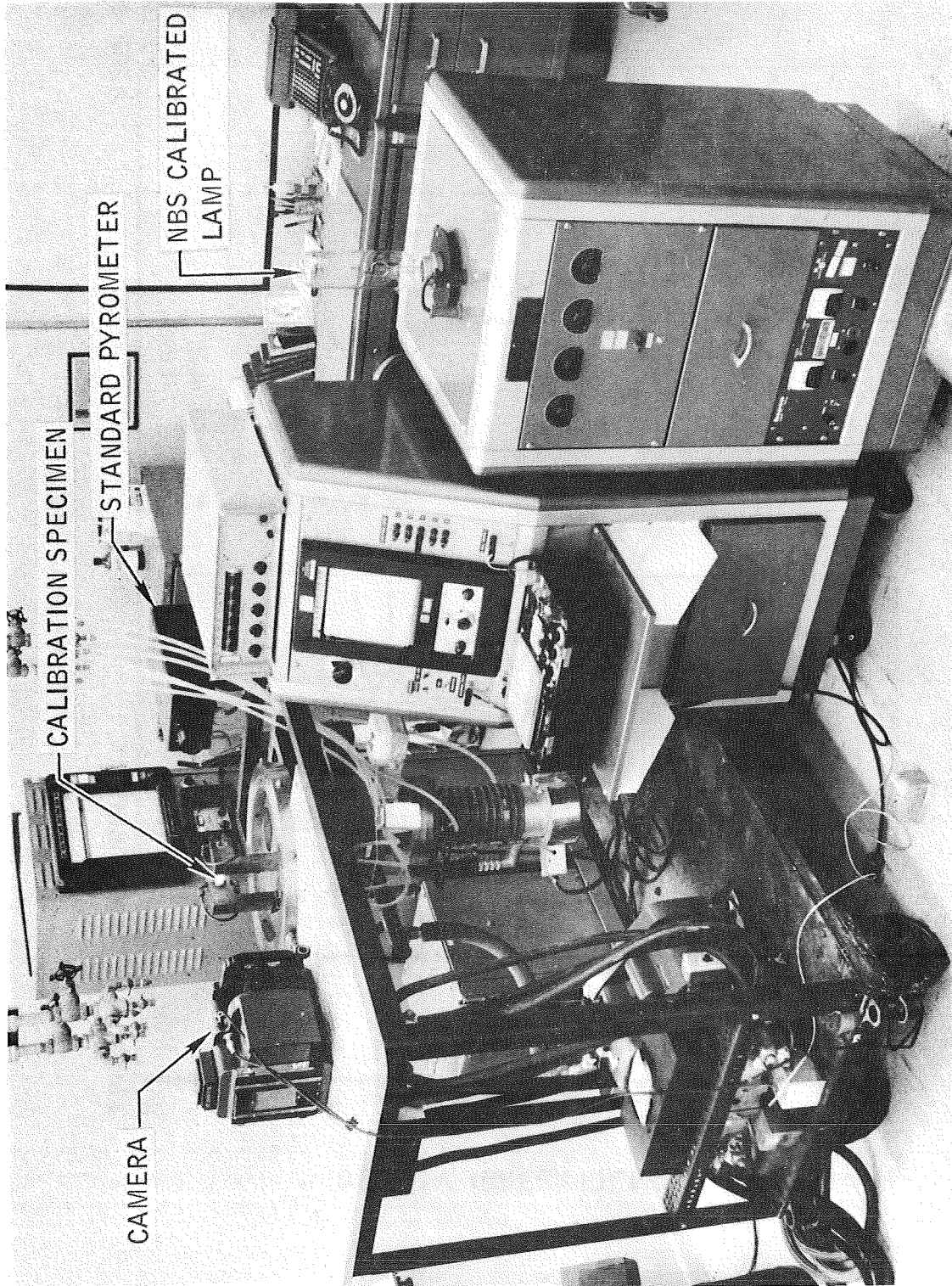
- E-1. Edgerton, Germeshausen, & Grier, Inc. Data Sheet for XR (Extended Range) Film, undated.
- E-2. Devos, J.C., "Physica XX", 1964, pp 669-689.
- E-3. Wood, W.D., H.W. Deem, and C.F. Lucks, "Thermal Radiative Properties of Selected Materials", D.M.I.C. Report No. 177, Vol. 1, Nov. 1962, p 9.
- E-4. Kostkowski, H.J., and R.D. Lee, "Theory and Methods of Optical Pyrometry", National Bureau of Standards Monograph 41.

TABLE E-I

EFFECT OF CAMERA-TO-SAMPLE DISTANCE ON DENSITY RESPONSE
FOR C-103 COLUMBIUM ALLOY

Camera-to-Sample Distance	Test Temperature		Color Density
	°F	°K	
0 Reference	1600	1144	0.33
	1700	1200	0.35
	1800	1255	0.41
	1900	1311	0.50
	2000	1366	0.67
	2100	1422	0.92
	2200	1478	1.14
	2300	1533	1.31
	2400	1589	1.51
	2500	1644	1.72
2 lens	1600	1144	0.33
	1700	1200	0.35
	1800	1255	0.40
	1900	1311	0.50
	2000	1366	0.67
	2100	1422	0.90
	2200	1478	1.12
	2300	1533	1.33
	2400	1589	1.51
	2500	1644	1.71
1-inch thick cell window	1600	1144	0.33
	1700	1200	0.35
	1800	1355	0.41
	1900	1311	0.50
	2000	1366	0.66
	2100	1422	0.90
	2200	1478	1.13
	2300	1533	1.31
	2400	1589	1.52
	2500	1644	1.69

Bellows extension = 3 3/4 inches (9.55cm)



CA8385-1

FIGURE E-1. Apparatus Used for Temperature Calibration

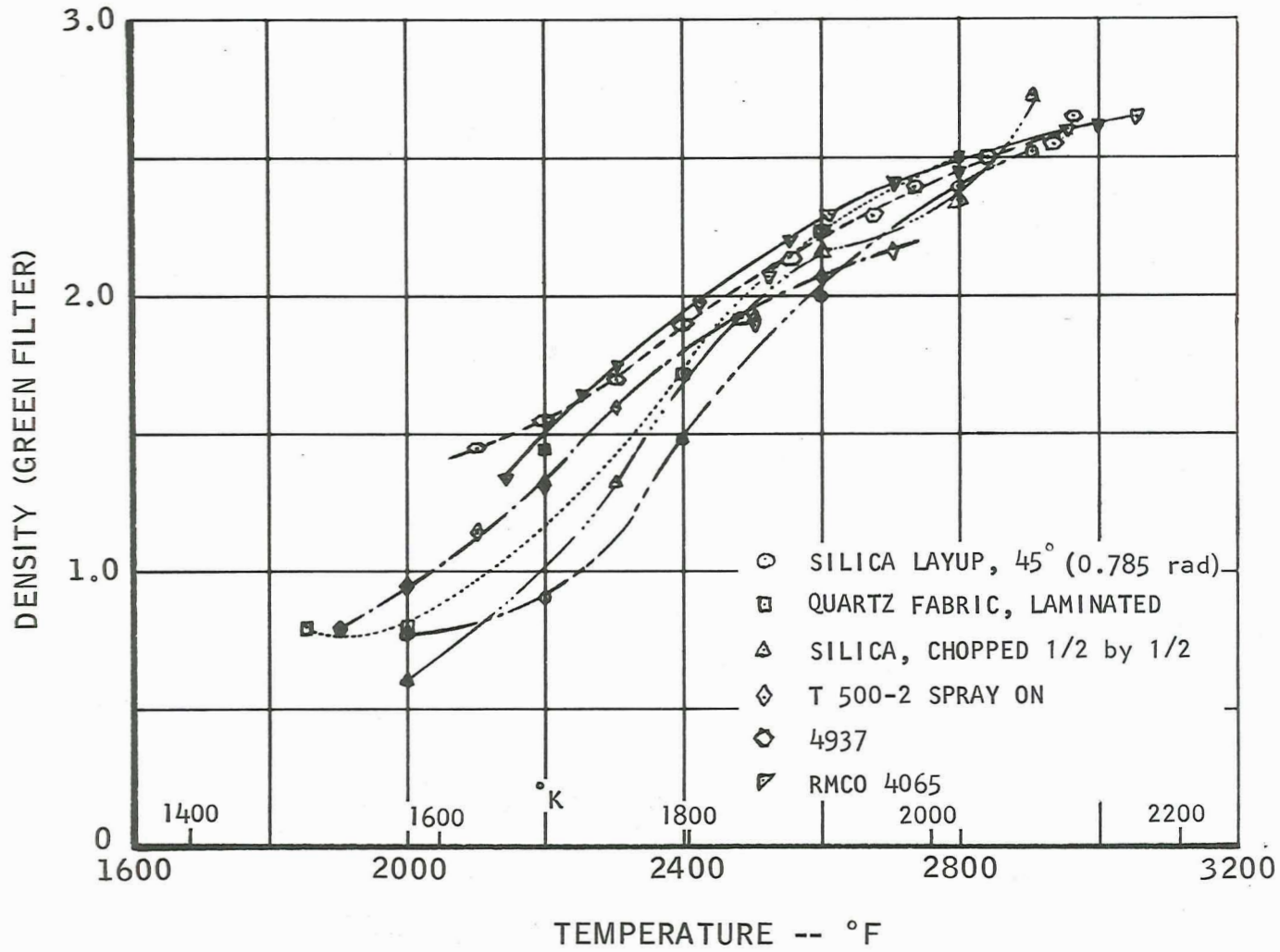


FIGURE E-2. Temperature vs. Density for Various Phenolics

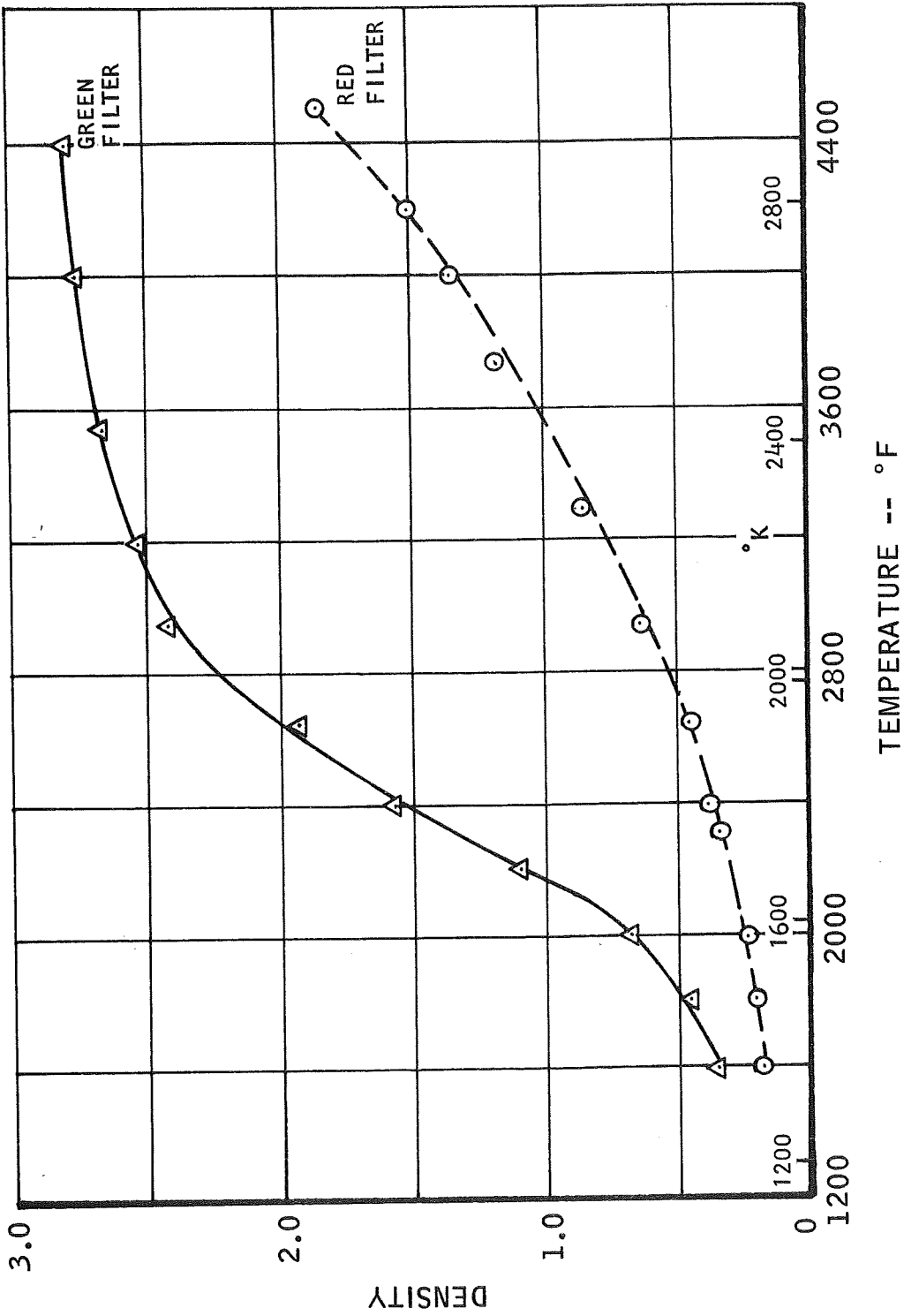


FIGURE E-3. Effect of Filter Color on Density vs. Temperature for Pyrographite

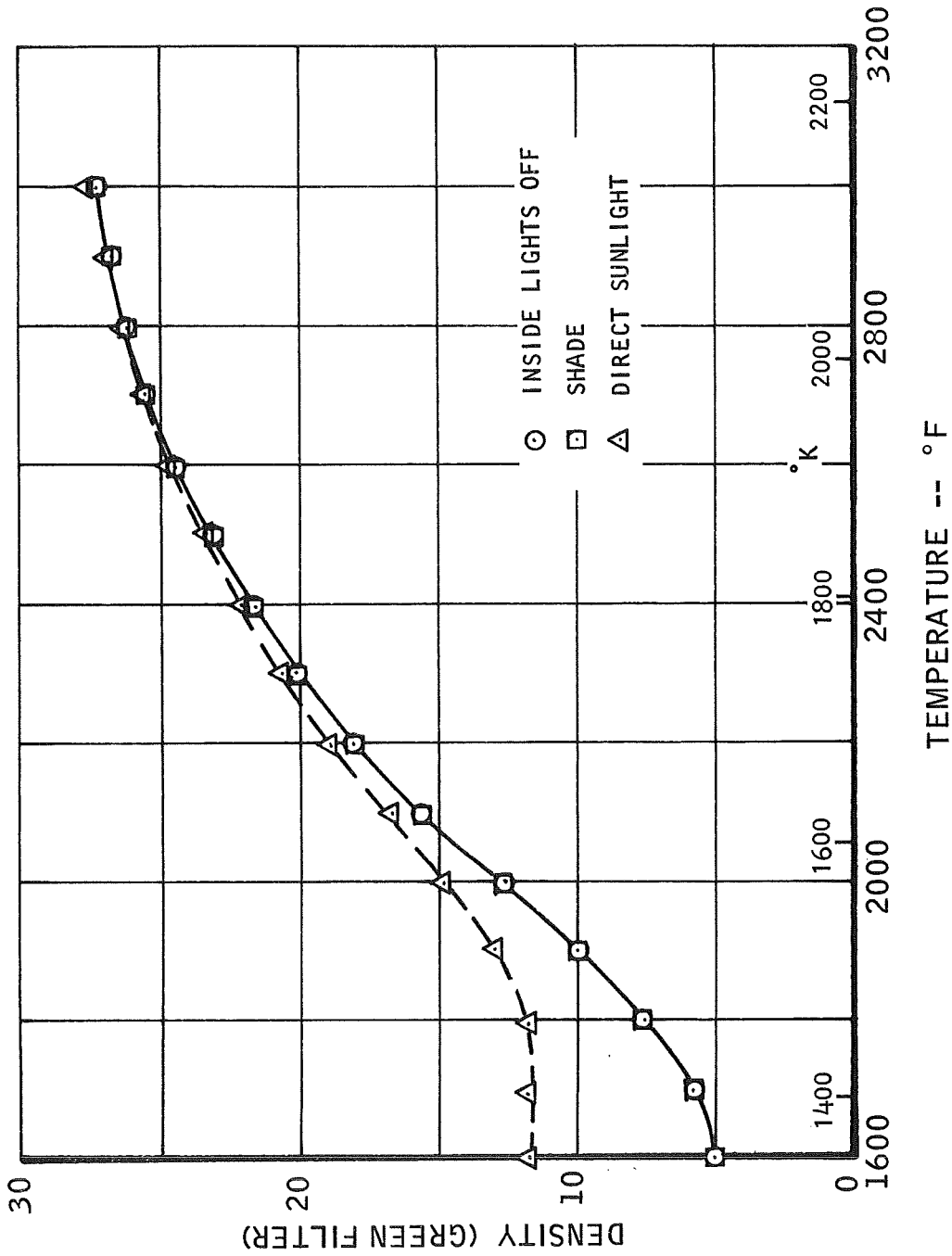


FIGURE E-4. Temperature Density for Various Lighting Conditions Using a Standard Tungsten Calibration Lamp

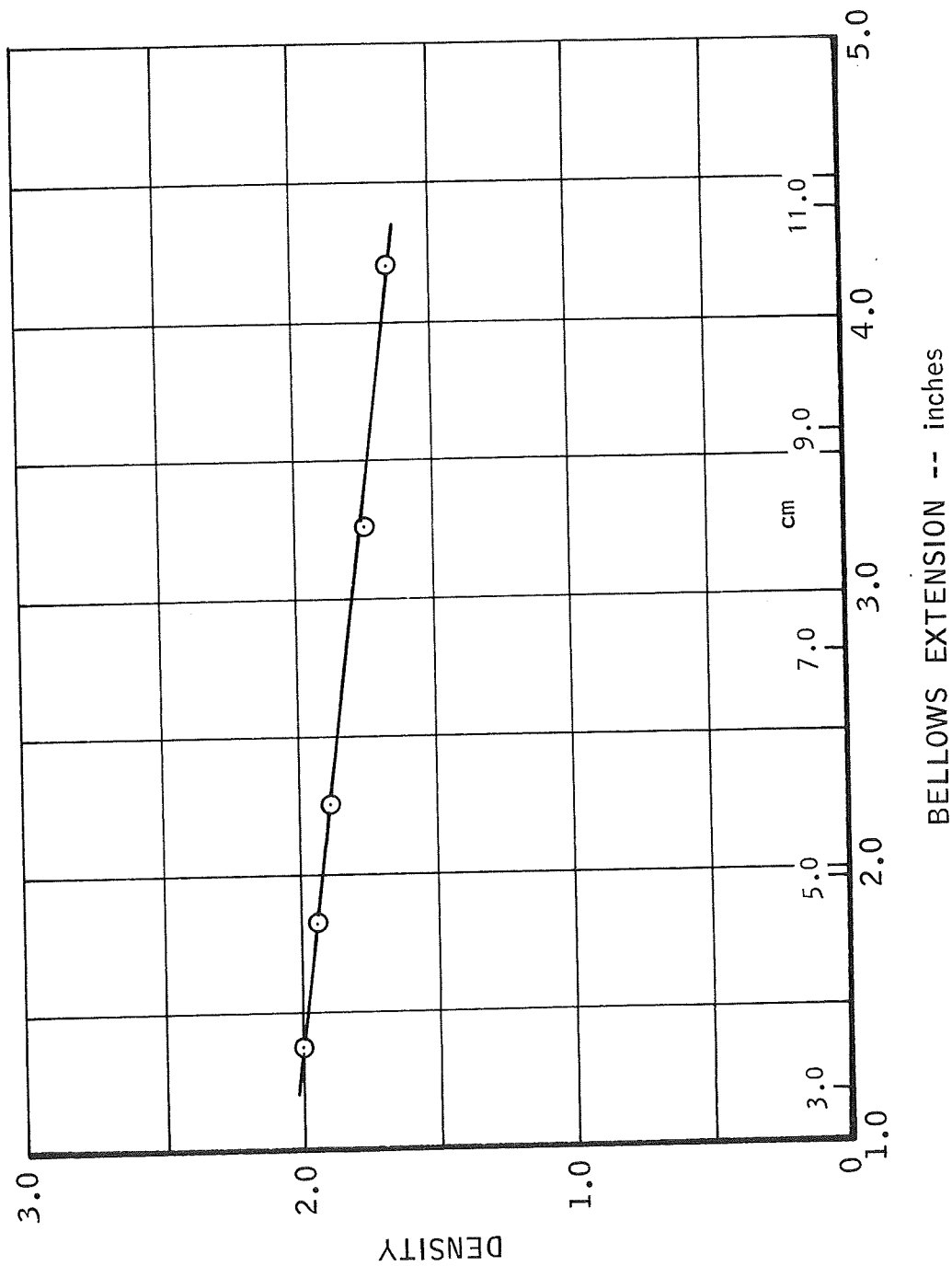


FIGURE E-5. Bellows Extension vs. Density at 2200°F (1478°K) for MoSi₂

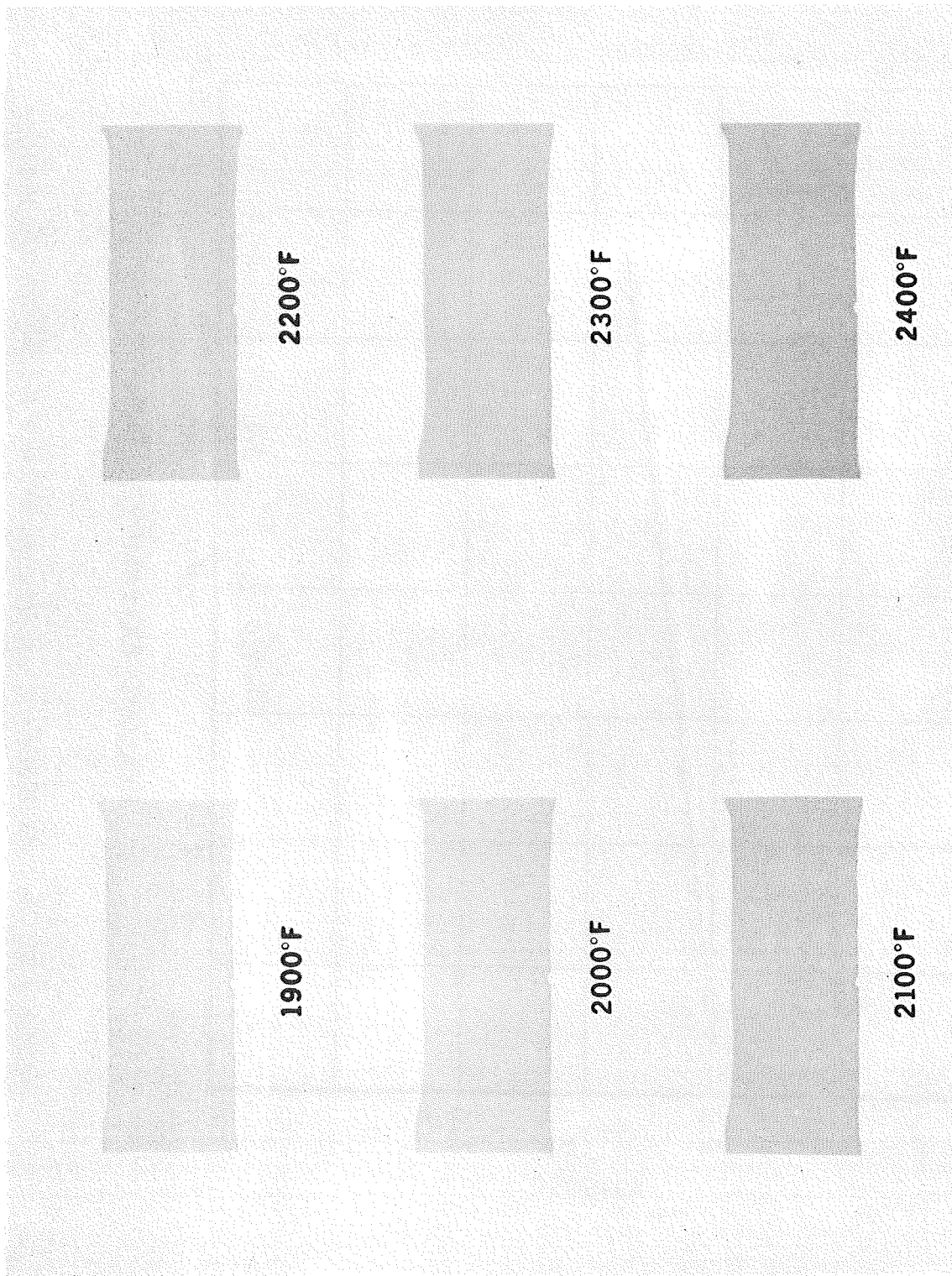
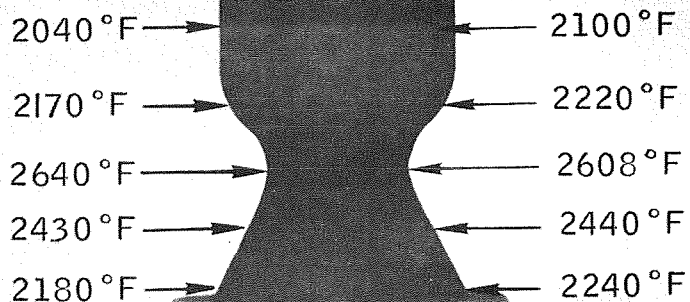


FIGURE E-6. Temperature Profile of Pyrolytic Graphite

V3469-1



ENGINE P/N T 12368
COMBUSTOR C129Y
COATING - SYLCOR 512
TEST NO. 3434
CELL NO. ATL PAD (D)
RUN NO. 24
MIXTURE RATIO 1.90
STEADY STATE CONDITION
DATE 7/19/66

v4388-

FIGURE E-7. Typical Chamber (Columbium) Evaluation using XT Film

This page intentionally left blank

<p>NASA CR-72526 National Aeronautics and Space Adm. SPACE STORABLE THRUSTOR INVESTIGATION C.D. Coulbert and R.J. Fiorito. 11 June 1969. 193 pp. A radiation cooled, 100-pound thrust, FLOX/CH₄, reaction control thruster of advanced pyrolytic refractory composite materials was designed and tested. A high performance injector was developed and long duration tests were performed with refractory composite, copper, and high density graphite chambers. Feasibility was demonstrated. Data are presented on injector performance, erosion rates, and carbon deposition.</p>	<p>I. Coulbert, C.D. II. Fiorito, R.J. III. NASA CR-72526 IV. Marquardt 6147</p> <p>NASA</p>
<p>NASA CR-72526 National Aeronautics and Space Adm. SPACE STORABLE THRUSTOR INVESTIGATION C.D. Coulbert and R.J. Fiorito. 11 June 1969. 193 pp. A radiation cooled, 100-pound thrust, FLOX/CH₄, reaction control thruster of advanced pyrolytic refractory composite materials was designed and tested. A high performance injector was developed and long duration tests were performed with refractory composite, copper, and high density graphite chambers. Feasibility was demonstrated. Data are presented on injector performance, erosion rates, and carbon deposition.</p>	<p>I. Coulbert, C.D. II. Fiorito, R.J. III. NASA CR-72526 IV. Marquardt 6147</p> <p>NASA</p>

Library Abstract Card

This page intentionally left blank

DISTRIBUTION

<u>Copy No.</u>	<u>Transmitted to</u>
1.	National Aeronautics and Space Administration Lewis Research Center 21000 Brookpark Road Cleveland, Ohio 44135 Attn: Contracting Officer, MS 500-313
2 to 9.	National Aeronautics and Space Administration Lewis Research Center 21000 Brookpark Road Cleveland, Ohio 44135 Attn: Liquid Rocket Technology Branch, MS 500-209
10.	National Aeronautics and Space Administration Lewis Research Center 21000 Brookpark Road Cleveland, Ohio 44135 Attn: Technical Report Control Office, MS 5-5
11.	National Aeronautics and Space Administration Lewis Research Center 21000 Brookpark Road Cleveland, Ohio 44135 Attn: Technology Utilization Office, MS 3-16
12, 13.	National Aeronautics and Space Administration Lewis Research Center 21000 Brookpark Road Cleveland, Ohio 44135 Attn: AFSC Liaison Office, MS 4-1
14, 15.	National Aeronautics and Space Administration Lewis Research Center 21000 Brookpark Road Cleveland, Ohio 44135 Attn: Library
16.	National Aeronautics and Space Administration Lewis Research Center 21000 Brookpark Road Cleveland, Ohio 44135 Attn: Office of Reliability and Quality Assurance, MS 500-111
17.	National Aeronautics and Space Administration Lewis Research Center 21000 Brookpark Road Cleveland, Ohio 44135 Attn: E.W. Conrad, MS 500-204

DISTRIBUTION (Continued)

<u>Copy No.</u>	<u>Transmitted to</u>
18.	National Aeronautics and Space Administration Washington, D.C. 20546 Attn: Code MI
19, 20.	National Aeronautics and Space Administration Washington, D.C. 20546 Attn: Code RPX
21, 22.	National Aeronautics and Space Administration Washington, D.C. 20546 Attn: Code RPL
23.	National Aeronautics and Space Administration Washington, D.C. 20546 Attn: Code SV
24 to 29.	Scientific and Technical Information Facility P.O. Box 33 College Park, Maryland 20740 Attn: NASA Representative, Code CRT
30.	National Aeronautics and Space Administration Ames Research Center Moffett Field, California 94035 Attn: Library
31.	National Aeronautics and Space Administration Ames Research Center Moffett Field, California 94035 Attn: C.A. Syvertson
32.	National Aeronautics and Space Administration Flight Research Center P.O. Box 273 Edwards, California 93523 Attn: Library
33.	National Aeronautics and Space Administration Goddard Space Flight Center Greenbelt, Maryland 20771 Attn: Library
34.	National Aeronautics and Space Administration John F. Kennedy Space Center Cocoa Beach, Florida 32931 Attn: Library

DISTRIBUTION (Continued)

<u>Copy No.</u>	<u>Transmitted to</u>
35.	National Aeronautics and Space Administration Langley Research Center Langley Station Hampton, Virginia 23365 Attn: Library
36.	National Aeronautics and Space Administration Manned Spacecraft Center Houston, Texas 77001 Attn: Library
37.	National Aeronautics and Space Administration George C. Marshall Space Flight Center Huntsville, Alabama 35812 Attn: Library
38.	National Aeronautics and Space Administration George C. Marshall Space Flight Center Huntsville, Alabama 35812 Attn: Keith Chandler, R-P&VE-PA
39.	Jet Propulsion Laboratory 4800 Oak Grove Drive Pasadena, California 91103 Attn: Library
40.	Office of the Director of Defense Research & Engineering Washington, D.C. 20301 Attn: Dr. H.W. Schulz, Office of Asst. Dir. (Chem. Technology)
41.	Defense Documentation Center Cameron Station Alexandria, Virginia 22314
42.	Arnold Engineering Development Center Air Force Systems Command Tullahoma, Tennessee 37389 Attn: AEOIM
43.	Aeronautical Systems Division Air Force Systems Command Wright-Patterson Air Force Base, Dayton, Ohio Attn: D.L. Schmidt, Code ASRCNC-2

DISTRIBUTION (Continued)

<u>Copy No.</u>	<u>Transmitted to</u>
44.	Air Force Missile Test Center Patrick Air Force Base, Florida Attn: L.J. Ullian
45.	Air Force Rocket Propulsion Laboratory (RPR) Edwards, California 93523
46.	Air Force Rocket Propulsion Laboratory (RPM) Edwards, California 93523
47.	Air Force Office of Scientific Research Washington, D.C. 20333 Attn: SREP, Dr. J.F. Masi
48.	Office of Research Analyses (OAR) Holloman Air Force Base, New Mexico 88330 Attn: RRRT
49.	Office of Research Analyses (OAR) Holloman Air Force Base, New Mexico 88330 Attn: Maj. R.E. Brocken, Code MDGRT
50.	U.S. Army Missile Command Redstone Scientific Information Center Redstone Arsenal, Alabama 35808 Attn: Chief, Document Section
51.	U.S. Army Missile Command Redstone Scientific Information Center Redstone Arsenal, Alabama 35808 Attn: Dr. W. Wharton
52.	Bureau of Naval Weapons Department of the Navy Washington, D.C. Attn: J. Kay, Code RTMS-41
53.	Commander U.S. Naval Missile Center Point Mugu, California 93041 Attn: Technical Library
54.	Commander U.S. Naval Ordnance Test Station China Lake, California 93557 Attn: Code 45

DISTRIBUTION (Continued)

<u>Copy No.</u>	<u>Transmitted to</u>
55.	Commander U.S. Naval Ordnance Test Station China Lake, California 93557 Attn: Code 753
56.	Commander U.S. Naval Ordnance Test Station China Lake, California 93557 Attn: W.F. Thorm, Code 4562
57.	Director (Code 6180) U.S. Naval Research Laboratory Washington, D.C. 20390 Attn: H.W. Carhart
58.	Picatinny Arsenal Dover, New Jersey Attn: I. Forsten, Chief Liquid Propulsion Laboratory
59.	U.S. Atomic Energy Commission Technical Information Services Box 62 Oak Ridge, Tennessee Attn: A.P. Huber, Code ORGDP Box P
60.	Air Force Aero Propulsion Laboratory Research & Technology Division Air Force Systems Command United States Air Force Wright-Patterson AFB, Ohio 45433 Attn: APRP (C.M. Donaldson)
61.	Aerojet-General Corporation P.O. Box 296 Azusa, California 91703 Attn: Librarian
62.	Aerojet-General Corporation 11711 South Woodruff Avenue Downey, California 90241 Attn: F.M. West, Chief Librarian

DISTRIBUTION (Continued)

<u>Copy No.</u>	<u>Transmitted to</u>
63.	Aerojet-General Corporation P.O. Box 1947 Sacramento, California 95809 Attn: Technical Library 2484-2015A
64.	Aerojet-General Corporation P.O. Box 1947 Sacramento, California 95809 Attn: Dr. C.M. Beighley
65.	Aerojet-General Corporation P.O. Box 1947 Sacramento, California 95809 Attn: D.T. Bedsole
66.	Aeronutronic Division of Philco Corporation Ford Road Newport Beach, California 92600 Attn: Dr. L.H. Linder, Manager
67.	Aeronutronic Division of Philco Corporation Ford Road Newport Beach, California 92600 Attn: D.A. Carrison
68.	Aeronutronic Division of Philco Corporation Ford Road Newport Beach, California 92600 Attn: Technical Information Department
69.	Aerospace Corporation P.O. Box 95085 Los Angeles, California 90045 Attn: J.G. Wilder, MS-2293
70.	Aerospace Corporation P.O. Box 95085 Los Angeles, California 90045 Attn: Library-Documents
71.	Arthur D. Little, Inc. Acorn Park Cambridge 40, Massachusetts Attn: A.C. Tobey

DISTRIBUTION (Continued)

<u>Copy No.</u>	<u>Transmitted to</u>
72.	Astropower, Incorporated Subs. of Douglas Aircraft Company 2968 Randolph Avenue Costa Mesa, California Attn: Dr. George Moc Director, Research
73.	Astrosystems, Incorporated 1275 Bloomfield Avenue Caldwell Township, New Jersey Attn: A. Mendenhall
74.	ARO, Incorporated Arnold Engineering Development Center Arnold AF Station, Tennessee 37389 Attn: Dr. B.H. Goethert Chief Scientist
75.	Atlantic Research Corporation Shirley Highway & Edsall Road Alexandria, Virginia 22314 Attn: A. Scurlock
76.	Atlantic Research Corporation Shirley Highway & Edsall Road Alexandria, Virginia 22314 Attn: Security Office for Library
77.	Battelle Memorial Institute 505 King Avenue Columbus, Ohio 43201 Attn: Report Library, Room 6A
78.	Beech Aircraft Corporation Boulder Facility Box 631 Boulder, Colorado Attn: J.H. Rodgers
79.	Bell Aerosystems, Inc. Box 1 Buffalo, New York 14205 Attn: T. Reinhardt
80.	Bell Aerosystems, Inc. Box 1 Buffalo, New York 14205 Attn: W.M. Smith

DISTRIBUTION (Continued)

<u>Copy No.</u>	<u>Transmitted to</u>
81.	Bendix Systems Division Bendix Corporation Ann Arbor, Michigan Attn: John M. Bureger
82.	The Boeing Company Aero Space Division P.O. Box 3707 Seattle, Washington 98124 Attn: Ruth E. Peerenboom (1190)
83.	The Boeing Company Aero Space Division P.O. Box 3707 Seattle, Washington 98124 Attn: J.D. Alexander
84.	Chemical Propulsion Information Agency Applied Physics Laboratory 8621 Georgia Avenue Silver Spring, Maryland 20910
85.	Chrysler Corporation Missile Division Warren, Michigan Attn: John Gates
86.	Chrysler Corporation Space Division New Orleans, Louisiana Attn: Librarian
87.	Curtiss-Wright Corporation Wright Aeronautical Division Woodridge, New Jersey Attn: G. Kelley
88.	Douglas Aircraft Company, Inc. Santa Monica Division 3000 Ocean Park Blvd. Santa Monica, California 90405 Attn: J.L. Waisman
89.	Douglas Aircraft Company, Inc. Santa Monica Division 3000 Ocean Park Blvd. Santa Monica, California 90405 Attn: R.W. Hallet

DISTRIBUTION (Continued)

<u>Copy No.</u>	<u>Transmitted to</u>
90.	Douglas Aircraft Company, Inc. Santa Monica Division 3000 Ocean Park Blvd. Santa Monica, California 90405 Attn: G.W. Burge
91.	Fairchild Stratos Corporation Aircraft Missiles Division Hagerstown, Maryland Attn: J.S. Kerr
92.	General Dynamics/Astronautics P.O. Box 1128 San Diego, California 92112 Attn: F. Dore
93.	General Dynamics/Astronautics P.O. Box 1128 San Diego, California 92112 Attn: Library & Information Services (128-00)
94.	General Electric Company Re-Entry Systems Department P.O. Box 8555 Philadelphia, Pennsylvania 19101 Attn: F.E. Schultz
95.	General Electric Company Flight Propulsion Lab. Department Cincinnati 15, Ohio Attn: D. Suichu
96.	Grumman Aircraft Engineering Corporation Bethpage, Long Island, New York Attn: Joseph Gavin
97.	IIT Research Institute Technology Center Chicago, Illinois 60616 Attn: C.K. Hersh, Chemistry Division
98.	Lockheed Missiles & Space Company P.O. Box 504 Sunnyvale, California Attn: Y.C. Lee, Power Systems R&D

DISTRIBUTION (Continued)

<u>Copy No.</u>	<u>Transmitted to</u>
99.	Lockheed Missiles & Space Company P.O. Box 504 Sunnyvale, California Attn: Technical Information Center
100.	Lockheed-California Company 10445 Glen Oaks Blvd., Pacoima, California Attn: G.D. Brewer
101.	Lockheed Propulsion Company P.O. Box 111 Redlands, California 92374 Attn: Miss Belle Berlad, Librarian
102.	Lockheed Propulsion Company P.O. Box 111 Redlands, California 92374 Attn: H.L. Thackwell
103.	Lockheed Missiles & Space Company Propulsion Engineering Division (D.55-11) 1111 Lockheed Way Sunnyvale, California 94087
104.	Martin-Marietta Corporation Martin Division Baltimore 3, Maryland Attn: John Calathes (3214)
105.	McDonnell Aircraft Corporation P.O. Box 6101 Lambert Field, Missouri Attn: R.A. Herzmark
106.	North American Aviation, Inc. Space & Information Systems Division 12214 Lakewood Boulevard Downey, California 90242 Attn: Technical Information Center, D/096-722 (AJ01)
107.	North American Aviation, Inc. Space & Information Systems Division 12214 Lakewood Boulevard Downey, California 90242 Attn: H. Storms

DISTRIBUTION (Continued)

<u>Copy No.</u>	<u>Transmitted to</u>
108.	Northrop Space Laboratories 1001 East Broadway Hawthorne, California 90250 Attn: Dr. William Howard
109.	Radio Corporation of America Astro-Electronics Division Defense Electronic Products Princeton, New Jersey 08540 Attn: S. Fairweather
110.	Republic Aviation Corporation Farmingdale, Long Island, New York 11735 Attn: Dr. William O'Donnell
111.	Rocket Research Corporation 520 South Portland Street Seattle, Washington 98108
112.	Rocketdyne Division of North American Aviation, Inc. 6633 Canoga Avenue Canoga Park, California 91304 Attn: Library, Department 596-306
113.	Rohm and Haas Company Redstone Arsenal Research Division Huntsville, Alabama 35808 Attn: Librarian
114.	Thiokol Chemical Corporation Alpha Division, Huntsville Plant Huntsville, Alabama 35800 Attn: Technical Director
115.	Thiokol Chemical Corporation Elkton Division Reaction Motors Plant Denville, New Jersey 07834 Attn: A. Sherman
116.	Thiokol Chemical Corporation Elkton Division Reaction Motors Plant Denville, New Jersey 07834 Attn: Librarian

DISTRIBUTION (Continued)

<u>Copy No.</u>	<u>Transmitted to</u>
117.	Thiokol Chemical Corporation Redstone Division Huntsville, Alabama 35808 Attn: John Goodloe
118.	TRW Systems, Incorporated 1 Space Park Redondo Beach, California 90200 Attn: G.W. Elverum
119.	TRW Systems, Incorporated 1 Space Park Redondo Beach, California 90200 Attn: STL Tech, Lib. Doc. Acquisitions
120.	TRW, Incorporated TAPCO Division 23555 Euclid Avenue Cleveland, Ohio 44117 Attn: P.T. Angell
121.	United Aircraft Corporation Corporation Library 400 Main Street East Hartford, Connecticut 06118 Attn: Dr. David Rix
122.	United Aircraft Corporation 400 Main Street East Hartford, Connecticut 06118 Attn: Erle Martin
123.	United Aircraft Corporation Pratt & Whitney Division Florida Research & Development Center P.O. Box 2691 West Palm Beach, Florida 33402 Attn: R.J. Coar
124.	United Aircraft Corporation Pratt & Whitney Division Florida Research & Development Center P.O. Box 2691 West Palm Beach, Florida 33402 Attn: Library

DISTRIBUTION (Continued)

<u>Copy No.</u>	<u>Transmitted to</u>
125.	United Aircraft Corporation United Technology Center P.O. Box 358 Sunnyvale, California 94088 Attn: Librarian
126.	Vought Astronautics Box 5907 Dallas, Texas 75222 Attn: Warren C. Trent